NRPB-R322

Atmospheric Dispersion Modelling Liaison Committee

Annual Report 1998/99

INCLUDING

Review of Deposition Velocity and Washout Coefficient

AND

Review of Flow and Dispersion in the Vicinity of Groups of Buildings

National Radiological Protection Board
Chilton
Didcot
Oxon OX11 0RQ

Approval date: June 2000
Publication date: June 2001
£30.00
ISBN 0 85951 454 4

Preface

In 1977 a meeting of representatives of government departments, utilities and research organisations was held to discuss methods of calculation of atmospheric dispersion for radioactive releases. Those present agreed on the need for a review of recent developments in atmospheric dispersion modelling, and a Working Group was formed. Those present at the meeting formed an informal Steering Committee, that subsequently became the UK Atmospheric Dispersion Modelling Liaison Committee. That Committee operated for a number of years. Members of the Working Group worked voluntarily and produced a series of reports. A workshop on dispersion at low wind speeds was also held, but its proceedings were never published.

The Committee has been reorganised and has adopted terms of reference. The organisations represented on the Committee, and the terms of reference adopted, are given in this report. The organisations represented on the Committee pay a small annual subscription. The money thus raised is used to fund reviews on topics agreed by the Committee, and to support in part its secretariat, provided by NRPB. The new arrangements came into place for the start of the 1995/96 financial year. This report describes the fourth year in which the Committee has operated under the new arrangements, and during which it placed two contracts, for reviews of the values of the deposition velocity and washout coefficient and for dispersion calculations for sites with groups of buildings. The technical specifications for these contracts are given in this report, and the contract reports attached as annexes to this report. The Committee funded six studies in previous years; they are described in its earlier annual reports.

The Committee intends to place further contracts in future years and would like to hear from those interested in tendering for such contracts. They should contact the Secretary:

Mr J G Smith
National Radiological Protection Board
Chilton
Didcot
Oxon OX11 0RQ

E-mail: justin.smith@nrpb.org.uk

Contents

Preface **iii**

Atmospheric Dispersion Modelling Liaison Committee

1 Organisations represented on the Committee **1**

2 Terms of reference **1**

3 Reports of the Committee and its earlier Working Group on Atmospheric Dispersion **2**

4 Specifications for technical annexes **2**

A Review of deposition velocity and washout coefficient 2

B Review of flow and dispersion in the vicinity of groups of buildings 3

Annexes

A Review of Deposition Velocity and Washout Coefficient **5**

B Review of Flow and Dispersion in the Vicinity of Groups of Buildings **53**

Atmospheric Dispersion Modelling Liaison Committee

1 Organisations represented on the Committee

Atomic Weapons Establishment, Aldermaston
British Nuclear Fuels plc
Department of the Environment Northern Ireland
Environment Agency
Health and Safety Executive
    Major Hazards Assessment Unit
Nuclear Installations Inspectorate
Magnox Electric
Ministry of Agriculture, Fisheries and Food
Meteorological Office
National Nuclear Corporation
National Radiological Protection Board
Nycomed Amersham plc
Royal Naval College, Greenwich
Rolls Royce and Associates plc
Scottish Nuclear
Scottish Environment Protection Agency
Urenco (Capenhurst)
Westlakes Research Institute

The Chairman and Secretary are provided by NRPB.

2 Terms of reference

1 To review current understanding of atmospheric dispersion and related phenomena and to identify suitable models for application primarily in authorisation or licensing, in the context of discharges to atmosphere resulting from nuclear industry activities.

2 The Committee shall consist of representatives of government departments, government agencies and primarily the nuclear industry. Each organisation represented on the Committee shall pay an annual membership fee of £1000.

3 The Committee will consider selected topics. These should be selected following discussion and provisional agreement at meetings of the Committee, followed by confirmation after the meeting. Where possible, it will produce reports describing suitable models for that topic. These will reflect either the views of an Expert Working Group appointed by the Committee or the outcome of a workshop organised on behalf of the Committee. The Working Group will determine who should be invited to speak at workshops, and will subsequently review their outcome and identify suitable models.

4 The money raised from membership fees and registration fees for the workshops will be used to support the Working Group, the drafting of reports, and any other matters which the Committee may decide.

3 Reports of the Committee and its earlier Working Group on Atmospheric Dispersion

Clarke, R H (1979). The first report of a Working Group on Atmospheric Dispersion: a model for short and medium range dispersion of radionuclides released to the atmosphere. Harwell, NRPB-R91

Jones, J A (1981). The second report of a Working Group on Atmospheric Dispersion: a procedure to include deposition in the model for short and medium range dispersion of radionuclides. Chilton, NRPB-R122

Jones, J A (1981). The third report of a Working Group on Atmospheric Dispersion: the estimation of long range dispersion and deposition of continuous releases of radionuclides to atmosphere. Chilton, NRPB-R123

Jones, J A (1981). The fourth report of a Working Group on Atmospheric Dispersion: a model for long range atmospheric dispersion of radionuclides released over a short period. Chilton, NRPB-R124

Jones, J A (1983). The fifth report of a Working Group on Atmospheric Dispersion: models to allow for the effects of coastal sites, plume rise and buildings on dispersion of radionuclides and guidance on the value of deposition velocity and washout coefficients. Chilton, NRPB-R157

Jones, J A (1986). The sixth report of a Working Group on Atmospheric Dispersion: modelling wet deposition from a short release. Chilton, NRPB-R198

Jones, J A (1986). The seventh report of a Working Group on Atmospheric Dispersion: the uncertainty in dispersion estimates obtained from the Working Group models. Chilton, NRPB-R199

Atmospheric Dispersion Modelling Liaison Committee. Annual Report 1995/96. Chilton NRPB-R292 Includes annexes

Atmospheric Dispersion at Low Wind Speed
Application of Computational Fluid Dynamics Codes to Near-field Atmospheric Dispersion
Rise of a Buoyant Plume from a Building Wake

Atmospheric Dispersion Modelling Liaison Committee. Annual Report 1996/97. Chilton NRPB-R302 Includes annexes

Atmospheric Dispersion at Low Wind Speed
Review of Models for Calculating Air Concentrations when Plumes Impinge on Buildings or the Ground

Atmospheric Dispersion Modelling Liaison Committee. Annual Report 1997/98. Chilton, NRPB-R316 Includes annex

Portability of Weather Data for Dispersion Calculations

4 Specifications for technical annexes

A Review of deposition velocity and washout coefficient

Calculations of the amount of material deposited under dry conditions are generally undertaken using the deposition velocity. A review of values of deposition velocity for particulate material and for those gases of interest to the nuclear industry is required. The review should concentrate on particles in the size range from about 0.1 to a few microns AMAD and iodine in elemental and organic forms. The review should consider deposition to a range of surfaces such as crops, grass and urban surfaces.

Calculations of the amount of material deposited by rain are generally undertaken using the washout coefficient. A review of values of washout coefficient for particulate material and those gases of interest to the nuclear industry is required. The review should concentrate on particles in the size range from about 0.1 to a few microns AMAD and iodine in elemental and organic forms. The review

should consider the variation of washout coefficient with rainfall rate and with the type of rain (eg rain from frontal systems or thunder storms).

B Review of flow and dispersion in the vicinity of groups of buildings

Dispersion calculations are often required for releases in sites consisting of many buildings. Predictions of concentration may be required at locations inside or outside the group of buildings. Such calculations have been undertaken in the past by representing the site as an area of increased roughness, or by replacing a group of buildings by a single ‘effective building’ and using a standard building wake model. The adequacy of such methods, and the way of representing a complex building or a group of buildings as a single ‘effective building’ should be discussed.

Recent experimental work has considered concentrations from releases in complex sites, either real sites or idealised arrays of buildings. The implications of this work for modelling should be addressed.

More complex calculations can be undertaken using computational fluid dynamics (CFD) techniques. The Committee has recently placed a contract to examine some features of CFD models; the report on that work has now been published.

While the report on this contract could include comments on the use of CFD, the emphasis should be on the ways in which calculations could be undertaken using the Gaussian plume model. The contractor should comment on the possibility of using existing Gaussian plume models with suitable choice of input parameter values such as roughness length or building dimensions. The possibility of making simple extensions to the Gaussian plume model should also be considered.

ANNEX A

Review of Deposition Velocity and Washout Coefficient

B UNDERWOOD, AEA TECHNOLOGY, HARWELL

Contents

Executive Summary **7**

1 Introduction **9**
- 1.1 Context 9
- 1.2 Objectives 9
- 1.3 Scope 9
  - 1.3.1 Physico-chemical form 9
  - 1.3.2 Dry deposition 10
  - 1.3.3 Wet deposition 10
- 1.4 Format 10

2 Dry deposition **11**
- 2.1 Particles 11
  - 2.1.1 Framework 11
  - 2.1.2 Meadow grass and crops 16
  - 2.1.3 Urban 19
  - 2.1.4 Forests 22
  - 2.1.5 Water 23
- 2.2 Iodine 23
  - 2.2.1 Framework 23
  - 2.2.2 Meadow grass and crops 24
  - 2.2.3 Urban 27
  - 2.2.4 Forests 28
  - 2.2.5 Water 28
- 2.3 Comparison with other approaches 29
  - 2.3.1 Data compilations 29
  - 2.3.2 Empirical relationships 29
  - 2.3.3 Semi-empirical approaches 30
  - 2.3.4 Theoretical models 31
  - 2.3.5 Present work 32
- 2.4 Summary 32
  - 2.4.1 Particles 32
  - 2.4.2 Iodine 33

3 Wet deposition **34**
- 3.1 Particles 34
  - 3.1.1 Below cloud 34
  - 3.1.2 In cloud 36
  - 3.1.3 Fog and hill cloud 37
- 3.2 Iodine 39
  - 3.2.1 Below cloud 39
  - 3.2.2 In cloud 44
  - 3.2.3 Fog and hill cloud 44
- 3.3 Comparison with other approaches 45
  - 3.3.1 Particles 45
  - 3.3.2 Gases 46
- 3.4 Summary 46
  - 3.4.1 Particles 46
  - 3.4.2 Iodine 47

4 References **48**

APPENDIX Notation **51**

Executive Summary

Dry and wet deposition play a major rôle in determining the environmental impacts of airborne pollutants. For major point-source releases, they determine the geographical extent over which airborne concentrations and ground contaminations exceed critical thresholds. In the specific context of nuclear accidents, they influence directly the levels of doses due to groundshine and the ingestion of contaminated foodstuffs, and they affect indirectly the doses due to inhalation and cloudshine by attenuating the amount of pollutant remaining airborne at a given distance from the release.

The data on the rate coefficients associated with wet and dry deposition processes are notorious for displaying a huge range of variation, pointing to the need for non-specialists to have access to practical advice on reasonable values to apply, together with an appreciation of what uncertainties to assume. The earlier recommendations made by the UK Atmospheric Dispersion Modelling Working Group (ADMWG) addressed this need, and the present work seeks to expand and update that advice, taking account of new information that has become available since then.

A key feature of the present work is the provision of an explanatory framework that assists in reviewing disparate experimental data and gives a context for specific recommendations. This enables sources of variation for which there is some understanding (such as the dependence of deposition velocity on particle size and windspeed) to be distinguished from residual sources which still await explanation (and therefore set the level of uncertainty).

The aims of the present work are:

(a) to review the literature on wet and dry deposition since the mid-1980s to assess whether more recent data indicate the need to revise or refine earlier recommendations, paying particular attention to the lessons learned from the Chernobyl plant nuclear accident,

(b) to develop a simple explanatory framework which enables a consistent set of recommendations to be made for a wide range of situations,

(c) to recommend values and simple methods of estimation which enable non-specialists to make practical assessments based on sound data and an appreciation of the underlying principles.

The work includes particles in the (aerodynamic) diameter range 0.1 μm to 10 μm and iodine either in elemental form or as methyl iodide. However, the discussion of elemental iodine embraces, as a limiting case, any highly reactive gas for which gas-phase transport processes are dominant.

For dry deposition, the dependence on surface type and on weather conditions is considered. The primary surface type of interest is taken to be grass and crop canopies, but separate consideration is given to forest canopies and water bodies. In addition, the particular features of the urban environment are discussed and corresponding recommendations made. The dependence on weather conditions is discussed in terms of windspeed and atmospheric stability. For wet deposition, both below-cloud scavenging and in-cloud scavenging are discussed. Separate consideration is also given to deposition in fog or in hill cloud.

Two types of values are given in the present work, a ‘best judgement’ value and a ‘conservative’ value, where ‘conservative’ means a value which is likely to lead to overestimation of the local deposition flux for a given airborne concentration. Although, notionally, the former aims to represent the most likely value of the relevant subjective probability distribution and the latter the, say, 90th percentile of that distribution, no formal statistical analysis has been carried out to obtain the values given.

For dry deposition, the key organising principle is to view the inverse of the deposition velocity as a transfer resistance which can be broken down into components. In particular, the

aerodynamic resistance – which relates to the transport of momentum or gas by eddy diffusion down to the vicinity of the surface roughness elements – provides a lower limit on total resistance. This is especially useful in setting conservative values in the face of large uncertainties, and in setting the limit on deposition velocity for larger particles as other resistance contributions become small. The values of sub-layer resistances (the extra resistance encountered once the roughness elements are approached) and surface resistance for iodine are set by reference to experimental data, including wind-tunnel data and field measurements (including post-Chernobyl data).

By this means, recommendations are made which are expected to be robust in terms of their dependence on meteorological conditions, on physico-chemical form of the pollutant, and in representing the trends in variation amongst a number of key surface types, whilst at the same time reflecting current uncertainties.

For wet deposition, the key step is an approximate expression for the scavenging coefficient (the rate coefficient for the decay of the total amount of pollutant airborne during rainfall), which focuses attention on the collection efficiency (the fraction of the pollutant in the air swept through by a raindrop as it falls that is actually collected by the drop). This helps to set, for particles at least, a conservative upper limit on scavenging coefficients, particularly important in the face of large discrepancies between theoretical estimates of collection efficiency and the values implied by field data for submicron particles. It also provides a simple route to expressing the dependence of scavenging coefficient on particle diameter. The best judgement values are tied to field data. Again, the overall aim is to provide recommendations which are robust in terms of their dependence on particle characteristics and rainfall intensity, whilst at the same time reflect current uncertainties.

For iodine, the implications of the reversibility of the uptake by raindrops is taken seriously, by demonstrating the differences in appropriate parameterisations for two limiting situations of interest.

For both particles and iodine, the conclusion is drawn that there is no pressing need to distinguish in-cloud and below-cloud scavenging, at the level of precision possible within the current level of uncertainty.

For both dry and wet deposition, the recommendations are summarised in terms of a simple decision tree, designed with the practical assessment context in mind.

1 Introduction

1.1 Context

Dry and wet deposition play a major rôle in determining the environmental impacts of airborne pollutants – for example, in terms of atmospheric residence times and the magnitude of pollutant inputs to sensitive ecosystems. For major point-source releases, they determine the geographical extent over which airborne concentrations and ground contaminations exceed critical thresholds. In the specific context of nuclear accidents, they influence directly the levels of doses due to groundshine and the ingestion of contaminated foodstuffs, and they affect indirectly the doses due to inhalation and cloud-shine by attenuating the amount of pollutant remaining airborne at a given distance from the release.

The literature on measurements and theoretical estimates of the rate coefficients associated with wet and dry deposition processes is vast, and the data are notorious for displaying a huge range of variation that is bewildering to the non-specialist. Those involved in estimating the consequences of airborne releases, however, need practical advice on reasonable values to apply, together with an appreciation of what uncertainties to assume. The recommendations made by the UK Atmospheric Dispersion Modelling Working Group (ADMWG) (Jones, 1983) addressed this need, and the present work seeks to expand and update that advice, taking account of new information that has become available since then.

In view of the large variability in the data, it is important to distinguish those sources of variation for which there is some understanding (such as the dependence of deposition velocity on particle size and windspeed) from residual sources which still await explanation (and therefore set the level of uncertainty). Thus, a key feature of the present work is the provision of an explanatory framework that assists in reviewing disparate data and gives a context for specific recommendations. Without this framework, values selected from the literature for use in parametric investigations of environmental impact may become inconsistent, leading to spurious trends being noted.

1.2 Objectives

The aims of the present work are:

(a) to review the literature on wet and dry deposition since the mid-1980s to assess whether more recent data indicate the need to revise or refine earlier recommendations, paying particular attention to the lessons learned from the Chernobyl nuclear plant accident,

(b) to develop a simple explanatory framework which enables a consistent set of recommendations to be made for a wide range of situations,

(c) to recommend values and simple methods of estimation which enable non-specialists to make practical assessments based on sound data and an appreciation of the underlying principles.

1.3 Scope

1.3.1 Physico-chemical form

Particles in the (aerodynamic) diameter range 0.1 μm to 10 μm are considered. The range 0.1 μm to 1 μm is especially important since many of the pollutant particles surviving well beyond the immediate vicinity of primary sources lie in this size range. Particles significantly larger than 10 μm in diameter have appreciable settling velocities and do not remain airborne many kilometres from the source unless they are released at elevation.

For smaller particles (<0.1 μm in diameter) physical diameter is more important than aerodynamic diameter (ie the diameter of a sphere of unit density having the same Stokes settling

velocity) but, for particles larger than about 1 μm in diameter, aerodynamic diameter is the key parameter. Particle density is often not recorded in measurements on small particles, so in practice the distinction is often ignored.

Usually the dry and wet deposition rate coefficients for particles are assumed not to depend on the chemical forms making up the particle, except where the hygroscopic nature of the particles might be particularly important (such as in dry deposition to a water surface and in-cloud scavenging involving nucleation).

For gaseous species, attention is directed solely towards iodine in either elemental form (sometimes termed molecular iodine) or as methyl iodide (sometimes termed organic iodine), because of their importance in nuclear accident consequence assessment. However, the discussion of elemental iodine embraces, as a limiting case, any highly reactive gas for which gas-phase transport processes are dominant.

1.3.2 Dry deposition

Besides its dependence on physico-chemical form, the other factors considered for dry deposition are its dependence on surface type and on weather conditions. The primary surface type of interest is taken to be grass and crop canopies, but separate consideration is given to forest canopies and water bodies. In addition, the particular features of the urban environment are discussed and corresponding recommendations made.

The dependence on weather conditions is discussed in terms of windspeed and atmospheric stability.

1.3.3 Wet deposition

The treatment of wet deposition includes below-cloud scavenging (material removed by raindrops passing through the pollutant plume) and in-cloud scavenging (material removed by incorporation into raindrops as they form). However, it is outside the scope of this work to consider the impact of the large-scale motions associated with thunderstorms, which can lead to pollutant being deposited at locations far removed from those implied by the boundary-layer wind field.

Consideration is also given to deposition in fog or in ground-contacting cloud on elevated terrain (sometimes termed ‘occult’ deposition).

1.4 Format

As discussed earlier, measured values of deposition rate coefficients show a wide variability and, even after accounting for the contributions that are readily understood, significant variation remains. This translates into uncertainty when a value for a particular situation has to be selected. Although it is usually straightforward to choose a ‘conservative’ value (a value that will almost certainly overestimate the impact under consideration), there is a well-known danger in impact assessment that the conclusions drawn may be jeopardised by excessive accumulation of conservative assumptions.

For this reason, two types of values are given in the present work, a ‘best judgement’ value and a ‘conservative’ value. Although, notionally, the former aims to represent the most likely value of the relevant subjective probability distribution and the latter the, say, 90th percentile of that distribution, no formal statistical analysis has been carried out to obtain the values given.

There is a difficulty in the definition of ‘conservative’ for deposition processes. Those parameter values which maximise the near-field deposition give greatest attenuation in the amount of pollutant remaining airborne at greater distances, so do not necessarily maximise the deposition there.

A conservative estimate of the airborne concentration at large range, however, is readily obtained by assuming zero depletion, and a procedure for delivering a conservative estimate of the deposition flux at long range would be to assume zero depletion en route coupled with a conservative estimate of deposition rate at the location of interest. Thus, in this work, 'conservative' means a value which is likely to lead to overestimation of the local deposition flux for a given airborne concentration.

2 Dry deposition

2.1 Particles

2.1.1 Framework

2.1.1.1 Resistance decomposition

The deposition velocity of a given pollutant at a specified reference height above a surface, $v_d(z_{ref})$, is defined as the downward flux of pollutant to the surface divided by the pollutant concentration at the reference height. For surfaces with roughness elements very much smaller than 1 m in height, z_{ref} is conventionally taken as 1 m. Far enough from the edges of an extended homogeneous surface, v_d is independent of location on the surface, but is dependent on the characteristics of the surface, the physico-chemical form of the pollutant and the meteorological conditions.

In the lower layers of the atmosphere, typically below a few tens of metres in height, the downward fluxes of momentum, heat and pollutants can be considered independent of height, and it is therefore convenient to discuss the bulk transfer to the surface in terms of a resistance decomposition. This is first applied to momentum. Representing the transport of momentum as an eddy-diffusion process give

$$K(z)\frac{\mathrm{d}u(z)}{\mathrm{d}z} = u_*^2 \tag{2.1}$$

where $K(z)$ is the eddy diffusivity of momentum, $u(z)$ is the windspeed at height z and u_* is termed the friction velocity. The left-hand side is proportional to the flux of momentum, and the constant on the right-hand side has been written as the square of a velocity.

Integrating equation 2.1 between two levels, gives

$$\int_1^2 \frac{\mathrm{d}z}{K(z)} = \frac{u_2 - u_1}{u_*^2} \tag{2.2}$$

The integral on the LHS can be identified as a transfer resistance, since the RHS is analogous to a voltage difference divided by a current. If additional layers are introduced, the ratio of the total change in u to the flux (total 'voltage drop' to 'current') is just given by the sum of the resistances 'in series' for the individual layers.

Although the constant-flux assumption ceases to be valid close enough to – and in amongst – the roughness elements projecting from the surface, the windspeed profile behaves as if there were some height, z_0 (for non-vegetative surfaces), down to which the flux is constant and at which the momentum is fully destroyed (a perfect sink for momentum). Here z_0 is termed the aerodynamic roughness length. Setting level 1 in equation 2.2 to z_0 and level 2 to the reference height z_{ref}, the RHS becomes $u(z_{ref})/u_*^2$ termed the *aerodynamic resistance* from z_{ref}.

In neutral atmospheric stability (no buoyancy forces, with only mechanical drag generating the turbulence), the eddy diffusivity of momentum can be written as

$$K(z) = ku_*z \tag{2.3}$$

where k is von Karman's constant (taken as 0.4). Equation 2.1 can be solved to give the neutral windspeed profile:

$$u(z) = \frac{u_*}{k} \ln\left(\frac{z}{z_0}\right) \qquad z > z_0 \tag{2.4}$$

and the aerodynamic resistance:

$$r_a(z_{ref}) = \frac{\ln(z_{ref} / z_0)}{k u_*} \qquad z_{ref} > z_0 \tag{2.5}$$

It is convenient to introduce the dimensionless form of the surface resistance R_a, defined as $u_* r_a$.

Tables of typical z_0 values for various surface types are included in many standard texts; an example is given in Table 2.1, taken from Clarke (1979).

TABLE 2.1 Typical roughness lengths

Surface type	z_0 (m)
Sea	0.0001
Sandy desert	0.001
Short grass	0.005
Open grassland	0.02
Root crops	0.1
Agricultural areas	0.2–0.3
Parkland, open suburbia	0.5
Cities, woodlands	1.0

Turning attention now to pollutants in gaseous or small-particle form, turbulent transport far enough from the surface is effected by the same eddies that transport momentum, and the eddy diffusivity can be taken as close to K. However, in the final layers close to the surface differences in the transport processes arise, leading to differences in the effective transfer velocity (or, equivalently, the total resistance). For particles much smaller in diameter than 0.1 μm, for example, the final transport has to be accomplished by Brownian diffusion, with no equivalent of the pressure forces operative for momentum. For larger particles, there is the possibility of inertia carrying particles across the final layers (a process termed inertial impaction).

For surfaces with bluff roughness elements (not vegetation), the difference in transfer has been represented traditionally in terms of a sub-layer Stanton number (Chamberlain, 1991), B, through

$$\frac{1}{v_d} = r_a + \frac{1}{u_* B} \tag{2.6}$$

(dropping the explicit reference to z_{ref} in v_d and r_a for convenience). In terms of dimensionless variables, this becomes

$$\frac{1}{V_d} = R_a + B^{-1} \tag{2.7}$$

where $V_d = v_d / u_*$. Normalising by u_* is advantageous since it is found that B^{-1} has a very weak dependence on u_*. Here R_a has no dependence on u_* for neutral stability and only a weak dependence

for other stabilities (see later). This implies that the principal dependence of v_d on windspeed enters through a near-linear dependence on u_*. (It has been noted often that normalisation by u_* significantly reduces the variability in deposition velocity measurements.)

To preserve the resistance terminology, B^{-1} is here relabelled R_b, the additional sub-layer resistance to transfer for gases and small particles. It is assumed that the surface itself is an infinite sink for particles (no bounce or resuspension), so that the concentration at the surface is zero. The extension to non-zero surface concentration is considered later for gases. With this change of terminology,

$$\frac{1}{V_d} = R_a + R_b \tag{2.8}$$

In the present work R_a plays an important rôle in that it is taken as a lower bound on the (dimensionless) transfer resistance (giving an upper bound on the deposition velocity) when there are major uncertainties on the magnitude of R_b. It is assumed that gases and small particles cannot be brought to the surface any faster than can momentum, which is generally a safe assumption. In principle, it would be possible for larger particles to be more efficiently transferred than momentum and thus have a slightly larger effective value of z_0 than that for momentum, but in practice the change in limiting resistance this represents is not significant.

2.1.1.2 Vegetative canopies

For vegetation, the windspeed profile behaves as if there is a shift in vertical origin, such that

$$u(z) = \frac{u_*}{k} \ln\left(\frac{z-d}{z_0}\right) \qquad z > d + z_0 \tag{2.9}$$

where d is termed the zero-plane displacement.

For grass and crop canopies where the height of the vegetation (h) is much less than 1 m, the aerodynamic resistance in neutral stability is simply

$$R_a(z_{ref}) = \frac{\ln((z_{ref} - d)/z_0)}{k} \qquad z_{ref} > d + z_0 \tag{2.10}$$

The ratios d/h and z_0/h vary with the characteristics of the individual vegetative elements and on their packing density in the canopy, but the values $d/h = 0.7$ and $z_0/h = 0.1$ (implying $d = 7z_0$) are reasonable values to use when little specific is known about the vegetation other than its height.

A modification to the methodology is needed for tall canopies such as forests (or, indeed, the urban canopy), where $h >> 1$ m. If the surface cover is extended enough, an 'equilibrium' vertical concentration profile will develop, and it is necessary to set a reference level for concentration in defining the bulk transfer velocity of pollutant. This cannot be set too close to the top of the vegetation since there are well-known anomalies induced by the individual elements of the canopy, but care has to be taken not to set the level so high that constant-flux assumptions no longer apply. Choosing a reference level at $2h$ would give

$$R_a = \frac{1}{k} \ln\left(\frac{2h-d}{z_0}\right) \qquad z_{ref} = 2h \tag{2.11}$$

in neutral conditions. Substituting the approximate values given above, gives $R_a(2h) = \ln(13)/k$, ie 6.4, taking von Karman's constant as 0.4. For a reference level of $2.5h$, R_a only increases to 7.2, so the precise value of the reference level is not critical.

2.1.1.3 Non-neutral stabilities

Departures from the logarithmic windspeed profile arise when the there is a flow of heat between the underlying surface and the air: the transport of momentum is enhanced (retarded) for a flow of heat from (to) the surface. The length scale determining the relative importance of buoyancy influences is the Monin-Obukhov length, L, defined as

$$L = -\frac{\rho c_p T u_*^2}{kgH_0} \tag{2.12}$$

where ρ is the air density, c_p its specific heat capacity at constant pressure, g is the acceleration due to gravity, T is the air temperature and H_0 is the heat flux (positive if the flow is from the ground to the air, giving negative L). Clearly, for a given heat flux, L is a strong function of windspeed.

The eddy-diffusivity for a gaseous species is now written as

$$K(z) = kz / \phi_g(z/L) \tag{2.13}$$

where
$$\begin{aligned}
\phi_g(z/L) &= 6 && z/L > 1 && \text{(very stable)} \\
&= 1 + 5\frac{z}{L} && 0 < z/L < 1 && \text{(stable)} \\
&= 1 && z/L = 0 && \text{(neutral)} \\
&= (1 - 16\frac{z}{L})^{-1/2} && z/L < 0 && \text{(unstable)}
\end{aligned} \tag{2.14}$$

adopting the recommendations of Brutsaert (1982).

Substituting ϕ_g into the integral leading to aerodynamic resistance gives, for $z_{ref}/L \le 1$,

$$R_a(z_{ref}) = \frac{1}{k}\left\{\ln\left(\frac{z_{ref}-d}{z_0}\right) - \left[f\left(\frac{z_{ref}-d}{L}\right) - f\left(\frac{z_0}{L}\right)\right]\right\} \tag{2.15}$$

where
$$\begin{aligned}
f(zlL) &= -5z/L && 0 < z/L \le 1 \\
&= 0 && z/L = 0 \\
&= 2\ln\left(\frac{(1+\eta^2)}{2}\right) && z/L < 0
\end{aligned} \tag{2.16}$$

with η short-hand for $(1 - 16\, z/L)^{1/4}$. For $z_{ref}/L > 1$,

$$R_a(z_{ref}) = R_a(L) + \frac{6}{k}\ln\left(\frac{z_{ref}}{L}\right) \qquad z/L > 1 \tag{2.17}$$

In view of the essential role that L plays in modern dispersion modelling, standard techniques exist for deducing it from routine meteorological observations (see, for example, van Ulden and Holtslag, 1985); indeed, it is possible sometimes to obtain values of L (together with u_*) as part of the meteorological data set for the site of interest.

For a reference height of 1 m, it is readily seen that knowledge of L is not critical to estimating R_a even in very stable or unstable conditions, since the numerical value of L is usually much greater than 1 m. Table 2.2 gives a typical value of L for each of the standard Pasquill stability categories, and the associated values of R_a for two example roughness lengths (assuming $d = 7z_0$). The deviation from the

neutral value is typically less than 10% for all but the extreme stable and unstable categories, and even there is at most 20%. Thus, for low canopies, in the absence of information on L it would be an adequate approximation to take the neutral value for R_a.

For tall canopies, the variation of R_a with stability is more significant, since z_{ref} is now likely to be comparable to L for a wider range of conditions. Here it is essential to have an estimate of L if R_a is required to better than a factor of two accuracy for even moderately stable or unstable conditions. Given L, equation 2.15 can be used to estimate R_a, although it should be noted that for extremely unstable or stable conditions z/L may now lie outside the range for which the Monin-Obukhov similarity profiles are strictly valid. Although the values of L in Table 2.2 are indicative, they should not be viewed as definitive, given the strong dependence of L on u_*.

TABLE 2.2 Typical values of R_a for various reference heights, roughness lengths and atmospheric stabilities

		R_a (1m)	
Category	L	z_0 = 0.01 m	z_0 = 0.03 m
A	–2	9.89	7.36
B	–10	10.89	8.23
C	–100	11.43	8.69
D	∞	11.51	8.77
E	100	11.62	8.86
F	20	12.05	9.21
G	5	13.67	10.55

2.1.1.4 Evaluation of u_*

The friction velocity, u_*, plays a key rôle in determining the dry deposition velocity, and it is an essential element in the recommended procedures given here for estimating v_d, for most surface types. As mentioned in discussing L, it is possible sometimes to obtain values of u_* (together with L) as part of the meteorological data set for the site of interest, although care must be taken that the meteorological station sits in a region of similar surface characteristics to the location of interest.

Where information on u_* is not directly available, it is possible to estimate u_* from routine meteorological data, in particular the windspeed at a reference height, z_w, usually 10 m height for low canopies. In neutral conditions, this is straightforward since the logarithmic profile applies, so u(10 m) and u_* are related by equation 2.9; the corresponding ratio u_*/u_{10} is shown in Table 2.3 for a range of values of z_0, assuming $d = 7z_0$.

In non-neutral conditions, a similar form to equation 2.13 applies to momentum, with $\phi_m = \phi_g$ for stable conditions and $\phi_m = \phi_g^{1/2}$ for unstable conditions. In this case, however, the extraction of u_* from u(10 m), given, say, the surface heat flux, is complicated by the fact that L itself depends on u_*.

TABLE 2.3 Ratio of friction velocity to 10 m windspeed for various roughness lengths (neutral stability; assuming $d = 7z_0$)

z_0 (m)	u_*/u_{10}
0.0001	0.0347
0.001	0.0434
0.005	0.0526
0.02	0.0645
0.1	0.0882
0.3	0.122

Nevertheless, there are now standard techniques for estimating the heat flux from routine meteorological data and then estimating u_* (van Ulden and Holtslag, 1985; Hanna and Chang, 1992), but it is not within the scope of the present work to review these.

If no information is available on which to base an estimate of the heat flux, the assumption of neutral conditions should give a value of u_* within a factor of two for low vegetative canopies except in extremely stable or unstable conditions, but by adopting this approximation the dependence of v_d on windspeed would not be properly represented if r_a makes a sizeable contribution to the total resistance.

To extract u_* from $u(z_{ref})$ for tall canopies requires that the windspeed be known at an appropriate reference height above the canopy (see the earlier discussion on R_a). If this is not available then, in neutral conditions, the value of u_* extracted from measurements over neighbouring lower vegetation may provide a reasonable approximation since u_* is a weak function of z_0 for a given upper level (geostrophic) windspeed (Davenport, 1982). However, in non-neutral conditions this will no longer be true unless z_{ref}/L is small.

2.1.1.5 Inclusion of gravitational settling

Generally, gravitational settling makes a small contribution to the total dry deposition velocity for particles with diameters less than 10 μm, except in circumstances where the turbulent transport is particularly slow. To an adequate level of accuracy, the gravitational settling velocity, v_s, of particles with aerodynamic diameter between 1 μm and 10 μm can be taken as $3.2\ 10^{-5}\ D^2$ m s^{-1} when the aerodynamic diameter, D, is given in microns.

In principle, it is not adequate simply to add the gravitational settling velocity to the dry deposition velocity that would have been obtained in the absence of settling, since the latter alters the vertical profile of concentration. In practice, when either of the two contributions dominates the inaccuracies of simple addition are immaterial but, when there is particular interest in situations where the two contributions are comparable, a better approximation is

$$v_d = \frac{v_s}{1-\exp(-v_s / v_d')} \tag{2.18}$$

where v_d' is the deposition velocity calculated as if settling were absent. (Equation 2.18 is only strictly valid in neutral conditions and when aerodynamic resistance dominates.) Simple addition gives at most about 30% deviation from the result using the above form.

Further discussion will now be given separately for each surface type.

2.1.2 Meadow grass and crops

The particle diameter range of interest, 0.1 μm to 10 μm is treated as two sub-ranges, 0.1 μm to 1.0 μm and 1.0 μm to 10 μm. All diameters are interpreted as aerodynamic diameters.

The particle diameter range from around 0.1 μm to 1.0 μm is of particular interest because none of the potential processes contributing to deposition – Brownian diffusion, interception[*], impaction[†] or gravitational settling – is particularly efficient for these sizes, so particles that survive deposition in the near-field tend to lie in this range: much smaller particles will agglomerate, attach to larger particles or deposit via Brownian diffusion; much larger particles will fall out by gravitational settling. For the same reason, most field data using naturally occurring aerosol relate to particles in this

[*] 'Interception' is capture of a particle by an element projecting from the surface as a result of the particle's finite spatial extent as it passes around the element on a streamline.

[†] 'Impaction' is capture of a particle by an element projecting from the surface due to its departure from the streamline as a result of particle inertia.

size range. Theoretical models of dry deposition usually manifest a shallow minimum in the curve of deposition velocity versus aerodynamic diameter in this range. In practice this may not be observed empirically if the particles sources are not monodisperse or if the elements projecting from the surface of deposition have a wide range of sizes and shapes (effectively, the 'minimum' for each element size occurs at a slightly shifted particle diameter).

It is judged, therefore, that a good starting point for specifying deposition velocities is to take a value independent of particle size for this diameter range. It is considered preferable to base recommended values on experimental data rather than on the predictions of a particular theoretical model: many of the complexities and non-idealities of dry deposition in the field are not represented by the models. There is much scatter in the empirical data on deposition velocity in this size range, a major fraction of which is unexplained by any model applied to a given data set, so the data themselves give a better idea of the true uncertainty in predicting values for an actual, rather than ideal, situation.

Expert B in the USNRC/EC Probabilistic Accident Consequence Uncertainty Analysis (Harper *et al*, 1994) analysed the extensive field data sets of Nicholson and Davies (1987) and Allen *et al* (1991) which encompassed deposition to a range of grass and crop surfaces for particles mainly in the 0.1 μm to 1.0 μm diameter range, and proposed a median value 4.85 10^{-4} m s^{-1} at a windspeed of 2 m s^{-1} and 8.32 10^{-4} m s^{-1} at 5 m s^{-1}, for the purposes of the expert elicitation exercise. Here, a slightly different approach based on the same experimental data is proposed. Nicholson and Davies analysed their data to derive values of the resistance r_b discussed above (termed by them $r_b + r_c$). In the following, it will be assumed that the systematic dependence of v_d on windspeed in this size range can be expressed by assuming the product $r_b\, u_*$ (termed R_b) is constant. Although there are theoretical arguments for both a weaker and stronger dependence on u_* than this, there is too much scatter on the data to give a clear indication, whereas it is well known that normalisation of small-particle deposition velocities by u_* reduces the scatter on the data. The data of Kinnersley *et al* (1996) suggest a much stronger dependence on u_* in this size range, but this has not been confirmed by others. It appears that only four data points were used in a fit involving three variables, and the data would actually give reasonable support to the hypothesis that v_d is proportional to u_*, within experimental uncertainty.

Based on the Nicholson and Davies data, a value of $R_b = 300$ is chosen for the 'best estimate' for meadow grass and crops (the average value, excluding instances of negative deposition velocity). At this value of R_b, aerodynamic resistance makes a small contribution to the total, and this implies that $V_d' = 3.3\ 10^{-3}$, which, for a typical value of $u_* = 0.2$ m s^{-1} gives $v_d = 7\ 10^{-4}$ m s^{-1} coincidentally equal to the overall mean of the data (including the negative values, however); gravitational settling contributes only 4% of the total at 1 μm. Although the data sets are more extensive, the values found in the more recent work are fairly consistent with the earlier data of Chamberlain (1967), Clough (1975) and others, although wind-tunnel values of deposition velocity to grass appear to be, typically, a few times lower than field data (but not in the work of Kinnersley *et al*).

The post-Chernobyl measurements of Horn *et al* (1987) gave a range for the deposition velocity of ^{137}Cs – in particles chiefly in the aerodynamic diameter range 0.1 μm to 1.0 μm – to grass of height 0.1 m to 0.15 m (Bonka, 1989) between 3 10^{-4} m s^{-1} and 1.5 10^{-3} m s^{-1}, with a mean of 7 10^{-4} m s^{-1}. Clark and Smith (1988) give a value of 5 10^{-4} m s^{-1} for the deposition velocity of 'Chernobyl' particles containing ^{137}Cs depositing to vegetation in England.

The 'conservative' value is chosen to reflect the fact that a number of deposition velocity measurements on submicron particles using the profile or eddy correlation techniques have given deposition velocities in the range 10^{-3} m s^{-1} to 10^{-2} m s^{-1} (Nicholson, 1988). Although there are suspicions that the higher values may reflect limitations of the experimental techniques, the issue is still open, so a 'conservative' value of $R_b = 50$ is recommended. At this value of R_b, aerodynamic resistance

cannot be ruled out as a significant contributor. Taking a typical value of $R_a = 12$, gives a V_d of 1.7 10^{-2} which, for a u_* of 0.2 m s^{-1}, gives a v_d of 3.4 10^{-3} m s^{-1}. Only around 10%–15% of the individual data values in Nicholson and Davies imply a value of R_b less than 50. If the data of Kinnersley *et al* for submicron particles are analysed in terms of R_b, the values lie between 80 and 240, comfortably within the range 50 to 300 implied by the current recommendations (although implying consistently higher values of deposition velocity than the 'best judgement' estimate).

There are fewer data for larger particles, although pollen grains have provided a natural source of larger particles for some field measurements. The data show a rapid increase of dry deposition velocity with increasing particle diameter. The older data have been reviewed by Underwood (1984). The data of Kinnersley *et al* were fitted to a power-law dependence on diameter, with exponent 0.91. For large enough particles gravitational settling becomes important, and the contribution from aerodynamic resistance cannot be ignored. In the few-micron range, Expert B (Harper *et al*, 1994) advocated extrapolating from the value selected for the 0.1 μm to 1 μm range assuming a proportionality of deposition velocity to the square of particle diameter above 1 μm diameter. This was in accord with the analysis of Fernandez de la Mora and Friedlander (1982) for canopies with blade-shaped elements. The latter did not include inertial impaction, but this would have led to a stronger dependence on particle diameter, which is not supported by the data (although it should be borne in mind that the contribution from aerodynamic resistance was not separated out, so the observed behaviour may have been the net effect of contributions with different dependence). Similarly, although there are theoretical reasons for expecting the dependence on u_* to be stronger than linear in this size range, the data usually give reasonable support to a linear dependence within experimental uncertainties.

Here, a modification to method of Expert B in Harper *et al* (1994) is advocated in which it is the contribution of $1/r_b$ that is assumed to increase with the square of the particle diameter. Thus the deposition velocity in the 1 μm to 10 μm range is calculated using

$$R_b(D) = R_b(D_1)\left(\frac{D_1}{D}\right)^2 \qquad \text{for } 1\ \mu\text{m} \le D < 10\ \mu\text{m} \tag{2.19}$$

where $R_b(D_1)$ is the value of R_b at 1 μm. Then v'_d is obtained from

$$\frac{u_*}{v'_d(D)} = R_a + R_b(D) \tag{2.20}$$

and thence v_d from v'_d and v_s using equation 2.18. This prescription allows for the fact that aerodynamic resistance will play an increasingly important role as diameter increases towards 10 μm, as will gravitational settling. The exact form of the dependence of R_b on D is not to be taken too seriously: the data would allow other ways of approaching the aerodynamic limit for the total resistance, as diameter rises from 1 μm to 10 μm.

In most circumstances, equation 2.18 can be replaced by

$$v_d = v'_d + v_s \tag{2.21}$$

but the more general form is retained for when there is particular interest in the regime where the two terms on the RHS of equation 2.21 are comparable.

Table 2.4 gives an example of the resulting deposition velocities for an assumed aerodynamic resistance R_a of 10 and $u_* = 0.2$ m s^{-1}, which are typical values. It is noteworthy that the net dependence of deposition velocity on diameter is much weaker than to the power of two due to the influence of aerodynamic resistance: the 'best judgement' value shows an approximately linear dependence over the 1 μm to 10 μm size range, somewhat similar to the empirical relationship found by Kinnersley *et al* (1996).

TABLE 2.4 Deposition velocities to meadow grass and low crops, for R_a = 10, u_* = 0.2 m s^{-1}

Aerodynamic diameter (μm)	v_s 'Simple formula' (m s^{-1})	v_d (m s^{-1}) 'Best judgement'* R_b = 300	'Conservative' R_b = 50
1	3.20 10^{-5}	6.61 10^{-4}	3.35 10^{-3}
2	1.28 10^{-4}	2.42 10^{-3}	8.95 10^{-3}
3	2.88 10^{-4}	4.76 10^{-3}	1.30 10^{-2}
4	5.12 10^{-4}	7.22 10^{-3}	1.55 10^{-2}
5	8.00 10^{-4}	9.50 10^{-3}	1.71 10^{-2}
6	1.15 10^{-3}	1.15 10^{-2}	1.81 10^{-2}
7	1.57 10^{-3}	1.32 10^{-2}	1.89 10^{-2}
8	2.05 10^{-3}	1.47 10^{-2}	1.96 10^{-2}
9	2.59 10^{-3}	1.59 10^{-2}	2.02 10^{-2}
10	3.20 10^{-3}	1.70 10^{-2}	2.07 10^{-2}

* The precision quoted is for convenience of working, and is not an indication of accuracy.

As expected, for a fixed R_a, the difference between 'best judgement' and 'conservative' values becomes small when aerodynamic resistance becomes dominant: uncertainties in deposition velocity are then related to uncertainties in the aerodynamic resistance. Settling makes a small contribution in this size range for R_a = 10 (at most a 10% contributor), and this is likely to be true in most (but not all) practical circumstances.

The form of the dependence of deposition velocity on particle diameter implied by equation 2.19 is assumed to apply to all surface types below, although the values of R_b may be different. For given R_a and R_b, equation 2. 20 gives a linear dependence of v_d' on u_* and thus, for neutral stability, on 10 m windspeed; however, the settling component to deposition velocity is independent of windspeed. Figure 2.1 shows the net dependence of the 'best judgement' deposition velocity (at 1 m reference height) on 10 m windspeed in neutral conditions for a vegetative canopy with z_0 = 0.02 m, assuming $d = 7z_0$, for two particle diameters (0.5 μm and 5 μm).

2.1.3 Urban

When considering the deposition in an urban environment, the chief interest lies in flux of pollutant to specific types of surface, such as house roofs, pavements, building walls and grass lawns. The 'bulk' deposition velocity to the urban canopy as a whole (the average downward flow of pollutant per unit plan area of the city) is usually of less interest, apart from in determining the overall attenuation of the amount of material airborne in passing over the city.

The concept of deposition velocity is problematic for individual surfaces within the city. Although it is always possible to define a 'local' deposition velocity as the flux to an element of the surface divided by a reference concentration, generally its value will depend on where the surface sits in relation to other surfaces (for example, how tightly packed are the buildings) and on location on the surface (for example how far from edges). Despite these difficulties, experimental data after Chernobyl have been analysed to give representative values of local deposition velocity to each of a number of surface types, for a 'typical' European suburban configuration of buildings and grassed areas (Nicholson, 1987; Roed, 1987). These local deposition velocities incorporate, in a typical or average sense, the effect of sheltering of one surface by another and the specific nature of the wind environment within the canopy. (In principle, concentrations will also vary through the canopy because of loss processes, implying that care has to be taken over which reference concentration is used. However, for low values of deposition velocity, this will not be a major factor.)

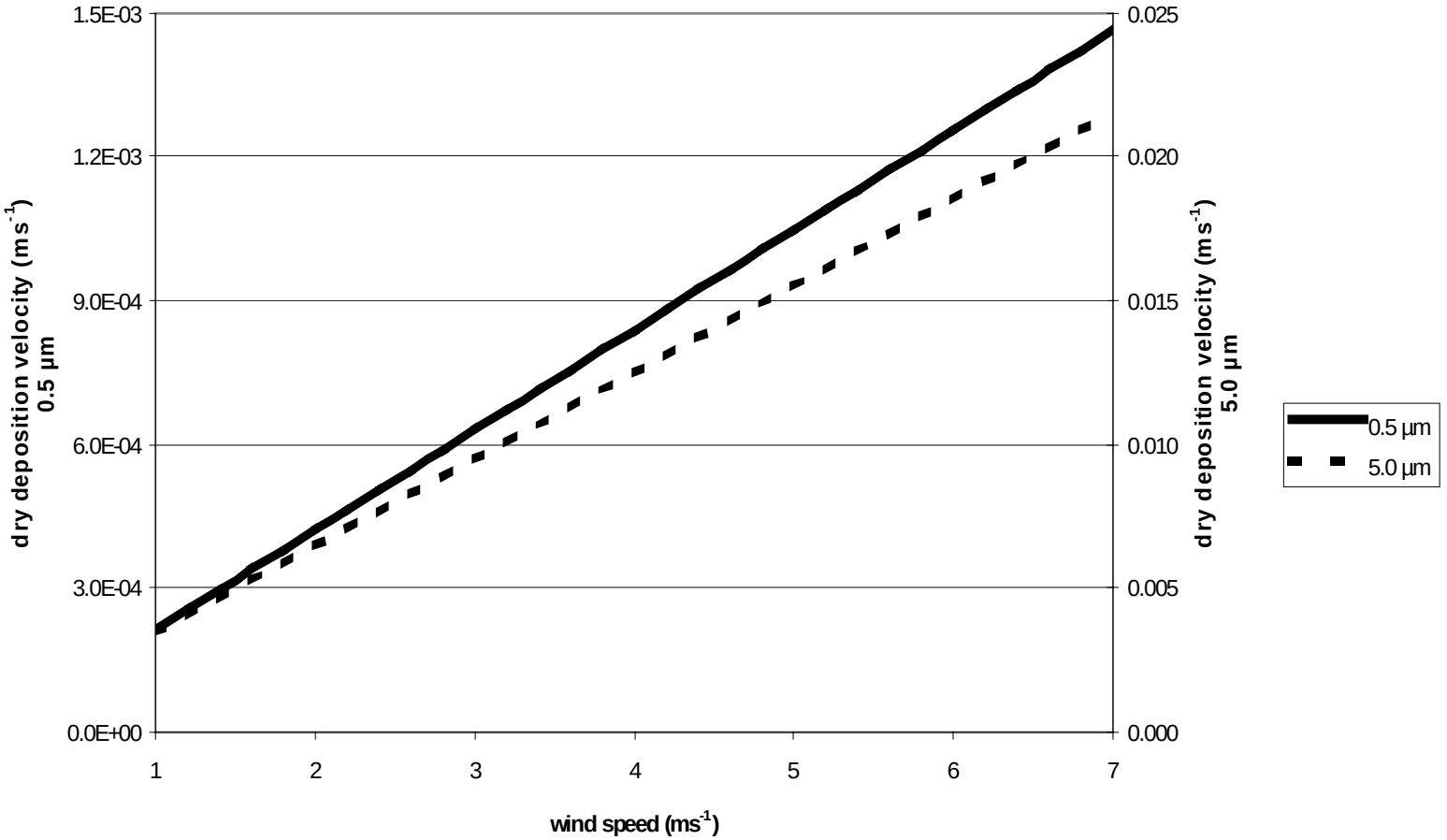

Figure 2.1 Particle dry deposition velocity to grass *vs* 10m wind speed for two particle sizes in neutral stability

A related difficulty for the urban canopy is to define an appropriate limiting aerodynamic resistance for an individual surface within the canopy. For submicron particles, this resistance contribution will be negligible, but for larger particles it is needed to set a sensible limit to local deposition velocities. In principle, it depends on the height within the canopy at which the individual surface sits, since the mean windspeed varies with height. However, the aerodynamic resistance will be dependent on the vertical profile of turbulence properties within the canopy as well as on the mean windspeed profile, since large-enough wake eddies act as quasi-mean flow to some individual surfaces.

In view of the uncertainties, the following *ad hoc* procedure is recommended: the local deposition velocity, v'_{dl} (excluding settling), is assumed to be given by

$$\frac{1}{v'_{dl}(D)} = r_{al} + r_{bl}(D) \tag{2.22}$$

where r_{al} acts as a lower limit on the local value of total resistance and $r_{bl}(D)$ is the local value of sub-layer resistance, for particles of diameter D. A value of 100 s m^{-1} is recommended for r_{al}.

It is assumed that $r_{bl}(D)$ is given by

$$r_{bl}(D) = r_{bl}(D_1)\left(\frac{D_1}{D}\right)^2 \qquad 1\ \mu\text{m} < D < 10\ \mu\text{m} \tag{2.23}$$

where D_1 is 1 μm and $r_{bl}(D_1)$ is the submicron value of r_{bl}. This prescription goes beyond what is supported by the field data, but enables a tentative extrapolation to larger particles to be made and a reasonable limit to be defined. It is not to be inferred from equation 2.22 that v'_{dl} is known to be independent of windspeed: the dependence on windspeed was not given by Roed (1987) and, in the complex canopy environment, it is difficult to speculate what it will be. Nicholson *et al* (1993) did not find a strong association between windspeed and the deposition velocity of small particles to building surfaces. Thus, the values v'_{dl} derived in the above manner are assumed to be for 'typical' values of windspeed, and no recommendation for the dependence on windspeed is provided.

Based on the data of Roed (summarised by Roed and Jacob, 1993, and IAEA, 1994), the 'best judgement' value of r_{bl} for submicron particles for grassed areas is taken to be 1500 s m^{-1}. This corresponds to a deposition velocity of around 6 10^{-4} m s^{-1} (taking the aerodynamic resistance to be 100 s m^{-1}) for particles in the 0.1 μm to 1.0 μm diameter range, close to the recommended value for extended grass/crop surfaces in the rural environment. The level of uncertainty on the deposition velocity for submicron particles is assumed to reflect that to extended vegetative canopies, and a 'conservative' estimate is based on taking r_{bl} as 250 s m^{-1}.

The data for roofs and paved areas, although more variable, suggest values comparable to those for grass, and the same prescription is therefore recommended, with r_{bl} values of 1500 s m^{-1} ('best judgement') and 250 s m^{-1} ('conservative') for submicron particles. It is important to bear in mind that the resulting values of deposition velocity are specific to the urban environment: Nicholson *et al* (1993) found significantly larger bulk deposition velocities to concrete slabs using a wind-tunnel technique.

The urban data of Roed (1987) indicate that vertical building surfaces (walls, windows and doors) are characterised by much lower values of the local deposition velocity for submicron particles; similar observations were made by Nicholson (1987). For submicron particles, this cannot be attributed simply to the absence of gravitational settling, but must relate also to the canopy environment in which the surfaces sit. Roed's data suggest one order of magnitude lower values of deposition velocity for walls and perhaps another factor of three lower for windows. Nicholson *et al* (1993) suggest using two orders of magnitude lower. The recommendation here is to use around one order of magnitude higher values of r_{bl} for all vertical surfaces (2 10^4 s m^{-1} for the 'best judgement' value and 2 10^3 s m^{-1} for the 'conservative' value for submicron particles).

These resistance values are summarised in Table 2.5, whereas Table 2.6 gives examples of the resulting deposition velocities for particles of three diameters – 1 μm, 3 μm and 10 μm.

For an isolated tree in the urban environment, the local deposition velocity can be defined as the flux per unit plan area covered by the tree. For a given above-canopy flow and pollutant concentration, the rate of deposit to an individual tree may be higher in the urban environment than if the tree sat in a forest canopy – since the wind (and possibly concentration) may be less attenuated with depth in the former than in the latter – but probably not by a large factor. In the absence of systematic data for isolated trees, it is recommended that the deposition velocity to forests be assumed. (Although the latter is defined in terms of unit plan area of the forest as a whole, it is assumed that there are no significant gaps in foliage from one tree to another.) Appropriate values for a forest are discussed below.

Nicholson *et al* (1993) used the measured values for individual surface types to derive an estimate of the bulk deposition velocity to an urban canopy, taking account of the average area of each surface type per unit plan area of the canopy. The resulting value for submicron particles was $8\ 10^{-4}$ m s^{-1}, rising to $1.6\ 10^{-2}$ m s^{-1} for 22 μm diameter particles. The value for large particles could, alternatively, be derived from considerations of bulk aerodynamic resistance and gravitational settling, as discussed earlier.

TABLE 2.5 Recommended values of the local sub-layer resistance for urban surfaces

	$r_{bl}(D_1)$ (s m^{-1})	
Surface type	'Best judgement'	'Conservative'
Grass (lawns etc)	1500	250
Roofs and paved areas	1500	250
Walls, windows and doors	20000	2000

TABLE 2.6 Example urban deposition velocities

	Local deposition velocity (m s^{-1})					
	'Best judgement'			'Conservative'		
Surface type	1 μm	3 μm	10 μm	1 μm	3 μm	10 μm
Grass (lawns etc)	$6.4\ 10^{-4}$	$3.8\ 10^{-3}$	$8.9\ 10^{-3}$	$2.9\ 10^{-3}$	$7.9\ 10^{-3}$	$9.9\ 10^{-3}$
Roofs and paved areas	$6.4\ 10^{-4}$	$3.8\ 10^{-3}$	$8.9\ 10^{-3}$	$2.9\ 10^{-3}$	$7.9\ 10^{-3}$	$9.9\ 10^{-3}$
Walls, windows and doors	$6.7\ 10^{-5}$	$4.8\ 10^{-3}$	$3.5\ 10^{-3}$	$4.9\ 10^{-4}$	$3.2\ 10^{-3}$	$8.5\ 10^{-3}$

2.1.4 Forests

There are no strong reasons to expect the values of R_b for forest canopies to differ systematically from those applicable to meadow grass/crop canopies. Naturally, there is a wide variation in foliage density and characteristics from one forest to another, but no more so than from one crop to another. A number of models of particle deposition to forests have been presented (early examples are cited by Chamberlain, 1991, and by Underwood, 1984); when expressed in terms of V_d (ie normalised by u_*), they lead to predicted deposition velocities in the 0.1 μm to 1 μm diameter range which are much the same as values for grass and crop surfaces measured in a wind tunnel (Chamberlain, 1991).

Field measurements of the bulk deposition velocity to forests are notoriously difficult. Profile methods (estimating fluxes from concentration gradients above the canopy) are unreliable because of the well-known anomalies often found above forests. Estimates based on scaling from measurements on individual leaves (see the collection of results by Expert B in Harper *et al*, 1994) show a wide variation, but the range overlaps to a large extent the range of field measurements for grass and crops.

Some of the predicted forest deposition velocities are apparently significantly larger than those to grass/crop canopies, but part of this difference derives from the assumption that significantly higher values of u_* are appropriate. Where the interest lies in forests on elevated terrain or in regions which experience high wind climatology this may be justified, but for low level forests the difference in u_* between grass/crop canopies and forest canopies for the same upper level (gradient) wind is expected to be modest, at least in neutral conditions.

In the light of these considerations, it is recommended that the same values of R_b are adopted for forests as for low grass/crop canopies, as detailed above. Care has to be taken over the definition of R_a for tall canopies, as discussed earlier in this section.

2.1.5 Water

The deposition velocity of small particles to a water surface has been measured in wind tunnels (Mőller and Schumann, 1970; Sehmel and Sutter, 1974), and the results are compatible with theoretical estimates for surfaces with small aerodynamic roughness (not quite smooth surfaces). Expressed in terms of V_d (ie normalised by u_*), the experiments gave much the same values as found in wind-tunnel measurements on grass and crop canopies (Chamberlain, 1991).

However, question-marks have been raised over the applicability of the wind-tunnel data to field conditions (Hicks and Williams, 1979; Sievering, 1984). Considerations of global budgets and atmospheric turn-over times suggest effective deposition velocities for submicron particles to the oceans considerably higher than wind-tunnel data and simple models would indicate. Additional mechanisms have been proposed – for example, impaction on to waves or capture by spray – but careful analysis seems to rule these out as adequate explanations of the discrepancy. The growth of hygroscopic particles in the near-saturated layers close to the liquid surface has also been proposed as a contributing mechanism, and may indeed play a rôle in lowering the effective value of R_b. The upper end of the range of proposed values for submicron particles would imply that the deposition velocity is comparable to or only a few times lower than the aerodynamic limit.

In the light of these considerations, there appears to be no strong reason for departing from the R_b values proposed for vegetative canopies.

2.2 Iodine

2.2.1 Framework

The formalism introduced above for particle dry deposition must be extended for gas dry deposition since the concentration of pollutant at the bounding surface may be non-zero. It is usually assumed that the flux at the surface is linearly proportional to this concentration, (although this is not necessarily true), leading to an extension to the resistance decomposition, namely

$$\frac{1}{v_d} = r_a + r_b + r_s \tag{2.24}$$

where r_s is termed the surface resistance, and represents, in the case of vegetation, the additional transfer resistance from the surface of the plant to the plant interior. For plants, it will depend on the solubility of the gas in plant fluids and on internal chemical reactions. It is assumed that pollutant material once taken up by the surface cannot subsequently be released when the external concentration falls, although in some circumstances this is an approximation.

In models of gas deposition to vegetation, r_s itself may be expressed in terms of a number of sub-resistances (in series and/or parallel) representing different parts of the plant.

2.2.2 Meadow grass and crops

Elemental iodine

In his review of data on the deposition of gases (and small particles), Sehmel (1980) commented on the large range (over three orders of magnitude) in values for elemental iodine to vegetation, although the form of the iodine may not have been carefully controlled in some early measurements. Even though most values lie between 1.0 10^{-3} m s^{-1} and 4.0 10^{-2} m s^{-1}, this is still a large range, and the resistance breakdown is helpful in interpreting this variability.

Examining the three resistance components r_a, r_b and r_s in turn, no further discussion of r_a is necessary. The sub-layer resistance, r_b, for gases has been extensively investigated for a wide range of gases, with results usually expressed in terms of R_b ($=u_* r_b$) as introduced above. It was noted that for natural fibrous surfaces such as vegetation R_b is a very weak function of u_* and of the details of the surface elements, such that for meadow grass and crops it is adequate to take R_b as independent of u_*. Also it does not vary strongly from one gas to another, and it is therefore adequate to take R_b as a constant, equal to 8, for vegetative canopies for both the gases of interest. Thus,

$$\frac{1}{v_d} = \frac{(R_a + 8)}{u_*} + r_s \qquad (2.25)$$

For $r_s = 0$, $R_a = 12$ and $u_* = 0.2$ m s^{-1}, v_d is 10^{-2} m s^{-1}. Thus, the observed large variation in deposition velocity can be attributed principally to variation in the surface resistance. At the upper end of the experimental range for molecular iodine, $u_* r_s$ cannot be large compared to 20, whereas at the lower end it must be much larger than 20.

Surface resistance has been found to depend on the character and state of the vegetation (for example, whether the stomata are open or closed, whether the cuticle is waxy or not, whether the vegetation is senescent or new, dry or wet). There is no reason to expect r_s to be directly dependent on u_* (although there could be an indirect dependence via the response of stomatal resistance to wind stress). For the 'best estimate' value of v_d, a representative value of r_s is chosen, based on the experimental data; for the 'conservative' value r_s is taken as zero.

The data suggest that, typically, v_d does not attain the limiting value that would apply for zero r_s, but also that the value obtained is not a small fraction of this limiting value. In addition, the data support an almost linear dependence on relative humidity (Heinemann and Vogt, 1980; Chamberlain, 1991), particularly at lower values. To reflect this, the following prescription is recommended when information on relative humidity is available:

$$r_s = \frac{25}{H} \text{ s m}^{-1} \qquad (2.26)$$

where H is the relative humidity expressed as a fraction, or 0.1, whichever is larger. In the absence of information on relative humidity, it is recommended that r_s is taken as 50 s m^{-1}.

Chamberlain and Chadwick (1966) measured surface resistances of around 100 s m^{-1} for individual bean leaves, with the resistance for a canopy a few times lower, reflecting the value of the Leaf Area Index (leaf area per unit plan area). For $R_a = 12$, $u_* = 0.2$ m s^{-1} and $H = 0.5$, the 'best-estimate' value of v_d is two-thirds of the 'conservative' value, and equal to 6.7 10^{-3} m s^{-1}. Even for especially low aerodynamic resistance, the 'best judgement' value cannot rise above a few times 10^{-2} m s^{-1}. For vegetation wetted by dew or previous rain, the value for $H = 1$ is recommended.

Figure 2.2 gives examples of the 'best judgement' values of the deposition velocity of elemental iodine to grass as a function of windspeed for two values of relative humidity, for a canopy with $z_0 = 0.03$ m in neutral conditions, assuming $d = 7z_0$, at a reference height of 1 m.

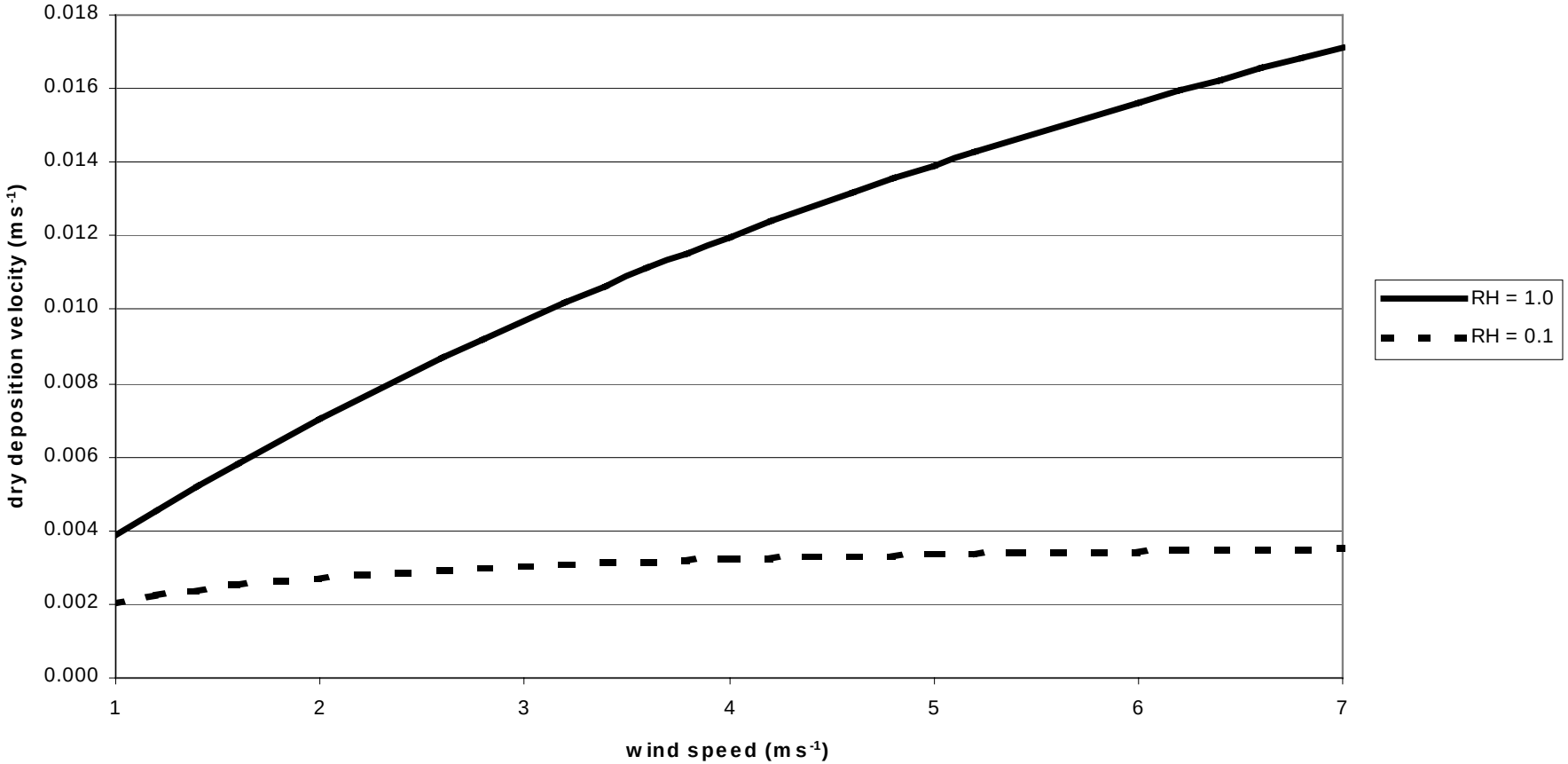

Figure 2.2 Dry deposition velocity of elemental iodine to grass vs 10m wind speed for two values of relative humidity (RH) in neutral stability

A systematic difference between day- and night-time values of the deposition velocity of elemental iodine has been observed in dry conditions, relating to the opening and closing of stomata, but the presence of dew on the vegetation increases the night-time value. The variation from day to night for a particular type of vegetation is expected to be less than the variation from one type of vegetation to another, and separate day- and night-time values are not given here.

Several authors (see, for example, Heinemann and Vogt, 1980; Roed, 1987; Chamberlain, 1991) have noted that normalising the deposition velocities of elemental iodine by herbage density (dry weight) reduces the scatter on the data (although in practice the reduction is often not dramatic). In the present formalism, this could be represented by assuming $r_s W_d$ (where W_d is dry weight density) is a constant. This may be a reasonable assumption when the herbage density increases through growth of a particular crop (although even here vegetation characteristics change with age), but it is unlikely to reduce much the variation in deposition velocity from one crop to another, considering the differences in leaf morphology, waxiness etc. Bearing in mind also that in an environmental impact assessment the herbage density will often not be known, the simpler prescription of a representative value of r_s for all vegetation is preferred, reflecting the variability in the data as a range of r_s values.

Measurements made after the Chernobyl accident were complicated by the fact that the iodine existed in three different forms, elemental, organic and particle-bound, although the latter could be separated out using particle filters. Maqua *et al* (1987), assuming 40% of the iodine was organic (and 30% particle-bound), inferred an overall mean value of deposition velocity for elemental iodine of 8.0 10^{-3} m s^{-1}. Livens *et al* (1992*)* inferred from post-Chernobyl measurements in England a deposition velocity for gaseous iodine to vegetation of 3.4 10^{-3} m s^{-1}, and deduced that this was 40% of the aerodynamic limit, implying a surface resistance of 170 s m^{-1}. However, methyl iodide was not distinguished from elemental iodine. If 50% of the gaseous iodine was methyl iodide (not inconsistent with some post-Chernobyl measurements), the inferred surface resistance for elemental iodine would be only 25 s m^{-1}. In their analysis of post-Chernobyl measurements in England, Clark and Smith (1988) derived a deposition velocity for iodine to vegetation of around 3 10^{-3} m s^{-1}, but this included particulate and organic species. Given that the elemental fraction was likely to have been several tens of per cent, this value is compatible with the recommendations made above for elemental iodine.

Wershofen and Aumann (1989) measured the deposition velocity of gaseous ^{129}I in the vicinity of a nuclear reprocessing plant, obtaining a value of 5.8(±2.6) 10^{-3} m s^{-1}. However, most of the airborne iodine (89.4%) was found to be organic in form, so the result implies a high deposition velocity for elemental iodine (around 7 10^{-2} m s^{-1}), if the value for methyl iodide is assumed to be at least two orders of magnitude lower. This is high even if the surface resistance is zero, although no meteorological information was provided. However, the experimental uncertainties are quite large, and the value quoted is consistent with the recommendations to within one to two standard deviations of the measurement uncertainty.

Methyl iodide

There are fewer data for methyl iodide than for elemental iodine, but all the data indicate that it is poorly absorbed by vegetation, such that surface resistance is by far the dominant resistance component. The early data have been reviewed elsewhere (Underwood, 1988; Harper *et al*, 1994) and no substantial body of new data is available. The measured values range between 10^{-6} and 10^{-4} m s^{-1} approximately. Again, there are no strong reasons for taking r_s to be a function of windspeed, so it is recommended that v_d is taken to be a constant. Based on the limited data available, the 'best judgement' value of v_d is taken as 10^{-5} m s^{-1} and the 'conservative' value as 10^{-4} m s^{-1}. Where there is uncertainty

as to the chemical species of the iodine, it is clearly safest to assume that it is all in elemental form from the viewpoint of making a conservative estimate of deposition flux.

2.2.3 Urban

Elemental iodine

The approach will be similar to that developed above for particle deposition to urban areas. A key source of data is the post-Chernobyl work of Roed (see Roed, 1987; Roed and Jacob, 1990). Although the results may have related to a mixture of gaseous and particulate iodine, arguments were presented there to indicate that the values were likely to be representative of elemental iodine.

As for particles, these results can be analysed in terms of local transport resistances, namely

$$\frac{1}{v_{dl}} = r_{al} + r_{bl} + r_{sl} \tag{2.27}$$

where r_{sl} is a surface resistance appropriate to the individual surface type in the urban environment, although, as discussed for particles, the concepts of local aerodynamic resistance and friction velocity are not fully coherent in the urban environment.

For grassed areas in the city there is no strong reason for expecting the surface resistance to be different to that for extended grass/crop canopies (equation 2.26), implying a value in the range 25 s m^{-1} to 250 s m^{-1}. The total local resistance implied by the measured value, 2.6 10^{-3} m s^{-1}, is 385 s m^{-1}, which implies that ($r_{al} + r_{bl}$) could lie between 135 s m^{-1} and 360 s m^{-1}. Thus the assumed variation of r_{sl} with relative humidity could generate at most about a factor of two variation in local deposition velocity, much less than the expected variability from one grassed area/urban canopy to another. The 'best judgement' value, therefore, is taken simply to be the experimental value, with no dependence on relative humidity or the state of the vegetation. There is no information on which to base a 'conservative' value of the deposition velocity, and it is set arbitrarily at 1.0 10^{-2} m s^{-1}, equivalent to zero surface resistance and ($r_{al} + r_{bl}$) = 100 s m^{-1}.

Similarly, the 'best judgement' values for roofs, paved areas, walls and windows are taken to be the quoted measured values, namely 3.3 10^{-3} m s^{-1}, 4.6 10^{-4} m s^{-1}, 3.0 10^{-4} m s^{-1} and 2.3 10^{-4} m s^{-1}, respectively, interpreted as values for typical windspeeds. Arbitrarily, for roofs the 'conservative' value is set at 1.0 10^{-2} m s^{-1} and for the other surfaces at five times the 'best judgement' value. These values are summarised in Table 2.7.

TABLE 2.7 Recommended values of local deposition velocity for elemental iodine to urban surfaces

	v_{dl} (m s^{-1})	
Surface type	'Best judgement'	'Conservative'
Grass (lawns etc)	2.6 10^{-3}	1.0 10^{-2}
Roofs	3.3 10^{-3}	1.0 10^{-2}
Paved areas	4.6 10^{-4}	2.3 10^{-3}
Walls	3.0 10^{-4}	1.5 10^{-3}
Windows and doors	2.3 10^{-4}	1.2 10^{-3}

Methyl iodide

There appear to be no data for the deposition of methyl iodide to building surfaces: the deposition velocity will be limited by adsorption processes and chemical reactions (if any) at the surface, for which specific data are required. No recommendations are given in this case. For vegetation within the urban area (lawns and parks etc), it is recommended that the values for extended grass surfaces be used.

2.2.4 Forests

There appear to be no data on the bulk deposition velocity of gaseous iodine (either species) to forests. In line with the discussion above for particle deposition to forests, the recommendation is to use the methodology advocated above for grass and crop canopies, adopting the values of r_s given there.

2.2.5 Water

The rôle played by surface resistance in deposition of gases to vegetation is here replaced by the gas solubility in water and the resistance to transfer in liquid layers beneath the surface. To an approximation, it is possible to express the overall deposition velocity as a sum of two resistances, namely

$$\frac{1}{v_d} = \frac{1}{v_g} + \frac{1}{pv_L} \tag{2.28}$$

where v_g is the deposition velocity that would apply if the water surface was a perfect sink for gas molecules ($1/v_g$ is the gas-phase resistance), p is the gas–liquid partition coefficient (which takes account of solubility and liquid-phase reactions), and $1/v_L$ is a transfer resistance on the liquid side. Similar terms enter into the discussion of the below-cloud scavenging of gaseous iodine (see Section 3).

Elemental iodine

For elemental iodine, the magnitude of p decreases with increasing airborne concentration and, if the latter is high enough, the second term may make a significant contribution. However, sufficiently high concentrations are unlikely to be experienced except in the immediate vicinity of major releases of iodine, and for most purposes it is adequate to assume that the gas-phase resistance dominates. This resistance can, as usual, be expressed as the sum of an aerodynamic resistance and a sub-layer resistance, ie (in normalised form):

$$\frac{1}{V_d} = R_a + R_b \tag{2.29}$$

The sub-layer resistance presented by molecular diffusion to a smooth surface is well known, but the surface of the sea or inland water bodies is rarely smooth. Correlations for R_b for rough (non-vegetative) surfaces have been widely studied, for both heat and vapour transfer, and a satisfactory representation is

$$R_b = 7.3\,\mathrm{Re}_*^{0.25}\,\sigma^{0.5} - 5 \tag{2.30}$$

The roughness Reynolds number, Re_*, is given by $u_* z_0/\nu$, where ν is the kinematic viscosity of air and σ is the Schmidt number, given by ν/Δ, where Δ is the diffusion coefficient of the gas in air.

The difficulty in applying this correlation to transfer to water lies in specifying – even approximately – the effective roughness length of the surface, which depends on windspeed and the character of the waves on the surface (although the dependence on z_0 in equation 2.30 is weak). A common approach is to use the relationship of Charnock (1955) for fully-developed wind waves, namely

$$z_0 = 0.014 u_*^2 / g \tag{2.31}$$

where g is the acceleration due to gravity, and the value of the numerical constant has been discussed by Garratt (1992). For a typical $u_* = 0.2$ m s^{-1}, this implies a z_0 of 6 10^{-5} m and R_b of around 5 (although the flow is then, in fact, barely turbulent). Other data reviewed by Garratt, based on drag coefficients, suggest typical values of around 2 10^{-4} m, giving $R_b = 8.7$, coincidentally close to the value adopted for

vegetative canopies. Although equation 2.30 implies a dependence on u_*, this is weak, and R_b can be taken as a constant over the range of u_* of interest. Thus, there appears no strong reason for departing from a choice of $R_b = 8$, as chosen for vegetative canopies, in setting the 'best judgement' value. (For water, however, the surface resistance should be taken as zero.)

Typically, R_a will be around 20 for the water surface so, for $u_* = 0.2$ m s^{-1} the deposition velocity would be 7 10^{-3} m s^{-1}, only 30% lower than the aerodynamic limit. The 'conservative' value should be taken as the aerodynamic limit, ie $v_d = u_*/R_a$.

Methyl iodide

For methyl iodide, with its low solubility in water, the magnitude of the liquid-phase resistance will determine the overall transfer velocity. This resistance component depends critically on motions within the liquid and, possibly, on the properties of thin surface films of other pollutants. In this case it is not possible to give a 'best judgement' value. A 'conservative' value for methyl iodide is obtained by taking the 'best judgement' value for elemental iodine.

2.3 Comparison with other approaches

Dry deposition velocities have been reviewed many times in the past, and it is not within the scope of this work to re-tread old ground. However, it is worthwhile to see how others have attempted to put some order into the huge data set on dry deposition velocities, with the aim of helping those faced with having to choose appropriate values to use in assessing the impact of releases to atmosphere.

2.3.1 Data compilations

Early systematisers of dry deposition velocity values such as McMahon and Denison (1979) and Sehmel (1980) performed a valuable service in compiling data available at the time, which highlighted the enormous range covered by the values and the need to search for ways to break down the variability into manageable components. McMahon and Denison noted the trends that deposition velocity is approximately a linear function of windspeed or friction velocity and that there is a systematic shape to the curve of deposition velocity versus particle size, with a minimum in the 0.1 μm to 1.0 μm range. This shape was manifest in the plots given in the well-known compilation of Slinn (1978), which were based principally on wind-tunnel data.

In examining the wide variation in measured deposition velocities, it has to be borne in mind that deficiencies in the experimental techniques may be a significant contributor. By whatever technique, deposition velocities are notoriously difficult to measure, particularly for small particles. Nicholson (1988) has highlighted the difficulties inherent in some of the modern techniques for measuring bulk deposition velocities and no doubt many of the early measurements suffered technical difficulties.

2.3.2 Empirical relationships

The development of empirical relationships is one approach that has been used to separate trends in data and to assist the selection of deposition velocity in a wide range of circumstances. A well-known example is the work of Heinemann and Vogt (1980) on the dry deposition velocity of elemental iodine to vegetation. They developed power-law regression fits, including as variables the herbage density (dry weight), relative humidity and friction velocity (the dependence on each being close to linear). A dependence on herbage density and relative humidity is easy enough to understand in terms of surface resistance. However, the precise fitted forms for the deposition velocity are puzzling since the values indicate that aerodynamic resistance would have played a significant role in many cases.

Indeed, some of the values quoted appear to exceed the limit that would be allowed by aerodynamic resistance, pointing to significant experimental uncertainties. The approach adopted here, linking the dependences to the surface resistance component, is preferred.

Another, more recent, example of this approach is the work of Kinnersley *et al* (1996) who made power-law fits to their own measurement of the dry deposition velocity of particles in the range 0.1 μm to 10 μm depositing to grass and crop canopies, using herbage density (dry weight per m^2), friction velocity and particle diameter (in the range above 1 μm) as variables. The dependence on herbage density is not strong (and is actually an inverse relationship for the submicron particles). There is an unexpectedly strong dependence on friction velocity for the submicron particles, but there are only four data points for a three-parameter fit and the data would fairly well support a linear dependence on friction velocity within experimental error.

One of the dangers in this type of approach – where the variable combinations used are not tied to a theoretical framework – is the 'over-fitting' of data, without due recognition of the measurement errors, leading to some trends being mere artefacts of the fitting procedure. In addition, in the examples cited above there seems little recognition of the varying contributions made by the separate components of the transfer resistance.

2.3.3 Semi-empirical approaches

Semi-empirical approaches are characterised by the identification of key dimensionless groups of parameters on which dry deposition might be expected to depend, guided by theoretical understanding of contributing processes.

Vapour and heat transfer to rough (non-vegetative) surfaces has been investigated in this way, with the dimensionless sub-layer transfer resistance represented as a function of the roughness Reynolds number and the Schmidt number (for gases, Prandtl number for heat). Chamberlain *et al* (1984) have shown that data for the transport of gases and very small particles (where Brownian diffusion is the dominant mechanism of transport across sub-layers) can be described by a single relationship across many orders of magnitude of roughness Reynolds number and a wide range of diffusion coefficients. The resulting relationship shows the dimensionless sub-layer resistance to be a very weak function of friction velocity and roughness length, a result which is exploited a number of times in the procedures recommended above.

For larger particles, where interception and impaction are important transfer processes, Sehmel and Hodgson (1978) developed a correlation in terms of a number of dimensionless groups, based on measurements to a variety of surfaces in a wind tunnel, and the results have been widely quoted. This work did take seriously the resistance decomposition, separating an aerodynamic part. However, vegetative canopies were represented by results on artificial grass and the correlation has been found not to be reliable for tall natural canopies. Over a number of years, the fits developed by Sehmel and Hodgson for essentially the same set of data varied remarkably in terms of the dimensionless groups used and the coefficients found, highlighting the sparsity of the data used to fit so many parameters and inviting caution in extending the results beyond the boundaries of the experiments. In addition, there are suggestions of systematic differences in values of particle deposition velocities measured in wind tunnels from those measured in the field, although this may derive partly from the fact that in the field the aerosol is often polydisperse.

Fernandez de la Mora and Friedlander (1982) introduced a set of dimensionless parameter groups which collapsed a wide range of data, including measurements for both gases and particles (up to 32 μm in diameter). The choice of pertinent groups was guided by theoretical considerations of transport to surfaces with blade-shaped elements, including Brownian diffusion and interception for

particles, but it is puzzling that there appeared to be no need to include dimensionless groups relating to inertial impaction (involving the particle stopping distance). It may be that the rapid dependence on particle diameter implied by impaction is moderated by re-bound in natural canopies (see below), such that the net effect mimics the dependence implied by interception alone (some support for this explanation is provided by the Slinn model – see later). A fit was made to data on deposition velocity to artificial grass in a wind tunnel. The fit implies a $u_*^{3/2}$ dependence for particles, somewhat faster than the linear dependence assumed in this work, but the data used would also support a linear dependence reasonably well. The work does not appear to recognise the contribution from aerodynamic resistance for the larger particles.

The relationship implies a dependence on the square of particle diameter, and the most impressive part of the fit is that it appears to perform well over a wide range of particle diameters (although on the large-scale log–log plots used for display even an order of magnitude discrepancy is barely noticeable). This gives some support to the inverse D^2 dependence of the dimensionless sub-layer resistance adopted above, although Fernandez de la Mora and Friedlander were working with the total deposition velocity, without separating the influence of aerodynamic resistance.

Schack *et al* (1985) extended the work of Fernandez de la Mora and Friedlander to a wider range of surface types (mainly in a wind tunnel). Widely different fitting coefficients are needed for each surface type, and there is no understanding of how the values for the coefficients relate to the properties of the surface, so the approach does not provide a basis for choosing deposition velocities for natural surfaces other than those included in the fits.

2.3.4 Theoretical models

Here, models of the micro-scale transfer of particles and gases to individual roughness elements are combined with a model of the fluid flow in the vicinity of the elements to generate a complete model for the bulk transfer to the surface. This type of approach has been applied particularly to particle deposition to vegetative canopies, in which bulk deposition is envisaged as filtration from the air flow by individual elements. An early example of such a model was that of Slinn (1976), but in a later key paper Slinn (1982) provided a more detailed model, which has been widely used as a basis for discussing deposition to vegetative canopies. This model takes seriously the resistance decomposition, and leads to a dimensionless 'canopy' resistance (equivalent to R_b introduced above) which is independent of u_*.

A key parameter of the model is the efficiency with which individual elements capture particles, and the mechanisms represented in the expression used include Brownian diffusion, interception, impaction and re-bound, and the dependence on particle size enters through this term and, for a specific choice of element dimensions, the results show the characteristic minimum in deposition velocity in the 0.1 μm to 1.0 μm range. However, in real canopies there are a variety of element dimensions, and the dip may be somewhat masked. In the data, the increase in deposition velocity with diameter above 1 μm is much less rapid for natural grass than for sticky artificial grass, which the Slinn model mainly attributes to re-bound, but the net result is that for real grass the deposition velocity rises by not much more than a factor of ten for a factor of ten increase in diameter, a type of behaviour also shown in the approach developed in the present work. With a few free parameters, Slinn was able to fit the data on deposition to grass, but it is not clear how generalisable the fit is to other surfaces.

Although the model is a valuable research tool, it is still idealised in that it does not take into account explicitly the 'sheltering' effect of one element on another (some other models recognise this), and in practice there will be a wide range of element orientations, size, shape and surface properties (stickiness, hairiness) in a natural canopy. In applying the model in an assessment context, the

parameters required to characterise the canopy, even to the extent represented in the model, will be unknown generally. Chamberlain (1991) noted that when normalised by friction velocity, a number of forest canopy models give closely similar results over a wide range of particle size, with values not far from those measured for grass swards in a wind tunnel. This suggests that the broad features of the dependence on windspeed and particle size can be represented in simpler ways, as adopted in the present work, and that the use of a canopy model with 'typical' values for the element characteristics will not account for much of the variability in the data on particle deposition to vegetative canopies. Thus, in framing recommendations, the approach adopted in the present work – tied to the measured data – is preferred to the reliance upon a specific model.

Canopy models have proliferated in the literature, and are proving a fruitful source of insight into the mechanisms controlling bulk deposition. In one variety (for an early example, see Belot *et al*, 1976), the individual-element collection efficiencies are themselves determined experimentally for a particular canopy type, but the model then becomes very specific to that type of canopy.

For gases, models for the deposition to vegetation have attempted to break down the surface resistance into further sub-components. Again, these models provide valuable research tools but require detailed knowledge of plant parameters, and are not readily generalisable.

2.3.5 Present work

The approach adopted in the present work is a type of 'expert judgement', based on the available data viewed from within a framework that recognises a number of guiding principles and broad features of the dry deposition process. The type of approach was suggested by the work of Expert B in the USNRC/EC Probabilistic Accident Consequence Uncertainty Analysis (Harper *et al*, 1994). By this means, it is hoped, recommendations are made which are robust in terms of their dependence on meteorological conditions, on physico-chemical form of the pollutant, and in representing the trends in variation amongst a number of key surface types, whilst at the same time reflecting current uncertainties.

2.4 Summary

The recommendations for dry deposition are summarised here in terms of a decision tree. Indented statements give a breakdown of how to carry out the preceding task.

2.4.1 Particles

2.4.1.1 Meadow grass/crops, forests and water

- Obtain $R_b(D)$:
  - Select a value of $R_b(D_1)$: 'best judgement' = 300; 'conservative' = 50.
  - Derive the value of $R_b(D)$ from $R_b(D_1)$:
    - if 0.1 μm ≤ D ≤ 1.0 μm, $R_b(D) = R_b(D_1)$,
    - else if 1.0 μm < D ≤ 10 μm, use equation 2.19.
- Obtain R_a (will have small impact if $R_b(D)$ is large enough):
  - Set z_{ref} (1 m for low canopies).
  - Obtain z_0: if no specific information, use Table 2.1.
  - Obtain d (zero for water surface):
    - if no specific information, assume $d = 7z_0$,
    - else if only height of canopy, h, known, $d = 0.7h$.
  - Obtain L: if no information, assume neutral conditions ($L = \infty$).
  - Calculate R_a from equation 2.15. (*Note*: see examples in Table 2.2.)

- Obtain u_*: if not available in meteorological data then
  estimate from $u(z_w)$, ie the windspeed at a reference height:
  if information on heat flux available, deduce u_* and L by standard techniques,
  else assume a neutral profile and use equation 2.9 – see examples in Table 2.3. (*Note*: could be significant errors for tall canopies.)
- Calculate v'_d from $u_*/(R_a+R_b)$.
- Calculate settling velocity: $v_s = 3.2\ 10^{-5}\ D^2$ m s^{-1} (1.0 μm < D ≤ 10 μm); ignore for D < 1.0 μm.
- Calculate v_d using equation 2.18 – see examples in Table 2.4 and Figure 2.1.

2.4.1.2 Urban surfaces

- Obtain r_{bl}:
  Choose $r_{bl}(D_1)$ from Table 2.5.
  Derive the value of $r_{bl}(D)$ from $r_{bl}(D_1)$:
  if 0.1 μm ≤ D ≤ 1.0 μm, $r_{bl}(D) = r_{bl}(D_1)$,
  else if 1.0 μm < D ≤ 10 μm, use equation 2.23.
- Set r_{al} = 100 s m^{-1} (will have small impact if r_{bl} is large enough).
- Calculate v'_{dl} using equation 2.22.
- Calculate v_{dl} using equation 2.18 – see examples in Table 2.6.

2.4.2 Iodine

2.4.2.1 Meadow grass/crops and forests

Elemental iodine

- Obtain r_s:
  if 'conservative' value required, r_s = 0,
  else if 'best judgement' value required:
  if relative humidity known, use equation 2.26,
  else r_s = 50 s m^{-1}.
- Obtain R_a – same procedure as for particles, see above.
- Obtain u_* – same procedure as for particles, see above.
- Calculate v_d using equation 2.25 – see examples in Figure 2.2.

Methyl iodide

- For meadow grass/crops and forests:
  if 'best estimate' value required, $v_d = 10^{-5}$ m s^{-1},
  else if 'conservative' value required, $v_d = 10^{-4}$ m s^{-1}.

2.4.2.2 Water

Elemental iodine

- r_s is set to zero.
- Obtain R_b:
  if 'best estimate' value required, set R_b = 8,
  else if 'conservative' value required, set R_b = 0.
- Obtain R_a – same procedure as for particles, see above.
- Obtain u_* – same procedure as for particles, see above.
- Calculate v_d as $u_*/(R_a+R_b)$.

Methyl iodide

- No 'best judgement' value.
  'Conservative' value: take the 'best judgement' value for elemental iodine.

2.4.2.3 Urban surfaces

Elemental iodine

- Set v_{dl} for the surface type of interest using Table 2.6.

Methyl iodide

- For vegetation in the urban area:
  'best judgement value of $v_{dl} = 10^{-5}$ m s^{-1},
  'conservative' value of $v_{dl} = 10^{-4}$ m s^{-1}.
- For other surface types, no recommendation.

3 Wet deposition

3.1 Particles

3.1.1 Below cloud

Below-cloud scavenging of particles is the process by which particles are taken into raindrops as they fall and are thence deposited on the ground. The following assumptions are made.

(a) Rainfall intensity is constant in time.
(b) Raindrop size spectrum is not a function of height.
(c) Particles once taken up by drops are not re-emitted before contacting the ground.

Under these assumptions, the removal of particles by scavenging does not alter the vertical distribution of particles in the air but simply causes an exponential decay in time of the total mass of pollutant airborne. The rate coefficient for the decay of the airborne mass is termed the scavenging coefficient, $\Lambda(D)$, which for particles of diameter D is given by

$$\Lambda(D) = \int \pi R_d^2 \, v_t(R_d) \, E(D, R_d) \, N(R_d) \, \mathrm{d}R_d \qquad (3.1)$$

where the integral is taken over the whole raindrop size spectrum and R_d is the drop radius, D is the particle diameter, $N(R_d)\,\mathrm{d}R_d$ is the number of raindrops per unit volume in the size range R_d to $(R_d + \mathrm{d}R_d)$, $v_t(R_d)$ is the settling velocity of raindrops of radius R_d, and $E(D, R_d)$ is the fraction of particles of (aerodynamic) diameter D which are collected from the volume of air swept out by a drop of radius R_d as it falls.

Assuming raindrops fall vertically downward, the wet deposition flux of pollutant (mass per unit area per second) at location (x, y), $W(x, y)$, can be written as

$$W(x, y) = \Lambda \int \chi(x, y, z) \, \mathrm{d}z \qquad (3.2)$$

(with easy generalisation to non-vertical rain), where the integral runs over the whole depth of the pollutant cloud and $\chi(x, y, z)$ is the airborne concentration of particulate at height z above the location of interest.

An alternative way of parameterising wet deposition is in terms of the 'washout ratio', w, defined as the ratio of the mass of pollutant per unit volume of rainwater deposited to the average mass of contaminant per unit volume in the column of air through which the rain has passed (Chamberlain, 1960). This can be written as follows.

$$w = \frac{W}{J\,\overline{\chi}} \tag{3.3}$$

where J is the rainfall intensity and $\overline{\chi}$ is the vertical average of the pollutant concentration in air. (It should be noted that sometimes w is defined using the ground-level concentration in the air rather than the vertical average, termed w_0). With these definitions,

$$w = \frac{\Lambda\, b}{J} \tag{3.4}$$

where b is the height of the column of air through which the precipitation falls.

Although w and Λ are thus related, it is worth remarking that they tend to be used in different situations: measured washout ratios are often long-term averages for continuously present pollutants and are thus averages over many rain events, whereas measurements of Λ tend to apply to specific episodes.

Slinn (1977) introduced a useful approximation to equation 3.1, expressing the scavenging coefficient as

$$\Lambda(D) = \frac{E(D, R_m)}{2R_m} J \tag{3.5}$$

where R_m is the volume-mean raindrop radius. This approximation relies upon the fact that the drop size range within which raindrops predominantly lie is fairly narrow. If R_m were independent of raindrop intensity (the total number of drops increases with increasing intensity but not the drop size spectrum) then the scavenging coefficient would be linearly proportional to rainfall intensity. In fact, R_m is known to increase slowly with rainfall intensity, and Slinn suggests (for steady frontal rain):

$$R_m = 3.5\ 10^{-4} \left(\frac{J}{J_0} \right)^{0.25} \tag{3.6}$$

where R_m is in metres and J_0 is a rainfall intensity of 1 mm h^{-1}. This leads to a net dependence of scavenging coefficient on $J^{0.75}$, ignoring the dependence of E on R_m. The best value for the numerical coefficient in equation 3.5 is uncertain, although definitely of the order of unity, and the Slinn suggestion is adopted. There is some evidence that the exponent in equation 3.6 varies with the type of rain, whether thunderstorm, frontal or orographic (discussed in Underwood, 1984) but the data are judged not to warrant making a distinction here.

Many mechanisms potentially contribute to efficiency E, including Brownian diffusion, interception and impaction. Theoretical collection efficiencies usually show a sharp dip in the particle diameter range 0.1 μm to 1 μm but, as with dry deposition, this has not usually been borne out by either controlled experiments or field data. Numerous additional mechanisms have been proposed to explain the data and 'fill in' the theoretical dip, such as phoretic processes, electrostatic effects, growth of hygroscopic particles, attachment of the primary particles to droplets or other particles and the polydispersivity of the primary particles, but the reasons for the discrepancies are not fully understood. Here, a procedure is adopted similar to that for dry deposition: the scavenging coefficient is taken to be constant for particles in the 0.1 μm – 1 μm (aerodynamic) diameter range, with the value based on data. Again, this approach is adopted to ensure realistic values are used in an assessment, given that conditions applicable to the assessment are likely to be closer to those pertaining in the experiments/field measurements than to the idealised conditions assumed for theoretical calculations.

Inspecting the field data for submicron particles (see, for example, Graedel and Franey, 1974, Radke *et al,* 1974, Davenport and Peters, 1978, and others cited in McMahon and Denison, 1979)

suggests a value of 0.1 for the collection efficiency, giving a 'best estimate' scavenging coefficient of 4 10^{-5} s^{-1} for a rainfall intensity of 1 mm h^{-1}. Post-Chernobyl measurements on caesium-bearing particles (Maqua *et al,* 1987; Clark and Smith, 1988) also point to values in the range 10^{-5} to 10^{-4} s^{-1} rather than the much lower values indicated by theory (but they may have included an in-cloud contribution). The 'conservative' estimate is obtained by taking $E = 1.0$, giving a scavenging coefficient of 4.0 10^{-4} s^{-1} at 1 mm h^{-1} rainfall intensity.

Theoretical calculations suggest a rise in scavenging coefficient (or, equivalently, collection efficiency) as particle diameter increases much above 1 μm until 'saturation' ($E = 1$) is attained for particles around 10 μm in diameter. The limited data available for larger particles (see, for example, Dana, 1970; Nicholson *et al,* 1991) support an increase in the few-micron size range. The procedure recommended here is to take

$$E(D) = E_1 + (1 - E_1)\frac{(D - D_1)}{(D_2 - D_1)} \qquad \text{for } D_1 \le D \le D_2 \tag{3.7}$$

where E_1 is the efficiency at D_1, taken as 1 μm, and D_2 is 10 μm, with $E(D)$ taken as unity for $D > 10$ μm.

Table 3.1 shows the resulting 'best estimate' scavenging coefficient as a function of particle diameter for a rainfall intensity of 1 mm h^{-1}. For all diameters in the range, the 'conservative' value is the same, namely 4.0 10^{-4} s^{-1} (ie the value for $E = 1$).

TABLE 3.1 'Best estimate' scavenging coefficient as a function of particle diameter (J = 1 mm h^{-1})

Diameter (μm)	Efficiency	Scavenging coefficient (s^{-1})
1	0.1	4.0 10^{-5}
2	0.2	8.0 10^{-5}
3	0.3	1.2 10^{-4}
4	0.4	1.6 10^{-4}
5	0.5	2.0 10^{-4}
6	0.6	2.4 10^{-4}
7	0.7	2.8 10^{-4}
8	0.8	3.2 10^{-4}
9	0.9	3.6 10^{-4}
10	1.0	4.0 10^{-4}

3.1.2 In cloud

A key question in assessing the contribution from in-cloud scavenging is what fraction of the pollutant resides within the cloud rather than below it. The dynamics of the interchange between clouds and boundary-layer air are complex, particularly for thunderstorm clouds, and are beyond the scope of this work. However, it is within the scope to consider how the rate of depletion of the mass of pollutant incorporated into the cloud (*via* liquid water loss from the cloud in raindrops) compares with the rate of washout of the material below the cloud.

Cloud droplet sizes are much smaller than raindrop sizes (tens of microns compared to fractions of a mm) and the dominant processes by which drop and particle associate could be quite different in the two cases.

It is convenient to consider the in-cloud removal process in two steps – the incorporation of pollutant material into cloud droplets (or ice crystals) and the growth of droplets to raindrop size – although, generally, the processes will be concurrent. The removal of cloud water by growth of droplets

to raindrop size has been studied extensively in the meteorology context, and rate constants are typically of the order of 1 h^{-1}, ie 3 10^{-4} s^{-1}. If all the particulate matter within the cloud became associated with water on a much shorter timescale than this – either via nucleation or attachment to existing droplets/ice crystals – then the overall rate coefficient for diminution of in-cloud pollutant would be of this order, which is close to the 'conservative' value of the scavenging coefficient adopted for below-cloud scavenging.

Whether or not substantial nucleation of the pollutant particles occurs depends on the absolute number concentration of the particles and their ability to compete with the ambient aerosol for water, so a general answer cannot be given. Even if nucleation is not a major factor, however, attachment to existing droplets can take place through a variety of mechanisms, such as Brownian and turbulent diffusion, with the latter capable of leading to attachment rates of the order of 10^{-1} h^{-1} to 1 h^{-1} for particles in the 0.1 μm to 1.0 μm diameter range. Early theoretical studies of attachment rates pointed to there being a dip (the 'Greenfield gap') in rates for particles in this size range but this is not borne out by field data and, as with below-cloud scavenging, additional mechanisms have been proposed to 'fill in' the dip, such as electrical charging.

The net result is that the effective scavenging rate coefficient for in-cloud pollutant is expected to lie in the range 0.1 h^{-1} to 1 h^{-1} (ie 3 10^{-5} s^{-1} to 3 10^{-4} s^{-1}), as borne out by field data (Underwood, 1984), which matches closely the range between the recommended 'best estimate' and 'conservative' values for below-cloud scavenging. This implies that there is no pressing need to differentiate between pollutant particulate matter within the cloud and below the cloud from the viewpoint of wet deposition, thereby bypassing the need to know how the pollutant is distributed between the two.

Wet deposition after Chernobyl in those countries far removed from the accident is likely to have resulted from a mixture of below-cloud and within-cloud scavenging, perhaps to varying degrees in various locations, and the measured values quoted earlier are consistent with the above suggestion.

3.1.3 Fog and hill cloud

3.1.3.1 Occult wet deposition

In fog or hill cloud there is the potential for submicron particles to have a higher deposition velocity than in dry conditions, due to their association with water droplets in the diameter range 10 μm to 20 μm.

Radiation fog is the most common type of fog at most low level inland sites in the UK, occurring mainly in winter months, and is characterised by low windspeeds and the absence of cloud. Thus, droplets deposit principally by gravitational settling (typically u_* is only a few times 10^{-2} m s^{-1}) with settling velocities of the order of 10^{-2} m s^{-1}, so particles associated with droplets experience deposition velocities around two orders of magnitude higher than those for particles which are not (around 10^{-4} m s^{-1}, according the prescription given earlier, at such low values of u_*).

In hill cloud, the (typically) 20 μm diameter droplets have deposition velocities up to 10^{-1} m s^{-1} (Carruthers and Choularton, 1986), at the higher values of friction velocity usually experienced there, but dry submicron particles would also have had higher deposition velocities, preserving the nearly two order of magnitude enhancement for particles in droplets. This type of deposition in hill cloud is often called 'occult' wet deposition, in that it is not captured efficiently in rain gauges but can be a significant contributor to the annual flux of ambient pollutants to hill-top vegetation.

To estimate the net enhancement to deposition, it is therefore necessary to know what fraction of particles in a given volume of air is associated with the droplets in that volume. There are two routes by which particles could end up in droplets: they may act as the kernels for heterogeneous nucleation of the droplets or they may attach to already existing droplets. For the latter, Underwood (1988)

examined the timescales of a number of potentially contributing processes, and concluded that they were too long for more than a few per cent of submicron particles to attach in the time available in the fog or cloud, which would give only a modest enhancement in average effective deposition velocity.

Turning to nucleation, the fraction of the pollutant particles of interest that would find themselves the kernels of forming droplets depends on the absolute number density of the particles and on how well they would compete with the background aerosol for the available water in the fog/cloud. Too many (hygroscopic) particles may interfere with the ability of fog or cloud to form in the first place since the water could be too widely shared for any droplet to be 'activated' (grow to droplet size) – the basis of some proposed fog control schemes and termed over-seeding in cloud physics. However, if the pollutant particles are completely insoluble in water, they will not compete with the background aerosol (which acts as if it includes several tens of per cent by volume of soluble material typically). Nevertheless, even a small amount of soluble material can dramatically affect the supersaturation level required for activation. For example, a 1 μm particle requires less than 1% by volume of (accessible) soluble material to be activated at the 0.1% supersaturation typical of radiation fog (higher values of supersaturation apply in hill cloud).

Since, usually, it will not be known how the pollutant particles of interest will fare in the competition with the background aerosol for available water, the approach here is to provide only a 'conservative' estimate of the deposition velocity based on the assumption that the released particles would always win the competition to become the kernels of newly formed fog or hill-cloud droplets. However, even for this value, the constraint is retained that the number of particles per unit volume that become droplets cannot exceed the number of droplets per unit volume that is typically supported by that type of fog or hill cloud, N_c, taken to be $2\ 10^8$ m^{-3} (200 cm^{-3}) in radiation fog and $3\ 10^8$ m^{-3} (300 cm^{-3}) in hill cloud. Thus, a 'conservative' estimate of effective deposition velocity cannot be made without also estimating the number concentration of particles, N_p, from the release information and dispersion modelling. If the particle number concentration is lower than the typical droplet number concentration given above, all particles are taken to have the deposition velocity of the droplets. If the particle number concentration is twice as high, half of the particles are assumed to be activated, with the other half retaining the dry deposition velocity. Generally, letting F be the maximum fraction of the pollutant particles that can become droplets, then

$$F = N_c / N_p \qquad N_p \geq N_c \tag{3.8}$$

To give an idea of scale, for a release rate of a few grams per second of 1 μm unit density particles in typical Pasquill category D weather, the particle concentration will fall to fog droplet concentration levels after about 1 km of downwind travel.

The recommended deposition velocity for the droplets is 10^{-2} m s^{-1} in radiation fog if, as is likely, detailed information on droplet size distribution and on u_* is not known. (If details are known, the standard prescription for particle deposition velocity given above can be applied.) Similarly, in hill cloud a value of 10^{-1} m s^{-1} is recommended in the absence of information on u_* (which, in this situation, is more difficult to deduce from routine measurements); similar values have also been found for wind-blown fog (Dollard and Unsworth, 1983). It is assumed that the fog or hill cloud extends throughout the depth of atmosphere primarily responsible for supplying the particles being deposited. Thus, the effective deposition velocity, v_{de}, is taken to be

$$v_{de} = F v_{do} + (1 - F) v_d \tag{3.9}$$

where v_{do} is the deposition velocity of the activated droplets and v_d the dry deposition velocity of the 'bare' particles.

3.1.3.2 Seeder-feeder mechanism

There is also the potential for enhanced precipitation scavenging in the presence of hill cloud via the 'seeder-feeder' effect, in which particles that are associated with droplets in the hill cloud (the 'feeder' cloud) are more easily washed out by raindrops falling from the higher level 'seeder' cloud than they would be if not in droplets. (This is not a viable mechanism for radiation fog since the appearance of a cloud sheet bringing precipitation would disperse the fog.)

An additional question has to be answered here to determine the degree of enhancement of the scavenging coefficient, even assuming that all the pollutant particles of interest in the 'feeder' cloud are associated with droplets: 'What (weighted) fraction of the vertical extent of polluted air through which the raindrops fall is occupied by the feeder cloud?' Thus,

$$\Lambda_{eff} = \frac{\Lambda_c \underset{hill\,cloud}{\chi(z)\,\mathrm{d}z} + \Lambda \underset{non-cloud}{\chi(z)\,\mathrm{d}z}}{\underset{full\,height}{\chi(z)\,\mathrm{d}z}} \tag{3.10}$$

where Λ_c is the enhanced value of the scavenging coefficient in cloud, Λ the value for the particles outside of cloud and Λ_{eff} the enhanced value. This is written as

$$\Lambda_{eff} = f\Lambda_c + (1-f)\Lambda \tag{3.11}$$

where f is the weighted fraction of the depth of the polluted layer that is occupied by the feeder cloud. If the vertical concentration is uniform then f is simply the fraction of the depth occupied by the cloud, but it should be noted that the presence of the hill may distort the vertical concentration profile.

Thus an effective scavenging coefficient cannot be given without an estimate of f. For a conservative value, f can be taken as unity, but it should be noted that the resulting value then combines two stages of potential overestimation, the first relating to the fraction of particles associated with droplets in the cloud and the second concerning the fraction of height occupied by the cloud.

The constraints on absolute number concentration given earlier are still assumed to apply, so that Λ_c itself is given by

$$\Lambda_c = F\Lambda_{dr} + (1-F)\Lambda \tag{3.12}$$

where Λ_{dr} is the value of scavenging coefficient appropriate to cloud droplets (calculated using $E = 1$) and F is the maximum fraction of particles that could be activated in the fog/cloud, discussed above.

For submicron particles Λ_{dr}/Λ is ten in the above prescription (the ratio of the collection efficiencies for particles larger than 10 μm particles to that for submicron particles).

3.2 Iodine

3.2.1 Below cloud

Two key features of the scavenging of particles by rainfall are

(a) the local rate of removal of pollutant is proportional to the local concentration of pollutant,
(b) once particles are taken into a drop they do not escape before the drop reaches the ground.

Under these conditions, the scavenging process attenuates material at each height by the same fraction per unit time, so does not alter the vertical profile of pollutant. For a constant rainfall intensity (and raindrop size spectrum), this leads to an exponential decay of the mass of airborne material.

For gases, in general, these conditions are no longer satisfied. For a given concentration in the surrounding air, the amount of gas transferred to the drop may approach a 'saturation' value, when the

concentration in the liquid phase is in equilibrium with that in the air. If the drop then falls to a region of lower concentration, gas may be released by the drop in its attempt to reach a liquid-phase concentration in equilibrium with the new surrounding air concentration. Thus the instantaneous rate of removal depends not only on the local air concentration but on the history of concentrations experienced by the drop; also, the scavenging process can lead to vertical re-distribution of the material in the air.

Although it is always possible to define an effective scavenging coefficient representing the rate of decay of the total mass airborne, in the case of reversible gas scavenging this is no longer independent of the vertical profile of airborne concentrations and will generally be time dependent. For example, the scavenging coefficient would be effectively zero if contaminated drops fall through a region of very low concentration before reaching the ground. Elevated narrow plumes could be simply vertically displaced (termed 'plume washdown').

Modelling the wet deposition of reversible gases in the general case is complex (see, for example, the work of Hales, 1982) but there are two limiting cases where a simple decay constant gives an adequate representation.

3.2.1.1 'Thin' ground-level plume

In this case, the pollutant gas is confined to a sufficiently shallow layer near the ground (a few tens of metres – see later) that (initially unpolluted) raindrops do not have time to approach saturation before reaching the ground; this situation then mimics the irreversible scavenging of particles. In this case, for highly soluble gases, the scavenging is limited only by the rate at which gas can reach the liquid surface; for less soluble gases it is also limited by the rate at which gas can be carried away from the liquid surface into the interior of the drop.

For convenience, the scavenging coefficient can be represented in terms of a transfer velocity, v_T, somewhat analogous to the dry deposition velocity, namely

$$\Lambda = \int 4\pi R^2 v_T N(R)\, \mathrm{d}R \tag{3.13}$$

with
$$\frac{1}{v_T} = \frac{1}{v_g} + \frac{1}{p v_L} \tag{3.14}$$

where $1/v_g$ can be interpreted as a gas-phase resistance and $1/v_L$ a liquid-phase resistance and p is the gas–liquid partition coefficient (ratio of liquid-phase concentration to gas-phase concentration at the interface). For simple solutions, p is the inverse of the Henry's Law constant for the pollutant gas, but more generally it takes on an enhanced value due to liquid-phase reactions.

Comparing equation 3.13 with equation 3.1, and adopting an approximation equivalent to equation 3.5, implies that

$$E_g(R_m) = 4 v_T(R_m) / v_t(R_m) \tag{3.15}$$

where the efficiency E_g is the ratio of the mass of gas transferred to the drop per second to the total mass of gas swept through by the drop per second.

The discussion now branches for elemental iodine and methyl iodide.

Elemental iodine

The washout of elemental iodine is complicated by the fact that the partition coefficient is dependent on the absolute concentration; this behaviour has been widely studied (for a summary, see Underwood, 1984). For the high airborne concentration that might exist close to a major release of elemental iodine, the partition coefficient may not attain the large values expected for low airborne

concentrations and, for a stagnant drop, liquid-phase resistance may then play a significant role. However, given that such high concentrations are only experienced in extreme circumstances (within, say, a few kilometres of a major nuclear reactor accident) and that internal drop circulation acts to lower the liquid-phase resistance, the 'best judgement' value can be based on the assumption that gas-phase resistance dominates.

The gas-phase transfer velocity is usually expressed in terms of the drop Sherwood number, S_g, through

$$v_g = S_g(R_d)\, \Delta_g / 2R_d \tag{3.16}$$

where Δ_g is the diffusion coefficient of the pollutant gas in air and, as before, R_d is the drop radius, giving

$$E_g(R_m) = \frac{2S_g(R_m)\, \Delta_g}{R_m v_t(R_m)} \tag{3.17}$$

An adequate correlation for the Sherwood number in the relevant drop size range is

$$S_g = 2 + 0.6\, \mathrm{Re}^{1/2}\, \sigma^{1/3} \tag{3.18}$$

where Re is the drop Reynolds number ($2v_t R_d/\nu$), ν is the kinematic viscosity of air, and σ is the Schmidt number, defined as ν/Δ_g. For elemental iodine, $R_m = 3.5\ 10^{-4}$ m and a rainfall intensity of 1 mm h^{-1}, this gives $E_g = 0.16$. Thus Λ is given by

$$\Lambda = 6\ 10^{-5}\ (J/J_0)\ \mathrm{s}^{-1} \tag{3.19}$$

(ignoring the dependence of E on R_m). Since this result corresponds already to the limit in which only gas-phase resistance limits the rate of transfer, no separate 'conservative' value is given.

Given that the dependence on the diffusion coefficient of the gas in air is weak, equation 3.19 can be used for any 'reactive' gas, ie for which the liquid-phase resistance is small compared to the gas-phase resistance. However, the estimate applies only to the 'thin plume' situation, unless the gas is taken up irreversibly by the drops.

Methyl iodide

For methyl iodide, the partition coefficient has been measured experimentally (see the results cited in Maeck *et al,* 1984). A value of seven is recommended at 15 C. Transfer on the liquid side would be enhanced by drop internal circulation and drop oscillation, but the laboratory measurements of Maeck *et al* gave a transfer rate even lower than that for a stagnant drop. Perhaps the presence of surface-active agents inhibited the transfer.

In light of the lack of understanding of the processes limiting the rate of transfer of methyl iodide to drops, no 'best judgement' value for the scavenging coefficient is provided. A 'conservative' value can be provided by assuming zero liquid-phase resistance, although this could be very conservative indeed for methyl iodide. In principle, even the limiting value will differ from that for elemental iodine due to the different diffusion coefficient in air (about a factor of two higher), but to the level of approximation involved this difference can be ignored.

3.2.1.2 Uniform concentration

Most discussions of the iodine scavenging coefficient appear to have in mind the gas-phase-resistance-only limit worked out above. However, the 'thin' ground-level plume situation is not likely

to be common in practice. The timescale for elemental iodine to approach equilibrium concentration is of order of ten seconds for a 0.5 mm drop (Underwood, 1984) and a few tens of seconds for methyl iodide (although the laboratory experiments of Maeck *et al* suggest it would take of the order of 100 m of fall for a 0.5 mm diameter drop to reach equilibrium). For elemental iodine this implies that equilibrium is attained in only a few tens of metres of fall and that the pollutant layer would have to be of this thickness or less for the above approximation to be valid.

Another idealised situation for which a simple exponential decay coefficient is adequate is more often approximated by field conditions. Here, the concentration is uniform over the full vertical extent of the pollutant, the latter height range is large compared to the distance needed to reach equilibrium concentrations in the drop, and the rate of diminution of the total amount airborne is comparable to or slower than the rate of vertical mixing in the atmosphere. In this case, although the flux of deposited pollutant is proportional to the airborne concentration in the last few tens of metres of fall, this concentration is representative of the concentration throughout the polluted layer. Also, although the loss of material to the drops is greatest when the drops first enter the polluted layer, the preferential loss at the top is shared over the layer by vertical dispersion.

Since the drops hitting the ground have liquid-phase concentrations in equilibrium with the air concentration, the 'washout ratio' (ratio of concentration in liquid to that in the air) is equal to the partition coefficient, p. Thus, the wet deposition flux, W (in kg m^{-2}), is given by

$$W = J\ p\ \chi \tag{3.20}$$

where χ is the airborne concentration (kg m^{-3}) and J is the rainfall intensity in units of m s^{-1}.

In this situation, a useful alternative concept is the wet deposition velocity, v_w, defined as the ratio of the flux to near-surface concentration (in an equivalent manner to dry deposition velocity). From the above,

$$v_w = J\ p \tag{3.21}$$

This velocity can be compared directly with the dry deposition velocity to provide information on the relative importance of wet and dry deposition. It is important to note, however, that there are subtle differences in the two concepts. The dry deposition velocity relates to mechanisms operative at the surface and is specific to a defined reference height, whereas most of the material removed in wet deposition may have entered the drops well above the surface and the concentration of interest is the 'average' value over a depth from the surface comparable to the height required to reach equilibrium in the drop. However, when it can be assumed, in both cases, that vertical dispersion is rapid enough to maintain a uniform concentration throughout the depth of the plume, both result in an exponential decay with time of the amount of material airborne. For wet deposition, the necessary condition is that the wet deposition velocity be small compared to vertical turbulence velocity scales in the vertical region where the removal from the plume is primarily taking place.

Tangentially, for reversible gas scavenging wet deposition velocity remains a useful concept even when the vertical concentration profile is not uniform. Then the above condition on v_w is equivalent to the condition under which the widely-used 'source depletion' approximation is valid for dry deposition. Although not giving a simple exponential decay with time of the amount airborne, this does lead to a simple way of estimating the effect of deposition by assuming the vertical concentration profile is the same as that in the absence of deposition. For wet deposition, however, it should be borne in mind that the principal uptake of gas may be near the top of the cloud, where vertical turbulent velocity scales may be quite different from those near the ground.

Elemental iodine

For elemental iodine, previous work (Underwood, 1984) suggests that p is likely to be of the order of 10^4 at low airborne concentrations and typical pH values, although it may be higher in some circumstances. It is recommended that 'best judgement' wet deposition fluxes of elemental iodine be calculated using equation 3.20, taking $p = 10^4$.

Assuming a uniform concentration throughout the height of the polluted layer implies that the decay rate constant for the airborne material, the scavenging coefficient (in s^{-1}), is given by

$$\Lambda = Jp / b \quad (= v_w / b) \tag{3.22}$$

where b is the height of the layer (in metres) and, again, J is in m s^{-1}. It is worth noting the linear dependence on J resulting from this simple analysis. Interestingly, taking $p = 10^4$, a polluted layer of 100 m depth and a rainfall intensity of 1 mm h^{-1} gives $\Lambda = 0.1$ h^{-1} or 3 10^{-5} s^{-1}, coincidentally much the same value as for the 'thin' plume case. More typically, b is expected to be of the order of 1000 m, giving $\Lambda = 10^{-2}$ h^{-1} (3 10^{-6} s^{-1}), an order of magnitude lower. Application of the above washout coefficient assumes that the background concentration of molecular iodine is small compared to release concentration at the distances of interest.

Few field measurements of gaseous iodine scavenging coefficients have been reported. The results of Engelmann and Perkins (1966) were reckoned to have been affected by attachment to large particles, whereas the tracer experiments of Engelmann *et al* (1966) were carried out at high iodine concentrations. Post-Chernobyl measurement of iodine scavenging relate (see, for example, Maqua *et al,* 1987) principally to the particle-bound component rather than the gaseous species.

Field experiments were carried out by Caput *et al* (1993) at two sites in France: at Brennilis the release was made at a high point of around 30 m, with measurements made at distances between 320 m and 1720 m from the source; at Roc'h Trédudon the release was from a mast at 12 m, with measurements made at 20 m to 50 m from the source. At Brennilis, the measured values of scavenging coefficient ranged from 2.1 10^{-5} s^{-1} to 4.0 10^{-4} s^{-1}, with a mean of 2.0 10^{-4} s^{-1}, but the measurements were assumed to include a dry deposition component. At Roc'h Trédudon the measurements were made close enough to the source that the plume had not diffused down to ground. The lower values of scavenging coefficient found there (from 1.5 10^{-5} s^{-1} to 3.0 10^{-4} s^{-1}, with a mean of 8.2 10^{-5} s^{-1}) were taken to confirm that dry deposition had played a part at Brennilis, but may also be interpreted as showing an influence of desorption from drops below the plume.

The overall results were taken to confirm that iodine uptake by drops is irreversible, with uptake rates reaching the limit imposed by gas-phase resistance. However, the analysis above has shown that if the partition coefficient is high enough similar effective values can be found in situations where the behaviour is far from irreversible. The liquid-phase concentrations in the Caput *et al* experiments were certainly low enough (around 10 μg l^{-1}) to achieve partition coefficients of the order of 10^4, as in the example given earlier. The apparent lack of influence of the ambient concentration of iodine was also adduced as evidence of irreversibility, but the ratio of background to signal was not really high enough for a firm conclusion. Overall, the values of scavenging coefficient found by Caput *et al* were generally in line with the recommendations made here.

In summary, in situations where b is one of the parameters known in the assessment, it is recommended that the rate of decay of airborne material be calculated using equation 3.22, with $p = 10^4$.

It is possible that the iodine partition coefficient could be significantly higher than 10^4 in particular circumstances, although this is not likely. For a 'conservative' value, it is recommended that p be taken as 10^5.

The decrease in Λ with increasing b indicates that wet deposition velocity is a more suitable concept in this situation. For a partition coefficient of 10^4, v_w is 2.8 10^{-3} m s^{-1} for a rainfall intensity of 1 mm h^{-1}, which is comparable to the dry deposition velocity of elemental iodine. However, dry deposition is continuously operative whereas rain falls for only a fraction of the time (albeit sometimes with higher intensity than 1 mm h^{-1}).

Methyl iodide

The value of p quoted earlier implies a wet deposition flux about three orders of magnitude lower for methyl iodide than for elemental iodine for the same rainfall intensity and thus an effective scavenging coefficient three orders of magnitude lower for the same layer depth. However, some field data suggest much higher concentrations of methyl iodide in rain and snow than given by equilibrium theory by around three orders of magnitude (Rasmussen *et al,* 1983). Although suggestions have been made to explain this discrepancy – involving attachment to particles or enrichment in cloud formation processes – the reasons are far from fully understood. Here, these higher values are assumed not to apply to below-cloud scavenging: the recommendation is to use the known low value of p (= 7) to give the 'best judgement' scavenging coefficient. For the 'conservative' value it is recommended that the iodine be assumed to be in elemental form.

3.2.2 In cloud

Elemental iodine

Given that the timescales for iodine concentrations in the water phase to reach equilibrium are expected to be much shorter than the cycling time for liquid water in clouds (even after allowing for the smaller drop sizes in clouds), there seems no strong necessity to distinguish in-cloud from below-cloud scavenging. Provided in-cloud airborne concentrations do not differ significantly from those below cloud, the 'uniform concentration' approximations introduced above can be taken to apply.

Methyl iodide

For methyl iodide, caution is necessary in the light of field observations which suggest much higher water-phase concentrations than given by an equilibrium calculation. Where in-cloud scavenging is a possibility, a 'conservative' procedure would be to assume a scavenging coefficient of 10^{-2} h^{-1} ($3\ 10^{-6}$ s^{-1}), and to assume that the uptake of methyl iodide was irreversible, although the mechanisms to achieve these values are not fully understood.

3.2.3 Fog and hill cloud

Elemental iodine

In the following, the implications of fog or hill cloud will be worked out only on the assumption that the concentration in droplets has reached equilibrium with that in the surrounding air, since the timescales to equilibrium are at most tens of seconds. In this case, that fraction of the iodine that resides in droplets will experience a deposition velocity appropriate to droplets of 10 μm to 20 μm diameter. In the type of conditions leading to radiation fog, the dry deposition velocity of the gas would likely be aerodynamically limited, and have a value of around 2 10^{-3} m s^{-1}. The droplets, however, experience gravitational settling, giving a deposition velocity around 10^{-2} m s^{-1}, so the differential is not as high as in the case of submicron particles.

The key factor now, however, is that only a small fraction of the total mass of gas in unit volume of air can actually reside in droplets. The fraction of gas in droplets, F, is given by

$$F = p\, L_w \qquad (3.23)$$

where L_w is the liquid water content of the fog/cloud, ie the fraction by volume that is water, and p is the partition coefficient. The value of L_w is, typically, around 10^{-7}, so even for a partition coefficient of 10^4 the fraction is only 0.1%. High values of the partition coefficient for elemental iodine are only realised at very low airborne concentrations and increase with increasing pH. Even though, theoretically, p may rise above 10^4, in practice higher values have rarely been observed. Thus, even if a conservative value of $p = 10^5$ is postulated, it is safe to ignore any enhancement of the effective deposition velocity of elemental iodine in fog and hill cloud. Of course, the droplets in fog and hill cloud may contain other trace compounds that affect the iodine partition coefficient but, since these are more likely to make the droplets acidic, the partition coefficient is unlikely to be increased.

The principal impact of foggy conditions on iodine deposition velocity would be to wet the vegetation and thus lead to a lowering of the surface resistance (see the earlier discussion on the influence of relative humidity on iodine deposition velocity).

A similar line of reasoning applies to the seeder-feeder mechanism: such a small fraction of the total iodine resides in the droplets that the enhanced scavenging experienced by this fraction (with one to two orders of magnitude higher effective scavenging coefficient) has little impact on the net wet deposition flux.

Methyl iodide

With the partition coefficient expected to be less than 10, only around 10^{-6} of the methyl iodide is expected to be in droplets. In radiation fog, even if the deposition velocity of this fraction increases from around 10^{-6} m s^{-1} to around 10^{-2} m s^{-1}, the net effect on the deposition flux is negligible. Similarly, even if in hill cloud the deposition velocity were increased from 10^{-5} m s^{-1} to 10^{-1} m s^{-1}, the net impact would be negligible. There is no information on the impact that wetting the vegetation has on the deposition velocity of methyl iodide, but its low solubility suggests that the surface resistance would remain high.

By a similar line of reasoning to that used for elemental iodine, the seeder-feeder mechanism is not expected to provide any significant enhancement of effective scavenging coefficient for methyl iodide.

3.3 Comparison with other approaches

3.3.1 Particles

There is less variety in the approaches recommended for precipitation scavenging than for dry deposition. The starting point is almost universally the Slinn expression – equation 3.5. Although this is an approximation, it does not differ in essence from the full expression (equation 3.1), but simply focuses attention on the key rôle played by the collection efficiency. Differences in approach relate to how the collection efficiency is estimated as a function of particle size. A large body of theoretical and experimental work has been devoted to the collection efficiency of raindrops, and an obvious approach is to distil this into the values selected for use in estimating scavenging coefficients.

Along these lines, Slinn (1977) suggested a semi-empirical form which included the Brownian diffusion, interception and impaction collection mechanisms, and this has been widely adopted (see, for example, Expert B in the USNRC/EC study – Harper *et al*, 1994). It implies collection efficiencies of the order of 10^{-4} to 10^{-3} for particles in the diameter range 0.1 μm to 1.0 μm, rising by several orders of magnitude as the particle diameter approaches 10 μm. However, these values of collection efficiency for submicron particles imply much lower scavenging coefficients than field data indicate (as collected by McMahon and Denison, 1974, and partly reviewed by Underwood, 1984). Numerous additional

mechanisms have been proposed to 'fill in the dip', such as thermophoresis and electrical charging. Calculations indicate that these may have a significant effect in some circumstances, but are unlikely to be able to explain all the discrepancies between theory and field data.

The discrepancies may derive from practical difficulties in the measurements, from the polydispersivity of the aerosol or from additional processes such as the growth of hygroscopic particles during the rain event. In addition, in experiments using the background aerosol, there may have been a contribution from in-cloud scavenging. Despite the lack of understanding of the reasons for the discrepancy, in the present work it was judged preferable to link the particle scavenging coefficients to measured values, an approach adopted by Expert G in the USNRC/EC study (Harper *et al,* 1994).

3.3.2 Gases

The difficulty that 'back diffusion' of gases presents to the scavenging-coefficient concept was recognised long ago, but that has not prevented many from using the 'irreversible' approximation for reactive gases such as iodine, even in conditions well removed from the 'thin' plume situation introduced above. In practice, however, the more appropriate 'uniform concentration' value for elemental iodine may, coincidentally, be quite similar to the 'thin' plume value, as shown above.

Other authors (see, for example, Dana, 1979) have recognised the efficacy of the washout ratio concept for gases when equilibrium conditions apply, with the focus of attention then directed to the partition coefficient at the air–water interface, which may be enhanced by liquid-phase reactions (as is the case for elemental iodine). This is the approach recommended above to calculate a scavenging coefficient when the pollutant gas has near uniform concentration over a substantial depth of atmosphere. The situation can also be treated in terms of a wet deposition velocity. For elemental iodine, partition coefficients have been investigated both theoretically and experimentally in the context of spray removal from indoor atmospheres and are known to depend on absolute concentration and on the pH of the liquid phase. Although very high partition coefficients are predicted at low concentrations, values much above the 10^4 recommended here rarely arise in practice.

3.4 Summary

3.4.1 Particles

3.4.1.1 Below-cloud and in-cloud scavenging

- Estimate collection efficiency, *E(D)*:
  - if 'conservative' value required, set $E = 1.0$,
  - else if 'best judgement' value required:
    - if $0.1\ \mu m < D \leq 1.0\ \mu m$, $E = 0.1$,
    - else if $1.0\ \mu m < D \leq 10\ \mu m$, use equation 3.7.
- Calculate $\Lambda(D)$ from *E(D)* and *J* (rainfall intensity) using equations 3.5 and 3.6 – see examples in Table 3.1.

3.4.1.2 Occult wet deposition (fog or hill cloud) ('conservative' value only)

- Set the droplet number concentration, N_c:
  - for radiation fog, take $N_c = 2\ 10^8\ m^{-3}$,
  - else if hill cloud, take $N_c = 3\ 10^8\ m^{-3}$.
- Obtain the particle number concentration, N_p (from release parameters, dispersion modelling etc).

- Calculate maximum fraction of particles that could be activated, F:
  if $N_p < N_c$, $F = 1$,
  else use equation 3.8.
- Calculate effective deposition velocity using equation 3.9.

3.4.1.3 Seeder-feeder mechanism ('conservative' estimate only)

- Obtain F as described above for occult wet deposition (hill cloud only).
- Calculate the value of the maximum fog/cloud scavenging coefficient, Λ_c using equation 3.12, calculating Λ_{dr} as for below-cloud scavenging with $E = 1$.
- Obtain f, the (weighted) fraction of the polluted layer occupied by hill cloud: if no information available take as 1 (but this is an extra stage of potential overestimation).
- Calculate the effective scavenging coefficient, Λ_{eff}, using equation 3.10.

3.4.2 Iodine

3.4.2.1 Below cloud

'Thin' plume

- *Elemental iodine* – 'best judgement' and 'conservative' values the same, obtained from equation 3.19.
- *Methyl iodide* – No 'best judgement' value; for 'conservative' value, take value for elemental iodine.

Uniform concentration

- Obtain partition coefficient, p:
  if *elemental iodine*
    if 'best judgement' value required, set $p = 10^4$,
    else if 'conservative' value required, set $p = 10^5$.
  else if *methyl iodide*
    if 'best judgement value required, set $p = 7$,
    else if 'conservative' value required, set $p = 10^4$ (ie assume the gas is elemental iodine).
- Calculate wet deposition velocity from equation 3.21.
- If required, go on to calculate scavenging coefficient:
  obtain b, the depth of the polluted layer, then use equation 3.22.

3.4.2.2 In cloud

- *Elemental iodine* – take as the same as below-cloud (uniform concentration) value for elemental iodine.
- *Methyl iodide* – no 'best judgement' value; 'conservative' value = $3\ 10^{-6}\ s^{-1}$.

3.4.2.3 Occult wet deposition (fog and hill cloud)

- No enhancement in deposition velocity for either gaseous species except through the effect of wetting of vegetation (elemental iodine).

3.4.2.4 Seeder-feeder mechanism

- No enhancement in scavenging coefficient for either gaseous species.

4 References

Allen A G, Harrison R M and Nicholson K W (1991). Dry deposition of fine aerosol to a short grass surface. *Atmos Environ,* **25A**, 2671–6.

Belot Y, Baillie A and Delmas L (1976). Modele numerique de dipsersion des pollutants atmospheriques en presence de couverts vegetaux. *Atmos Environ,* **10**, 89–98.

Bonka H (1989). Measured radioecological parameters after the Chernobyl accident. IN *The Radioecology of Natural and Artificial Surfaces* (W Feldt, Ed). TUEV Rheinland.

Brusaert W (1982). *Evaporation into the Atmosphere*. Kluwer Academic Publishers.

Caput C, Camus H, Gauthier D and Belot Y (1993). Etude expérimentale du lavage de l'iode pa la pluie. *Radioprotection,* **28**, 15–22.

Carrruthers D J and Choularton T W (1986). The microstructure of hill cap clouds. *Quart J R Met Soc*, **112**, 113–29.

Chamberlain A C (1960). Aspects of the deposition of radioactive and other gases and particles. *Int J Air Pollut,* **3**, 63–8.

Chamberlain A C (1967). Transport of Lycopodium spores and other small particles to rough surfaces. *Proc Roy Soc Lond*, **A296**, 45–70.

Chamberlain A C (1991). *Radioactive Aerosols*. Cambridge, University Press.

Chamberlain A C and Chadwick R C (1966). Transport of iodine from atmosphere to ground. *Tellus,* **17**, 226–39.

Chamberlain A C, Garland J A and Wells A C (1984). Transport of gases and particles to surfaces with widely spaced roughness elements. *Bounday-Layer Meteorol*, **29**, 343-60.

Clark M J and Smith F B (1988). Wet and dry deposition of Chernobyl releases. *Nature,* **322**,245–9.

Clarke R H (1979). The first report of a Working Group on Atmospheric Dispersion: a model for short and medium range dispersion of radionuclides released to the atmosphere. Chilton, NRPB-R91.

Clough W S (1975). The deposition of particles on moss and grass surfaces. *Atmos Environ,* **9**, 1113–19.

Dana M T (1970). Scavenging of soluble dye particles by rain. IN *Precipitation Scavenging 1970:* Proceedings of a Symposium held in Richland, Washington.

Dana M T (1979). Overview of wet deposition and scavenging. IN Proceedings Symposium on Potential Environmental and Health Effects of Atmospheric Sulphur Deposition, Gatlinburg, USA.

Davenport A G (1982). The interaction of wind and structures. IN *Engineering Meteorology* (E Plate, Ed). Elsevier Scientific Publishing Co.

Davenport H M and Peters L K (1978). Field studies of atmospheric particulate concentration changes during precipitation. *Atmos Environ,* **12**, 997–1008.

Dollard G J and Unsworth M H (1983). Field measurements of turbulent fluxes of wind-driven fog drops to a grass surface. *Atmos Environ*, **17**, 775–80.

Engelmann R J and Perkins R W (1966). Snow and rain washout coefficients for process plant radioiodine vapour. *Nature*, **211**, 61–2.

Engelmann R J *et al* (1966). Washout coefficients for selected particles and gases. Battelle Northwest Laboratories, BNWL-SA-657.

Fernandez De la Mora J and Friedlander S K (1982). Aersol and gas deposition to fully rough surfaces: filtration model for blade-shaped elements. *Int J Heat Mass Transfer,* **25**, 1725–35.

Garratt J R (1992). *The Atmospheric Boundary Layer.* Cambridge, University Press.

Graedel T E and Franey J P (1974). Field measurements of submicron aerosol washout by rain. IN *Precipitation Scavenging 1974*. Proceedings of a Symposium held at Champagne, Illinois.

Hales J M (1982). Mechanistic analysis of precipitation using a one-dimensional time-variant model. *Atmos Environ,* **16**, 1775–83.

Hanna S R and Chang J C (1992). Boundary layer parameterisations for applied dispersion modelling over urban areas. B*oundary-Layer Meteorol,* **58,** 229–59.

Harper F T *et al* (1994). Probablistic accident consequence uncertainty analysis. Washington DC, US Nuclear Regulatory Commission (European Commission), NUREG/CR-6244 (EUR 15855EN, SAND94-1453).

Heinemann K and Vogt K J (1980). Mearuements of the deposition of iodine onto vegetation and of the biological half-life of iodine on vegetation and of the biological half-life of iodine on vegetation. *Health Phys,* **39**, 463-74.

Hicks B B and Williams R M (1979). Transport and deposition of particles to water surfaces. IN Proceeding Symposium on the Potential Environmental and Health Effects of Atmospheric Sulphur Deposition, Gatlinburg, USA.

Horn H G, Bonka H and Maqua M (1987). Measured particle bound activity size distribution, deposition-velocity and activity concentration in rainwater after the Chernobyl accident. J Aerosol Sci, **18**, 681–4.

IAEA (1994). Modelling the deposition of airborne radionuclides into the urban environment. Vienna, International Atomic Energy Agency, IAEA-TECDOC-760.

Jones J A (1993). The fifth report of a Working Group on Atmospheric Dispersion: models to allow for the effects of coastal sites, plume rise and buildings on dispersion of radionuclides and guidance on the value of deposition velocity and washout coefficient. Chilton, NRPB-R157.

Kinnersley R P, Goddard A J H, Minski M J and Shaw G (1996). Deposition and canopy interception of submicron particles and caesium-bearing simulated rain. London, Imperial College Report to MAFF (Reference IB005).

Livens F R, Fowler D and Horrill A D (1992). Wet and dry deposition of ^{131}I, ^{134}Cs and ^{137}Cs at an upland site in northern England. *J Environ Radioact,***16**, 243–54.

Maeck W J *et al* (1984). Laboratory measurements of parameters affecting wet deposition of methyl iodide. Westinghouse Idaho Nuclear Co, Idaho Falls, USA, NUREG/CR-4014.

Maqua M, Bonka H and Horn H-G (1987). Deposition velocity and washout coefficient of radionuclides bound to aerosol particles and elemental radioiodine. *Radiat Prot Dosim*, **21**, 43–9.

McMahon T A and Denison P J (1979). Empirical atmospheric deposition parameters – a survey. *Atmos Enviro,* **13**, 571–85.

Möller U and Schumann G (1970). Mechanisms of transport from the atmosphere to the earth's surface. *J Geophys Res,* **75***,* 3013–19.

Nicholson K W (1987). Deposition of caesium to surfaces of buildings. *Radiat Prot Dosim,* **21,** 37–42.

Nicholson K W (1988). The dry deposition of small particles: a review of experimental measurements. *Atmos Environ* **22**, 2651–66.

Nicholson K W and Davies T D (1987). Field measurements of the dry deposition of particulate sulphate. *Atmos Environ,* **21**, 1561–71.

Nicholson K W, Branson J R and Geiss P (1991). Field measurements of the below-cloud scavenging of particulate material. *Atmos Environ*, **25A**, 771–7.

Nicholson K W *et al* (1993). The dry deposition of particulate materials in an urban environment. Harwell, AEA Technology, AEA-EE-0424.

Radke L F, Hindmann E E and Hobbs P V (1974). A case study of plume scavenging by a rain shower. IN *Precipitation Scavenging 1974*. Proceedings of a Symposium held at Champagne, Illinois.

Rasmussen R A, Khalil M A K and Hoyt S D (1983). Trace gases in snow and rain. IN *Precipitation Scavenging, Dry Deposition and Resuspension* (Pruppacher *et al*, Ed). Elsevier Science Publishing Co.

Roed J (1987). Dry deposition in rural and urban areas in Denmark. *Radiat Prot Dosim*, **21**, 33–6.

Roed J and Jacobs P (1990). Deposition on urban surfaces and subsequent weathering. IN Proceedings Seminar on Methods and Codes for Assessing the Off-Site Consequences of Nuclear Accidents. Luxembourg, European Commission, EUR 13013/1EN.

Schack C J Jr, Pratsinis S E and Friedlander S K (1985). A general correlation for deposition of suspended particles from turbulent gases to completely rough surfaces. *Atmos Environ* **19**, 953–60.

Sehmel G A (1980). Particle and gas dry deposition: a review. *Atmos Environ,* **14**, 983–1011.

Sehmel G A and Hodgson W H (1978). Improved predictive dry deposition velocity correlation. IN Pacific Northwest Laboratory Annual Report for 1977, Part 3. Atmospheric Sciences.

Sehmel G A and Sutter S L (1974). Particle deposition rates on a water surface as a function of particle diameter and air flow. *J Rechs Atmos*, **III**, 911–8.

Sievering H (1984). Small-particle dry deposition on natural waters' how large the uncertainty? *Atmos Environ,* **18**, 2271–2.

Slinn W G N (1976). Dry deposition and resuspension of aerosol particles – a new look at some old problems. IN Proceedings Atmosphere–Surface Exchange of Particulate and Gaseous Pollutants – 1974 Symposium. Richland VA, NTIS CONF-740921.

Slinn W G N (1977). Some approximations for the wet and dry removal of particles and gases from the atmosphere. *Water, Air Soil Pollut,* **7**, 513–43.

Slinn W G N (1978). Parameterizations for resuspensions, and for wet and dry deposition of particles and gases for use in radiation dose calculations.

Slinn W G N (1982). Predictions for particle deposition to vegetative canopies. *Atmos Environ,* **16**, 1785–94.

Underwood B Y (1984). Dry deposition. IN Review of specific effects in atmospheric dispersion calculations. Luxembourg, European Commission. EUR 8953EN.

underwood b y (1984). wet deposition. in review of Specific Effects in Atmospheric Dispersion Calculations. Luxembourg, European Commission, EUR 8935EN.

Underwood B Y (1988). Deposition in foggy conditions. Risley, UK/AEA, SRD R487 (now AEA Technology).

van Ulden A P and Holtslag A A M (1985). Estimation of atmospheric boundary-layer parameters for diffusion applications. *J. Clim Appl Meteorol*, **24**, 1196–207.

Wershofen H and Aumann D C (1989). Dry deposition of iodine-29 onto grass as obtained by field measurements in the environment of a nuclear fuel reprocessing plant. *J Radioanal Nucl Chem Lett,* **137**, 373–9.

APPENDIX

Notation

b	Depth of the polluted layer, m
B	Sub-layer Stanton number (re-defined as R_b)
c_p	Specific heat of air at constant pressure, J kg^{-1} K^{-1}
d	Zero-plane displacement, m
D	Aerodynamic diameter, μm
D_1	Aerodynamic diameter at the end of the submicron range, μm
E	Collection efficiency of raindrop for particle
f	(Weighted) fraction of polluted layer occupied by hill cloud
$f( )$	Function appearing in integration of similarity profile
F	Fraction of particles in fog or hill cloud that are activated
g	Acceleration due to gravity, m s^{-2}
h	Canopy height, m
H	Relative humidity, expressed as fraction or 0.1, whichever is larger
H_0	Heat flux at the surface, W m^{-2}
J	Rainfall intensity, m s^{-1}
J_0	Rainfall intensity of 1 mm h^{-1}, m s^{-1}
k	von Karman's constant
$K(z)$	Eddy diffusivity at height z, m^2 s^{-1}
L	Monin-Obukhov length, m
L_w	Liquid water content (as a volume fraction)
N_c	Number of droplets per unit volume in fog or hill cloud, m^{-3}
N_p	Number of particles per unit volume, m^{-3}
$N(R_d)$	Raindrop number density per unit radius interval, m^{-4}
p	Partition coefficient at the air/water interface
r_a	Aerodynamic resistance, s m^{-1}
r_{al}	Local value of aerodynamic resistance in urban environment, s m^{-1}
r_b	Sub-layer resistance, s m^{-1}
r_{bl}	Local sub-layer resistance in urban environment, s m^{-1}
r_s	Surface resistance, s m^{-1}
r_{sl}	Local value of surface resistance in urban environment, s m^{-1}
R_a	Normalised aerodynamic resistance ($u_* r_a$)
R_b	Normalised sub-layer resistance ($u_* r_b$)
R_d	Drop radius, m
Re	Drop Reynolds Number (= $2v_t R_d / \nu$)
Re_*	Roughness Reynolds Number (= $u_* z_0 / \nu$)
R_m	Volume-mean raindrop radius, m
T	Temperature, K
$u(z)$	Windspeed at height z, m s^{-1}
u_*	Friction velocity, m s^{-1}
v_d	Deposition velocity, m s^{-1}

v_{dl} Local deposition velocity in urban environment, m s^{-1}

v_{de} Effective deposition velocity in fog or hill cloud, m s^{-1}

v_{do} Deposition velocity of the droplets in fog or hill cloud, m s^{-1}

v'_d Deposition velocity in the absence of settling, m s^{-1}

v'_{dl} Local deposition velocity in the absence of settling, m s^{-1}

v_g Gas-phase transfer velocity to water surface, m s^{-1}

v_L Liquid-phase transfer velocity, m s^{-1}

v_s Gravitational settling velocity, m s^{-1}

v_t Terminal velocity of falling raindrops, m s^{-1}

v_w Wet deposition velocity, m s^{-1}

V_d Normalised deposition velocity (v_d/u_*)

V'_d Normalised form of v'_d ($=v'_d/u_*$)

w Washout ratio

w_0 Washout ratio using the ground-level concentration

W Wet deposition flux, kg m^{-2} s^{-1}

W_d Herbage density (dry weight), kg m^{-2}

z Height from the surface, m

z_{ref} Reference height for deposition velocity, m

z_0 Aerodynamic roughness length, m

$\chi(z)$ Airborne concentration of pollutant at height z, kg m^{-3}

Δ Diffusivity of gas in air, m^2 s^{-1}

φ_g Similarity function for turbulent diffusion of matter

φ_m Similarity function for turbulent diffusion of momentum

$\Lambda(D)$ Scavenging coefficient for particles of diameter D, s^{-1}

Λ_c Scavenging coefficient applicable within the hill cloud, s^{-1}

Λ_{dr} Scavenging coefficient for the droplets in hill cloud, s^{-1}

Λ_{eff} Effective scavenging coefficient (layer is part hill cloud), s^{-1}

ν Kinematic viscosity (molecular diffusivity of momentum), m^2 s^{-1}

ρ Air density, kg m^{-3}

ANNEX B

Review of Flow and Dispersion in the Vicinity of Groups of Buildings

ALAN ROBINS, UNIVERSITY OF SURREY, AND ROBERT MACDONALD, UMIST & UNIVERSITY OF WATERLOO (CANADA)

Contents

Abstract **54**

1 Introduction **55**

2 Flow and dispersion – the physical processes involved **55**
- 2.1 Single buildings 55
- 2.2 Groups of buildings 59
- 2.3 Porous obstacles 62
- 2.4 Internal boundary layers 63
- 2.5 Extensive array of buildings 64
- 2.6 Stages of plume development over arrays of obstacles 65
  - 2.6.1 Dispersion in the first regime: short range around single or multiple obstacles embedded in an array 66
  - 2.6.2 Dispersion in the second regime: intermediate range in arrays of obstacles 68
  - 2.6.3 Dispersion in the third regime: long-range neighbourhood and urban scale modelling 68

3 Current practices in dispersion modelling **69**
- 3.1 Single buildings 69
  - 3.1.1 Virtual source and related models 69
  - 3.1.2 NRPB-R91 model 70
  - 3.1.3 ISC model 70
  - 3.1.4 ADMS modelling 71
  - 3.1.5 PRIME modelling 76
- 3.2 Groups of buildings 77
  - 3.2.1 Virtual source modelling 77
  - 3.2.2 ISC modelling 77
  - 3.2.3 ADMS modelling 77
- 3.3 Urban dispersion modelling 78
  - 3.3.1 Gaussian models 78
  - 3.3.2 Street canyon and related models 79
  - 3.3.3 Hybrid models 80

4 Role of more complex approaches **82**
- 4.1 Physical modelling 83
- 4.2 Field experiments 86
- 4.3 Computational modelling 86
  - 4.3.1 Transport equation modelling 87
- 4.4 Model evaluation 89
- 4.5 Model development 91

5 Results of recent experimental work **92**
- 5.1 Emissions above building arrays 92
- 5.2 Porous obstacles 100

5.3 Recent experimental work on dispersion within groups of obstacles 106
5.3.1 Research at the University of Cambridge 106
5.3.2 Research at the University of Karlsruhe 108
5.3.3 Physical modelling studies at BRE and UMIST 108
5.3.4 Other recent experimental studies 118
5.4 Aerodynamics of arrays of obstacles 121

6 Implications of recent experimental work 123
6.1 Extensions within the ADMS approach to treat building groups 123
6.2 Considerations for modelling dispersion in large groups of obstacles 123
6.3 Characterisation of the bulk flow over urban roughness and the effect of limited fetch 124
6.4 Modelling the plume advection velocity in urban dispersion 126
6.5 Plume partitioning and near-field dispersion in large obstacle arrays 128
6.6 Averaging time effects in urban dispersion 128
6.7 Effect of wake residence times on dispersion 129

7 Limitations of current understanding 130
7.1 Array dispersion modelling 130
7.2 Some modelling issues 131
7.3 Some validation issues 132
7.4 Simple models – are they possible? 132

8 Modelling – prospects and limitations 133
8.1 General topic areas 134
Research topics 134
8.2 Passive emissions and near-neutral boundary layers 135
8.2.1 Near-field dispersion (1st and 2nd obstacles) for sources within the canopy 135
8.2.2 Intermediate-field dispersion (2nd to 4th or 5th obstacle) for sources within the canopy 136
8.2.3 Far-field dispersion (beyond 5th or 6th obstacle) for sources within the canopy 137
8.2.4 Downstream dispersion (beyond all obstacles) for sources within the canopy 138
8.2.5 Elevated plumes above large and medium sized arrays 138
8.2.6 Plumes reaching surface at long-range; size much larger than obstacles 139
8.2.7 Plume reaching surface at short-range; size similar to obstacles 140
8.2.8 Dispersion within porous arrays 141
8.2.9 Dispersion downstream from porous arrays 142
8.2.10 Elevated plumes downstream from small regular and irregular arrays 143
8.3 Dispersion and obstacle arrays; atmospheric stability effects 144
8.4 Dispersion and obstacle arrays; emission effects 145

9 References 146

APPENDIX Notation 155

Abstract

This review concerns atmospheric flow and dispersion processes in the vicinity of groups of buildings and structures. In practice, this topic covers both large and small industrial sites and built-up areas. The physical processes involved are first described and then current dispersion modelling methods outlined The role of more complex physical and numerical approaches is then discussed and recent wind tunnel and full scale experimental research and its consequences are outlined. The prospects for model development in a number of sub-topics are then summarised, following a discussion of the limitations to current understanding. A comprehensive bibliography is included.

1 Introduction

Dispersion in the vicinity of groups of buildings is an issue affecting health and safety and air quality concerns at and near industrial sites and in built-up areas. The industrial context generally involves the consequences of routine discharges from stacks and vents and accidental discharges from stacks, vents, safety relief systems, failed plant items and buildings, and evaporating pools. Such emissions may be positively or negatively buoyant and may contain significant momentum. Applications in built-up areas frequently concern the behaviour of emissions from vehicles, but the question of fixed low and high level sources is also important. Research across all these areas has much in common, since it basically concerns the interaction of the obstacles (buildings, plant items, etc) with the external boundary layer flow, the flow field generated within the obstacle group (ie below roof level) and the consequent effects on dispersion behaviour.

Satisfactory prediction of dispersion behaviour implies that concentrations and doses within and downwind from a site can be adequately determined for releases at any location on the site. In this context, 'adequately' means sufficient for the purposes of assessing and protecting air quality, health and safety. The discharge itself may be steady or transient and possess significant momentum and buoyancy. Clearly, we are some way from the solution of all such problems by the use of conventional dispersion modelling techniques or even through the application of complex techniques such as wind tunnel or computational fluid dynamics simulations. However, considerable progress has been made in understanding many aspects of the subject.

In this review we concentrate on basic flow and dispersion processes, making only passing reference to the associated topics involving emission momentum and buoyancy and traffic induced flow and dispersion. The bulk of the detailed research has concentrated on single large buildings or extensive arrays of identical buildings, with releases at or below roof level, and this is reflected in the review. The dispersion of stack emissions over and downwind of regular and irregular arrays, a topic of common industrial concern (though much less studied), is also treated.

The review is organised in the following manner: Section 2 treats the physical processes involved; Section 3, current modelling practices; Section 4, the results of recent experimental studies; Section 5, the implications of this work; Section 6, the role of more complex modelling methods; Section 7, the limits to our understanding; Section 8, the prospects for model development and fruitful further research.

2 Flow and dispersion – the physical processes involved

2.1 Single buildings

There have been a number of informative studies and reviews of flow and dispersion around simple surface mounted obstacles in neutrally stable boundary layers, (see, for example, Hunt *et al*, 1978; Robins and Fackrell, 1980; Meroney, 1982; Hosker, 1984; Foster and Robins, 1985). These have shown how the basic flow features depend on the obstacle shape and orientation, and the characteristics of the approach flow, and how dispersion processes are subsequently affected. Figure 2.1 illustrates typical flow fields around cuboid shaped obstacles. They are very complex, though the relative importance of the main features varies according to obstacle shape and orientation.

The approach flow rolls-up ahead of the obstacle in forming a horseshoe vortex system. This may be particularly strong if the approach flow is steady, with low turbulence intensity, and the mean shear is large over the height of the building. The flow separates over the roof and may reattach if conditions are favourable; ie the approach flow is sufficiently turbulent and/or the roof long enough. Behind the building is a complex and very unsteady recirculating flow region. This

does not have a closed boundary and material passes in and out both by turbulent and mean flow transport. The size of the recirculation region depends on building geometry and orientation, and approach flow conditions. For a cuboid, the extent downwind of the rear face is between one and three obstacle heights; it increases for wider buildings. An arch vortex forms just downstream of the side walls and is often clearly visualised by swirling leaves and litter lifted from behind buildings.

A pair of roof vortices is generated by the roll-up of the flow up the forward facing walls when the approach flow is not normal to the front face. The vortices trail off downstream at or near roof height. In general, one is stronger than the other, but in strictly symmetrical orientations (eg a cube at 45º to the wind) they are of equal strength. The trailing vortices may persist as important flow features far downwind if the approach flow is relatively steady and turbulence levels low.

The main wake is a simple 'momentum deficit wake' if any trailing vortex systems generated in the flow over the obstacle are weak. Such wakes are characterised by a region of velocity deficit and turbulent excess. Wake decay, typically over a fetch of 10 to 30 building

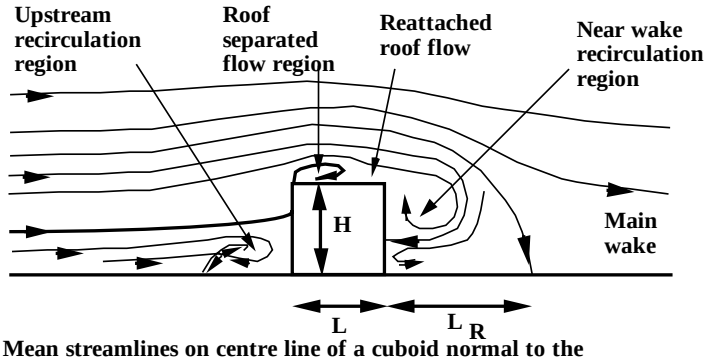

(a) Mean streamlines on centre line of a cuboid normal to the approach flow

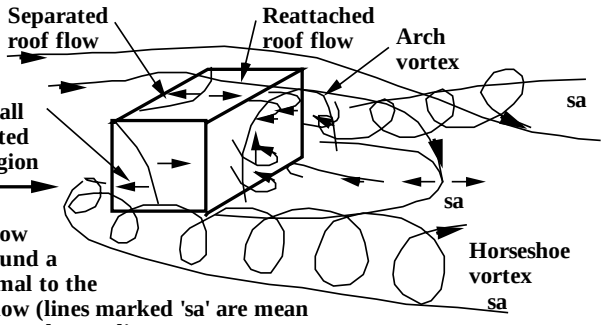

(b) Mean flow pattern around a cuboid normal to the approach flow (lines marked 'sa' are mean separation/attachment lines

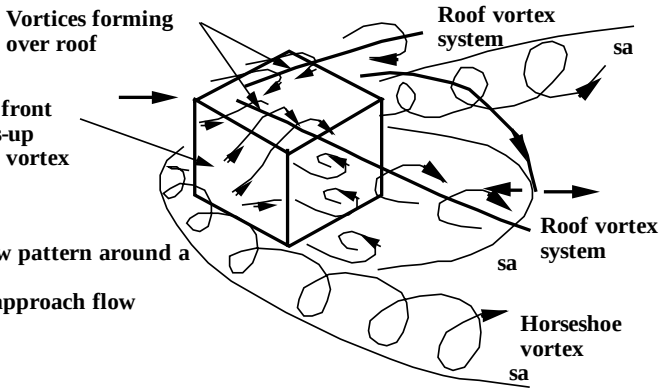

(c) Mean flow pattern around a cuboid at incidence to approach flow

FIGURE 2.1 Main features of the flow around cuboids at 0º and 45º to the approach flow in a deep boundary layer

heights, creates secondary flows outside of the wake itself which provide a net flow into the wake. These interact with the secondary flows generated by the horseshoe vortex system. A 'vortex wake' develops when stream-wise, trailing vortex systems play a significant role, and resulting secondary flows may continue beyond the position where a momentum deficit wake would have decayed to insignificance. In some parts of the flow field, the persistent secondary flows transport external fluid towards the surface and, as a result, produce regions of local mean velocity excess. Both momentum deficit and vortex wake components are found in many circumstances. Indeed, a most complex combination may exist downwind of a group of buildings due to the interactions between individual wake components.

The flow over a flat roof may or may not reattach, depending on geometry and ambient turbulence levels. The boundaries of the roof flow regimes have been derived from neutral flow wind tunnel studies (Castro and Dianat, 1983; Dianat and Castro, 1984; Fackrell, 1984a). At the boundary between reattached and separated flow, reduced turbulence makes separated flow more likely. Increasing stability may therefore mark the onset of fully separated flow for some building shapes, although even greater stability may cause attachment to occur again as vertical motion becomes affected. The vertical extent of the recirculation region is greatest for fully separated flow. These changes in roof flow conditions will influence elevated emissions through streamline displacement and entrainment processes.

Pollutant dispersion near buildings reflects the complexity of the flow fields. As an illustration, Figures 2.2(a)–(e) show typical dispersion patterns for ground-level emissions upwind, downwind and to the side of a simple block-shaped obstacle. Plume shape and position and, by inference, dilutions are clearly strongly dependent on source position and wind direction. The situation becomes even more complicated if the building shape is more complex, or additional buildings are involved. Small features close to the source may play an important role; Figure 2.2(k) illustrates how a small building to the left of the source may force most of the emitted material to pass to one side of the main building, thus breaking the symmetry that would otherwise exist (Fackrell and Robins, 1982). The implication is that the effects of source position and wind direction are likely to dominate other influences – in the case of flow stability, at least until the mean flow around the building changes significantly.

Figures 2.2(f)–(j) show that a wide range of dispersion patterns also applies to elevated emissions, depending on source location, wind direction and flow conditions. Of particular importance can be the strong plume deflection due to roof vortex systems, which occurs for 'diagonal winds'. Material entrained from an elevated emission into the recirculation region is re-emitted from that region as a diffuse, ground-based plume. The concentration field downwind of the near wake can be pictured in terms of two components. One is the diffuse, ground-based plume and the other the remains of the elevated plume, at a reduced height because of streamline deflection and of reduced strength because part of the original emission is entrained into the recirculation region. In contrast to the case of ground-level releases, ambient conditions have a direct bearing on the dispersion of elevated emissions, largely determining the rate of plume spread and dilution outside of the wake.

Wind tunnel studies of the unsteadiness of dispersion from ground-level sources near buildings clearly illustrate the unsteadiness of the wake flow (Lee *et al*, 1991). A single realisation of the flow reveals a very sinuous plume shape and a patchy concentration distribution. A smooth distribution only emerges after averaging over a large number of realisations, corresponding to the sampling of several hundred, perhaps a thousand, large eddies of the flow. These conclusions apply to dispersion in a turbulent boundary layer with steady mean conditions. However, some meteorological conditions are not sufficiently steady for smooth dispersion patterns to emerge from

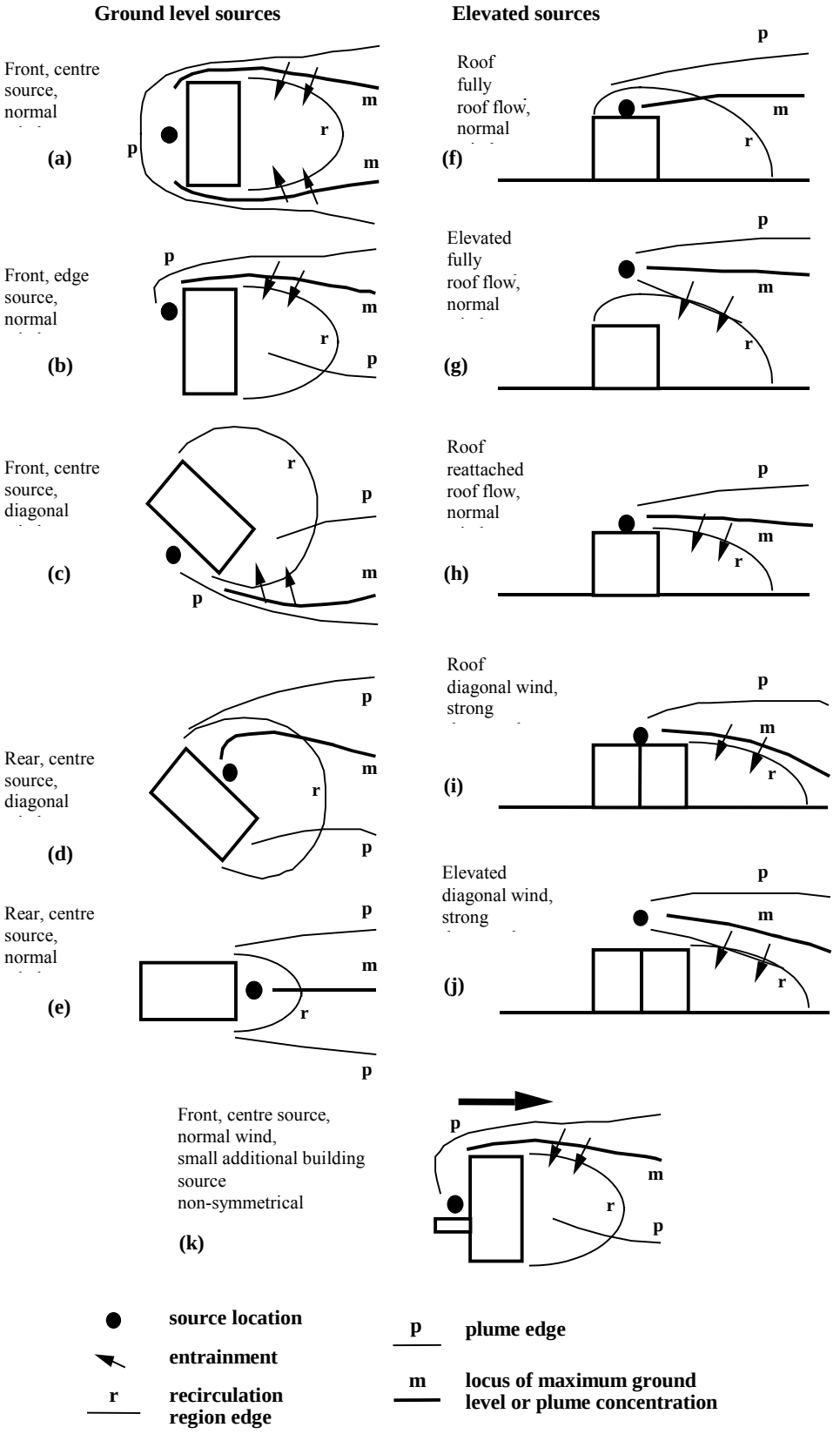

FIGURE 2.2 Dispersion patterns for passive emissions above and to the side of a cuboid, showing regions of entrainment

a single experiment or observation of an hour or two in duration. For example, the large eddy time scale of a convective boundary layer may be a few hundred seconds, so that only 20 or so are sampled in an hour-long period. Clearly, irregular and somewhat patchy concentration fields can be anticipated in conditions of this sort.

2.2 Groups of buildings

The features apparent in the flow around a single, isolated building are also present for a group of buildings, although their relative and absolute significance is generally affected by interactions within the group. There are some obvious limiting cases for a small group as the spacing between members becomes very large or very small. In the first case we simply have a set of isolated buildings and the cumulative effects of the group can be treated by linear addition of the effects due to each in turn. This is most simple when the spacing is so large, typically greater than 10–20 building heights, that each effectively experiences undisturbed boundary layer conditions. For smaller separations, the flow conditions at downwind buildings are perturbed by those upstream, but to a sufficiently small extent that linear superposition remains acceptable. Generally, this is a useful approximation for separations down to around $5H$, where H is the obstacle height. These limiting separations actually depend on building geometry, orientation and approach flow conditions and the values quoted are intended to be no more than typical for cuboid shapes and neutral flow. The limits are larger for buildings of extended lateral dimensions or in stable flow conditions, and smaller in unstable conditions.

Figure 2.3 illustrates the three regimes frequently identified in discussion of flow in and above the urban canopy; it is based on classifications described by Hosker (1985), Hosker and Pendergrass (1987), Hussain and Lee (1980) and Oke (1987). The figure applies to relatively regular arrays of block shaped obstacles more or less normal to the wind direction and the

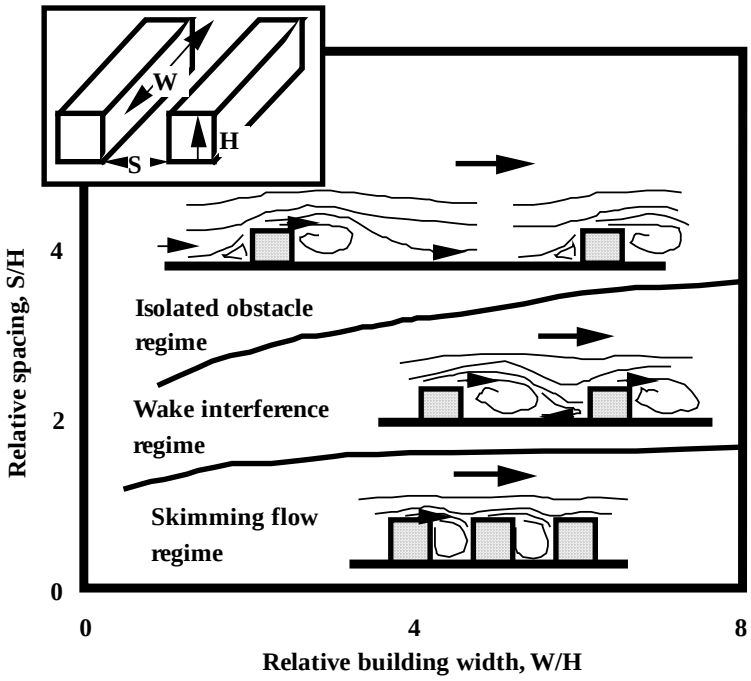

FIGURE 2.3 Regimes of flow over an obstacle array and the main flow features associated with each

boundaries between the regions respond to variations from this state (see, for example, Johnson and Hunter, 1995). The external flow is bodily displaced by the building height in the skimming regime, where the space between buildings is occupied by a simple recirculating motion. This becomes a particularly important feature of the overall flow once the building width, W, is large enough (say, $W/H > 4$). Of course, mean flow through the array still occurs along longitudinal channels. Exchange between the recirculation region and the external flow occurs through turbulent diffusion, with some external flow penetrating into the region at its downstream end. The apparent aerodynamic roughness of the array is relatively low and decreases as the spacing, S, between buildings decreases. At the other extreme lies the isolated obstacle regime, where the near-wake flows associated with individual buildings are only weakly perturbed by surrounding buildings. The flow becomes a superposition of many independent building wake flows as the separation is increased. Again, the apparent aerodynamic roughness of the array is relatively low, but now decreases as the spacing, S, between buildings increases. The aerodynamic roughness is greatest in the wake interference regime, which is transitional between the skimming and isolated obstacle regimes. A variety of complex and rather unsteady flows can now occupy the spaces between buildings. There are regions of recirculation and often regions where the external flow penetrates to the ground. The displacement height (ie the effective zero velocity height in the log-law wind profile of the external flow) tends to zero as the relative spacing, S/H, becomes large, and increases monotonically as the spacing decreases, tending to H as S/H tends to zero. Many industrial and urban building configurations lie in the skimming regime which, when the buildings are sufficiently extensive across the wind, gives rise to so-called urban street canyon flows, discussed further in Section 2.6.

Figure 2.4 illustrates some of the features of the wind field above and within a three-dimensional array. Regions of recirculation are shown as well as regions between buildings which are relatively well ventilated. The flow can be divided into three layers: the canopy layer (below typical roof level), the external boundary layer (where surface detail is unimportant), and a sub-layer between them. Flow features created by individual buildings cannot be distinguished in the external layer and the surface can be represented in terms of a roughness length, z_o, and a zero plane displacement, d. Since the perturbations due to an isolated building die out at a height of about three building heights, we can expect the outer layer to commence at a height between $d + 3H$ and $d + 3(H - d)$, where H is the typical building height. The mean flow in the sub-layer, whilst free of

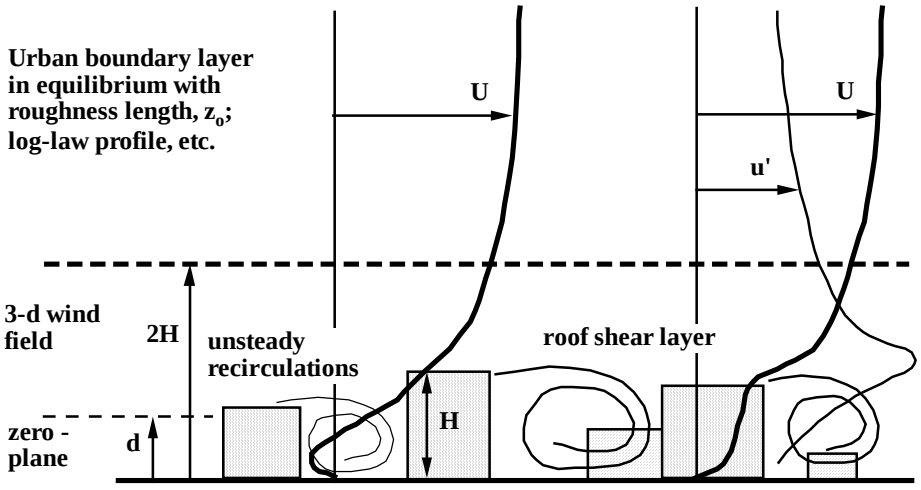

FIGURE 2.4 General features of the wind and turbulence fields over an urban area showing regions of recirculation and ventilation

recirculation, is significantly three-dimensional. Peak turbulence levels also occur in the layer, associated with strong mean shear just above roof level.

A variety of flow conditions will generally exist within irregular arrays (irregular in terms of shape, size and orientation) depending on location within the array and wind direction (see, for example, Hosker and Pendergrass, 1987). Regions where the flow is channelled, diffused, deflected, displaced, accelerated, stagnated, or recirculated may all be observed. Dispersion conditions will be variable to an equivalent degree. Poorly ventilated regions, such as tightly enclosed courtyards, are characterised by weak mixing with the external flow and hence long residence time for locally emitted pollutants. However, buoyant discharges may rise relatively rapidly because of the quiescent ambient state. In other sections of the array ventilation may be very efficient, driven by mean flow advection as well as turbulent diffusion. The mechanisms involved include direct penetration of the external wind into open areas and streets aligned with the wind and upwards mean flow in the wakes of the larger obstacles within the array. Figure 2.5 illustrates flow at a street intersection with a tall building on the upwind side of one of the streets. The additional secondary flows created by the tall building both mix external air into the canopy and draw air from it, in particular up the building's rear face. Significant exchanges take place between the intersecting streets. As shown, the wind is somewhat off-normal to the cross-street and this modifies the basic street canyon vortex, changing it into a helical vortex. Predictions of dispersion in these circumstances cannot account for this level of detail and some drastic simplifications are normally applied, such as treating a large building as if it were in isolation or modelling the whole group as an equivalent, homogeneous array.

The characteristics of the wake downwind of an array depend on the division of the approach flow between the so-called bleed flow through the array and the displaced flow over and around it. Only when the bleed flow becomes very weak indeed can the array truly be treated as a single, solid, bounding body. Otherwise, the wake begins as a very complex affair, comprising regions

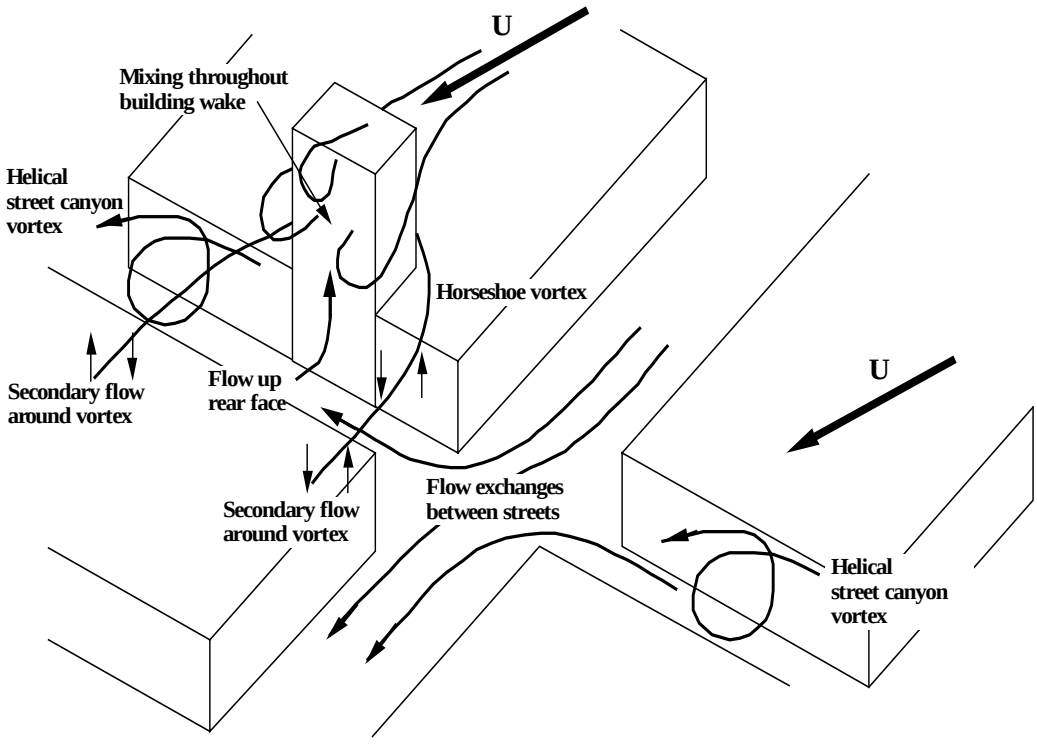

FIGURE 2.5 Flow field at a street intersection with a tall building illustrating exchanges between the streets and additional mixing processes due to the large building

of recirculation directly behind obstacles and bleed flow where there are spaces. These features then merge until finally, far enough downwind, a simple wake is formed, similar to that behind a single obstacle. The effects of bleed flow on wake structure are discussed in the following section.

2.3 Porous obstacles

The wakes of two-dimensional obstacles, such as fences and wind breaks, have been subject to extensive study (see, for example, Plate, 1971; Raine and Stevenson, 1977; Perera, 1981) and the basic features of the perturbed flow are reasonably well understood. However, investigation of the equivalent three-dimensional problem was, until recently, quite limited. Work by Speirs (1998) has rectified much of this deficiency and shown that the main flow features are common to both the two- and three-dimensional cases (see also Robins *et al*, 1999). A number of flow regimes can be identified, depending on the porosity of the obstacle (defined as the ratio of the open area to the total area). The important factor is the ratio of the 'bleed flow' through the porous obstacle and the 'displaced flow' over and, in the three-dimensional case, around it. Recirculation immediately behind a solid body is eliminated by sufficient bleed flow, although recovery in the near-wake and entrainment into its bounding shear layers may lead to a recirculation region forming downwind. This region shrinks and eventually vanishes as the porosity and associated bleed flow are increased. The shear at the edge of the near-wake is strong when the bleed flow is weak but gradually lessens as the bleed flow increases. Streamline deflections follow these patterns, since weak bleed flow implies strong displaced flow and vice versa. Four flow regimes, illustrated in Figure 2.6, can be summarised as follows:

(a) solid plate (zero porosity) case – recirculating flow 'attached' to the obstacle and bounded by zones of strong shear,

(b) low porosity case – recirculating flow 'detached' from the obstacle and bounded by zones of strong shear,

(c) intermediate porosity case – no mean flow recirculation, shelter in the near wake, bleed flow deceleration, a near-wake bounded by zones of strong shear which converge downstream to form a deep and vigorous turbulent mixing region,

(d) high porosity case – persistent mean flow shelter for cases of low blockage, weak shear layers and low levels of wake turbulence.

The strength of the wake, as exemplified by the mean velocity deficit, steadily weakens as the porosity increases. The vigorous mixing associated with recirculation regions in regimes 1 and 2 is also a feature of regime 3. This subsequently decreases in importance as the porosity increases.

The changing character of the wake flows has obvious effects on dispersion characteristics. Regions of high turbulence intensity are associated with rapid mixing and plume growth, especially when combined with recirculation. Variations in mean longitudinal velocity imply secondary flows which bodily displace dispersing plumes. The behaviour of a plume emitted in the near-wake depends on source height, reflecting the properties of the wake itself, the bounding shear layers, and the displaced external flow.

An array of buildings may be considered as a porous obstacle, but of a rather different sort than those discussed above because of the geometry of the elements within the array. Broadly speaking, a building array can be described as a set of vertical members and spaces of comparable lateral dimensions, whereas most research has concentrated on bodies either of more-or-less homogeneous porosity or comprised of a number of horizontal elements (eg fences). The individual recirculating regions immediately behind each member of the final row of an array of buildings may merge if the spacing between members is small enough; ie the bleed flow weak enough.

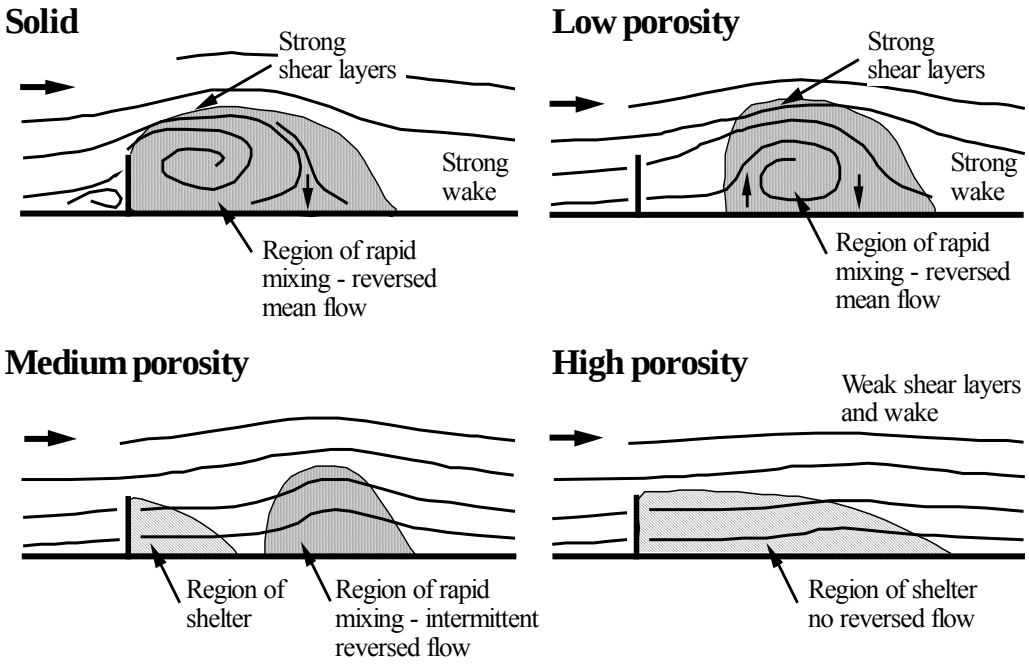

FIGURE 2.6 Regimes of flow in the wake of a three-dimensional porous obstacle

Whether a detached recirculation region can form some distance downwind of a building array is not known. It may well be possible when the extent of the recirculation regions behind the individual members is smaller than the formation distance for the downwind recirculation.

2.4 Internal boundary layers

An internal boundary layer grows over an obstacle array, deepening with distance from the upstream edge. The situation is shown schematically in Figure 2.7. The internal boundary is the layer near the ground in which the flow is in equilibrium with the new surface roughness. The friction velocity, the scaling velocity for mean velocities and turbulence intensities, is, however, a function of fetch from the edge of the new roughness. As the layer deepens the friction velocity tends to the limit appropriate to a fully developed atmospheric boundary layer above the new surface roughness. However, the fetch needed for the friction velocity to be within, say, 10% of its final value may well be much greater than the streamwise extent of an industrial site.

There is a transition layer between the internal boundary layer and the external flow. Conditions in the external flow are not modified directly by the new surface, although, in general, there will be an overall displacement of the flow due to changes in the mass flux in the internal boundary layer. The layer depths, δ_i, can be expressed as

$$\delta_i = d + a\, f(z_{o1}, z_{o2}) x^m \tag{2.1}$$

where d is the zero plane displacement, a is a constant, x is the distance from the roughness change and z_{o1} and z_{o2} are the upwind and downwind roughness lengths. The roughness function, $f(\,.\,.)$, depends on the nature of the roughness change (ie whether or not $z_{o2} > z_{o1}$), as does the exponent m, which typically lies between 0.5 and 0.75. Multiple roughness changes can be described and treated in an analogous manner (see, for example, Cook, 1990a).

Plume dispersion in the internal boundary layer reflects the behaviour of the flow field and takes some time to adapt to fully developed conditions over the new surface. Similarly, dispersion

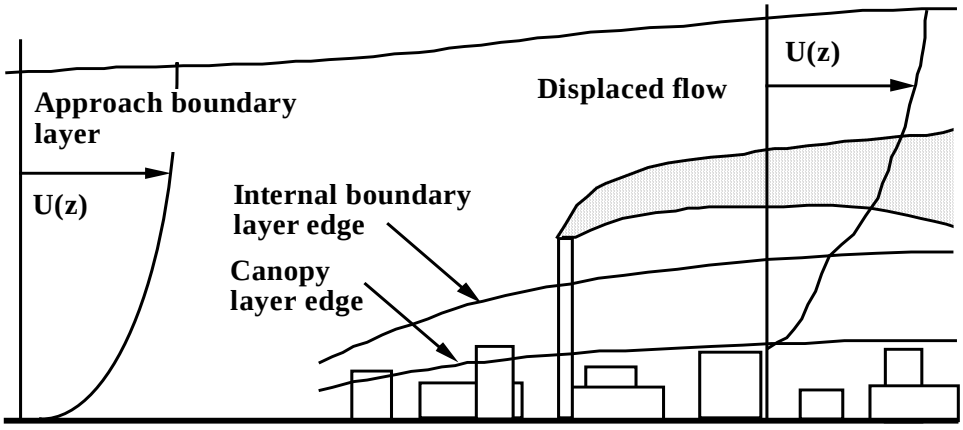

FIGURE 2.7 Developing internal boundary layer over an obstacle array, showing the retarded mean flow and enhanced turbulence levels

above the transition region continues as in the upstream flow, with the addition of an overall displacement due to changes in the mass flux in the internal boundary layer. Of course, the internal boundary layer eventually grows to encompass elevated plumes and their dispersion is then governed by the new surface.

2.5 Extensive array of buildings

In dispersion modelling there is no obvious demarcation between what constitutes a group or cluster of buildings, and what can be considered an extensive array of buildings. In practical terms, the following two features determine an extensive array: (a) at least three or four rows of obstacles, and (b) a building packing density greater than about 5%. (A building area density of at least 5% is required for application of urban corrections in some of the German air pollution standards; VDI, 1987).

The first point follows from the results of recent field experiments (Macdonald, 1997, and Macdonald *et al*, 1998a) and wind tunnel experiments by Hall *et al* (1996b,c), also reported in Macdonald (1997). In these experiments it was found that ground-level plumes dispersing in the first two rows of a regular array are significantly distorted by the aerodynamic features of individual buildings. Additionally, the wind approaching an array of buildings from a smooth upwind surface requires at least three rows to adjust to a form which is slowly varying. There are quite rapid changes in the first two rows of an array of obstacles due to streamline divergence and adjustment to the new drag force (Jerram *et al*, 1995; Davidson *et al*, 1996; Macdonald *et al*, 1997). This necessitates a different treatment from that inside an extensive array. If there are only one or two rows of obstacles, it may be best to treat the problem as dispersion about individual or small groups of interacting obstacles.

A key feature characterising an extensive array is the packing density of obstacles. If the mean plan area of the obstacles covering the ground is A_p and the mean frontal area of the obstacles presented to the wind is A_f, then it is possible to define two area densities (Plate, 1995; Theurer, 1995):

$$\lambda_p = A_p/A_d; \qquad \lambda_f = A_f/A_d \tag{2.2}$$

where A_d is the mean lot area of the obstacles. If the obstacles are roughly cubic in shape, then $\lambda_f = \lambda_p$. It is possible to relate the area density in a regular cube array to the face-to-face spacing between obstacles, S, and the cube dimension, H, as follows.

$$\lambda_p = 1/(1 + S/H)^2 \quad (2.3)$$

Thus, an area density less than 5% corresponds to an element spacing $S > 3.5H$. The flow over arrays of elements which are sparsely laid out falls in the isolated roughness regime (Morris, 1955; Hussain and Lee, 1980). In this regime the separation bubble behind the obstacles is able to reattach to the ground before the next downwind obstacle is encountered, limiting the interaction between the obstacles. Such sparsely laid out obstacles are probably best treated as isolated obstacles, although the levels of turbulence will be enhanced relative to isolated obstacles in open terrain.

2.6 Stages of plume development over arrays of obstacles

The development of a low level plume released in an urban environment can be broken down into different stages or regimes, with different levels of modelling appropriate to each regime. A crude division in terms of length and time scales was suggested by Munn (1981) who defined the microscale (0–100 m), neighbourhood scale (100–2000 m), and urban scale (>2 km). At a given location, air pollution from sources at each of the scales will affect the local pollutant concentration levels. Although it is not generally possible to decompose measured concentrations into individual contributions, one can observe that concentration fluctuation time scales will generally be of the order of seconds for microscale sources, minutes for neighbourhood scale sources and hours for urban scale sources. The three regimes of plume development illustrated in Figure 2.8 can be defined in terms of the size of the plume (characterised by σ_y and σ_z) relative to the mean height H, and mean width W, of obstacles in the urban area (Hall *et al*, 1996) as follows.

(a) **First regime.** The region close to a discharge, where the plume dimensions are smaller than the individual obstacles, typically $\sigma_y < W/4$ and $\sigma_z < H/3$. In this regime the local aerodynamic effects around individual obstacles dominate the plume path and very high levels of spatial and temporal variation exist. Dispersion patterns tend to be highly individualistic and site dependent.

(b) **Second regime**. In this intermediate regime (corresponding to Munn's neighbourhood regime) the plume may encompass one or more obstacles, with values of σ_y between about $W/4$ and W, and σ_z between $H/3$ and H. A large portion of the plume is still within the urban canopy. Although there is less spatial and temporal variation in this regime, the dispersion rate is still strongly influenced by the details and layout of the obstacles. This is perhaps the least studied regime.

(c) **Third regime**. Far enough from the source, the plume will have grown above the urban canopy and the concentration within the canopy will be relatively uniform over its depth. The plume dimensions are sufficiently larger than the obstacles ($\sigma_y > W$ and $\sigma_z > H$) such that the details of the individual obstacles and their layout pattern are no longer important. Here the surface features can be modelled as a uniform roughness. This is the regime of conventional urban dispersion modelling, where the urban surface affects the dispersion through the high level of mechanical turbulence generated by the surface drag of the buildings.

There are no precise boundaries between the above regimes. Plate and Baechlin (1988) introduced the concept of a 'radius of homogenisation' to divide the first two regimes from the far-field where conventional Gaussian plume models could be used. This is typically about 1 km from the source (10 or 20 obstacle rows), which corresponds to the limit of the neighbourhood scale.

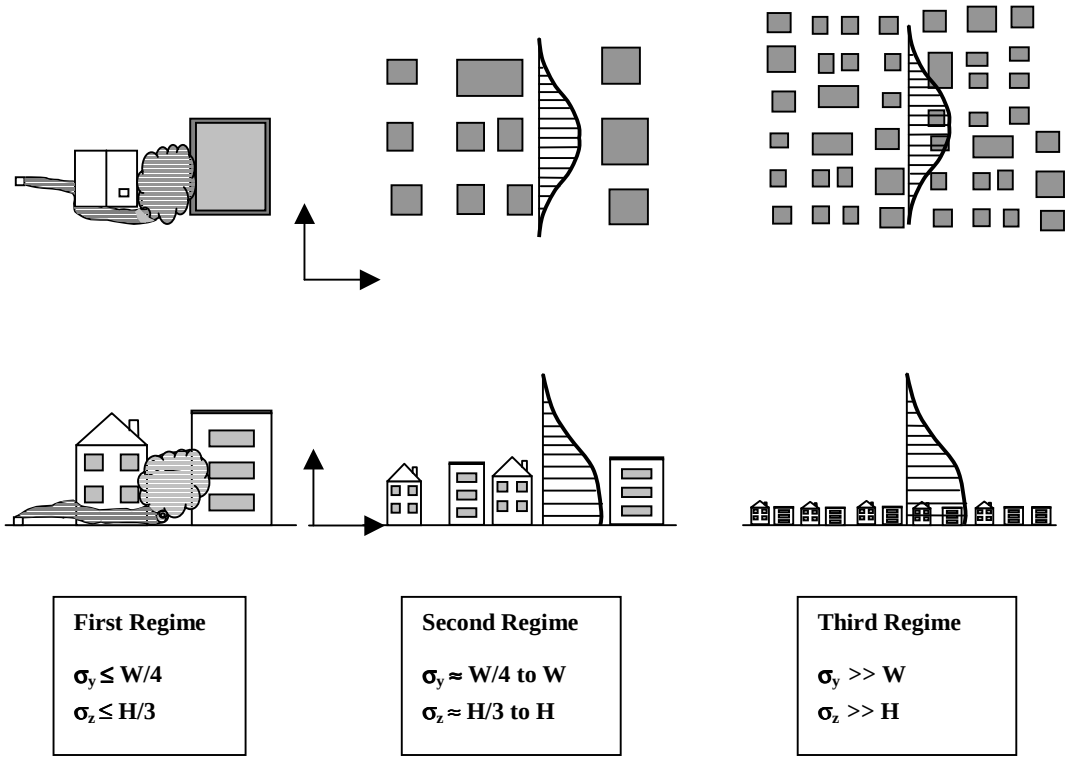

FIGURE 2.8 Schematic representation of three dispersion regimes depending on the relative size of the plume and individual obstacles. Lateral and vertical plume concentration profiles are shown in the plan and elevation views

2.6.1 Dispersion in the first regime: short range around single or multiple obstacles embedded in an array

The features of short-range dispersion around one or more obstacles imbedded in an array of obstacles are similar to those for flow and dispersion around isolated obstacles discussed in Section 2.1. In this regime there can be large variations in the dispersion characteristics due to the multiplicity of possible obstacle shapes and orientations, and the relative position of source and receiver. For example, if the source is located in a street or a gap between obstacles, while the receiver is located downwind in the same street, the received plume may be relatively undiluted. However, a plume released in the wake of an obstacle will quickly disperse to fill the wake, and is thus subject to a substantial initial dilution. A plume released just upstream of an obstacle will, if the obstacles are far enough apart, be entrained in the horseshoe vortex around the obstacle and possibly be split by the obstacle (Foster and Robins, 1985; Macdonald, 1997; Hall *et al*, 1998).

The main difference between the near-field problem within an extensive array and that of flow and dispersion around isolated or small groups of obstacles is the enhanced level of sheltering and turbulence production within the array. The aerodynamic influence of an obstacle located within an array may extend considerably far afield. Cook (1990b) provides useful diagrams of the region of influence of an obstacle immersed in an array. The study by Hosker and Pendergrass (1987) gives some idea of the flow features around small groups of three to five buildings, and includes a discussion of proximity effects such as sheltering, wind jetting, vortex production and shear layer impingement. Because of the sensitivity of the obstacle interactions to wind direction, large variations in plume concentration can occur in this regime for small changes in configuration. The precise prediction of concentrations resulting from specific arrangements of source and obstacles

generally requires wind tunnel or field experiments, as observed distributions of concentration are usually quite different from those found for obstacles in isolation. For example, Wilson and Chui (1987) suggest that the high levels of turbulence generated by even one building upwind can increase the local dilution by a factor of two to ten times over that of an isolated building.

Perhaps the most studied and best-understood problem in the near-field regime is the short-range dispersion of a line source due to traffic in a street canyon. When rows of buildings are close together, there is a sheltering effect when the wind blows perpendicularly to the street, and 'skimming flow' occurs. This results in a recirculating vortex decoupled from the main flow overhead, and it is generally observed that pollutant dilution is controlled by mean flow transport out of the canyons rather than by turbulent diffusion (Wedding *et al*, 1977). The typical flow pattern is illustrated in Figure 2.9. The local wind near street level is in the opposite direction to the external wind. A more complicated helical circulation arises as the wind direction moves from normal towards parallel to the street, the vortex component disappearing when the wind blows along the street. Street intersections generate very complex, three-dimensional flow patterns due to the interactions between the flows separating from roof and wall edges. There are large gradients across the street canyon and large variations in concentration where a street canyon is intersected by a cross street (Hoydysh and Dabbert, 1994). The flow field, and hence the associated dispersion behaviour at intersections, is very sensitive to the local geometry (Scaperdas *et al*, 1998a,b). Buoyancy forces generated by solar heating of building surfaces or traffic within the street may modify the circulation patterns. For example, heating of the downwind wall of the canyon illustrated in Figure 2.9 would create buoyancy forces that opposed the air flow down the wall and at low enough wind speeds these might be strong enough to reverse the flow, thus cutting-off the supply of 'clean' air into the canyon. This is discussed further in Section 4.3.1. The movement of traffic creates additional turbulence and, possibly, mean flows that become important when wind speeds are low. Traffic-induced mixing tends to reduce the very high concentrations that would otherwise result from street level emissions in calm conditions.

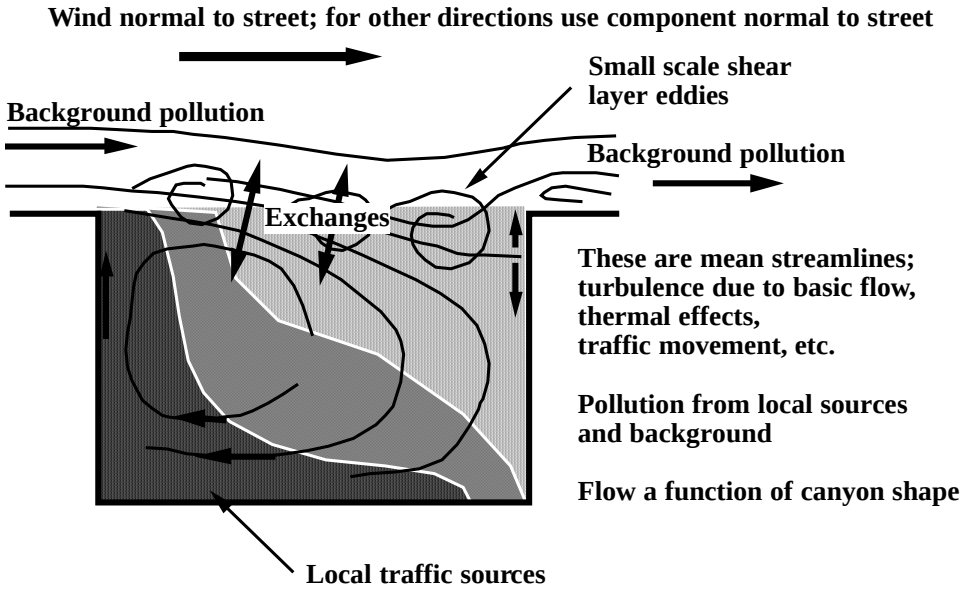

FIGURE 2.9 Simple street canyon vortex flow with associated concentration levels due to street-level sources

2.6.2 Dispersion in the second regime: intermediate range in arrays of obstacles

The intermediate range of plume dispersion in arrays of obstacles is perhaps the least well understood and most studies are relatively recent (see, for example, Baechlin *et al*, 1991, 1992; Davidson and Hunt, 1991; Davidson *et al*, 1995, 1996; Theurer, 1995; Theurer *et al*, 1996; Hall *et al*, 1996c; Macdonald *et al*, 1997, 1998b; Poreh, 1997). There has been considerably more interest in the aerodynamics of buildings and the measurement of force coefficients (wind loading) for civil engineering applications (Hussain and Lee, 1980; Ho *et al*, 1991, 1992; Theurer *et al*, 1992). Another application is the estimation of displacement height and surface roughness for meteorological applications (Counihan, 1971; Wooding *et al*, 1973; Raupach *et al*, 1980; Fang and Sill, 1992; Bottema, 1996, 1997; Petersen, 1997; Macdonald *et al*, 1998a).

The dispersion problem in this regime is two-fold. There is, firstly, the influence of the obstacles on the plume dimensions σ_y and σ_z and, secondly, the modified wind field, in terms of reduced mean advection velocity and enhanced turbulence. The effect of the obstacles on the plume depends mainly on the relative size of the plume and obstacles. The lateral concentration profile is typically Gaussian or near-Gaussian in this regime (Davidson *et al*, 1995; Macdonald *et al*, 1997, 1998b; Hall *et al*, 1998), and σ_y is mainly related to mean obstacle width. The vertical plume distribution has a more complex profile, but appears to be well represented by a reflected Gaussian. The portion of the plume within the obstacle canopy can be expected to be well mixed, because of the low advection velocity and the high turbulence intensity in the recirculating secondary flows. Thus, the concentration gradients in the urban canopy are small once the plume has encountered a few rows of obstacles.

Most studies of urban diffusion show an enhanced vertical diffusion relative to open terrain, and an early recommendation for urban dispersion modelling was to use the empirical Pasquill-Gifford charts of σ_z shifted by one stability class towards more unstable (Gifford, 1972; Yersel *et al*, 1983). This is especially important at short distances (<200–400 m) where the dispersion is most strongly affected by the enhanced mechanical turbulence induced by the flow in the canopy and immediately above the buildings. One other effect of the high levels of turbulence in the urban canopy is that sharp gradients of concentration are smoothed out. This produces a rapid reduction in concentration fluctuations (Davidson *et al*, 1995; Macdonald, 1997). The high level of vertical mixing also tends to limit the range of thermal stratification found in an urban area, so that the range of atmospheric stability found in the urban boundary layer is reduced, even in low wind speed conditions (Gifford, 1972).

Although the dispersion parameters σ_y and σ_z are usually enhanced by the increased urban roughness the increased drag leads to a reduction in mean transport velocity). These effects tend to counteract one another, since $C \propto 1/U\sigma_y\sigma_z$, so it is difficult to say whether the mean ground-level concentration will be reduced in an urban plume relative to one in open terrain. In certain configurations σ_y may actually be reduced, relative to a plume in open terrain, due to channelling effects in along-wind streets (Poreh, 1997).

When the building aspect ratio W/H is greater than one (low, wide buildings or buildings joined in rows), the wind may be deflected along the streets within the urban canopy. A plume may then experience a significant lateral shift in the canopy, and may not follow the direction of the overhead wind (Baechlin *et al*, 1992; Theurer *et al*, 1996; Hall *et al*, 1998; Macdonald *et al*, 1998b). Most existing plume models do not include such a lateral shift, although it can be easily accounted for by relocating the source to a virtual origin.

2.6.3 Dispersion in the third regime: long-range neighbourhood and urban scale modelling

The longer-range dispersion of pollutants in the urban environment is the subject of most air quality simulation models. There are many approaches available for estimating concentrations

within this regime for averaging times greater than a few minutes. Several good reviews of this type of modelling can be found (Johnson *et al*, 1976; Turner, 1979; Benarie, 1980; Turner *et al*, 1989; Zannetti, 1990). These include Gaussian plume models (see, for example, Turner, 1994), box models (see, for example, Gifford and Hanna, 1970, 1973), gradient transport models and trajectory models. Most of these require some estimate of the emissions affecting an area (source inventory), of the meteorological conditions (for transport and dilution), and any removal processes. Some of the models are discussed in Section 3. In general, they are used to predict concentrations from plumes whose size is much greater than the roughness elements, and may even be approaching the height of the mixing layer. Typically, clusters of ground-level sources are combined into area sources, although the largest point sources can be calculated individually. The longer-range urban models do not generally have the ability to resolve the concentration field to a high degree, and cater more towards modelling background pollution levels due to a multiplicity of sources. Specific adjustments are usually made to account for significant local sources such as major motorways or street canyons where pollutant levels are enhanced over the spatially averaged values. A popular method of dealing with plume dispersion in this regime is to make use of modified Gaussian plume parameters for urban terrain, although most simple models include only a broad roughness category for urban dispersion. More recently, there had been a tendency in sophisticated models to include the effects of the actual surface roughness directly (see, for example, Roberts *et al*, 1994).

3 Current practices in dispersion modelling

3.1 Single buildings

3.1.1 Virtual source and related models

A whole class of early and some current building effects models are based on a form of virtual origin representation of the extra spread or effective stack height representation of the reduction in plume height due to downwash generated by building wakes (see, for example, Gifford, 1960; Huber and Snyder, 1976; Turner, 1979; Jones, 1983). Virtual origin models are usually applied to emissions below roof level and effective stack height models to stack releases above roof level. A review of simple models and their performance is presented by Fackrell (1984b).

The model for lateral or vertical plume spread, σ_B, is typically expressed by one of the following:

$$\sigma_B(x) = \sigma(x + x_o); \qquad \sigma_B(x) = \sigma(x) + \sigma_o; \qquad \sigma_B^2(x) = \sigma^2(x) + \sigma_o^2 \tag{3.1}$$

where σ is the spread in the undisturbed flow, x_o a virtual origin chosen and σ_o an initial spread, both chosen to satisfy conditions of the form:

$$\sigma_B(0) = \sigma(x_o) = f(H, W) \qquad \text{or} \qquad \sigma_B(0) = \sigma_o = f(H, W) \tag{3.2}$$

where H and W are the building height and lateral extent.

Effective stack height rules can be expressed as

$$\begin{aligned} &h \le h_{max}: && h_e/h_{max} = (h - H)/(h_{max} - H) \\ &h > h_{max}: && h_e = h \\ & && h_{max} = N_h H \end{aligned} \tag{3.3}$$

where h_e is the effective height of a stack of height h, and H is the building height. This assumes no variation with fetch or wind direction and that the effect of the building vanishes above h_{max}. With $N_h = 2.5$ we have the so-called 'two and a half times rule'. The origins of this are rather obscure (see, for example, Lucas, 1972) and appear to be based on the observation that the disturbance due to the recirculation region behind a two-dimensional, solid fence or plate in a uniform flow is

approximately 2.5 fence or plate heights deep at most. No doubt there are other 'origins' to the rule but the point is that there is nothing fundamentally significant in the choice of 2.5, although in practice it has proved not to be excessively large or small. There are of course variations on this theme which may introduce further features of the building shape and variations with wind direction. For example, a common extension is to define a length scale, L_B, as the lesser of the building height and width, $L_B = \min(H, W)$, and then define:

$$N_h = 1 + 1.5L_B/H \tag{3.4}$$

In all cases, the adjustment to the plume height becomes an adjustment to the stack height, with the actual height being replaced by an effective one. This creates some difficulties when applied to rising plumes. Application of the full stack height reduction is clearly excessive when plume rise is significant and some compromise has to be sought based on, say, the average plume height over the building and its near-wake.

3.1.2 NRPB-R91 model

The NRPB-R91 dispersion model (Clarke, 1979; Jones, 1983) proposes the use of a virtual source model for emissions which are fully entrained into the building wake. The condition for the model to be applicable to a passive emission at height h is formally written as

$$(h - H)/(x' + 0.1H) < 0.1 \tag{3.5}$$

where x' is the distance of the source downwind from the leading edge of the building. A virtual source, Gaussian plume model is used to calculate dispersion downwind of the recirculation region, with

$$\sigma_y(0) = W/3; \qquad \sigma_z(0) = H/3 \tag{3.6}$$

and an effective source height of $H/3$. Concentrations in the recirculation region are calculated from a box model very like that used in the ADMS building effects model described in Section 3.1.4.

3.1.3 ISC model

The current ISC approach (Huber and Snyder, 1976; USEPA, 1992) defines a region where building effects dominate plume behaviour. Dispersion in this region is matched to dispersion further downstream by use of a virtual source model. The method applies to a stack which falls within the zone of influence of a building, which itself may be one of a group of buildings. The zone of influence, sketched in Figure 3.1, is determined by the length scale, L_B, which is defined as the lesser of H and W. The zone is taken to extend $2L_B$ upwind, $5L_B$ downwind, and to be of lateral extent $W + L_B$ and vertical extent $H + 1.5L_B$. Building effects on dispersion are calculated within the range $3H \le x \le 10H$ by writing expressions of the form: $\sigma = \sigma(x, H, W)$, the precise functional form depending on the source height and building shape. The ISC building effects model is not applicable for $x < 3H$.

The basic dispersion relations in the zone of influence are

$$\sigma_z = 0.7H + 0.067(x - 3H) \tag{3.7a}$$

$$\sigma_y = 0.7W/2 + 0.067(x - 3H) \tag{3.7b}$$

where x is measured from the rear of the building. Both σ_y and σ_z are calculated from the above equations when the source height is below $1.2H$, but otherwise only σ_z, with σ_y given by the appropriate dispersion relationship for the external flow. Plume rise is calculated by a modified version of the conventional Briggs-type plume rise model, adjusted to simulate extra dilution in the

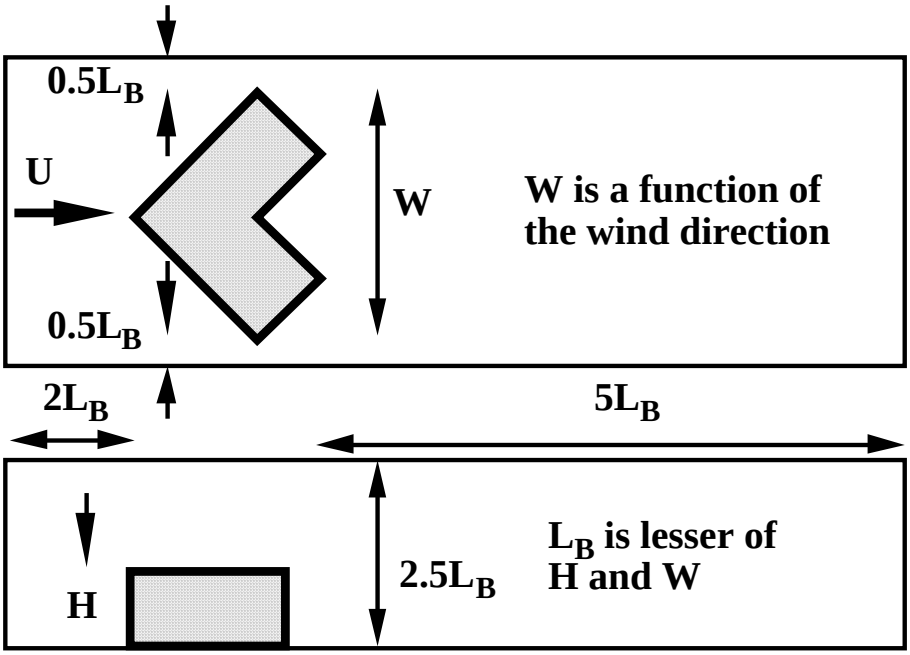

FIGURE 3.1 ISC building effects region and its relation to the building dimensions

initial phase of the rise. An important feature of this model is that mean streamlines are assumed to be horizontal within the zone of influence. This is a surprising assumption in view of our understanding of flow patterns around cuboids and probably reflects the fact that the underlying experimental study only addressed approach flows normal to the building.

The ISC model is being replaced by an advanced Gaussian plume model, AERMOD (Lee *et al*, 1996). AERMOD was first released without a new building effects module, the intention being for this to be added at a later date. Meanwhile, a new building effects model, PRIME, has been developed and tested (Schulman *et al*, 2000). This is discussed in Section 3.1.5, following a summary of ADMS in Section 3.1.4.

3.1.4 ADMS modelling

The ADMS approach (Apsley, 1988; Carruthers *et al*, 1994; Robins *et al*, 1997) is much more sophisticated than those so far described. A set of sub-models is used to represent behaviour in a number of regions within the flow. These are illustrated in Figure 3.2. The building effects region, B, is divided into five sub-regions where specific processes dominate: U, upwind; N, near wake; S, surrounding; E, external; W, wake. In general, a number of these will be involved in any particular dispersion problem.

A distinction was drawn in reviewing flow and dispersion around buildings (Section 2.1) between momentum deficit and vortex wakes, since analytical theory exists for the former but not the latter. This situation is reflected in the way the two-wake components are modelled within ADMS where simple empirical relationships are used to describe mean streamline deflections due to roof vortices. These relationships are based on wind tunnel observations (see, for example, Robins and Castro, 1977) and describe streamline deflections as a function of initial height, building orientation and distance downstream.

Application of the ADMS model begins by converting the actual building or buildings to be studied into an effective obstacle, which is a rectangular block (dimensions L, W, H) normal to

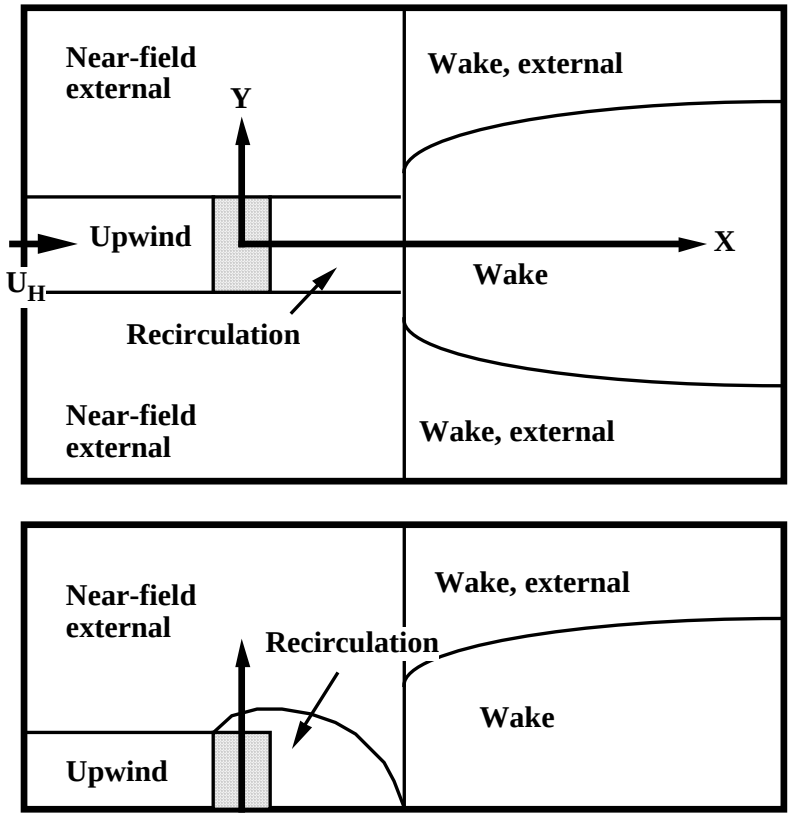

FIGURE 3.2 Regions used in ADMS building effects module; from Robins *et al* (1997)

the oncoming flow. An effective orientation, θ, is also defined which is later used to determine mean streamline displacements around the obstacle and its near-wake. The orientation is set between 0 and $\pi/4$, with 0 corresponding to an approach flow normal to the front face of the main building.

3.1.4.1 Upwind region

The upwind region, U, is defined to include all upwind sources whose emissions are significantly perturbed by the building and its wake. Concentrations in U are given by the underlying ADMS dispersion model. A slight modification is made if the source lies within a sub-region, UI, the forward projection of the obstacle cross-section, as the plume then impacts on to the front face of the building. In this case the wind speed is set to U_H, the roof level wind speed, to ensure compatibility with modelling in subsequent regions.

3.1.4.2 Near-wake region

The near-wake region, N, is the well-mixed area of recirculating flow created by separation of the mean flow from the building surfaces. The bounding surface is defined as parallel sided in the x–y plane and elliptical in the x–z plane, emanating from the upwind or downwind wall and roof edges according to a separation criterion based on building geometry. For the height and length of the near-wake, z_R and L_R, we write

$$z_R = z_{R\max} f(x) = z_{R\max} \{1 - [(x - x_{R\max})/(x_R - x_{R\max})]^2\}^{1/2} \tag{3.8}$$

$$L_R = [1.8(L/H)^{-0.3}]/[1 + 0.24W/H]; \qquad x_R = L_R + \mathrm{L}/2 \tag{3.9}$$

based on wind tunnel observations (Fackrell, 1984a).

Mixing is assumed to be sufficient to produce uniform near-wake concentrations, at least for buildings whose geometry satisfies $W \leq 3H$, otherwise mixing is assumed to create uniform concentrations in part of the near-wake of width $3H$. The basic dispersion model is a simple mass flux balance within N, which can be expressed as

$$\mathrm{d}/\mathrm{d}t(V_R\, C_R) = Q - \langle u_n\, c\rangle\, S_R \tag{3.10}$$

where V_R is the region volume, Q the source strength within N, and $\langle u_n\, c\rangle$ the concentration flux across the boundary of area S_R due to turbulent and mean flow processes. Using scaling arguments this becomes

$$\mathrm{d}C_R/\mathrm{d}t = Q/V_R - b\, U_H\, C_R\, S_R/V_R = Q/V_R - C_R/T_R \tag{3.11}$$

where b is a similarity constant and T_R the concentration decay time scale. In the steady state the non-dimensional concentration is given by

$$C_R\, U_H H^2/Q = (T_R\, U_H/H)/(V_R/H^3) \tag{3.12}$$

$$V_R/H^3 = (\pi/4)\,(z_{Rmax}\, W\, L_R/H^3) \tag{3.13}$$

$$T_R\, U_H/H = [11(W/H)^{3/2}]/[1 + 0.6(W/H)^{3/2}] \tag{3.14}$$

with the empirical relationship for the time scale again based on extensive wind tunnel data (Fackrell, 1984a). No concentration field structure is modelled within the recirculation region, although some could quite simply be added, based on data correlations of the sort discussed by Wilson and Britter (1982); eg by writing

$$C\, U_\mathrm{H}\, H^2/Q \approx C_R\, U_H H^2/Q + \beta\, (s/H)^{-2} \tag{3.15}$$

where s is the distance from the source and β an empirical constant.

Three cases need to be treated: 'effectively-passive' emissions into N; 'non-passive' emissions into N; emissions external to N. Effectively-passive is here taken to describe emissions which do not escape directly from N by virtue of their initial buoyancy and momentum and for these Q is simply the source strength. For the others it must be calculated from the external concentration field and this is dealt with in a subsequent section. A simple criterion based on the source momentum and buoyancy fluxes is used to distinguish between effectively-passive and non-passive emissions.

3.1.4.3 Surrounding region

The surrounding region, S, is the space surrounding the building and its near-wake (but not extending upwind of the front face). Plume spread is predicted by the underlying ADMS dispersion model, but the plume centreline is displaced by mean streamline deflections. These are known to be strongly dependent on the orientation of the building to the oncoming flow, as this determines the strength of the streamwise 'roof' vortex system and hence the magnitude of the associated secondary flow. Mean streamline deflections, Δz, are estimated as a function of the effective orientation, θ, with $\Delta z = 0$ for all z when $\theta = 0$ and Δz a maximum for $\theta = 45°$, satisfying the limits that $\Delta z = H$ for $z = H$ and $Dz = 0$ for $z = z_\mathrm{B}$. The mean streamline height, z_{SL}, and plume height, z_P, are written as

$$\mathrm{d}z_{SL}/\mathrm{d}x = w/U_\mathrm{H} = \{\mathrm{d}z_R/\mathrm{d}x\}\ \{[z_{R\max} - z]/[z_{R\max} - z_\mathrm{R}(x)]\}\ \{4\theta/\pi\} \tag{3.16}$$

$$\mathrm{d}z_\mathrm{p}/\mathrm{d}x = \mathrm{d}z_{SL}/\mathrm{d}x + (\mathrm{d}z_p/\mathrm{d}x)_{\text{plume rise}} \tag{3.17}$$

where z_B is the height of the building effects region, B.

To some degree, material from a plume in S is entrained into the near-wake, N. Modelling follows Puttock and Hunt (1979) by assuming very efficient and rapid mixing within the near-wake so that the resulting concentration in N, C_R, is the average over the boundary S; ie

$$C_R = \iint_S C_S(x, y)\, dA / \iint_S dA = \iint_S C_S(x, y)\, dA / S_R \tag{3.18}$$

where C_S is the concentration on the surface S.

The near-wake results derived in Section 3.1.4.2 link C_R to an effective source strength within the near-wake, Q_R, and the fraction, ε, of the original release which is entrained:

$$C_R\, U_H\, H^2/Q_R = (T_R\, U_H/H)/(V_B/H^3); \qquad \varepsilon = Q_R/Q \tag{3.19}$$

This process also defines boundary conditions for use in the two downstream regions, E and W, where a double plume structure is assumed. This comprises an elevated (or external) part of strength $Q–Q_R$ from the original emission, and a ground-based part of strength Q_R from the near-wake.

3.1.4.4 Main wake region

The main wake region, W, stretches downwind from the near-wake and here the flow field is modelled by a simplified, three-dimensional version of the constant eddy viscosity wake theory described by Counihan *et al* (1974). This can be written as

$$U_H\, \partial u/\partial x + \partial/\partial y(-\nu_y\, \partial u/\partial y) + \partial/\partial z(-\nu_z\, \partial u/\partial z) = 0 \tag{3.20}$$

where $U_W = U_H + u$ is the mean longitudinal velocity in the main wake, u, v, w the perturbation mean velocities, $\nu_y = k\, u^*\, H$ and $\nu_z = 2\, k\, u^*\, H$ are the eddy viscosities, k von Karman's constant and u^* is the friction velocity. A similarity solution is found of the form: $u = \Delta u(x)\, g(\zeta)\, h(\eta)$, where η and ζ are normalised coordinates, y/L_y, z/L_z, and L_y and L_z are characteristic wake length scales. An integral constraint relates u to the coefficient of the turning moment on the obstacle, c_B, and fixes the inevitable unknown similarity constant. The other two velocity perturbation components are expressed so as to satisfy the continuity condition. There is really very little experimental information on which to base c_B as a function of obstacle geometry so a constant value of 0.8 is used (Counihan *et al*, 1974).

The predicted velocity perturbations are used to calculate the path of any plume within W:

$$dz_p/dx = w/U_H + (dz_p/dx)_{\text{plume rise}} \tag{3.21}$$

Otherwise wake-averaged values are used to calculate modifications to plume spreading rates and plume advection speeds for use with a Gaussian concentration field model. The wake-averaged surface shear stress perturbation, $\Delta\tau$, taken also to be the scale for the perturbation turbulent stresses, Δv^2 and Δw^2 (ie assuming $\Delta v^2/\langle v^2\rangle = \Delta w^2/\langle w^2\rangle = \Delta\tau/u^{*2}$) is given by the momentum integral equation:

$$U_H\, d/dx\, ({}_0\int^\infty dy\, {}_0\int^\infty u\, dz) = L_y\, \Delta\tau \tag{3.22}$$

A standard Gaussian model is then applied with the advection speed set to $U_H–\Delta u$ and the plume spreading rates modified to account for streamline convergence and enhanced wake turbulence:

$$d\sigma_y^{(W)}/dx = 1/2\ \sigma_y^{(W)}\, d/dx(\Delta u/U_H) + [(1 + \Delta v^2/\langle v^2\rangle)^{1/2}/(1 - \Delta u/U_H)]\, d\sigma_y^{(E)}/dx \tag{3.23a}$$

$$d\sigma_z^{(W)}/dx = 1/2\ \sigma_z^{(W)}\, d/dx(\Delta u/U_H) + [(1 + \Delta w^2/\langle w^2\rangle)^{1/2}/(1 - \Delta u/U_H)]\, d\sigma_z^{(E)}/dx \tag{3.23b}$$

where $^{(W)}$ denotes wake conditions and $^{(E)}$ external conditions (ie the underlying ADMS plume spread model). A description of the implementation of the Gaussian model follows in Section 3.1.4.6.

3.1.4.5 External region

The decay of the main wake (ie acceleration in the streamwise direction) generates inwards secondary flow in the external region, E, which in turn affects plume centreline trajectories. The secondary flow components, v and w, are given by the main wake results, since these are valid as $z \to \infty$, $y \to \pm\infty$, and the plume trajectory is calculated from

$$dz_p/dx = w/U(z_p) + (dz_p/dx)_{\text{plume rise}} \tag{3.24}$$

3.1.4.6 Concentration field in the main wake and external regions

These two regions are taken together because a plume in either one will extend into the other. Gaussian formulae apply in W and E but with different parameters, whilst ensuring that the concentration field is continuous across the boundary between the two regions. As illustrated in Figure 3.3, E has to be subdivided to achieve this, giving six regions in all: WW (the whole of W), two times EW, two times EE, and WE. The reason behind this becomes apparent when we consider, for example, the boundary between WW and WE. This is a horizontal boundary and consequently the lateral concentration profiles must be the same on both sides, whereas the vertical profiles may reflect a more rapid variation with z above the boundary than below. In general, we write the concentration in a region $\alpha\beta$ as

$$C/Q = [q_{\alpha\beta}(x)/U_H]\, C_Y(y, y_p, \sigma_{y\alpha\beta})\, C_Z(z, z_p, \sigma_{z\alpha\beta}, D) \tag{3.25}$$

with $\sigma_{y\alpha\beta}$, $\sigma_{z\alpha\beta}$ chosen according to $\alpha\beta$ and the plume centre location, as defined in Table 3.1. The four coefficients, $q_{\alpha\beta}$, are chosen so that concentrations are continuous on the boundaries and the flux of material conserved; ie

$$\int_0^\infty \int_{-\infty}^{\infty} (U_H + u_{\alpha\beta})\, C/Q\, dy\, dz = 1 \tag{3.26}$$

$u_{\alpha\beta} = -\Delta u$ if $\alpha\beta$ = WW; = 0 otherwise

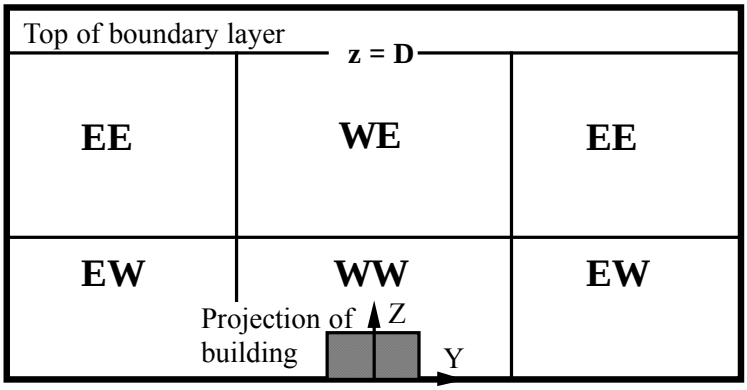

FIGURE 3.3 Regions used in ADMS to describe concentrations within the main wake; from Robins *et al* (1997)

TABLE 3.1 Definition of $\sigma_{y\alpha\beta}$, $\sigma_{z\alpha\beta}$ according to modelling region and plume centre position

Model region	WW	WE	EW	EE
Centre in WW	αβ= WW	WE	EW	EE
Centre in WE	EW	EE	EW	EE
Centre in EW	WE	WE	EE	EE
Centre in EE	EE	EE	EE	EE

Section 3.1.4.3 describes the basic double plume structure which results from the modelling in N and S. So with C(entrained) and C(non-entrained) representing the concentration fields for unit source strength in the entrained and non-entrained cases, the total concentration field in W and E becomes:

$$C/Q = \varepsilon\, C(\text{entrained}) + (1 - \varepsilon)\, C(\text{non-entrained}) \qquad (3.27)$$

3.1.5 PRIME modelling

In many respects PRIME (Schulman *et al*, 2000) is quite similar to ADMS, although there are important differences in detail. The wake is divided into a near-wake (the recirculation region) and a far-wake. The dimensions and shape of the near-wake are taken from the correlations proposed by Fackrell (1984) and Wilson (1979), using effective along-wind and across-wind building dimensions. The depth and width of the main wake grow as $x^{1/3}$, based on results for the growth of a three-dimensional wake in uniform, free flow. Mean streamline patterns outside of the near-wake are derived empirically from a database of measurements reported by Snyder and Lawson (1994).

Entrainment into the near-wake is calculated from the flux of plume material within the boundaries of the near-wake, which leads directly to the fraction, ε, of the emitted flux captured and subsequently re-emitted from the near-wake. Concentrations within the near-wake are calculated by assuming a Gaussian lateral distribution and a uniform vertical distribution and a mean convection velocity proportional to the roof level wind speed, U_H. As in ADMS, a two-component, Gaussian plume model is then used in the far wake, as per equation 3.27.

Lateral and vertical spreading rates are enhanced in the wake regions, using the methods developed by Weil (1996). Weil uses 'local' linear spread relations in the near-field (ie $\mathrm{d}\sigma_z/\mathrm{d}x = w'(x)/U(x)$, etc) and an eddy viscosity model in the far-wake. The mean flow and turbulence levels used in these relationships are based on the results for a three-dimensional wake in uniform, free flow. Virtual source modelling is used to represent the initial size of the ground-based plume emanating from the near-wake. A transition zone, equal in length to 15% of the recirculation region length, is assumed between the near- and far-wake within which a linear variation of concentration with distance is imposed to ensure a smooth transition in concentration levels between the two wake regions. PRIME predictions have been compared with both field and wind tunnel data, showing that the model performs significantly better than the ISC model described in Section 3.1.3.

There are three key differences between PRIME and ADMS modelling, relating to prediction of the mean streamlines, entrainment into the recirculation region, and flow and dispersion in the wake. PRIME uses interpolation in a database of measurements to derive mean streamlines, whereas ADMS calculates them from a combination of empirical and analytical models. The latter approach is the more general, whereas the former should be the more accurate for the range of geometrical and flow conditions covered by the database. However, models must be applied to real sites, where site detail can have a profound effect on the flow field, and must be used with the full range of approach flow conditions (wind direction, roughness, stability etc). The ADMS approach essentially places upper and lower bound limits on likely streamline displacements, acknowledging that greater accurate is not generally possible; the same could be achieved with PRIME by careful choice of effective building shapes. Which of the two methods for calculating entrainment into the recirculation region is the better is not clear. Neither is a very faithful representation of the processes found in practice, but both are simple and readily implemented. They should display similar sensitivities, as both depend on the diffusion of external emissions to, or across, the recirculation region boundary. PRIME uses a wake model based on free

wake theory, ADMS one based on wall-wake theory. The former is better founded, but not formally applicable in boundary layer flow. In practice, the extra rates of spread in the wake are of secondary importance to the vertical deflection of the plume centre (see Robins *et al*, 1998a), so the consequences of the different modelling approaches might not be too significant.

3.2 Groups of buildings

3.2.1 Virtual source modelling

The virtual source approach to modelling dispersion affected by a single building may in principle be extended to treat a group of buildings. In other words, the basic algorithm may be extended not only to predict the upstream location of the virtual source but also to determine its effective height and lateral position. The latter two parameters are necessary because plumes, are, in general, deflected from the downwind direction and mixed vertically in moving through an array. In fact, these are also features of dispersion around a single building, especially for upwind sources, but often ignored in simple models.

The real difficulty lies in determining the relationships that determine the effective source parameters from the input data describing the actual situation. There is no simple answer to this. One approach is to ignore the lateral deflection, arguing that this only affects the location of plumes, not the concentrations within them. There is some weight in this argument and for many cases it will be acceptable. Simple approaches based on the single building algorithms will also be acceptable when the spacing of obstacles in an array places them in the isolated obstacle regime. However, this fails as the packing becomes denser. Wind tunnel modelling may then be used to determine near-field dispersion behaviour and a standard Gaussian plume model patched to the results to extend predictions to greater distances downwind. Alternatively, wind tunnel studies may be used to extend the empirical, single building virtual source specification to building arrays. These matters are returned to in Section 3.3.3.

3.2.2 ISC modelling

The ISC buildings effect procedure is extended to a group of buildings by calculating the zones of influence for each building, identifying those within which the stack lies, and then forming an effective building to represent their combined effects. Plume dispersion does not depend on the relative positions of the stack and the effective building, nor the orientation of this building.

3.2.3 ADMS modelling

A building complex is simulated in ADMS by a single ‘equivalent’ building aligned with the flow. This is formed from the set of wind aligned blocks equivalent to the buildings comprising the complex. The centre, dimensions and orientation of each building in the complex are used to define its wind aligned equivalent with centre x_i, y_i, dimensions H_i, W_i, L_i, and roof orientation, θ_i. As before, the roof orientation lies between $\pm\pi/4$ and is used to specify the degree of streamline deflection due to the roof vortex system.

The equivalent building to be used to simulate the array is then determined. The user defines the main block from the set of individual wind aligned blocks. This defines the height and orientation, H_B and θ_B, of the equivalent building and the initial plan dimensions, L_B and W_B. The equivalent building is expanded to enclose all blocks satisfying

$$H_{Bi} \geq H_B/2 \tag{3.28a}$$

$$\Delta x_i \leq L_B/2, \qquad \Delta y_i \leq W_B/2 \tag{3.28b}$$

where Δx_i and Δy_i are the distances between the 'current' equivalent building and block *i*. This algorithm is applied iteratively until converged.

The algorithm is based on very little observational evidence and must therefore be treated with some scepticism. Users are advised to carry out sensitivity studies by varying the information input to define the building array. For example, all but the main building may be omitted or some other effective building dimensions directly input.

3.3 Urban dispersion modelling

A wide range of urban air quality models exists, reflecting the abundance of end requirements as, for example, laid down by the UK air quality strategy (DoE, 1997) or the American air quality standards (US-EPA, 1998). Some form of Gaussian plume model is frequently used in operational models, with special algorithms added to treat specific circumstances such as street canyons and highways. Atmospheric chemistry is commonly included because of its importance in determining levels of pollutants such as NO_2 and O_3. However, in this review we concentrate on the physical aspects of dispersion modelling.

3.3.1 Gaussian models

Gaussian plume models are used in a wide variety of urban dispersion models because of their relative simplicity and the ease with which additional effects due to source buoyancy, stability, deposition, surface roughness and averaging time may be included (Hanna *et al*, 1982; Turner, 1994). They form the basis of the NRPB-R91 model (Clarke, 1979) and most of the US-EPA 'preferred' models. Their accuracy depends on the appropriate selection of the plume spread functions, $\sigma_y(x)$ and $\sigma_z(x)$, and plume advection velocity U_p. The basic model is generally limited to time-averaged concentrations of at least ten minutes or more, over terrain for which the meteorological and surface features have remained constant during the plume travel time (although the latter restriction can be removed by the addition of segmented plume or puff modelling). Most present knowledge on plume spreading rates is based on experimental diffusion trials over open country, at relatively short distances from the source. Data applicable to urban areas or large industrial complexes were relatively scarce.

The increased roughness of the urban surface and its effects on stability and turbulence levels must be accounted for in defining plume spread relationships for urban areas. McElroy (1969) analysed some of the first measurements of urban plume spread in St Louis and found values about twice those expected from the standard Pasquill-Gifford relations at short distances (x < 200 m) from the source. Gifford (1972) later suggested that the increased turbulence in an urban area could be approximated by first estimating the standard Pasquill stability class from the insolation data, and then shifting to the next more unstable class. Variations in surface roughness may also be accounted for by adjusting σ_z valid for a reference surface roughness z_{oref} to another roughness length z_o Zannetti (1990) proposed the relation

$$\sigma_z(z_o) = \sigma_z(z_{oref})\,(z_o/z_{oref})^{0.2} \tag{3.29}$$

whereas the NRPB-R91 model (Clarke, 1979) adopts a correction based on work by Hosker (1974). This defines a function $F(x, z_o)$, which gives the ratio of σ_z at any roughness length to that at $z_o = 0.1$ m. This ratio is virtually independent of the atmospheric stability class.

Briggs (1973) provides specific algebraic functions for calculating plume spread in an urban boundary layer as a function of fetch and Pasquill stability class. The expressions are given in Table 3.2, and are valid for $z_o \approx 1$ m and $10^2 < x < 10^4$ m. The variation of σ_y with distance from the source is approximately linear at short distances, but varies at longer distances in accordance with

the classical statistical dispersion theory. As noted by Griffiths (1994), there are many typographical errors in the tabulation of these parameters throughout the literature, a situation which may lead to considerable error in the calculated values of plume spread by an uninformed user.

TABLE 3.2 Urban dispersion coefficients according to Briggs (1973)

Pasquill stability class	Urban σ_y (m)	Urban σ_z (m)
A–B	$0.32x(1 + 0.0004x)^{-0.5}$	$0.24x(1 + 0.0014x)^{0.5}$
C	$0.22x(1 + 0.0004x)^{-0.5}$	$0.20x$
D	$0.16x(1 + 0.0004x)^{-0.5}$	$0.14x(1 + 0.0003x)^{-0.5}$
E–F	$0.11x(1 + 0.0004x)^{-0.5}$	$0.08x(1 + 0.0015x)^{-0.5}$

All distances are in metres.

3.3.2 Street canyon and related models

The air pollution impact of emissions from most transport systems in urban areas involves source–receptor distances that are very short and pollutant concentrations that can be very high. Such local effects cannot be resolved by large-scale urban models, and are therefore usually treated by some form of street canyon or highway model. These sub-models must treat two driving forces for flow and dispersion, one due to the ambient wind and the other due to moving vehicles. A recent review of street canyon modelling has been published by Berkowicz (1997).

The simplest of street canyon models is probably a simple box model, which is an expression of conservation of pollutant flux. The spatially averaged concentration, C_b, in a straight, parallel sided street can be expressed in the general form:

$$d(V_S C_b)/dt = Q - a_1 U_p A_S(C_b - C_u) - a_2 U_n S_S(C_b - C_o) \tag{3.30}$$

where V_S is the volume of the street element under consideration, A_S its cross-sectional area, S_S its plan area, U_p and U_n the components of the roof level wind speed parallel and perpendicular to the street, Q the pollutant emission rate within the box, C_u the concentration at the upwind end of the element and C_o the background concentration above the street; a_1 and a_2 are constants. A recent application of box modelling is described by Hassan and Crowther (1998). Other terms might be included to represent exchanges with the background in calm conditions, plume chemistry and so on; the constants are usually determined empirically. Such models have their uses but provide no information concerning the spatial distribution of pollutants.

In urban street canyons local aerodynamic effects can result in dispersion patterns that are highly variable, though they can be related in a simplistic way to the above-canopy wind speed and direction relative to the street canyons. The typical flow pattern, with the overhead wind direction perpendicular to the street, was discussed in Section 2.3. For a line source of traffic pollution, the local street-side pollutant concentrations (eg of carbon monoxide) can vary significantly from one side of the street to the other. Experimental studies in San Jose and St Louis were used by Johnson *et al* (1973, 1976) to develop the following empirical expressions for the concentrations on the leeward side, C_L, and windward side, C_W:

$$C_L = C_o + b_S N_v V_v^{-0.75}/[(U_H + 0.5)\{(x^2 + z^2)^{1/2} + 2\}] \tag{3.31a}$$

$$C_W = C_o + b_S N_v V_v^{-0.75}/[W_S(U_H + 0.5)] \tag{3.31b}$$

Here C_o is the background concentration, b_S a constant, N_v the traffic flow rate, V_v the average vehicle speed, U_H the rooftop wind speed (m s^{-1}), x the horizontal distance (m) from the line source, and W_S the width of the street (m). These equations are used in one of the earliest canyon dispersion models, STREET (Johnson *et al*, 1973).

Concentrations on the leeward side of the street can be much larger than that on the windward side, due to the cross-street circulation. This type of local dispersion behaviour creates strong concentration gradients and is poorly predicted by large-scale models. Johnson *et al* (1976) give corrections for non-orthogonal approach wind directions and Hoydysh and Dabberdt (1994) and Scaperdas *et al* (1998a, b) have studied the problem of the urban intersection. Meroney *et al* (1996) note that in tall narrow canyons the vortex structure tends to be located in the upper part of the canyon. This results in relatively stagnant flow at ground level, and concentration levels much higher than those found in more open surroundings, all else being equal. Such conditions can be experienced in heavily built-up, city centre streets in light wind conditions with heavy traffic.

Local structure in the concentration field can be added to the box model by expressing the concentration experienced at a given point, C, as the sum of the mean value predicted by the box model, C_b, and a plume contribution due to direct advection from nearby sources, C_d, so that

$$C = C_b + C_d \tag{3.32}$$

Such an approach was first introduced by Yamartino and Wiegand (1986) and used in their Canyon-Plume Box Model, CPBM. It is also used in OSPM, the Danish Operational Street Pollution Model (Hertel and Berkowicz, 1991, Berkowicz *et al*, 1997a,b), AEOLIUS, the UK Meteorological Office model (Manning *et al*, 1998), ADMS-Urban (McHugh *et al*, 1997) and other models.

The direct contribution at distance x from a ground-level source (either a point source or an element of a line source) is typically expressed in terms of a Gaussian plume model. The chief modelling issues then become the definition of appropriate street level plume spreads. In OSPM the concentration contribution, δC_d, from an element of line source, δQ, is written as:

$$\delta C_d = \sqrt{(2/\pi)}\, \delta Q / U_S\, \sigma_z(x) \tag{3.33}$$

with $$\sigma_z = w'x/U_S + \sigma_o \tag{3.34}$$

where U_S is the street-level wind speed, σ_z the vertical plume spread, σ_o the initial spread and w' the vertical turbulence velocity. The turbulence velocity is related to both the wind speed and the traffic flow by

$$w'^2 = b_1 U^2 + b_2 V_v^2 N_v \tag{3.35}$$

where N_v is the vehicle density and b_1 and b_2 constants. Models of this type are now widely used for predicting air quality at street level. Their performance can be reasonably satisfactory (Berkowicz *et al*, 1997a,b; Buckland, 1998; Manning *et al*, 1998). However, a number of important issues have yet to be resolved; some of these relate to the source term, others are

(a) determination of the roof-level wind from standard meteorological data,
(b) evaluation of the street-level wind from the roof-level winds,
(c) effects of atmospheric stability and local building surface heating and cooling,
(d) limits to the geometrical configurations that can be treated.

3.3.3 Hybrid models

The problem with simple parameterisations of the urban surface is that no account is taken of the near-field details of the urban layout. These certainly influence the dispersion at near to intermediate distances from the source (microscale and neighbourhood scale), whereas in the far-field (urban scale) the simplified roughness length approach is probably adequate. Figure 3.4 shows a comparison between plume spread in neutral conditions as calculated from the Briggs urban equations and measured in a wind tunnel study with simple arrays of cubes of height H (10 m at full

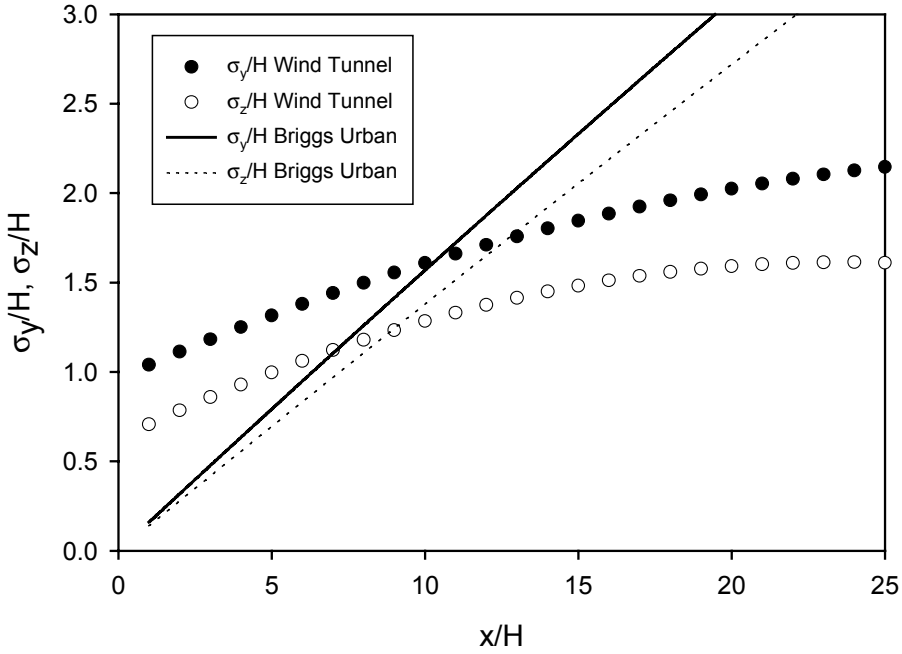

FIGURE 3.4 Briggs urban dispersion parameterisation compared with experimental data, from Hall *et al* (1998)

scale). The Briggs predictions tend to underestimate the dispersion very close to the source, where the local aerodynamic effects around individual obstacles dominate the plume path and initial dispersion. A similar observation was made by McElroy (1969) in analysing the St Louis urban data. Clearly, the agreement could be greatly improved if the Briggs model was used with some form of virtual source specification. However, dispersion patterns at this range tend to be highly site dependent so that a general and straightforward definition of the virtual source might prove difficult to find. Such an approach is far more plausible for intermediate distances, although there is often a need to incorporate the dependence of the dispersion parameters on the topography in this case.

Petersen *et al* (1991) recommend a hybrid modelling approach, in which fluid modelling is used to simulate the flow and dispersion in the near-field. This is then matched to a Gaussian plume model or simple numerical model at some intermediate distance. The hybrid model is thus able to account for the site-specific behaviour close to the source, while making use of the basic underlying model by interpolation. The main disadvantages are the initial cost and effort of conducting the wind tunnel simulation of the industrial installation around the release, and the time delay thereby imposed.

For the near-field behaviour, Theurer *et al* (1996) suggest that a basic database can be generated to account for the functional dependence of the plume spread on the near-field urban topology using

$$\sigma_y, \sigma_z = f_{y,z}(s, H, \sigma_H, W, \sigma_W, L, \sigma_L, W_S, \lambda_f, \lambda_p, \text{shape, pattern}) \qquad (3.36)$$

The argument list is not exhaustive, but includes the main parameters of interest. These are the distance from the source, s, the mean height of buildings H (with standard deviation σ_H), the mean building width W (with standard deviation σ_W), the mean depth L (with standard deviation σ_L), the packing (plan area) density λ_p, the frontal area density λ_f, the mean street width W_S, the mean obstacle shape, and the layout pattern (eg square or staggered). The wind direction is treated as a meteorological input and is not explicitly included in the list (although it may well be implicit in some of the other parameters).

Theurer *et al* (1996) describe a semi-empirical or hybrid Gaussian plume model, SAMPU, which combines the advantages of the basic plume model with wind tunnel modelling to account for the details of the urban topology near a source. In the near-field, where the dispersion depends strongly on the local arrangement of buildings, there is flow channelling and distortion of the plume. Here the use of the Gaussian model is not reliable. Further from the source, beyond a 'radius of homogenisation', the effect of the individual obstacles becomes negligible, and the flow field can be considered homogeneous. In this regime the Gaussian model can provide acceptable concentration predictions provided that the dispersion parameters are adjusted to ensure a smooth matching to the concentration distribution at shorter range. This involves the specification of an effective plume height, a lateral offset and virtual origins for lateral and vertical spread.

A programme of wind tunnel experiments was conducted by Theurer *et al* (1996) to determine the concentration distributions in the near field for different building arrangements, and thus to estimate the parameters for the semi-empirical model. The bulk of the tests used arrangements with high area density ($\lambda_f > 20\%$), high height variability ($\sigma_H > 0.20$) and high width-to-height ratio ($W/H > 2$). These types of arrangements have the strongest influence on the dispersion in terms of channelling and other building effects. The radius of homogenisation was determined for each case, and the German standard method, VDI 3783 (VDI, 1987), was used for the calculation of the Gaussian parameters in the far-field (treating the building pattern as a homogeneous roughness). The virtual origins were selected to ensure a smooth transition from the near-field to the far-field concentrations.

For point sources in built-up areas the SAMPU results are more realistic than those calculated by the unmodified Gaussian model and results can be obtained far quicker than with full, three-dimensional numerical calculations. Although small changes in building geometry may result in large changes in near-field concentrations, it is assumed that interpolation is possible between the results for different structures, approach flow directions, and height variability. There is thus a compromise between accuracy and effort to account for real geometries which differ from the idealised wind tunnel configurations. The SAMPU model is a useful alternative to full physical modelling, and can be used to give upper and lower concentration estimates close to sources where concentration distributions are not Gaussian shaped, but are dominated by local building effects.

4 Role of more complex approaches

Simple models cannot represent the details of flow and dispersion in building arrays. Something more complex is needed where this is an issue (eg in predicting the transport and dispersion of a narrow plume near a building) and realistic modelling is required. Installing and operating instrumentation in busy streets or industrial sites is difficult and expensive so that usually only a few locations may be selected. Modelling allied to such site measurements becomes essential in order to interpret results in circumstances where a high degree of spatial variability is normally present in the concentration field. In general, the flow field has to be predicted to a sufficient accuracy before pollutant dispersion can be determined. Predicting the concentration field cannot be separated from simulating the flow field.

There are three distinct approaches to dispersion modelling: field studies, physical simulation, and numerical modelling. Each has advantages and disadvantages and few would doubt that the most reliable (and most expensive and time consuming) approach to dispersion prediction involves all three to some degree. There is nothing particularly different in the application of these methods to a single building, a small group or a large array, except possibly the overall scale of the problem and the number of parameters involved. To a degree, there are even some possible

simplifications as the flow and dispersion are less sensitive to the upwind boundary conditions, and vortex shedding may be suppressed by surrounding obstacles.

4.1 Physical modelling

Wind tunnels are and have been most commonly used for the physical modelling of dispersion in arrays of obstacles, although water channels were used by civil engineers in some early studies of the flow and drag characteristics of arrays (see, for example, Morris, 1955; Sayre and Albertson, 1963). Water channels do offer some advantages for the visualisation of dispersion since simple dyes can be used and the much lower flow speeds produce longer time scales which are more suitable for video recording. Recently, a water channel was used at the University of Waterloo to study the flow and dispersion in a staggered cube array at 16% area density (Coulson, 1998). However, wind tunnel work predominates and the remainder of this section is written from that perspective, although the discussion is generally equally valid for water tanks and flumes. The application of wind tunnel techniques to the study of flow and dispersion in building arrays is briefly reviewed in Plate (1999).

A site model installed in a dispersion modelling wind tunnel is included as Figure 4.1. This clearly illustrates the level of detail that can be included (in this case at 1 : 500 scale). Physical modelling criteria for undertaking scale-model dispersion experiments and relating their outcome to their atmospheric counterparts have been widely discussed (see, for example, Poreh and Kacherginsky, 1981; Snyder, 1981; Obasaju and Robins, 1998). Although these are generally discussed in terms of an isolated stack or a single building, they apply equally to arrays of obstacles.

FIGURE 4.1 A detailed site model installed in an environmental wind tunnel

There are two aspects to be treated: (a) the simulation of the ambient flow and its modification in passing around buildings, and (b) the simulation of emissions into this flow. Neutral boundary layer simulation is a well-established procedure (eg using the systems developed by Counihan, 1969, or Irwin, 1981). However, the situation is not so satisfactory with regard to stable and unstable boundary layers. Here there are no established methods, although there is general agreement as to what broadly needs to be done, and where the pitfalls lie. Suitable facilities are much rarer than those where neutral boundary layer work is possible, experiments are more complex to carry out and more time consuming in their execution. Nevertheless, some convincing simulations have been reported by Ohya *et al* (1997) and Robins *et al* (2000) for stable boundary layers, and Fedorovich and Kaiser (1998) for the unstable case.

We will not discuss this any further, concentrating instead on the simulation of flow over buildings and emission modelling. Reynolds number independence of the flow past sharp edged obstacles is satisfied when the obstacle Reynolds number, R_H, is sufficiently large:

$$R_H = U_H H/\nu > 10^4 \tag{4.1}$$

where $U_H = U(H)$; Snyder (1981). The situation for rounded shapes is less well founded. Another Reynolds number limit arise in the maintenance of fully rough surface conditions in the ambient flow. This requires the flow speed to be large enough for the roughness Reynolds number, Re*, to be high enough Snyder and Castro (1997):

$$Re^* = u^* z_o/\nu \geq 1 \tag{4.2}$$

Both limits must be satisfied in an acceptable simulation. There are two rather weak constraints affecting the choice of simulation scale. These are that the ratios of the obstacle or building size relative to the roughness length and the boundary layer depth must be maintained in the laboratory simulation. The first, coupled with similarity of u^*/U_H in the ambient flow, ensures the required velocity profile over the building height, and the second the appropriate large eddy scales relative to the building dimensions. The latter is often relaxed, particularly when short-range building-affected dispersion is being simulated, the justification being that building-generated processes and scales dominate. However, this is a line of argument that cannot be taken too far without compromising the standard of the simulation.

In some ways obstacle arrays may be easier to work with than single buildings. Deep within an array of obstacles, the turbulence is mainly due to the upwind obstacles themselves and there is little 'memory' of the approach flow turbulence characteristics, except at the largest scales in the lateral direction. This means that where only flow and dispersion within the array are of issue, the simulation of the approach flow is not as critical as it is for an elevated source over simple terrain. The high levels of turbulence created by the obstacles implies that large departures from neutral stability will frequently not need examination. There is also likely to be less dependence of the flow on the surface details of the models. The obstacle Reynolds number needed for Reynolds number independent flow will often be lower than the value given above because of the high levels of turbulence generated within the array which promote fully turbulent flow over the obstacles.

Emission simulation frequently determines the operating speed of a wind tunnel study. For example, the appropriate parameters to conserve when modelling a buoyant discharge are

$$F_B/U^3H, \qquad F_M/U^2H^2, \qquad \Delta\rho/\rho \tag{4.3}$$

where F_B is the source buoyancy flux, F_M the source momentum flux, $\Delta\rho$ the density difference between the emission and the ambient flow, and ρ the ambient density. In many circumstances

conservation of the density ratio can be ignored which leads to a more favourable relation between the tunnel operating speed and the wind speed, since conservation of F_B/U^3H and F_M/U^2H^2 gives

$$U_M/U)^2 = \gamma\varphi \tag{4.4}$$

$$\varphi = [(\Delta\rho/\rho)_M]/[\Delta\rho/\rho]\,[(\rho/\rho_s)/(\rho/\rho_s)_M]^{1/2}$$

where γ is the geometrical scale ratio ($\gamma < 1$), the suffix 'M' denotes the model and 's' the source. With $\Delta\rho/\rho$ conserved we have $\varphi = 1$ and $U_M/U = \gamma^{1/2}$, implying very low tunnel speeds, but with $(\Delta\rho/\rho)_M \geq \Delta\rho/\rho$ we see that $\varphi > 1$ and hence the required tunnel speed is increased.

Wind tunnel studies of dispersion at industrial sites, commonly nuclear power plant, have been widely reported. A review of such work up to 1985 is given in Foster and Robins (1985); another important review is Hosker (1984). In nearly all the cases described the site is dominated by a single large building and little is learnt about the manner in which groups of buildings affect dispersion. These earlier studies are more useful for assessing the treatment of complex building shape and, in some cases, complex flow conditions. Some more recent and relevant work is described in Section 5.

One of the problems often encountered in generic studies with simple arrays is to limit the large number of trials required by a factorial-type experimental design. Not only may the mean obstacle shape (L, W and H) be varied, but the variability of these dimensions (σ_L, σ_W, and σ_H) and a variety of packing densities and element spacing in the array may also be considered. These factors must be combined with changes in mean wind angle, source location within the array, distance from the source, etc. In order to avoid impracticably large numbers of runs, it is necessary to isolate the most influential parameters and to limit the number of variations. This exercise is not helped by the rather limited degree of fundamental information available.

Difficulties can arise with interpolating the limited data from a factorial experiment. For example, even if five wind angles (0º, 30º, 45º, 60º and 90º) are selected, there may be strong discontinuities between the measured results for wide obstacles ($W/H >> 1$). In arrays of this type there may be large deflections of the plume for small changes of wind angle from normal to the rows. Actually, obtaining lateral symmetry in the concentration field within an array aligned normal to the approach flow is not easy or, indeed, always achieved. As Rafailidis and Schatzmann (1996) note, it is almost impossible to avoid lateral drift in street canyon flows with two-dimensional obstacle arrays.

The lateral scales of turbulence in a wind tunnel simulation are determined entirely by boundary layer processes, which means that they depend on height above the ground and the boundary layer depth. Additional factors come into play in the atmosphere, generating temporal and spatial variability, which increase the lateral scales beyond the values attained by boundary layer turbulence alone. As a result, concentration data from a scale-model experiment are representative of relatively short sampling times in the atmosphere. The precise equivalence is debatable but is probably in the range from 10 to 30 minutes. For long time averages (> 1 hour), the lateral concentration profile in the prototype problem is likely to be largely governed by the probability distribution of wind direction, which is often nearly Gaussian. In order to account for the lateral wind direction variability, it is necessary to look in some detail at the effect of variation in wind angle about the mean direction. A simple approach to account for this behaviour has been used by Mitsubishi Heavy Industries in Japan (Okabayashi *et al*, 1991). In their facility the relevant model and its surrounding terrain are mounted on a large turntable on the wind tunnel floor, which allows continuous variation in the approach wind angle θ to the model. If $C(x, y, \theta)$ is the concentration at ground level at a point (x, y) downwind of the source for the mean wind angle

θ, then the concentration at the same point when the wind direction varies about the mean, C_θ, is given by

$$C_\theta = \int F(\theta)\, C(x, y, \theta)\, \mathrm{d}\theta \tag{4.5}$$

Here $F(\theta)$ is the probability distribution of the wind direction variations. In this way, the influence of the large-scale wind direction variations which contribute to plume meandering can be synthesised in the wind tunnel.

4.2 Field experiments

One way to avoid some of the problems of scaling and resolution in a wind tunnel model (both in time and space) is to perform experiments in obstacle arrays erected in the atmospheric boundary layer. This method has been used successfully by Davidson *et al* (1995), Macdonald *et al* (1997, 1998b) and Briggs *et al* (1997). The basic idea is to choose an appropriate intermediate obstacle scale (about 1 : 10) using suitable obstacles which can then be laid out on flat terrain such as a mowed field. In this way the full spectrum of atmospheric turbulence conditions can be used, including naturally occurring stable or unstable conditions. The scaling problems are discussed in a report by Hall and Walker (1995), with applications to dense gas experiments. In the field there is no control over the wind direction and speed at any given time, so it is usually necessary to wait for the appropriate winds. In addition, experimental conditions can never be exactly replicated and ensembles of experiments in nominally similar conditions have to be analysed to derive satisfactory statistical properties of the dispersion process. Without such ensemble averaging, field experiments effectively become a collection of individual realisations and their use in model development or evaluation is greatly weakened by the inherent uncertainty attached to each. These factors greatly reduce productivity relative to wind tunnel work. Nevertheless, field data are an essential component of model testing and development because they encompass all the features of dispersion in the atmosphere. Important advantages may accrue when measuring concentration fluctuations, since the ranges of turbulence space and time scales are larger than in a wind tunnel and this implies considerably increased fluctuation levels, especially for plumes from small sources. There are also portable field instruments now available which can continuously measure concentration fluctuations up to 100 Hz (Griffiths *et al*, 1998).

Full-scale urban dispersion experiments at intermediate distances using point source tracers are quite rare and only a handful of studies are available (see, for example, Barrett, 1970; Yersel *et al*, 1983). It is difficult to find suitable tracers that can be measured at low concentrations, since dilution rates are very high. It is equally difficult to locate arrays of detectors in a busy urban environment, especially for measuring vertical concentration profiles. Characterisation of the mean wind field and turbulence is also difficult, as usually only a limited number of anemometer positions is available. Results with some tracers may be interfered with by naturally occurring background levels and local sources near the detectors. These can cause larger concentrations at the detectors than those due to the controlled source, completely invalidating the data. Despite the many problems of working at full scale, such experiments are essential for the validation of complex dispersion models and for obtaining insight into the natural variability of the dispersion process.

4.3 Computational modelling

The use of numerical solutions of modelled forms of the fundamental equations governing flow, heat and mass transfer is really in its infancy as far as building-affected, short-range atmospheric dispersion is concerned. The topic was reviewed by Hall (1997) who discussed the

practice and application of numerical modelling. The main application area has probably been the assessment of the hazards posed by accidental emission of hazardous material, in particular flammable gases.

The main practical difficulty is very simple. Consider estimating urban or building-affected dispersion to assess concentrations or doses relative to regulatory or other limits. To do this many hundreds, if not thousands, of calculations are usually carried out to cover the full range of meteorological conditions that are experienced at a given site (ie wind speed, wind direction, stability, precipitation etc). The whole calculation needs to be carried out in a reasonable time and this is just not feasible with numerical modelling, where one relatively simple case may take several hours to complete and a complex case the best part of a day. Computing power continues to improve, but the time when environmental assessment may be conducted solely through numerical modelling remains very distant.

The most likely impact of numerical simulations is as an alternative to wind tunnel modelling. Indeed, this already happens, probably driven more by the economics of the matter than by considerations of accuracy and reliability. We can expect this trend to continue, sometimes in the form of dual wind tunnel and numerical investigations. The latter approach is very promising, because of the in-built checks on accuracy and applicability, and is to be encouraged. For the present, we need a better understanding of the errors and variability implicit in the application of numerical techniques so that we can judge their use from an informed position.

4.3.1 Transport equation modelling

Diffusivity theory can be regarded as the first level of complex modelling beyond Gaussian plume and related methods. At first sight, it offers more flexibility in treating a variety of source types, time-dependent emissions and meteorological conditions, as well as the full structure of the atmospheric boundary layer. Assuming the flow field is known or can be specified, the model solves the advection-diffusion equation:

$$U\,\partial C/\partial x + V\,\partial C/\partial y + W\,\partial C/\partial z - \partial/\partial x(\kappa_x\,\partial C/\partial x) - \partial/\partial y(\kappa_y\,\partial C/\partial y) - \partial/\partial z(\kappa_z\,\partial C/\partial z) = 0 \qquad (4.6)$$

where κ_x, κ_y and κ_z are the turbulent diffusivities associated with diffusion in the x, y and z directions, respectively. Specification of these diffusivities is based on atmospheric observations and surface characteristics. The parameterisation of the surface characteristics typically involves estimating the relevant value of the friction velocity, u^*, and the surface roughness, z_o. Several approaches are available for this (see, for example, Arya, 1975). The usual approach to surface roughness estimation is to assign roughness values to relatively homogeneous sub-areas and then to combine these using some form of horizontal averaging to arrive at an effective roughness value for the whole area (Wieringa, 1993). Existing methods for estimating roughness lengths of built-up areas have been reviewed by Petersen (1997); improved models are provided by Bottema (1996, 1997) and Macdonald *et al* (1998a).

Diffusivity theory may be useful in situations where standard Gaussian models are not appropriate, such as for ground-level releases where the mean wind speed and turbulent diffusivity can vary strongly with height above the ground (the standard Gaussian model assumes homogeneous turbulence). However, advanced Gaussian models (such as ADMS) already take account of boundary layer structure and in many ways are comparable in performance with standard diffusivity theory.

For specific microscale problems, such as dispersion around a building or a group of buildings, the flow properties (U, κ_x, κ_y and κ_z) cannot be specified and have to be calculated.

This involves linking the diffusion calculation to a flow field prediction, the most common form of which is based on the two-equation k–ε turbulence model. Computing times are now dominated by the flow field calculation and become substantial (at least several hours per case). To a degree, the availability of high power work stations may offset this penalty, although in practice most of the increases in computing power are utilised in the search for more accurate solutions (ie reducing the numerical errors associated with solution procedures). Accurate solutions can sometimes be obtained in which modelling errors are off-set by numerical errors (see, for example, Cowan *et al*, 1997) but this does not form the basis of an acceptable simulation technique as there is no formal procedure for ensuring that the balance can be achieved. Further, approaches of this form should be regarded as bad practice, although there is a fine line between this and an acceptable practice that attempts to keep error levels equivalent across solutions through enforcing CFD modelling guidelines.

As noted previously, the solution of the dispersion problem follows directly from the initial calculation of the flow field, provided the concentrations are low enough not to change the fluid properties. The flexibility of the computing environment allows one to change parameters, such as the Schmidt number, arbitrarily to investigate their influence on the concentration field, which may be very difficult to do in a physical model. Because of the direct simulation of the different mechanisms of convective transport and diffusion, it is possible in a numerical solution to isolate the relative contribution of these two mechanisms to the transport of the pollutant. This has been done by Lee and Park (1994), in the case of a street canyon dispersion model. The numerical simulation can also calculate very low velocity secondary flows, such as secondary vortices in street canyons which can be difficult, if not impossible, to measure in physical models. Additionally, the simultaneous calculation of the pressure and drag forces in a numerical simulation provides useful information that can be used in later analyses. For example, it may be necessary to correlate the pressure field and concentration field on the surface of a building in an array, when considering the problem of street pollution infiltration into buildings via windows and vents.

Complex issues that may be difficult to treat experimentally may be tackled. As an example, the interaction between the wind driven, two-dimensional street canyon circulation and buoyancy forces generated by solar heating of the surfaces of the canyon has been studied computationally by Sini *et al* (1996). Computations for a street running from north to south and a wind speed normal to the street of 5 m s^{-1} (at 100 m) showed that a temperature difference of around 5 K was sufficient to disrupt the canyon vortex and significantly weaken the mixing between the canyon flow and the boundary layer above. This arose when the buoyancy forces opposed the basic wind driven circulation. In a subsequent paper, Mestayer and Sini (1998) simulated pollution concentrations due to traffic emissions in the canyon during a diurnal cycle. The results showed the changing character of the flow within the canyon and the consequent effects on air quality, in particular the occurrence of periods of poor air quality when the buoyancy forces effectively cut off the flow near street level from that in the upper part of the canyon. The calculations, run on a CRAY C98, provide a good illustration of how advanced computational methods can be applied to a complex problem to yield important insight into air quality issues, although the predictions have yet to be confirmed through comparison with experiment.

The use of complex numerical models for making regulatory decisions with serious economic and political consequences is still relatively uncommon, although it is easy to be over-optimistic about the capabilities of numerical modelling. In a recent paper discussing the use of a commercial code for the analysis of pollution around the exit of an urban traffic tunnel, Delauney

(1996) concludes that 'it is now possible to simulate gas dispersion in urban environments using a (Reynolds-averaged) Navier-Stokes solver.' A number of codes are currently being marketed which claim to be capable of simulating the dispersion of pollutants in topographically complex areas such as cities, and to allow the calculation of gas concentrations in the near-field of a release in a complex area. However, a note of caution is necessary, as there are a number of reasons why it is unlikely that numerical simulations will soon overtake the more simple Gaussian plume models in regulatory applications; some are discussed below.

Numerical models are not limited in their potential ability to model the physical phenomena occurring in complex flow and dispersion problems, in contrast to the more simple parameterisations commonly used. Even standard k–ε models can provide resolution of concentration gradients in regions of separated and secondary flows, without making the gross assumption of uniform concentration that is sometimes used in simple wake cavity and street canyon parameterisations. However, in complex flows with separation and recirculation their accuracy is compromised by turbulence modelling and numerical errors. Standard k–ε models are unable to handle flows in which large-scale structures dominate the turbulent transport or where high streamwise strain rates are important and a number of modifications have been proposed to overcome such limitations. However, these have yet to be fully evaluated in the present context. More advanced numerical modelling techniques (eg large eddy simulation) can reproduce the spatial and temporal behaviour of the large turbulent scales and some applications to environmental problems are appearing. Phenomena such as vortex shedding and wake flushing have been simulated (Rodi *et al*, 1997). However, these methods are primarily research tools and at the present time they can only be used by highly skilled personnel. Calculations are extremely time-consuming (eg 160 hours for one large eddy simulation of flow over a cube; Rodi *et al*, 1997). Even then, the solutions may not provide estimates of the natural variability of the results and the uncertainty associated with any calculated concentration. For the foreseeable future numerical modelling will employ k–ε (and its derivatives) and Reynolds stress modelling.

There are advantages to the computational approach, not least of which are the lower overheads associated with a microcomputer compared to a wind tunnel modelling facility. Computational fluid dynamics has now reached a state where it is claimed that problems such as flow and dispersion in large groups of obstacles can be solved with acceptable precision (Hall, 1997). Unfortunately, only small numbers of such solutions are ever published in the open literature, and these usually show only the best results obtained. Several examples of computational modelling of flow and dispersion in urban or built-up sites can be found in the air pollution literature: see, for example, the Proceedings of the First International Symposium on Computational Wind Engineering, Tokyo 1992, Guenther *et al* (1990) and Delauney (1996). These are in addition to the many detailed studies dealing with the idealised cube (Murukami and Mochida, 1988; Raul and Bernard, 1991), specific work on street canyon flows (Lee and Park, 1994; Johnson and Hunter, 1995), and modelling of street intersections (Scaperdas *et al*, 1998a,b).

4.4 Model evaluation

An acceptable level of model evaluation is needed before a method can be accepted for serious regulatory applications. It can be difficult to put complex models through sufficiently detailed and wide-reaching validation procedures involving comparison with data sets from experiments or analytical solutions to dispersion. This is especially a problem for large obstacle arrays where the detailed data may not even exist. Model benchmarking and testing in basic generic flows remains an academic pursuit (Rodi *et al*, 1997; Hanjalic *et al*, 1998) and funding for such

purposes is limited. Schatzmann *et al* (1997) discuss some of the considerations that make model validation difficult. To make a proper evaluation of a model one requires:

(a) detailed model description (including the modelling concepts, the performance of algorithms, and inherent limitations),
(b) model verification (that the computer code correctly represents the specification),
(c) scientific verification (that appropriate basic conservation and physical principles are satisfied),
(d) model evaluation, by comparison of the results with data sets.

The model evaluation stage is one of the most difficult parts of the process. Comparison of the model with field and laboratory data is complicated because there are fundamental differences in such results related to instrument time and space resolution, and there is also an inherent variability in any field measurement. The question of averaging time becomes important, and field results often show considerable sensitivity to this. Laboratory experiments often result in higher concentrations compared to field results because of the lower intermittency and the reduced plume 'meander'. To what data should the computer model be compared?

For very complex models, with many equations and empirical coefficients, it is extremely difficult to undertake validation tests without also a comprehensive statement of modelling practice. For example, solutions depend on decisions made by the model user, such as the choice of numerical methods or grids. Statements of performance must be linked to these issues and there is no guarantee that the achievement of an acceptable solution has any validity outside of the circumstances under which it was obtained (see, for example, Cowan *et al*, 1997; Robins *et al*, 1998b; Castro *et al*, 1999). Solutions change with adopted solution procedures and the problems are too complex to obtain solutions which are not dependent on the grid and set-up.

Uncertainties in computational modelling of gas dispersion have recently been investigated in Project EMU (Evaluating Modelling Uncertainties; Hall, 1997, 1998). In this work a single, commercial computational fluid dynamics code was applied by each of four research teams to the calculation of a series of specified problems concerning building-affected dispersion. Problems

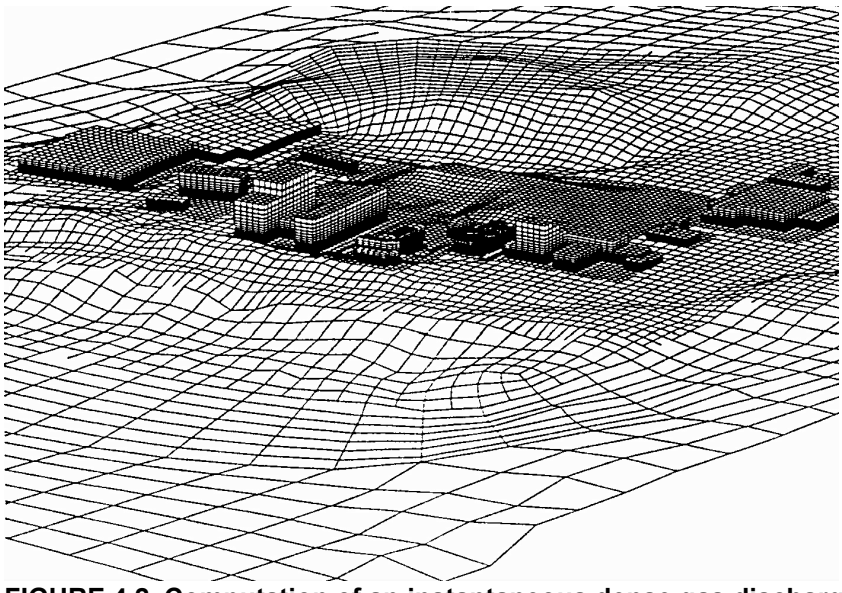

FIGURE 4.2 Computation of an instantaneous dense gas discharge at an industrial site, showing a typical mesh arrangement; note the simplified topography which results

ranged in complexity from a passive release from a doorway in an isolated, L-shaped building to an instantaneous heavy gas discharge at an industrial site, the latter shown as Figure 4.2. Results for one of the simpler problems, a dense gas discharge from a 1 m diameter source in a wall of the L-shaped building, are shown in Figure 4.3. In the figure the plume centre, ground-level concentration is plotted as a function of fetch from the building. Eight sets of predictions are shown (two attempts from each partner, denoted P1,1, P1,2 etc), together with wind tunnel data. Clearly there are considerable differences amongst the solutions and hazard ranges (the fetch to a given concentration level) vary by well over an order of magnitude.

Overall, solutions were found to be very sensitive to the modelling decisions employed by the teams and, as a consequence, calculated hazard ranges often varied by an order of magnitude between solutions. This clearly demonstrates the need for 'codes of best practice' to ensure a degree of uniformity in both evaluation studies and practical application. Continuing research in these areas will lead to increasing credibility and general acceptability of numerical models for complex flow and dispersion problems. Similar comments apply to any complex modelling method whose application depends on numerous user decisions. Even advanced Gaussian-based dispersion models, such as ADMS, are affected to a certain degree.

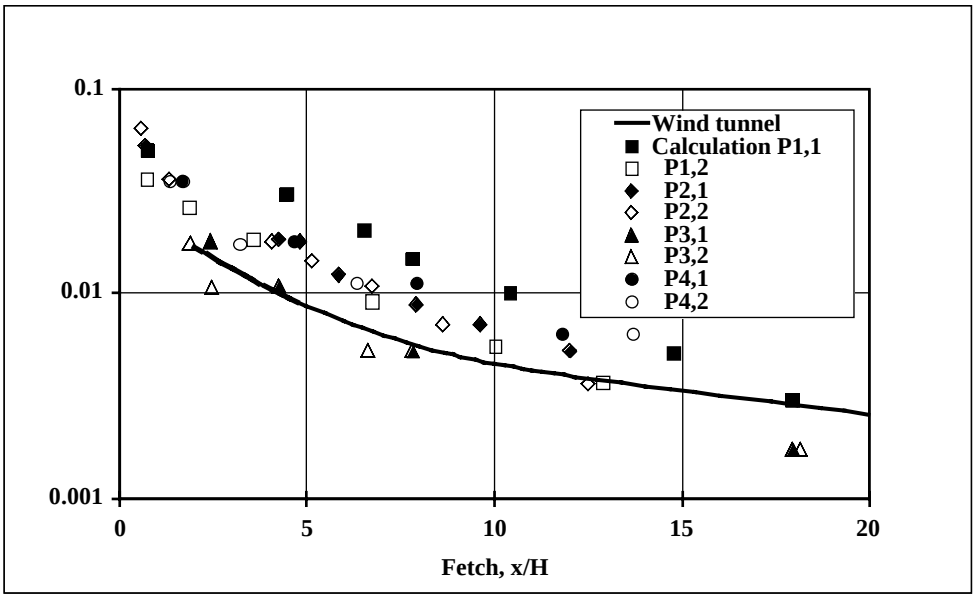

FIGURE 4.3 Sets of hazard ranges predicted for a dense gas jet from a wall of an L-shaped building. All calculations performed with the same computational model; from Hall (1996)

4.5 Model development

Desirable attributes of models to be used for regulatory and related purposes include:

(a) robustness in estimating concentrations and their probability of occurrence (providing reasonable concentration estimates over a wide range of conditions with minimal discontinuities),

(b) straightforward implementation with reasonable input data requirements and computer resources,

(c) a clear statement of best practice,

(d) utilisation of current knowledge, capturing the essential physical processes whilst avoiding unnecessary complexity,

(e) structural flexibility that will allow ready revision as and when the science evolves.

There is usually a considerable time-lag between advances in understanding of atmospheric boundary layer processes and the inclusion of such developments in regulatory models. This is not surprising given a typical time scale of at least five years for the development, verification and initial evaluation of an advanced dispersion modelling system. The monetary investment is also a very significant factor, being around £1,000,000 (Schulze, 1999).

The standards used in selecting a regulatory model make it very difficult for new models to become generally accepted, and presently rule against using most of the sophisticated numerical techniques for such purposes. Numerical simulations do not generally satisfy the criteria of robustness, high standard of validation, ease of implementation (especially as detailed boundary and source condition data is required), fundamental simplicity and ease of revision and modification. They are also too time consuming in application. To reiterate, a typical regulatory application may require running a model for an industrial site for a range of wind speeds and directions, and stability and emission conditions. This may well amount to several hundred different calculations (given that some combination of events do not arise). Clearly attacking such a task with a computational fluids package that takes, say, five to ten hours per case is impractical. As noted by Hall (1998), it takes four to six months to properly train someone to use such a package, and even then user errors are quite common, such as inputting the wrong sign for the surface heat flux. Presumably, with the continuing development of pre-processors and graphical user interfaces, many of these undesirable traits will eventually disappear and it will become less objectionable to use numerical simulations for regulatory purposes. Overall run times will remain a key factor and for the foreseeable future this will exclude routine use of complex computational methods.

5 Results of recent experimental work

5.1 Emissions above building arrays

The prediction of atmospheric dispersion in the vicinity of building groups is frequently required in assessments of the environmental consequences of emissions from industrial sites. Secondary flows (ie lateral and vertical mean motions) and increased turbulence levels are typical features of the perturbations to the approach flow generated by site buildings. These perturbations decay downstream of the site, but their overall effect is generally to increase (often by substantial amounts) ground-level concentrations due to site stack emissions. The bulk of the detailed research concerning building-affected dispersion has concentrated on single large buildings or extensive arrays of identical buildings, with releases at or below roof level. These situations are not typical of operational discharges from industrial installations, where the dispersion of stack emissions over and downwind of the site is of common concern. The work summarised here was undertaken in response to this situation and concerns the dispersion of elevated plumes above groups of buildings and is reported in full in Hayden (1998) and in part in Robins *et al* (1998a).

A series of wind tunnel experiments was used to investigate the requirements of 'practical' dispersion models, in particular for the determination of ground-level concentration or exposure downwind from a site. The experiments were carried out in the University of Surrey's EnFlo stratified flow wind tunnel, which has a 20 m long working section, 3.5 by 1.5 m in cross-section. The majority of the study was generic in nature, with flow and dispersion measurements being made in the undisturbed flow, in the wake of a single block and in the wakes of arrays of nine blocks, all the blocks being simple 1 : 500 scale models of a reference building at the Sellafield site of British Nuclear Fuels Ltd. Similar measurements were made over a 1 : 500 scale model of the site.

Building-affected dispersion studies began with the single building case, then concentrated on a number of building groups, as summarised in Table 5.1. In the table, a separation factor of one implies that the spacing between blocks in an array is the same as the equivalent block dimension. The final two arrangements in the list occupied the same plan areas as the nine block arrays of separation factors one and two, respectively, and were introduced as potential limiting representations of those arrays. Figure 5.1 illustrates the arrays studied and defines a notation for referencing them. All sources were located above array or block centres and emitted horizontally at the local flow speed. The model of the Sellafield site is shown in Figure 4.1.

TABLE 5.1 Experiments carried out in the neutral boundary layer

Number of blocks	Separation factor, S	Wind directions (degrees)	Measurements
1	0	0, 45	Velocity and concentration
9	0	0, 45	Velocity and concentration
9	1	0, 45	Velocity and concentration
9	0.5, 2	0, 45	Concentration
(25)	0	0, 45	Concentration
(49)	0	0, 45	Concentration
Building block dimensions: 125 tall by 94 by 64 mm Boundary layer depth: 1 m; roughness length: 0.35 mm; u^*/U_{ref} = 0.046			

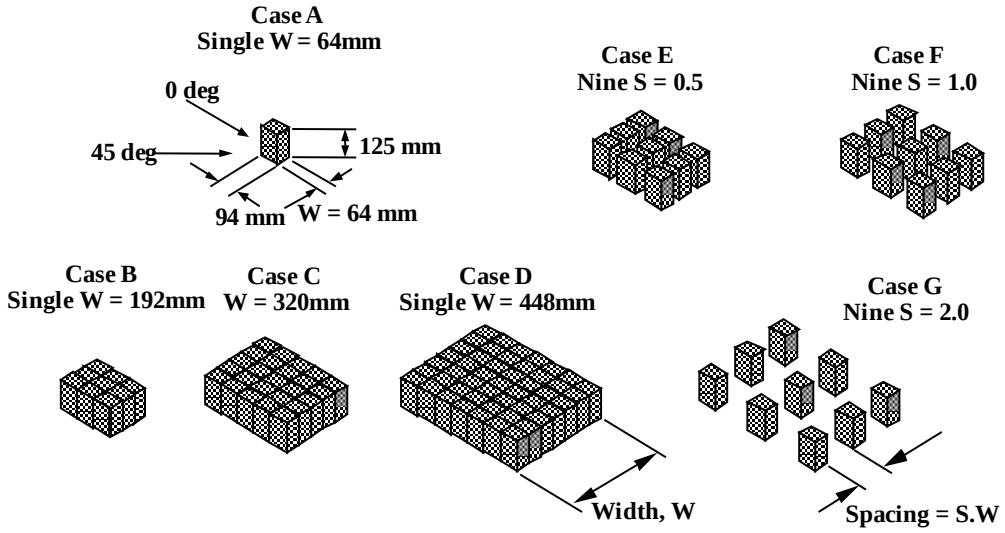

FIGURE 5.1 Details of the arrays studied by Hayden (1998) and the notation for describing them; S is the spacing factor

Wake flow and dispersion characteristics of the Sellafield reference building were then studied over a 1 : 500 scale model of the site and surrounding terrain, firstly with the building located in its true position, B1, and subsequently with an identical building located in a number of other positions around the site. Ground-level concentration mappings were obtained between $x = 0$ and 4 m, for source heights between 1.2H and 2.6H, for four wind directions and four building positions; the configurations are defined in Table 5.2. In its true position, B1, the reference building is surrounded by somewhat shorter buildings, typically H/2 tall. As B1 is located towards the north-west side of the whole site, the first set of results provided two pairs of contrasting cases in which the majority of the site was either upwind or downwind. In the other three cases, all for wind direction 330º, the additional reference building was located in three contrasting locations.

TABLE 5.2 Cases investigated with the site model (wind directions measured relative to site north)

Building location	Wind direction (degrees)	Source height range, *h*/*H*
True location, B1	90, 270, 150, 330	1.2 – 2.6
Denoted D1	330	1.2 – 2.0
Denoted D2	330	1.2 – 2.0
Denoted U1	330	1.2 – 2.0

In two cases it was placed just downwind (location D1) and just upwind (location U1) of a very extensive, flat-roofed building and in the other case (location D2) just downwind of a building of similar height to itself.

Maximum ground-level concentrations and their location were determined as functions of stack height, geometry and wind direction. These were then used in conjunction with equivalent sets of data for emissions in the undisturbed boundary layer to evaluate effective stack heights. The effective stack height was defined as that which in the undisturbed flow produced the same maximum ground-level concentration as measured in the wake flow. Results were also analysed in the context of standard Gaussian plume modelling, the objective being to examine which modifications were critical in adapting such models to the successful prediction of building wake dispersion. The Gaussian plume parameters which best described the undisturbed flow data were taken as the starting point and the consequence of changing each of them was then examined. This showed that the strength and persistence of the vertical velocity perturbation was the key factor for the successful prediction of the full concentration field downwind from the arrays. Put another way, the most important feature to model correctly was plume downwash over the longitudinal extent of the wake.

Relative to results for an isolated stack, maximum ground-level concentrations were increased downwind of the single block for all the stack heights examined. The influence of the building groups was analysed in terms of the reductions in effective stack height, $\Delta h/h$, which they brought about. Figures 5.2 and 5.3 show the results for wind directions of 0º and 45º. Dispersion behaviour was modified by the presence of the obstacles in all the experiments undertaken; ie for stack heights $h \leq 2.6H$ for the single buildings and $h \leq 3.2H$ for the arrays.

For a wind direction of 0° there was a clear minimum in the variation of $\Delta h/h$ with spacing, at a spacing factor, S, of about 1. The most appropriate simple modelling assumption for arrays with $S > 0.5$ was to ignore the array and use a single block model, whereas for $S \leq 0.5$ the best option was to use the equivalent array with zero spacing. However, in the 45° case a minimum in $\Delta h/h$ was only apparent for source heights below about $1.5H$, the minimum occurring at about $S = 1.5$. For this orientation the most appropriate simple modelling assumption for arrays was to treat them as the equivalent array with zero spacing.

Figure 5.4 illustrates the relative importance of modifications to a standard Gaussian dispersion model, applicable to the undisturbed flow, in predicting behaviour downwind of buildings. Vertical and longitudinal concentration profiles are shown for a single obstacle at 45° to the approach flow with a release height of $h = 2H$. Similar analyses were applied to the full set of observations. Overall, the main conclusions are that:

(a) plume height reductions are the predominant cause of increased ground-level concentrations,
(b) vertical spread is largely unaffected by the presence of the buildings,
(c) lateral spread is significantly enhanced in plumes released at heights of around $1.5H$ or less.

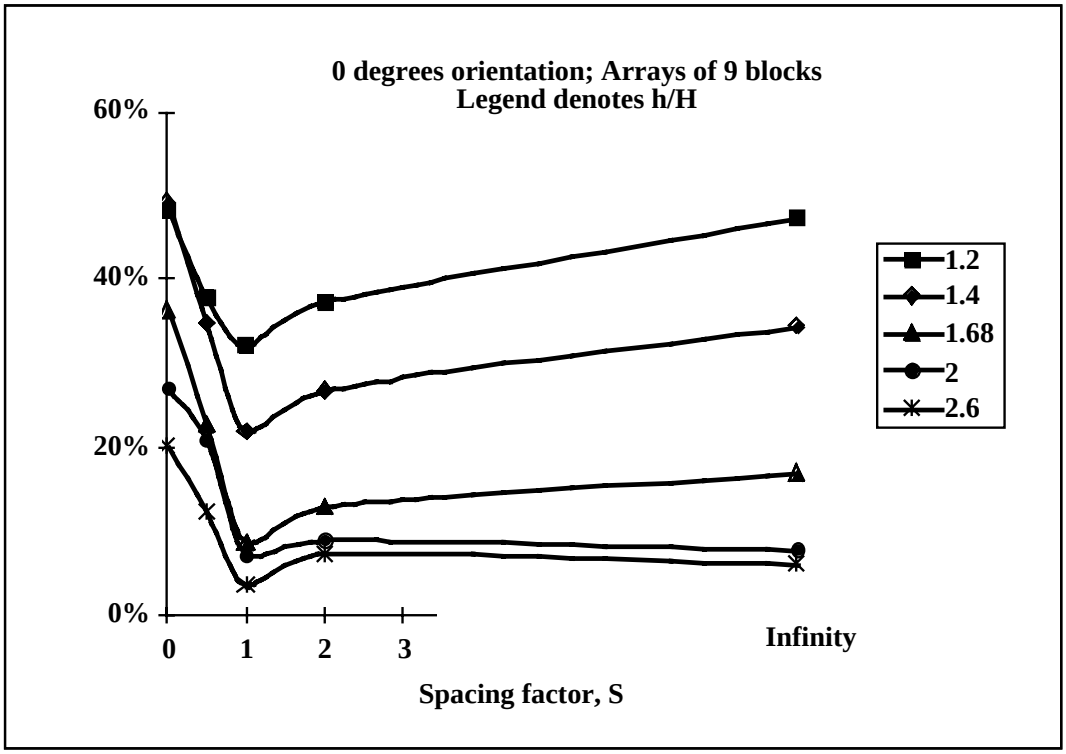

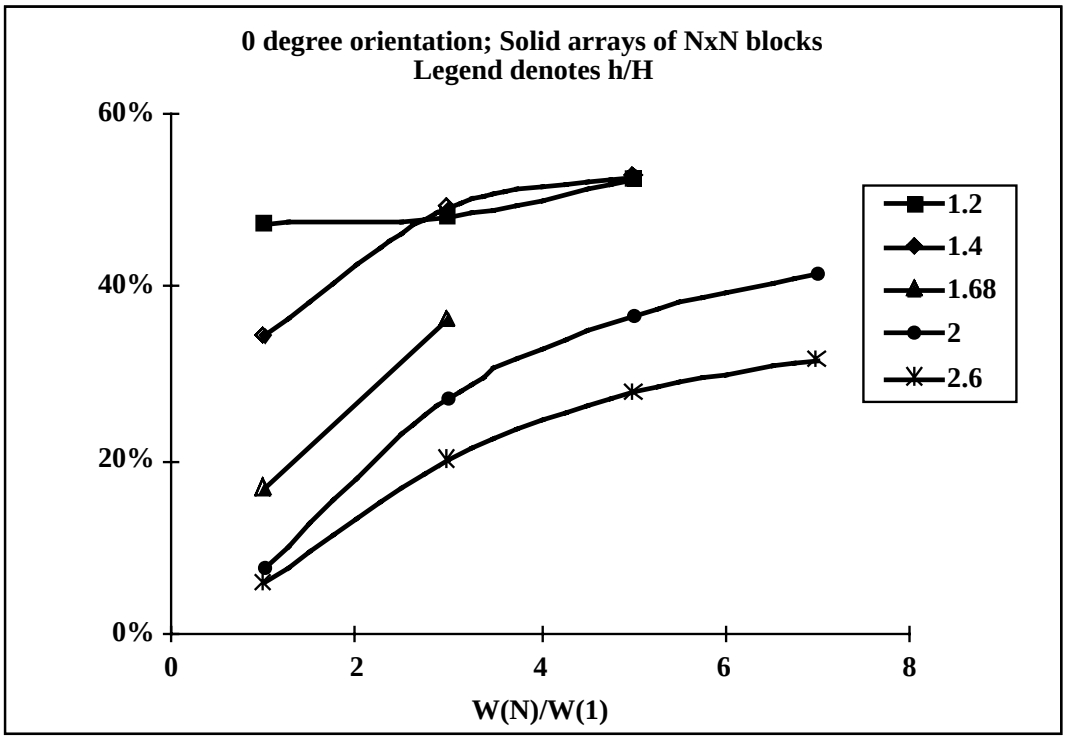

FIGURE 5.2 Reductions in effective stack heights as a function of spacing factor, *S*, and source height, *h/H*, over arrays of nine blocks (top) and solid arrays (bottom), with the wind at 0º to the front face (Robins *et al,* 1998b)

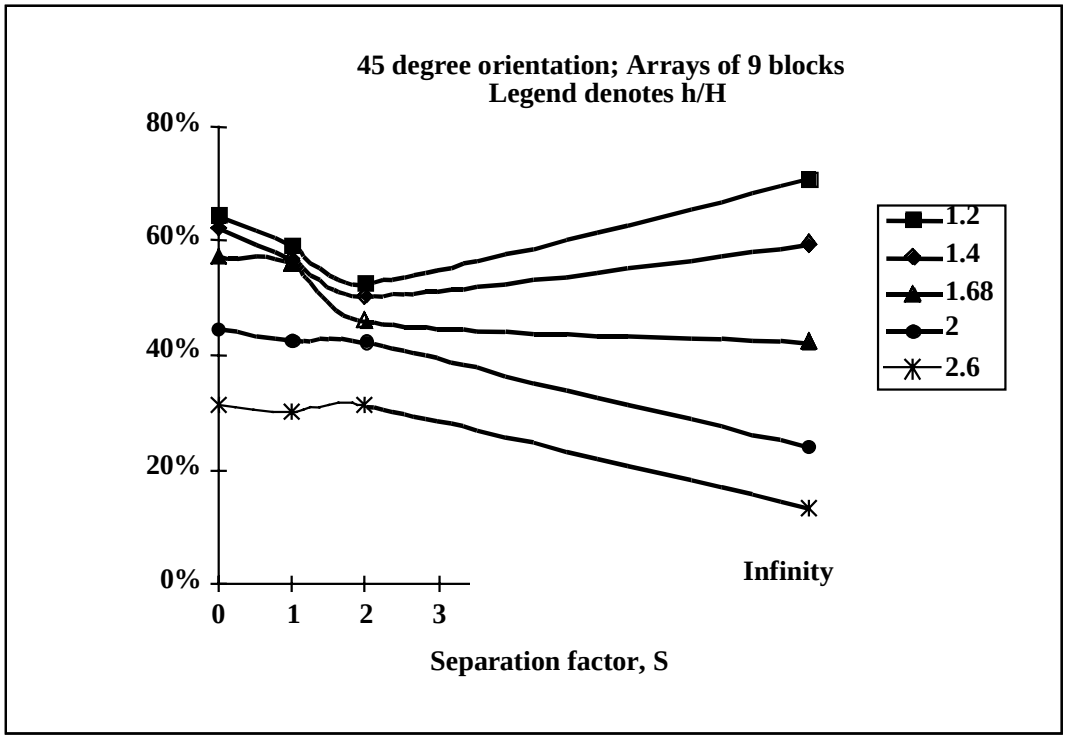

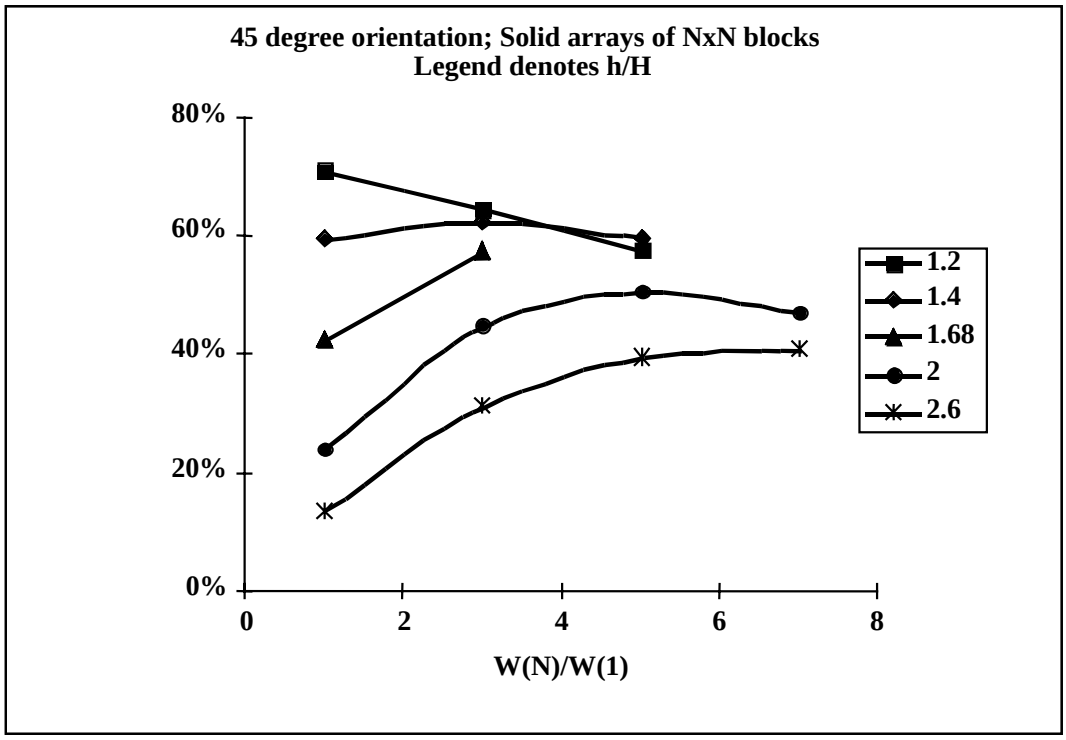

FIGURE 5.3 Reductions in effective stack heights as a function of spacing factor, *S*, and source height, *h/H*, over arrays of nine blocks (top) and solid arrays (bottom), with the wind at 45º to the front face (Robins *et al,* 1998a)

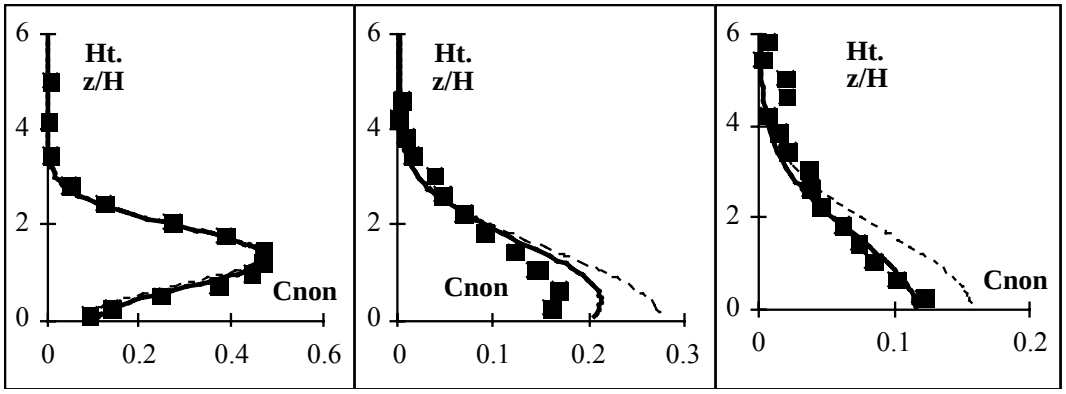

Vertical concentration profiles at x/H = 10, 20 and 32

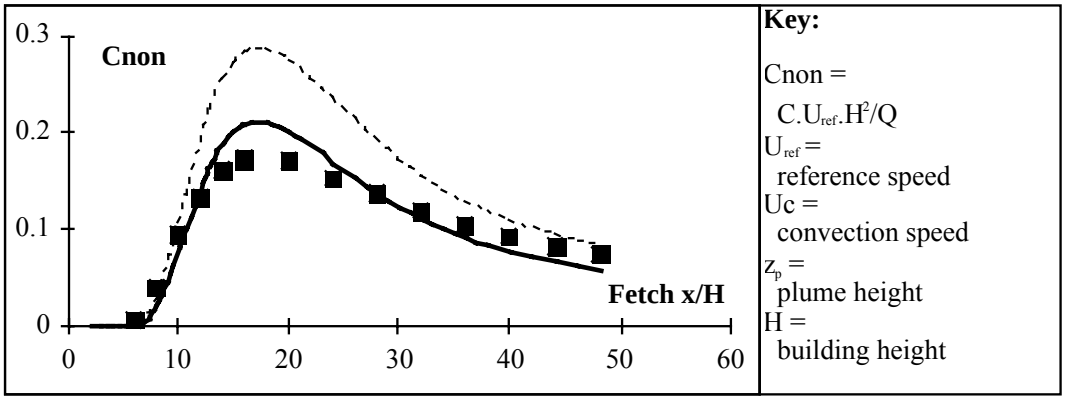

Ground level concentrations

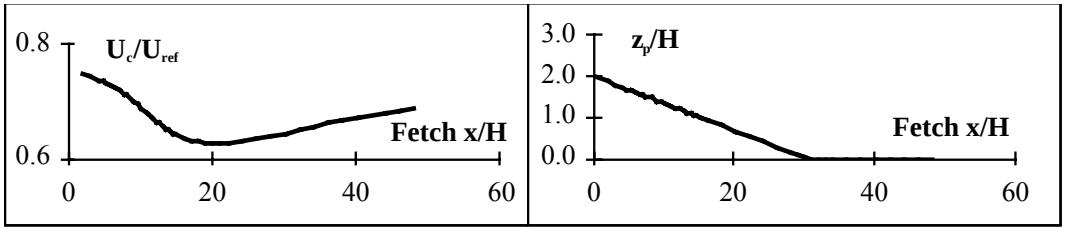

Convection speed **Plume height**

FIGURE 5.4 Predicted and measured concentrations for a source at height 2*H* above a single block of height *H*; wind direction 45º; square symbols, measurements; dashed line, Gaussian model with downwash; solid line, modified Gaussian model with downwash (Robins *et al,* 1998a)

In general, the Gaussian plume model with these modifications provided accurate predictions of the measured concentration fields. The lateral spread had to be made a function of height to ensure accurate prediction of both the ground-level and vertical distributions of concentration for low sources, $h/H \leq 1.5$. In other words, the concentration, C, is given by

$$C/Q = (1/2\pi U_c \sigma_{yu} \sigma_{zu}) \exp[-y^2/2\{\sigma_{yu}[1 + \psi(z/H)]\}^2] \times \quad (5.1)$$
$$[\exp\{-[z - z_p(x/H)]^2/2\sigma_{zu}^2\} + \exp\{-[z + z_p(x/H)]^2/2\sigma_{zu}^2\}]/[1 + \psi(z/H)]$$

where Q is the source strength, U_c the mean convection speed, σ_{yu} and σ_{zu} the plume spreads in the undisturbed flow, $z_p(x/H)$ the plume height and $1 + \psi(z/H)$ the variation of lateral spread with height. In general, U_c is a weak function of x and little error accrues by treating it as a constant, ie $U_c = U(H)$. The performance of a building effects dispersion model will depend on how well it represents the key variables identified above, which in order of significance are: $z_p(x/H)$, $\psi(z/H)$ and $U_c(x/H)$. In general, we expect these functions to depend on the emission height, the building or array geometry and orientation, and the approach flow conditions.

The results show that modelling based on virtual or effective source conditions can work reasonably well, at least sufficiently far from the site. The difficulty lies in defining the effective source properties as a general function of building geometry and orientation. Simple guidelines, such as the 'two and a half times rule', may be very misleading and in practice some form of numerical or wind tunnel modelling may be needed to determine appropriate functions. The virtual source model then offers a simple means of using what is learnt in the context of regulatory modelling.

Taken as a whole, the results plotted in Figure 5.5 show that effective stack heights over the site model were generally greater than for the equivalent release from an isolated reference building. Put another way, ground-level concentrations were generally smaller. The only significant exceptions were observed when the emitting building was placed in locations D1 and U1, close to a large building with an extensive flat roof. The explanation probably lies in the roof vortex system

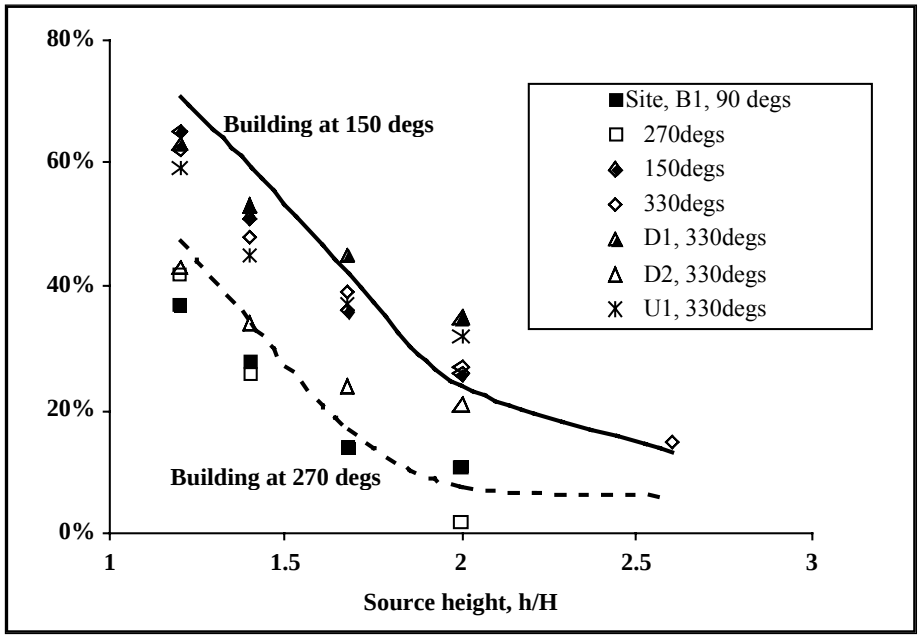

FIGURE 5.5 Fractional reduction in effective stack heights over a site model compared with data for an isolated building; B1, D1, D2, U1 are selected locations on the site (Robins *et al,* 1998b)

generated over this building. Presumably, the vortices were not immediately broken up by small-scale structural features and adjacent buildings and so persisted for some distance downwind. Even so, the increase in the maximum ground-level concentration was much less than the uncertainty generally associated with any prediction of atmospheric dispersion. Taken as a whole, the comparisons made between the site data and the results from the experiments with building arrays lead to the conclusion that the small-scale features and irregularities of geometry at the site generally played a significant role in suppressing organised flow features of the kind which might develop in a regular array of cuboids and thereby lessened the tendency to increase ground-level concentrations.

The main conclusions for stack emissions above buildings and building arrays are listed below; they are not applicable to releases at or below roof level.

(a) The 'two and a half times rule' should not be relied upon as an indicator of the significance of building effects, especially over building arrays where even a 'three and a half times rule' may not be adequate.

(b) The most appropriate simple modelling assumption for arrays with wind directions close to 0° is to ignore the array and use a single block model for spacing factors $S > 0.5$ and use the equivalent $S = 0$ array if $S \leq 0.5$. The most appropriate simple modelling assumption for arrays with wind directions around 45° is to treat them as the equivalent zero spacing factor (ie $S = 0$) block.

(c) In adapting Gaussian plume models to building wake dispersion the most important property to predict accurately is the plume height. The enhancement of lateral spread and its variation with height are also important for stack heights $h \leq 1.5H$. Vertical spread need not be modified.

(d) The effects of the large-scale irregularities of geometry at real sites should not be disregarded as they suppress the kind of organised flow features which might develop in a regular array of cuboids and can thereby lessen the tendency to increase ground-level concentrations.

(e) The extensive body of data for isolated obstacles may often provide a satisfactory first estimate of dispersion at an industrial site, at least within the level of uncertainty generally associated with predictions of atmospheric dispersion.

(f) Wind tunnel tests with a model of limited extent and detail are likely to be acceptable in providing a first estimate of dispersion behaviour.

Further research is needed to determine how downwash and lateral plume spread vary with release height for a range of building groups. The objective should be to provide the links, empirical if need be, between the primary variables, geometry and wind direction, and the plume height and lateral spread, the parameters which need to be modified in a Gaussian plume model. Another objective would be to generalise the rules for representing building groups by effective buildings. Improvements are also needed to the wake flow theories used in models such as ADMS. Current methods do not predict the development of the secondary flows generated by streamwise vortex systems and therefore resulting effects on dispersion behaviour have to be introduced empirically.

The importance of atmospheric stability, both stable and unstable, needs a thorough investigation. The work described by Hayden (1998) indicates some intriguing processes, particularly for emissions near the edge of a stable boundary layer. There has been some progress in the simulation of stable and unstable boundary layers in wind tunnels but not to the level where generally accepted procedures can be said to exist; nor is it clear how such simulations can be

adapted when large site models are to be installed. Resolving these issues is really a necessary precursor to successful dispersion studies at the level of detail already achieved in neutral flows.

5.2 Porous obstacles

The body of research concerning the wakes of two- and three-dimensional, surface mounted porous obstacles, such as fences and wind breaks, is not particularly extensive (see, for example, Gandemer, 1981; Perera, 1981; Raine and Stevenson, 1997). Indeed, the three-dimensional problem has been largely neglected, even though it is of considerable industrial relevance; eg to understand pollutant dispersion near industrial sites that can best be classified as a mixture of solid and porous installations. To address some of the issues, an experimental study (Speirs, 1998; Robins *et al*, 1999) was carried out at the University of Surrey in the EnFlo wind tunnel, using generic, three-dimensional porous plate models. Smoke and laser sheet lighting were used for flow visualisation studies, hot wire, pulsed hot wire and laser Doppler anemometers for velocity field measurements, and a gas sampling and analysis system for concentration measurement. Passive emissions containing a hydrocarbon tracer were used for all dispersion studies.

Porous plates of size 0.3×0.2 m were manufactured from regular grids of rectangular bar, covering a range of porosity from 0% (a solid plate) to 85%. These were mounted either singly or multiply in a nominally 1 m deep, turbulent boundary layer in the EnFlo wind tunnel. The boundary layer characteristics were rural in character, with roughness length 0.3 mm and friction velocity $0.045U_e$, U_e being the free stream velocity. The spacing between plates was 10% of the plate height and up to four plates were installed. The effective porosity of the arrays of plates was not the issue, simply the flow characteristics that resulted. The notation used to describe the models is: $M(p,n)$, where 'p' is the percentage porosity of the individual plate and 'n' the number installed. Sources were located either just upwind or just downwind of the model, at heights of 0.05, 0.25, 0.55 and $0.85H$, although here only the data for upwind sources at heights of 0.25 and $0.85H$ are considered.

Initial flow visualisation studies revealed a number of regimes of near-wake behaviour that can be classified as:

(a) recirculating flow 'attached' to the obstacle – the solid plate case,
(b) recirculating flow 'detached' from the obstacle – the low porosity case,
(c) non-recirculating mean flow with intermittent flow reversal – the intermediate porosity case,
(d) non-recirculating flow – the high porosity case.

The strength of the wakes, as exemplified by the mean velocity deficit, was seen to decrease steadily as the porosity increased. Characteristic configurations were selected on the basis of the flow visualisation work and subject to detailed mapping of the mean and fluctuating velocity fields through both the near- and far-wake regions. Mean concentration fields were also mapped for sources located near the base, mid-height and near the top of the porous plates.

A series of mean velocity and turbulence intensity profiles at constant height, $z = H/2$, through the wake is shown in Figures 5.6 and 5.7. Both are made non-dimensional by $U(H)$, the approach flow wind speed at height $z = H$, where H is the plate height, and plotted against x/H, where x is measured from the rear of the model. The recirculation region behind the solid plate, $M(0,1)$, stretches to about $x/H = 2.5$, where the highest turbulence intensity is seen. Introduction of a small degree of porosity enables bleed flow to pass through the plate causing the recirculation region to be displaced a small distance downstream, as well as reducing its overall length. This is illustrated by the results for model $M(30,4)$. Turbulence intensities are just slightly greater than approach levels ahead of the first mean stagnation point, then high throughout the recirculating

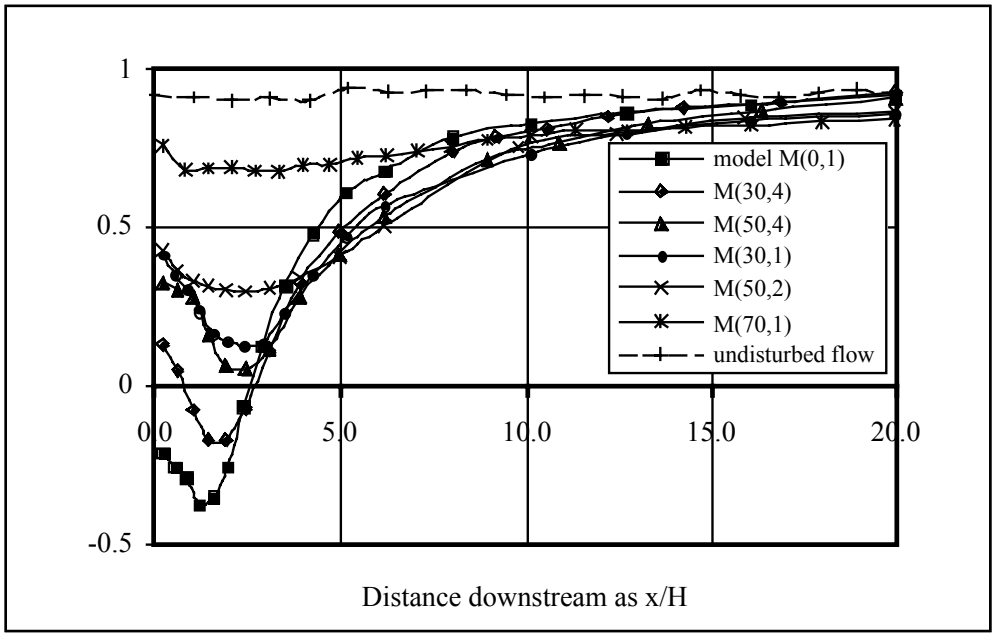

FIGURE 5.6 Longitudinal variation of mean velocity at a height of 0.5*H* (*y* = 0) behind porous three-dimensional fences, from Speirs (1998)

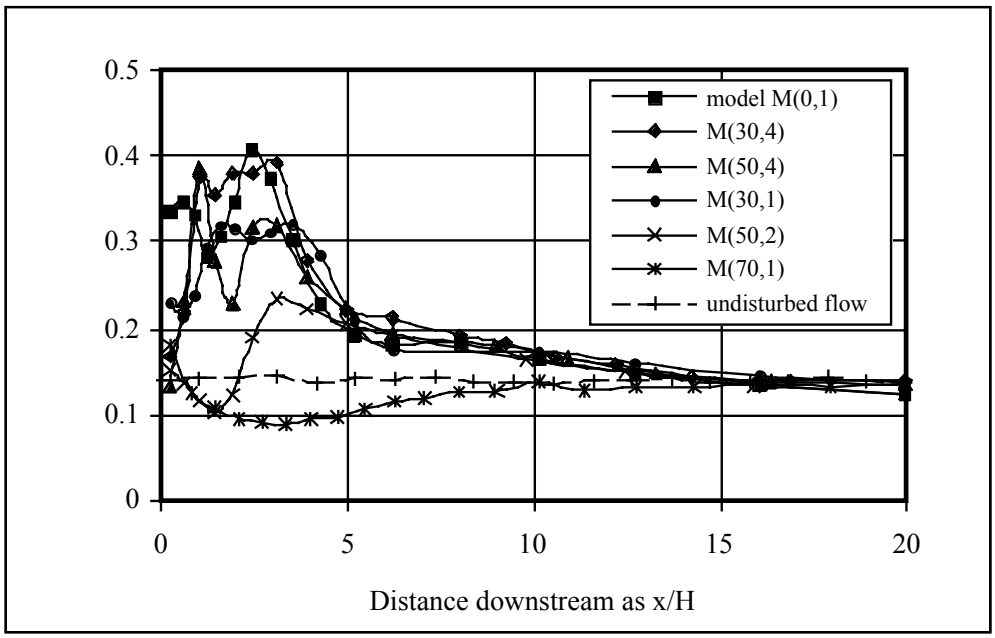

FIGURE 5.7 Longitudinal variation of longitudinal turbulence at a height of 0.5*H* (*y* = 0) behind porous three-dimensional fences, from Speirs (1998)

region. As the porosity is further increased the first mean stagnation point is displaced further downstream, accompanied by an overall reduction in recirculation region size.

Results for cases *M*(50,2) and *M*(30,1) are similar, showing a minimum mean velocity of about 0.1*U*(*H*) at about *x*/*H* = 2.5 and high turbulence levels between *x*/*H* = 1 and 3. The turbulence intensity in this region is about 0.3*U*(*H*), so there is clearly a substantial region of intermittent flow reversal at this height with a distinct possibility of mean flow reversal closer to the surface. There is

a small region of shelter between the model and x/H = 1, although immediately behind the model turbulence levels are somewhat increased above ambient values due to generation by the plate grid.

The mean flow recovery is somewhat slower than for the more solid models, with ambient conditions attained at approximately x/H = 20. Ambient turbulence levels are reached a little sooner, at about x/H = 15 in all but one case; this, however, is peculiar to the height of the traverse as more detailed measurements of the vertical distribution show (see below). The bleed flow strengthens as the blockage is further decreased. For M(50,2) the velocity defect is around 40%–50% in the fetch x/H < 6, although turbulence levels grow rapidly at about x/H = 2.5. The area of shelter is much more extensive behind model M(70,1), though the velocity deficit is only around 25%. Turbulence intensities are also lower than ambient levels throughout the area of shelter (ie for x/H < 10).

The results show the existence of three regimes of wake behaviour for high, medium and low blockages, respectively:

(a) *regime I*: near-wake flow recirculation for high blockages; attached recirculation for solid plate, otherwise detached; recirculation region bounded by zones of strong shear; eg M(0,1), M(30,4),

(b) *regime II*: no mean flow recirculation; shelter in the near-wake, with bleed flow deceleration; near-wake bounded by zones of strong shear which converge downstream to form a deep and vigorous turbulent mixing region; eg M(30,1), M(50,4),

(c) *regime III*: persistent mean flow shelter for cases of low blockage; weak shear layers and low levels of wake turbulence; eg M(70,1).

Centreline measurements provide only a limited picture of wake behaviour and, to establish a more comprehensive understanding of the three-dimensional flow mechanisms which determine the respective flow regimes, a small subset of model cases was selected: regime I – M(30,4), regime II – M(50,2), and regime III – M(70,1). The solid model, M(0,1), was also used as a reference case.

Detailed mean flow and turbulence mappings were carried out for these cases, followed by dispersion studies. Examples of mean velocity profiles for M(30,4) are shown in Figure 5.8.

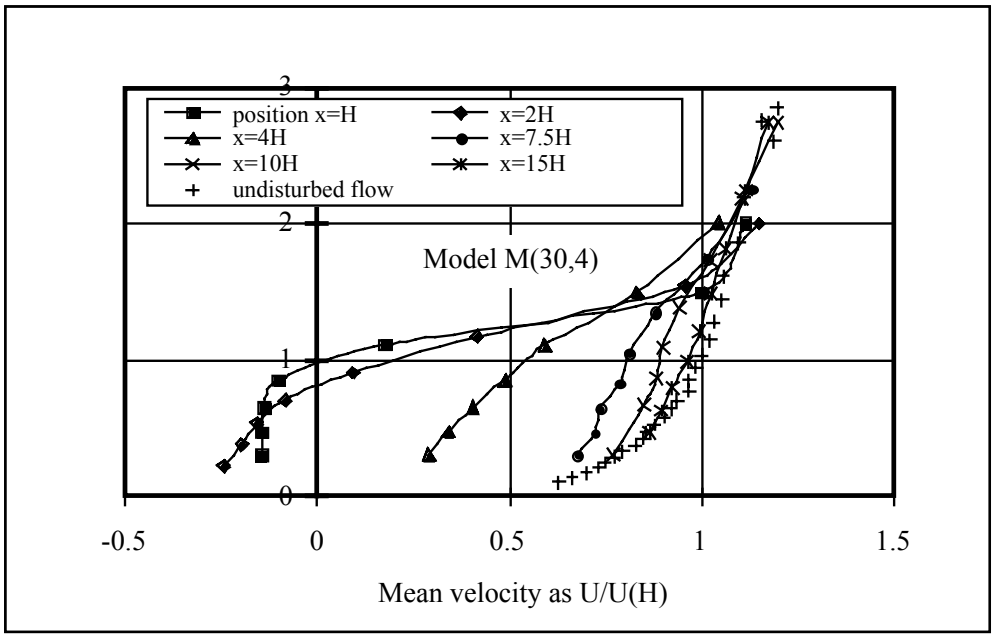

FIGURE 5.8 Vertical profiles of mean velocity behind a three-dimensional porous fence, from Speirs (1998)

Reversed flow extends vertically to about $z/H = 1$ and laterally to about $y/W = 0.4$ (where W is the total plate width). Excess turbulence levels extend vertically to at least $z/H = 2$ and persist throughout the region investigated (ie to $x/H = 15$). The height of the maximum excess rises from around $z/H = 0.5$ at $x/H = 1$ to $1.5H$ at $15H$.

Figures 5.9 and 5.10 show the variations of ground-level, centreline concentration for a range of model porosity (ie flow regimes), with source heights of $0.85H$ and 0.25, respectively.

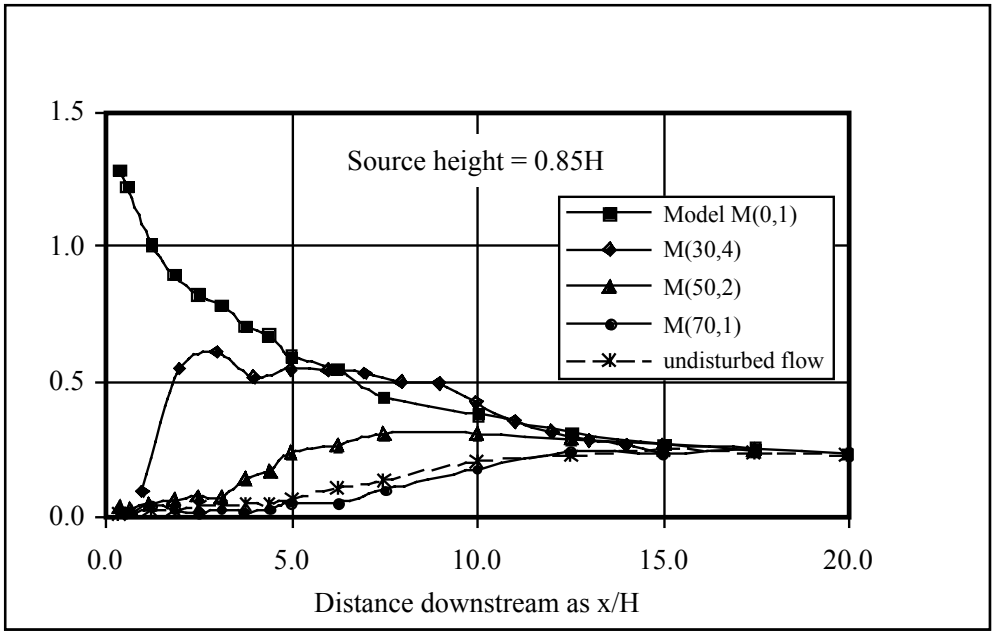

FIGURE 5.9 Longitudinal distribution of ground level concentration on $y = 0$ behind three-dimensional porous fences with an upwind source at a height of $0.85H$, from Speirs (1998)

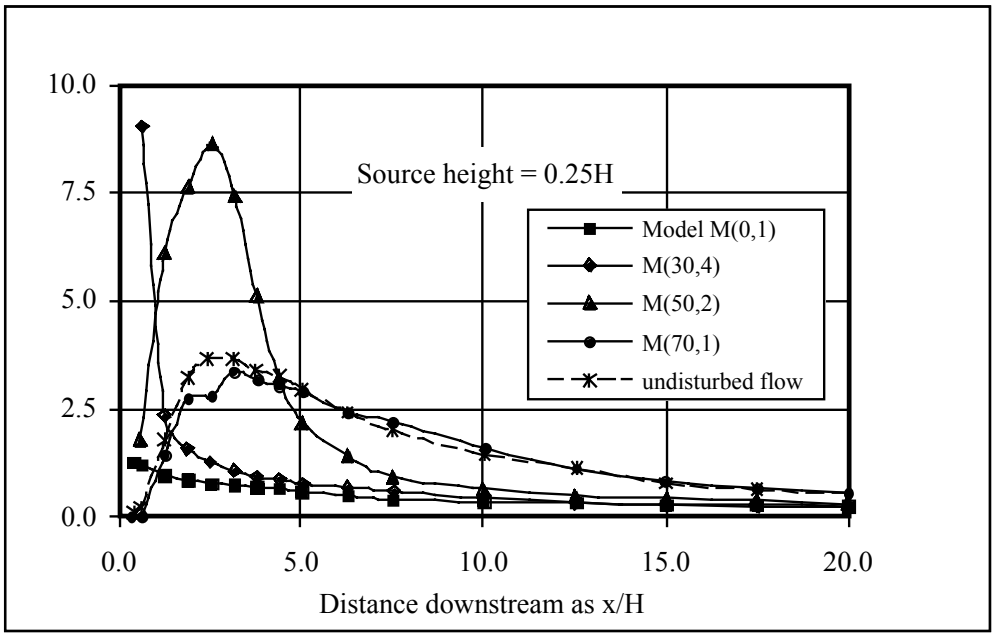

FIGURE 5.10 Longitudinal distribution of ground level concentration on $y = 0$ behind three-dimensional porous fences with an upwind source at a height of $0.25H$, from Speirs (1998)

Concentrations are non-dimensionalised as CUA/Q, where U is the reference wind speed at height H, A the projected frontal area of the model and Q the volume emission rate. Results for the solid plate are essentially the same in both cases and results for $M(70,1)$ are approximately the same as those in the undisturbed flow. Enhanced mixing clearly affects the other two cases. The detached recirculation and associated high turbulence levels downwind of $M(30,4)$ disperse the elevated plume very rapidly to the surface, which is made apparent for the source at $0.85H$ by a sudden increase in ground-level concentrations at the upstream edge of the recirculation region. The plume from the lower source is mixed to the ground in the low velocity flow behind the plate, producing high ground-level concentrations that decay rapidly through the recirculation region and immediately downwind. Results for $M(50,2)$ also show the most significant changes affecting the plume from the lower source height.

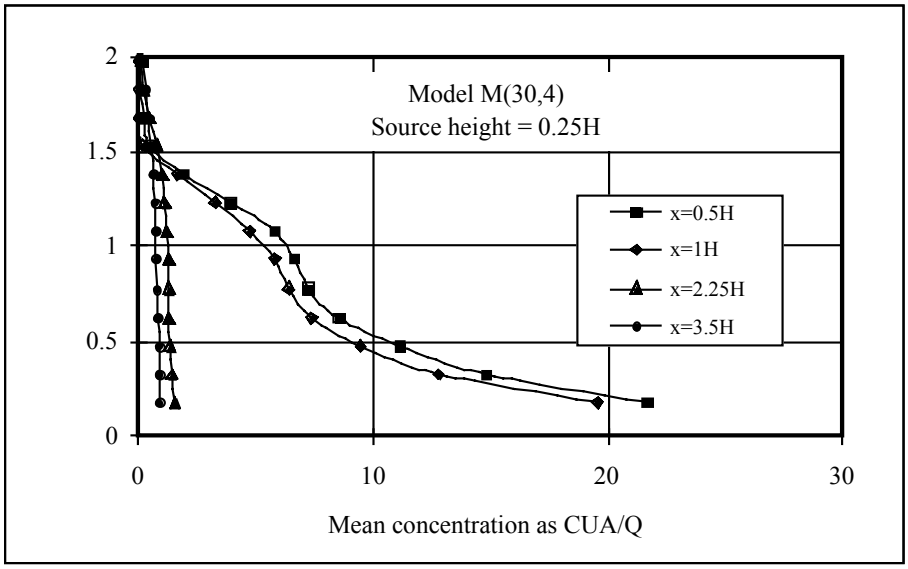

FIGURE 5.11 Vertical profiles of mean concentration behind fence *M*(30,4) for an upwind source at a height of 0.25*H*, from Speirs (1998)

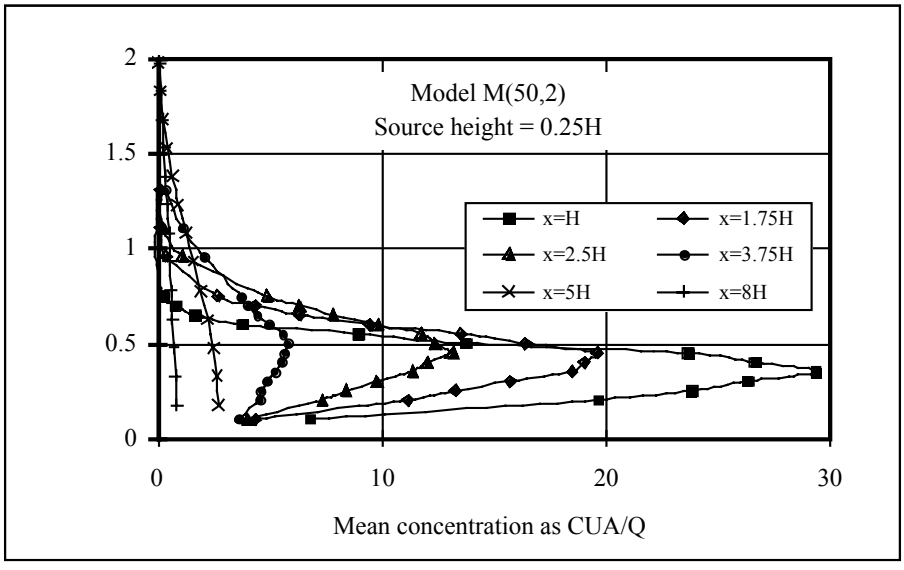

FIGURE 5.12 Vertical profiles of mean concentration behind fence *M*(50,2) for an upwind source at a height of 0.25*H*, from Speirs (1998)

These observations are supported by vertical concentration profiles measured downwind from *M*(30,4) and *M*(50,2) and shown here as Figures 5.11 and 5.12, for a source height of 0.25*H*. Intense mixing in the detached recirculation region behind M(30,4) deepens the plume very rapidly so that even at $x/H = 0.5$ the concentration field extends through the full depth of the wake. Flow visualisation showed essentially the same picture, with the recirculation lifting material from near the leading stagnation point almost vertically to heights in excess of the plate height. A somewhat simpler pattern is found downwind from *M*(50,2). The flow deceleration caused mean streamlines to be displaced upwards, carrying the plume with them. High turbulence levels from about $x/H = 3$ then mix the lower part of the plume to the ground. These two figures should be compared with Figure 5.13, which shows equivalent data for the undisturbed flow (but only for $x/H = 1$, 2.25 and 3.5). Here the plume height remains at the emission height and plume spread is slower.

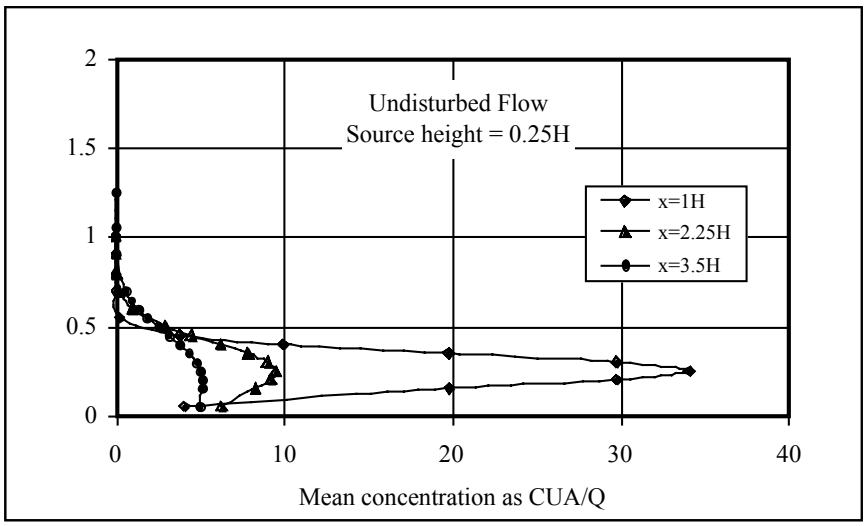

FIGURE 5.13 Vertical concentration profiles in the undisturbed flow for a source of height 0.25*H*, from Speirs (1998)

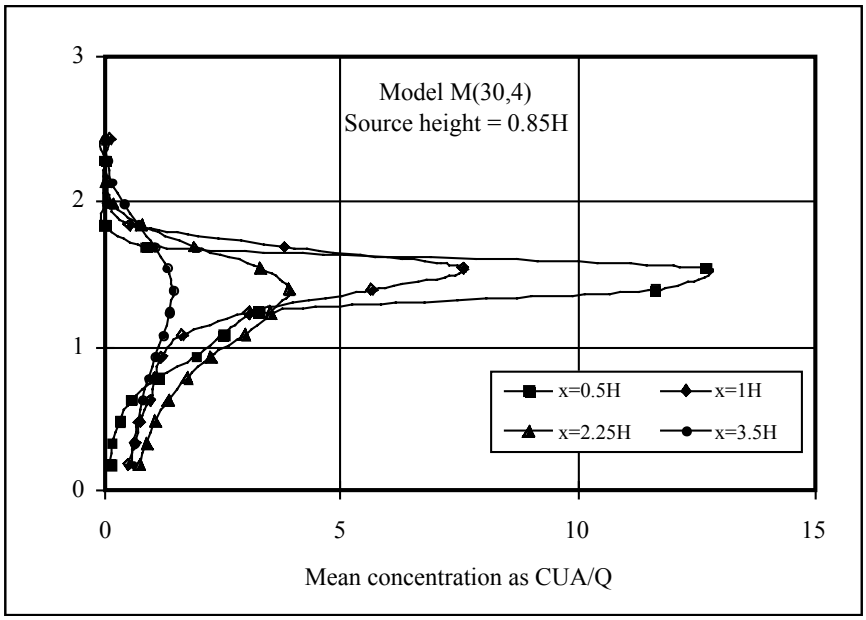

FIGURE 5.14 Vertical profiles of mean concentration behind fence *M*(30,4) for an upwind source at a height of 0.85*H*, from Speirs (1998)

The deep, detached recirculation downwind from $M(30,4)$ is accompanied by considerable mean streamline displacement, which manifests itself as increases in the plume centre height, as is clearly apparent in the concentration profiles for a source at height $0.85H$ shown in Figure 5.14. The plume height has increased to slightly less than $1.5H$. Increased mixing also affects plume development through the high turbulence levels in the wake. Skewed concentration distributions form as the lower part of the plume is mixed to the surface by the high turbulence levels associated with the detached recirculation region between $x/H = 1$ and 3.

Existing building wake dispersion models have been developed to account for the effects of near-wake recirculation (see, for example, Huber, 1987; Robins *et al*, 1997). Such models are likely to be suitable for regime I flows since recirculation plays an important role in the dispersion process. It is important to realise that in the calm bleed flow immediately behind the model, local concentrations can be high. Solid building wake models are therefore only useful beyond the first stagnation point for such cases. Regime II and III flows show quite different dispersion behaviour due to the absence of mean recirculation and presence of zones of decreased mean flow and turbulence levels. The shape of the concentration distributions suggests that a Gaussian modelling approach may be appropriate. Careful modelling of plume spread and vertical plume displacement is needed, together with the development of a mean flow model.

5.3 Recent experimental work on dispersion within groups of obstacles

An experimental or empirical approach is presently the most feasible means of developing an understanding of the physical mechanisms that influence plume behaviour in complex man-made terrain, and for developing models of urban dispersion. Since full-scale atmospheric experiments are costly, simulations using scaled-down models in wind tunnels or water channels tend to dominate the literature. The intermediate range of plume dispersion is the least-well-understood regime, with most published investigations occurring in the past 20 years. The current knowledge base consists of major ongoing studies in the UK, USA and Germany, along with various individual contributions. The major British studies consist of field and wind tunnel experiments at Cambridge (Davidson and Hunt, 1991; Davidson *et al*, 1995, 1996) and at UMIST and BRE (Hall *et al*, 1996b,c, 1997b; Macdonald, 1997; Macdonald *et al*, 1997, 1998b), with research continuing at BRE and the University of Surrey. The major German studies have been carried out at the University of Karlsruhe (Plate and Baechlin, 1988; Baechlin *et al*, 1991, 1992; Theurer, 1995; Theurer *et al*, 1996) and the University of Hamburg (see, for example, Rafailidis, 1997, Rafailidis and Schatzmann, 1996 and 1997). American research includes work by Petersen and Ratcliff (1989), Petersen and Hosoya (1991), Petersen *et al* (1991) and Petersen (1997). Some of the results of these programmes and some specific contributions of other individuals are discussed below.

5.3.1 Research at the University of Cambridge

The report of Davidson and Hunt (1991), which is summarised in Davidson *et al* (1995), identified several important characteristics of plume behaviour for ground-level plumes released upwind of a regular array of obstacles at 11% packing area density. This report describes a field study of dispersion using an array of 2 m cubes at a scale of about 1 : 10. During the field study a second plume was simultaneously released in the open terrain parallel to the obstacle array, to allow a direct comparison with the obstacle-affected dispersion. It was found that the influence of the array on the plume depended on the relative size of the plume to the obstacles. Within the obstacle array (typically six rows deep) the lateral plume profiles, averaged over 20 minutes, were Gaussian. Plume meandering appeared to be less in the arrays, although as the plume meandered, the obstacle wakes became secondary sources due to the entrainment and delayed release of contaminant. The

plume width inside the array appeared to be mainly related to the upstream turbulence statistics, as opposed to the turbulence scales imposed by the cubes. Thus, the plume width σ_y within the array was the same as in the unobstructed control plume at the same travel distance. This is not particularly surprising, given the long averaging time used (20 minutes). The time-averaged plume would have included the effects of large-scale horizontal eddies with periods of several tens of seconds and scales much larger than the obstacles or their characteristic wake residence times.

Some material was seen to be brought to the ground by the horseshoe vortices in the impact row of the array, but a portion of the plume was also deflected upwards because of the mean flow deceleration and the requirements of continuity. This is illustrated in Figure 5.15, which also shows the rapid deepening of the plume from an emission within the array and the role of the recirculation regions behind individual obstacles in enhancing plume spread. Davidson *et al* (1995) found that the vertical plume concentration profiles in the obstacle array were in the form of a reflected Gaussian and enhanced vertical dispersion occurred inside the obstacle array. Mean wind speed within the array was about 50% less than that upwind. This tended to counteract the dilution caused by the increased plume dimensions so that mean concentrations within the arrays were similar to those in the open terrain. Concentration fluctuations were observed to be more rapidly damped out within the array compared to the control plume in open terrain, due to the small-scale, high intensity turbulence generated by the obstacles. Retention of material in recirculation regions was also important in this respect as a mechanism for reducing the importance of the contribution of lateral plume meander.

Davidson *et al* (1996) found that the results of the field and wind tunnel trials (using the same array geometry) could be made to collapse on to non-dimensional curves if length scales of the turbulence in the approach flow were used. This is justified by their argument that if the plume is large compared to the obstacle scales then the obstacle scales can have little relevance compared to those of the upstream turbulence. The portion of the plume that passes over the array and its internal boundary layer will also be mainly influenced by the upstream turbulence.

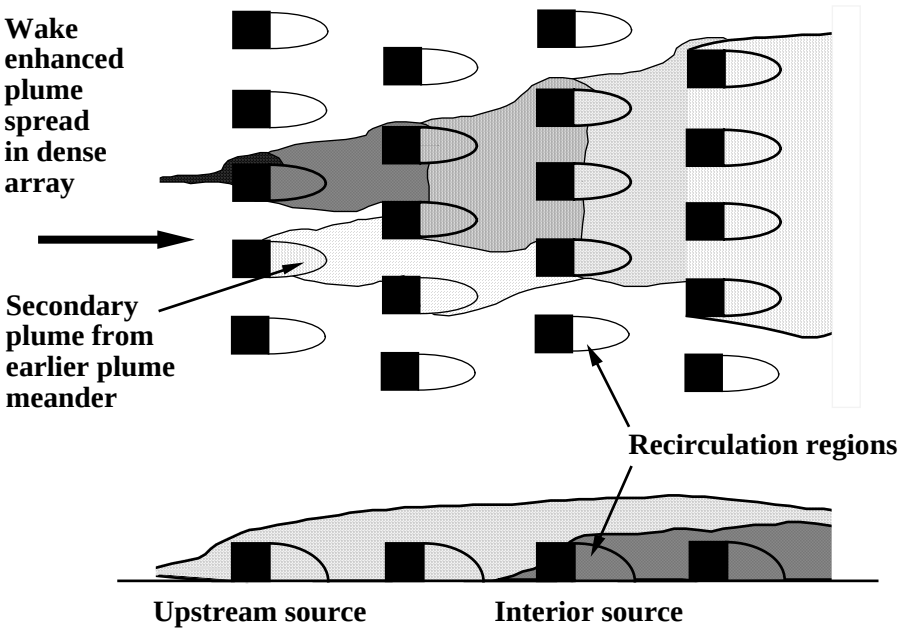

FIGURE 5.15 Simplified diagram of some mixing mechanisms in a building array

5.3.2 Research at the University of Karlsruhe

Work at the University of Karlsruhe was initially concerned with the validation of wind tunnel methods for the measurement of flow and dispersion around specific industrial sites. Plate and Baechlin (1988) discussed the possibility of using a limited number of scaled wind tunnel tests to characterise the transport and dispersion of contaminants from accidental releases at industrial plants. They proposed that a catalogue of plume behaviour, as a function of typical building configurations, could be generated and used in safety assessment and emergency planning, much like the proposal by Petersen *et al* (1991) in the USA. The Karlsruhe experiments were conducted in a boundary layer wind tunnel. A thick boundary layer flow with appropriately scaled mean speed and turbulence profiles was generated upwind of a scale model of the plant of interest. In the region near the source the local characteristics of the industrial complex and its surroundings determined the cloud spreading, and highly distorted, non-Gaussian concentration profiles occurred. At large distances from the source, the profiles were smooth and Gaussian. In this regime the gas cloud was larger than the roughness elements and the concentration was uniform within the roughness canopy. Baechlin *et al* (1991) also compared the wind tunnel and full-scale results measured at a chemical plant. They found excellent agreement between the model and prototype, thus validating the physical modelling.

The first generalised semi-empirical model was proposed by Baechlin *et al* (1992). This model used wind tunnel data to predict local flow direction and dispersion patterns around buildings in the near-field of industrial releases, where the flow was strongly influenced by the building arrangement. Geometrical parameters such as height H and width W of buildings, the street width S, the standard deviation of building height σ_H, and the plan and frontal area density (λ_p and λ_f) were systematically varied in the wind tunnel. The radius of homogenisation L_H was also measured. In some cases the plumes experienced significant lateral displacements which could not be predicted by existing urban Gaussian models. This lateral plume displacement was a result of flow channelling in arrays of wide buildings aligned at an angle to the mean wind vector.

Theurer *et al* (1996) provide a comparison of results from further wind tunnel work and selective full-scale measurements with the semi-empirical model SAMPU which is based on their previous work. The wind tunnel experiments were conducted with arrays of buildings which had particularly strong near-field effects such as street canyon channelling. Because of strong local variations in the built-up areas, the reference wind speed was determined in the approach flow over homogeneous roughness at 10 m height. For wind directions between 0° and 30°, it was found that the flow in the near-field was mainly parallel to the streets. The radius of homogenisation R_H was found to be typically between 50 and 100 building heights (1000–2000 m from the source), a distance corresponding to the neighbourhood scale. The SAMPU model was found to give good predictions of the concentration field, except very close to the source where the local concentrations differed from the model due to the idealisation of the building configurations.

5.3.3 Physical modelling studies at BRE and UMIST

5.3.3.1 Dispersion studies

A major comprehensive study of the urban dispersion problem UDM (Urban Dispersion Model) is currently being funded by DERA, Porton Down. The experimental work was undertaken at the Building Research Establishment Limited and at the Environmental Technology Centre at UMIST. The goal of the UDM project is to develop a computer model for predicting the dispersion of continuous and instantaneous releases in all types of urban environment and for all regimes (near, intermediate and far-field). A major experimental effort has been under way since 1995, including a series of field experiments (Macdonald, 1997; Macdonald *et al*, 1997, 1998b,d) and wind

tunnel experiments at BRE (Hall *et al*, 1996b,c, 1997b, 1998). An algorithm outlining the procedures for a first generation computer model has also been produced at BRE (Hall *et al*, 1997a).

Macdonald (1997) and Macdonald *et al* (1997, 1998b) conducted field experiments using extensive arrays of cuboid obstacles of height 1.12 m, at a scale of about 1 : 10, in order to study the effect of obstacle plan area density on the plume dispersion. A gas tracer of methane was released upwind of the arrays and concentration profiles were measured at various locations within the array. The experiments were carried out on a flat test area of low-cut grass at the UMIST Environmental Technology Centre dispersion test site at Altcar on the Lancashire Coast. The surface roughness of the site was approximately 5 mm for the most common wind direction (from the west). Examples of arrays installed at the test site are shown in Figure 5.16 and a smoke visualisation experiment is shown in Figure 5.17, illustrating the entrainment of a ground-level plume into the horseshoe vortex system around the base of a cube in the front row of the array.

Many of the qualitative features of the dispersion that were previously observed by Davidson *et al* (1995) in an 11% area density array were also identified in this study, in particular:

(a) a deceleration of mean flow in the array and a reduced mean advection velocity,
(b) an effective lifting of the plume centre of mass and enhanced vertical mixing,
(c) downwash of plume material in the impact region due to the horseshoe vortex system, resulting in high ground-level concentrations in the near-field,
(d) Gaussian lateral concentration profiles in the arrays, at all the area densities studied, except very close to the source,
(e) some enhancement of lateral dispersion at short distances, but the results in the arrays were generally similar to those in the open terrain,
(f) mean plume centreline concentrations in the arrays were similar to those in the open terrain, as the reduced advection velocity cancelled out the increased dispersion,
(g) peak-to-mean concentration ratios for different sampling times in the range 10 seconds to 15 minutes obeyed a similar law to the behaviour in open terrain.

Further experimental results from the field are reported by Macdonald *et al* (1998b). These support the original conclusion that a Gaussian plume model for the time-averaged concentration field in obstacle arrays is a plausible model, except in the first couple of rows of obstacles where the behaviour is more variable. Some interesting effects of obstacle width-to-height ratio were noted in the second round of field experiments. These include:

(a) an increase of plume width by a factor of two to four in the array for obstacle aspect ratios $W/H \geq 2$,
(b) a greater initial dispersion rate for a release inside the array as opposed to upwind of the array, due to the rapid initial mixing in an obstacle wake in the former case,
(c) lateral deflection of the plume was observed in arrays of wide obstacles due to wind channelling – when combined with the natural wind meander in the field, this tends to amplify the meander and cause wider plumes in the field.

Good agreement was found between the field experiments and the wind tunnel work reported by Hall *et al* (1998). A much larger range of obstacle parameters was tested in the wind tunnel experiments, including area density (5%, 11%, 16%, 20%, 33%, 44%, 69% and 91%), width to height ratio (W/H = 1, 2, 4, 8 and two-dimensional), obstacle height ($0.5H$ to $3H$), and height variability (up to ±50%). Flow visualisation experiments carried out as part of this work we discussed and illustrated in Section 5.3.4 below. Measured lateral and vertical concentration profiles are plotted in Figure 5.18. The rapid deepening of the plume is again apparent. Most of the

(a) Low-density array of obstacles (λ_p = 6.25%) with wide obstacle spacing *S*/*H* = 3

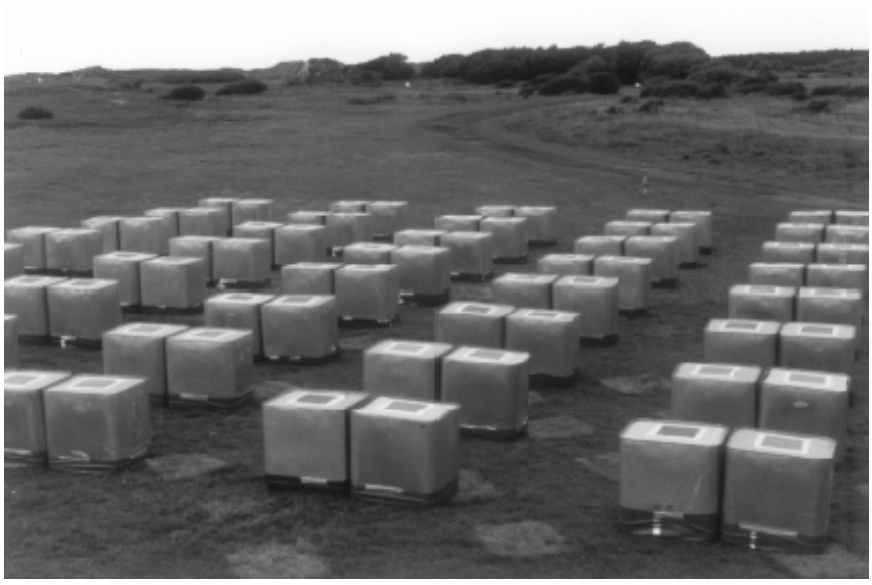

(b) Eight-row array of obstacles with width to height ratio *W*/*H* = 2 in the field; row spacing *S*/*H* = 2

FIGURE 5.16 Obstacle arrays at the UMIST Altcar test site (from Macdonald *et al*, 1998b, courtesy of Atmospheric Environment)

FIGURE 5.17 Entrainment of a ground-level plume into the horseshoe vortex system around the base of a cube in the front row of an array of 16% plan area density (Macdonald *et al*, 1998b, courtesy of *Atmospheric Environment*)

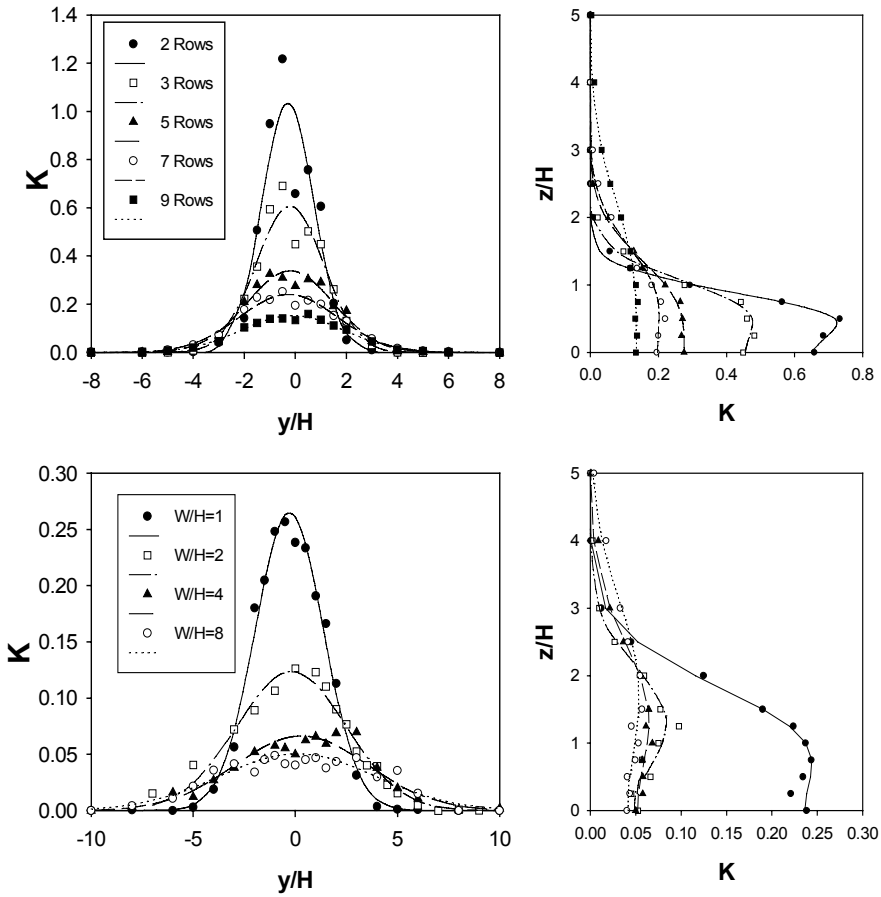

FIGURE 5.18 Lateral and vertical concentration profiles measured in obstacle arrays showing rapid growth in plume height in passing the first row of obstacles and complex lateral profiles at short range (Hall *et al*, 1998); non-dimensional concentration, $K = C\,U_H H^2/Q$

concentration distributions measured in the wind tunnel were Gaussian, except very close to the source and, in general, the rates of dispersion, σ_y and σ_z, were closely tied to the heights and widths of the obstacles. Figure 5.19 compares plume spreads with values from the undisturbed flow, as well as the effective plume height (the sources were at ground level) and the non-dimensional mean concentration. The enhanced lateral spread is clearly seen over the full range of downstream fetch investigated. However, concentrations beyond about x/H = 10 are more-or-less the same as in the undisturbed flow, due to the reduced plume advection speed over and in the array.

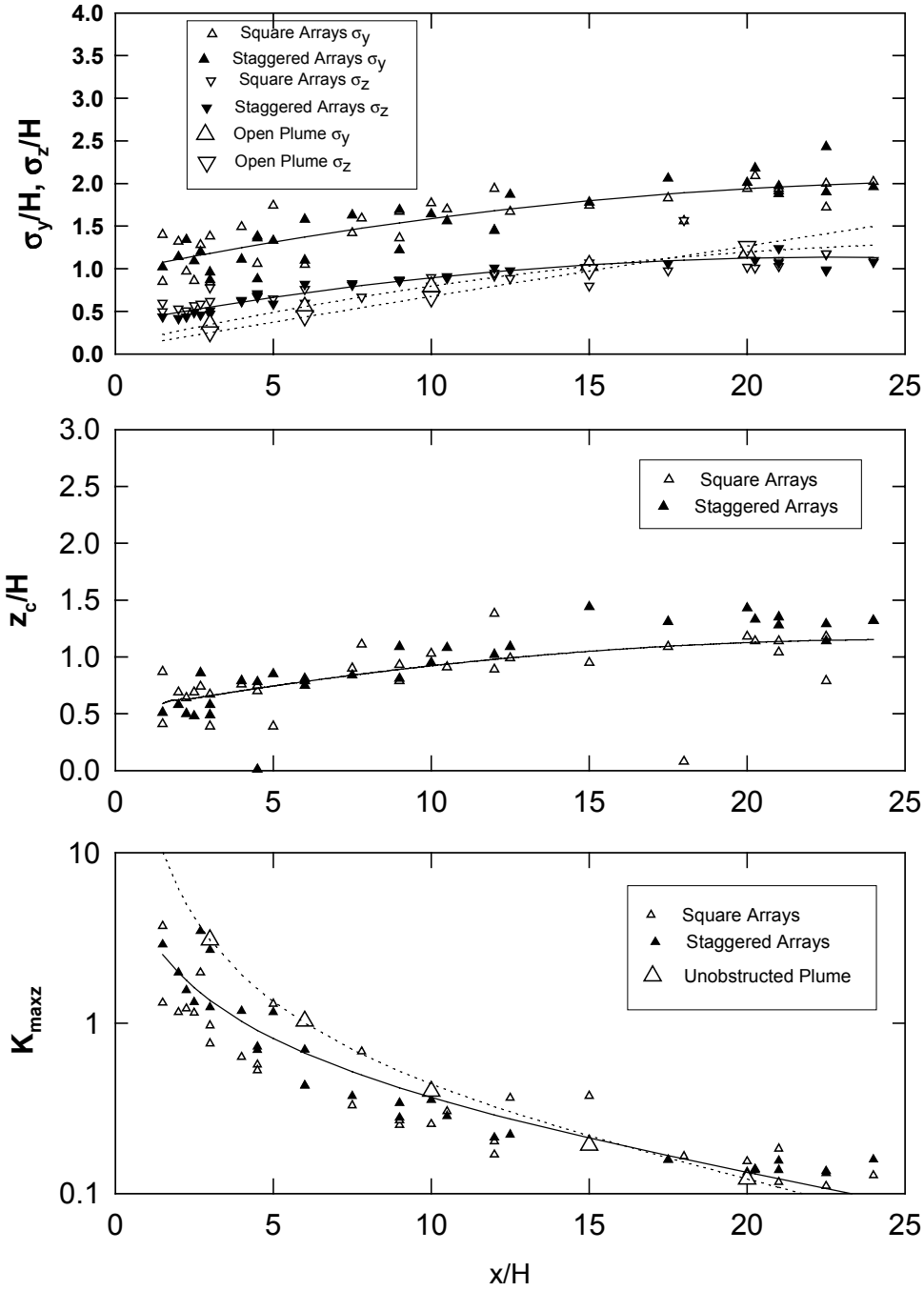

FIGURE 5.19 Plume spread, height and centreline ground-level concentrations in obstacle arrays compared with data from the undisturbed flow (Hall *et al*, 1998); non-dimensional concentration, $K = C\,U_H H^2/Q$

Wind direction generally had little effect on the dispersion rates in arrays of cube obstacles, but resulted in marked lateral shifts of the plume centreline for large W/H obstacles. Velocity profiles were also measured within the arrays. These showed more sensitivity to array density and variability in obstacle height than did the dispersion alone. The velocity profiles above the obstacles were generally logarithmic, and the values of effective roughness length z_o and displacement height d could be predicted by well-ordered functions of the obstacle geometry (Macdonald *et al*, 1998a: Grimmond and Oke, 1998).

Most of the results so far reported in the project have been for continuous ground-level releases. This was done to maximise the influence of the obstacles on the plumes. Work is currently underway to look at the effect of time-dependent releases, the effect of release height, and the details of the non-Gaussian behaviour very close to the source. It can be expected that the release height will have a major effect on the influence of the obstacle array on the plume. For high enough releases the influence of the obstacles will be minimal, and they will act as a homogeneous roughness. It is expected that there will be a critical boundary at the transition between the internal boundary layer above the obstacle arrays and the free stream flow outside that will demarcate the main influence of the obstacle array on an elevated plume.

5.3.3.2 Flow visualisation studies

This series of flow visualisations comes from the study of dispersion around isolated obstacles and arrays of obstacles reported by Hall *et al* (1997b). The work was conducted in the Dispersion Modelling Wind Tunnel at the BRE Cardington Laboratory, using dense white oil smoke. The models comprised groups of 100 mm cubes in a 1 m deep simulated boundary layer, with a characteristic roughness length of the upstream flow z_0 = 2.5 mm (z_0/d = 0.025, where d is the boundary layer depth).

Figures 5.20–5.23 show plan and isometric views of plumes for a wind direction normal to four in-line arrays. The figures are presented in order of increasing plan area obstacle density (ie decreasing obstacle spacing), with λ_p = 8% (S/H = 2.5), 16% (S/H = 1.5), 25% (S/H = 1) and 44% (S/H = 0.5), respectively. In each case, the plume was released from ground level, approximately 2H upwind of the array, on the centreline of a cube.

In Figure 5.20 the cubes are relatively sparse (S/H = 2.5) and the resulting flow falls into the isolated roughness flow regime (ie the wakes of each cube reattach upstream of the subsequent downwind cube. The initial rapid expansion around the 'impact' cube in the first row is clear, as the plume is carried in the horseshoe vortex system and spread laterally about the base. Following this, the plume is constrained in the gaps between the columns of cubes until the third or fourth rows where it is entrained into the wakes of the obstacles on either side. At this point there is a rapid increase in the lateral growth. The isometric view shows rapid vertical mixing behind the first row of cubes, with the plume rising above the tops of the obstacles. Beyond the first two rows, the plume density appears uniform within the obstacle canopy (between z = 0 and $z = H$).

In Figure 5.21 with an obstacle spacing of S/H = 1.5, the behaviour of the plume is similar to that in Figure 5.20, but the lateral plume growth occurs in the second and third rows in this case. Enhanced lateral dispersion caused by lateral jumps was also observed by Davidson *et al* (1995) in the field. The isometric view is similar to that in Figure 5.20, showing the entrainment into the horseshoe vortex system and rapid vertical mixing in the wake of the first obstacle row.

At 25% area density, Figure 5.22, the lateral spread is very rapid, with lateral jumps into adjacent obstacle wakes at almost every row. The plume spreading angle in this case is about 60°, much larger than that associated with plumes in neutral stability conditions in the open atmosphere.

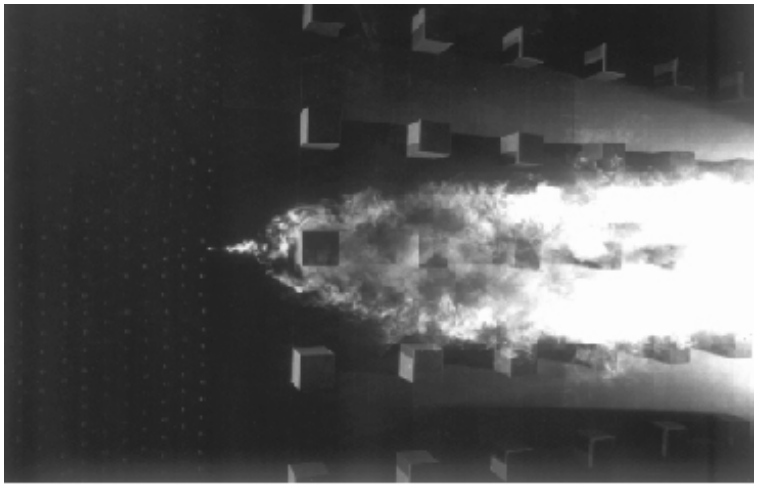

(a) Plan view

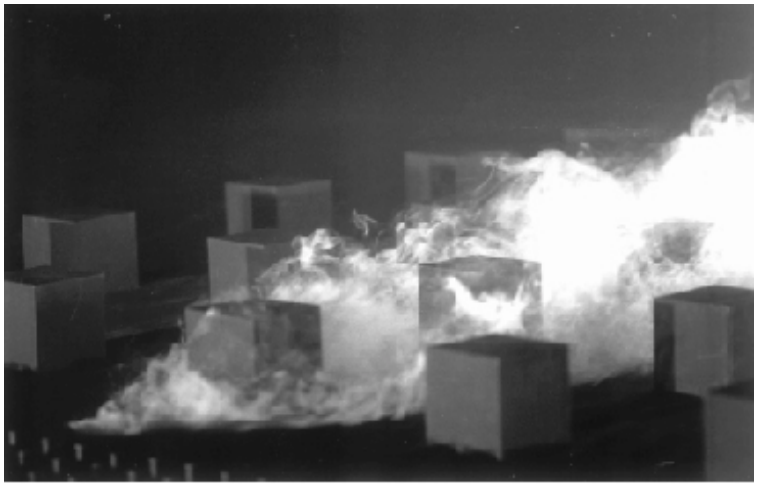

(b) Isometric view

FIGURE 5.20 Interaction between a plume and a square array of cubes at 8% plan area density (S/H=2.5)

The maximum plume spreading angle occurs at approximately the same obstacle plan area density that produces the maximum roughness length. The vertical dispersion in this case is similar to that for the two arrays discussed above.

In the most densely packed array, $\lambda = 44\%$, shown in Figure 5.23, the aerodynamic blockage is relatively high and the plume appears to go mainly over the top of the cubes. At high obstacle area density the dispersion behaviour is quite unsteady and slow meandering of the plume material through the narrow gaps in the array is apparent. This is a result of large-scale fluctuations in the flow and small irregularities in the array geometry. The isometric view of this array indicates that the vertical extent of the plume is greater than in any of the preceding examples.

Figure 5.24 shows a plume dispersing through a staggered array of 25% area density. In staggered arrays, the along-wind gaps between columns of obstacles are broken up because each alternate row is shifted laterally. The aerodynamic blockage of the array is greater than that of the equivalent square array. Dispersion in staggered arrays can be more rapid than in the equivalent square array, and in this example the lateral jump occurs in each of the first few rows. The lateral rate of plume spread is approximately the same as the diagonal angle of the obstacles within the

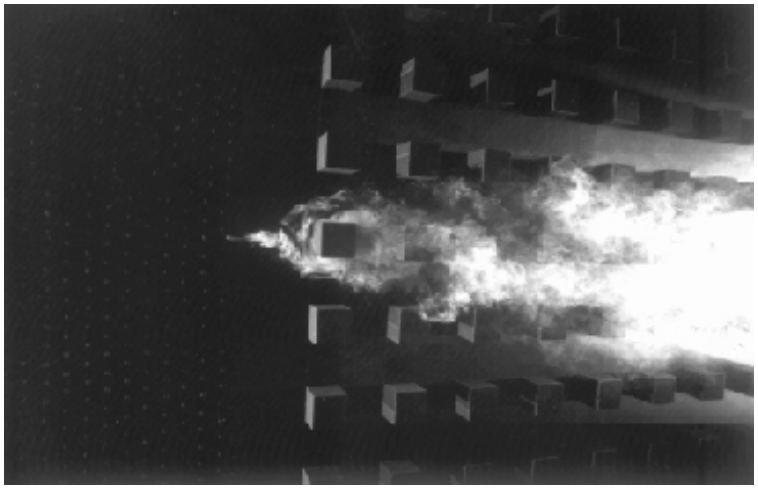

(a) Plan view

(b) Isometric view

FIGURE 5.21 Interaction between a plume and a square array of cubes at 16% plan area density (*S*/*H* = 1.5)

array; ie the dispersion appears to be dictated by the obstacle arrangement. This can only occur when the bulk of the plume is within the obstacle canopy. Once it rises above the obstacles, the plume material is dispersed by the turbulence in the internal boundary layer and lateral dispersion proceeds at a reduced rate.

The effect of wind angle is illustrated in Figure 5.25, which shows a plume travelling through an in-line array at 25% area density. At the wind angle of 45°, there are no clear 'streets' in the along-wind direction, so that the behaviour is similar to that of a staggered array. The dispersion around the first row differs from that shown in the previous figures, as the front row horseshoe vortex is not as prominent. However, strong trailing vorticity initiated by the roll-up of the vortices around the top edges of the cubes is indicated in the isometric view. One of the effects of an acute wind angle is a lateral shift of the plume centreline caused by channelling of the flow along 'lateral' street canyons. This phenomenon can be seen in the figure, but the effect is not as dramatic as in arrays of wider obstacles ($W/H > 1$). Lateral displacement of plumes is a significant feature of dispersion through arrays and one that may need to be correctly modelled if concentrations downwind are to be predicted with any accuracy.

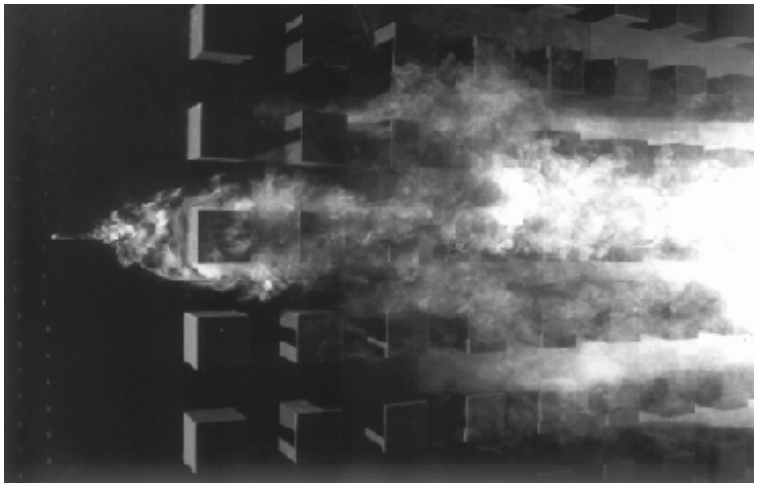

(a) Plan view

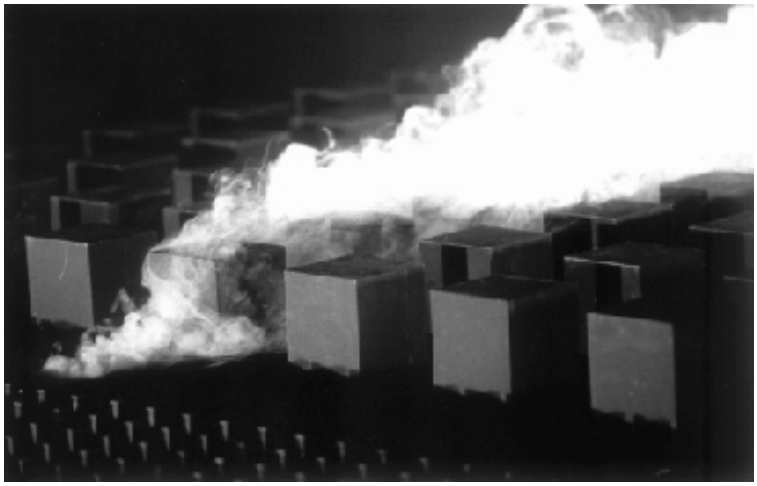

(b) Isometric view

FIGURE 5.22 Interaction between a plume and a square array of cubes at 25% plan area density (*S/H* = 1.0)

In the final example, Figure 5.26, the effect of a single tall obstacle (3*H* high) located in the third row of an obstacle array at 26% area density (*S*/*H* = 1.5) is shown. The tall obstacle draws the plume material from within the obstacle canopy up to a height of $z = 3H$, the plume height remaining at this value further downwind of the tall obstacle. This ventilation process is a beneficial consequence of tall buildings in urban areas, although the benefit of improved ventilation is often somewhat offset by pedestrian discomfort caused by increased wind speeds around the base of such structures.

5.3.3.3 Ventilation studies

Kukadia *et al* (1999) review the problem of the impact of urban air pollution on indoor air quality. The report discusses current ventilation strategies, relationships between external and internal pollution levels, building ventilation and dispersion patterns around buildings. Successful prediction of indoor levels of external pollutants requires knowledge of the nature and proportional impact of local and background pollution sources, the resulting distribution of pollutant concentrations over building surfaces, the pressure distributions generated on building surfaces by

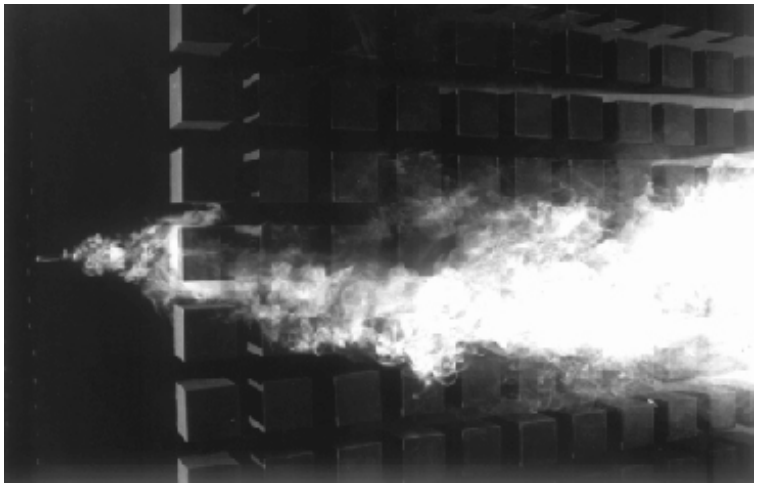

(a) Plan view

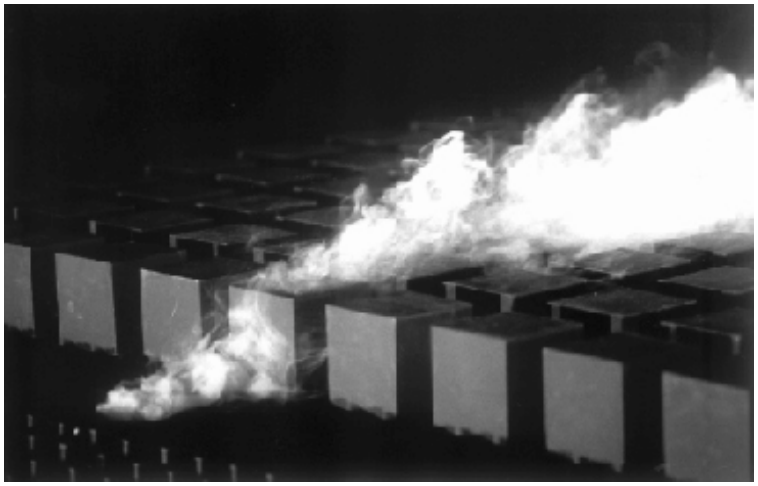

(b) Isometric view

FIGURE 5.23 Interaction between a plume and a square array of cubes at 44% plan area density (*S/H* = 0.5)

the ambient wind field (which itself is determined by the local urban canopy) and the behaviour of pollutants in transit through natural and forced ventilation systems. These topics have all been investigated to varying degrees, but not sufficiently to provide sound design rules. The report highlights the need for more extensive and detailed research in the following areas:

(a) relationships between indoor and outdoor pollution levels,

(b) small-scale spatial and temporal structure of concentration and pressure fields on buildings (both isolated and in urban locations).

An important requirement of (b) is that measurements be made of both fields on the same model (or building) in the same configuration, flow field, etc.

Hall *et al* (1999) carried out wind tunnel experiments to address these research needs, measuring pressure and concentration distributions on cubical and $4 \times 1 \times 1$ blocks, in isolation and in regular arrays of area density, λ_p, 0.16 and 0.44, the former being typical of suburban housing and the latter of urban centres. Sheltering in urban arrays considerably reduced the pressure differences across building surfaces; in the most dense array to about 10% of the values on the

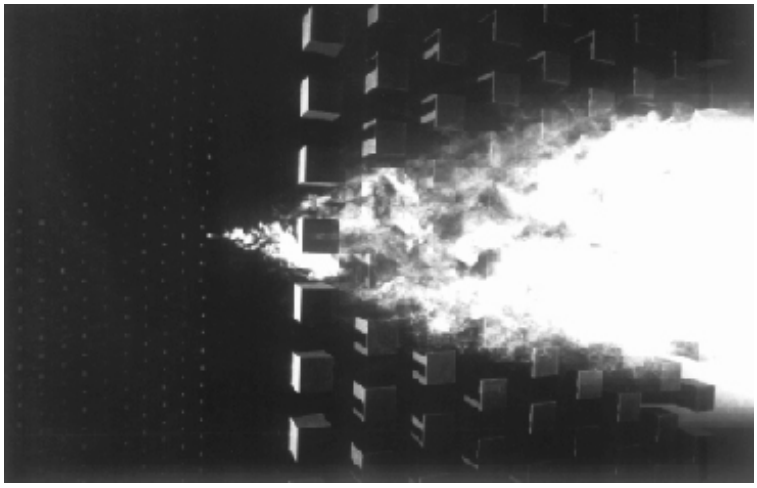

FIGURE 5.24 Interaction between a plume and a staggered array of cubes at 25% plan area density (*S/H* = 1.0); plan view

equivalent isolated building. This has an important impact on ventilation patterns, making buoyancy driven ventilation generally more likely than wind driven ventilation by considerably increasing the critical wind speed at which the latter dominates. Concentration differences across building surfaces were least in the most open array because of the high levels of turbulence and efficient mixing that prevailed. They were much greater in the dense array, reflecting the low wind speeds and dispersion rates in that case.

The regions of building surface where both high surface pressure and concentration were observed (where the infiltration of external pollution would be greatest) were found to vary considerably with building shape, wind direction and array density. The upwind surface most regularly met this condition (when the main sources were upwind).

5.3.4 Other recent experimental studies

Poreh (1997) investigated plume dispersion in a wind tunnel over regular arrays of rectangular obstacles with a plan area density of 21%. The obstacles were wider than they were deep ($W/H = 2.25$, $L/H = 1$) so that there was a difference in the obstacle aspect ratio depending on wind direction. This resulted in considerable variation of the dispersion rates with wind direction. In particular, σ_y and σ_z were lower for winds parallel to the predominant street direction, resulting in higher ground-level concentrations for these configurations. For some wind angles there was a lateral shift of the plume that persisted for large distances from the source. As noted by Baechlin *et al* (1992), this behaviour necessitates the use of a virtual source position to describe the dispersion further downwind where a Gaussian model might be used.

Some very high quality experimental information is currently being generated by researchers at the Institute of Meteorology at the University of Hamburg. They are primarily interested in the physical modelling of dispersion in urban street canyons in order to provide detailed data for the validation and testing of urban dispersion codes (Meroney *et al*, 1996; Pavageau *et al*, 1997; Rafailidis and Schatzmann, 1997), Pavageau *et al* (1997), studied the influence of street width and roof-top configuration on the pollutant concentration in two-dimensional street canyons. A line source of tracer gas was released from the centre of the street canyon and concentration measurements were made on the building surfaces around the street canyon. The canyon flow was also visualised using a laser sheet. In square canyons there was a single dominant vortex, whereas in a narrow canyon ($S/H = 0.5$) two counter-rotating vortices were observed, one on

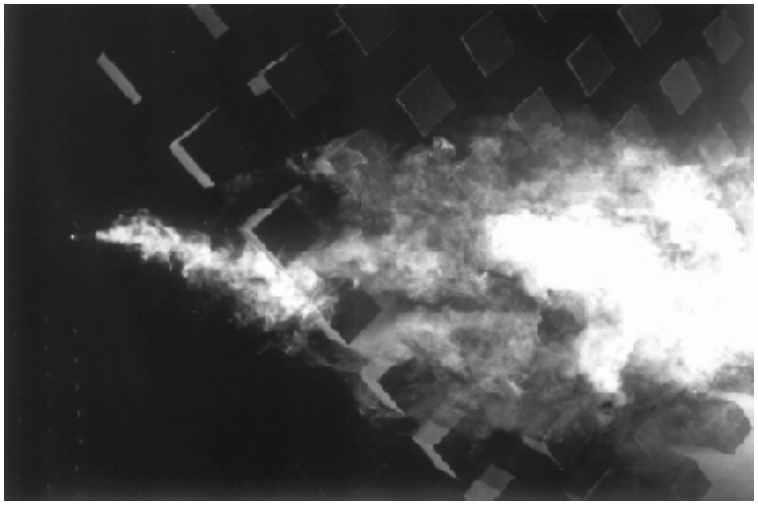

(a) Plan view

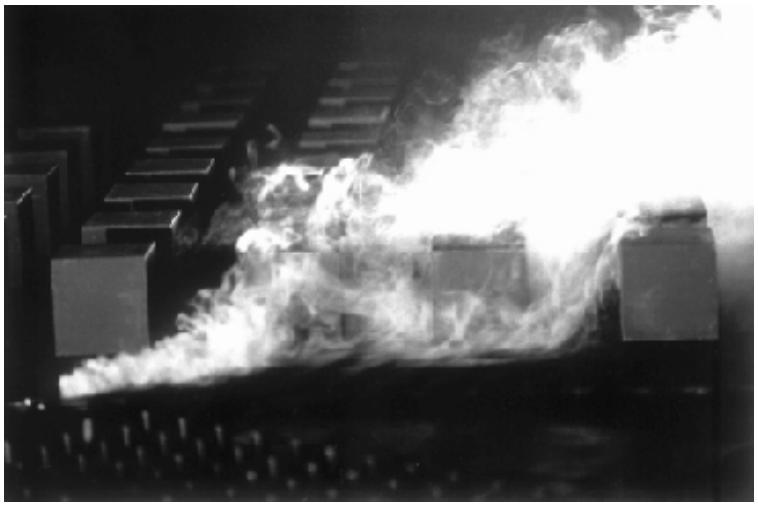

(b) Isometric view

FIGURE 5.25 Interaction between a plume and a square array of cubes at 25% plan area density (*S/H* = 1.0) for a wind direction at 45˚ to the array

top of the other. These vortices periodically collapsed and released pollutants out of the canyon. Rafailidis and Schatzmann (1997) found that street width had little influence on total pollution retained in the canyon in the range $S/H = 0.5–1$. The configuration of the roof tops on the sides of the canyon could have a major influence on the canyon re-aeration. In particular, if the roofs of the upstream buildings were slanted, the total pollution retained in the street canyon could be reduced by one-half.

Scaperdas *et al* (1998a,b) investigated dispersion at an intersection formed between four building blocks. The experimental work, carried out in the EnFlo wind tunnel at the University of Surrey, was undertaken in parallel with computational studies, using a modern, commercial CFD code. Of particular interest in this work was the transfer of pollutant from one street into the others at the intersection. This process was found to be exceptionally sensitive to small changes in the geometrical arrangement from the symmetrical base case, either due to a lateral offset of the downstream pair of buildings or a change in orientation of the group relative to the approach flow.

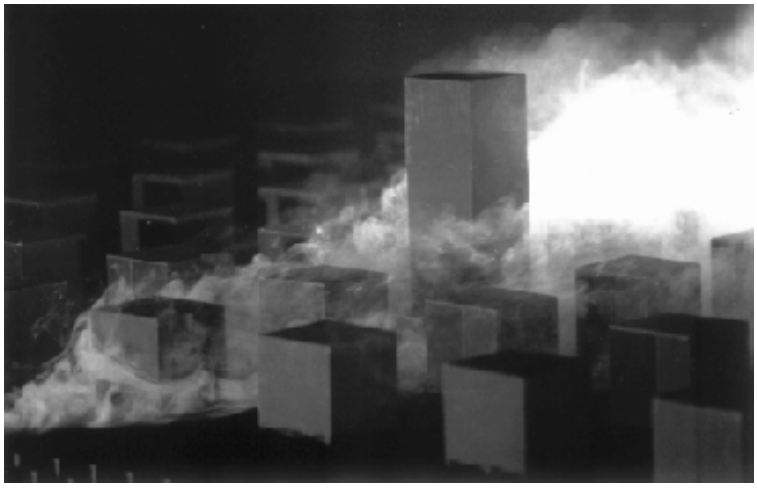

(a) Isometric view

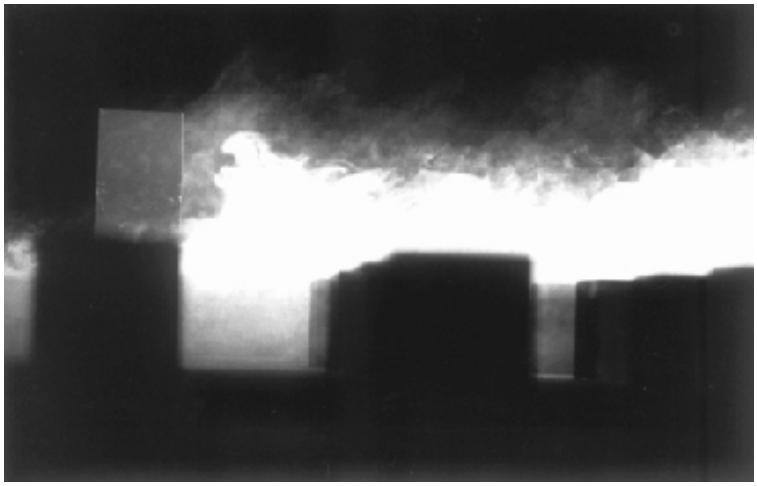

(b) Side view

FIGURE 5.26 Interaction between a plume and a square array of cubes at 16% plan area density (*S*/*H* = 1.5) with a single tall obstacle (height 3*H*) in the third row of the array

The sensitivity to lateral offset is illustrated by Figure 5.27, where concentrations in the 'cross-wind' street are plotted as a function of the offset, Dy. High concentrations are induced in the cross-street for an offset as low as 0.1*H*. Comparisons between the experiments and computations showed that the latter revealed similar sensitivities to the former, both for the flow and concentration fields. The sensitivity to small changes in geometrical parameters has also been observed in other studies (see, for example, Kastner-Klein and Plate, 1995).

One of the few full-scale urban dispersion studies in which near-field and intermediate profiles were measured was by Yersel *et al*. (1983) in the USA. They found that the ground-level lateral plume profiles for 15–20 minute averages were Gaussian at distances between 200 and 600 m from the source. The lateral dispersion coefficient σ_y was compatible with the standard Pasquill-Gifford relations, but shifted by one or two classes more unstable. Close to the source, the vertical dispersion coefficient σ_z was much larger than any value predicted by the P-G curves, but at larger distances it was close to the P-G curve for stability class A. The results were reasonably predicted

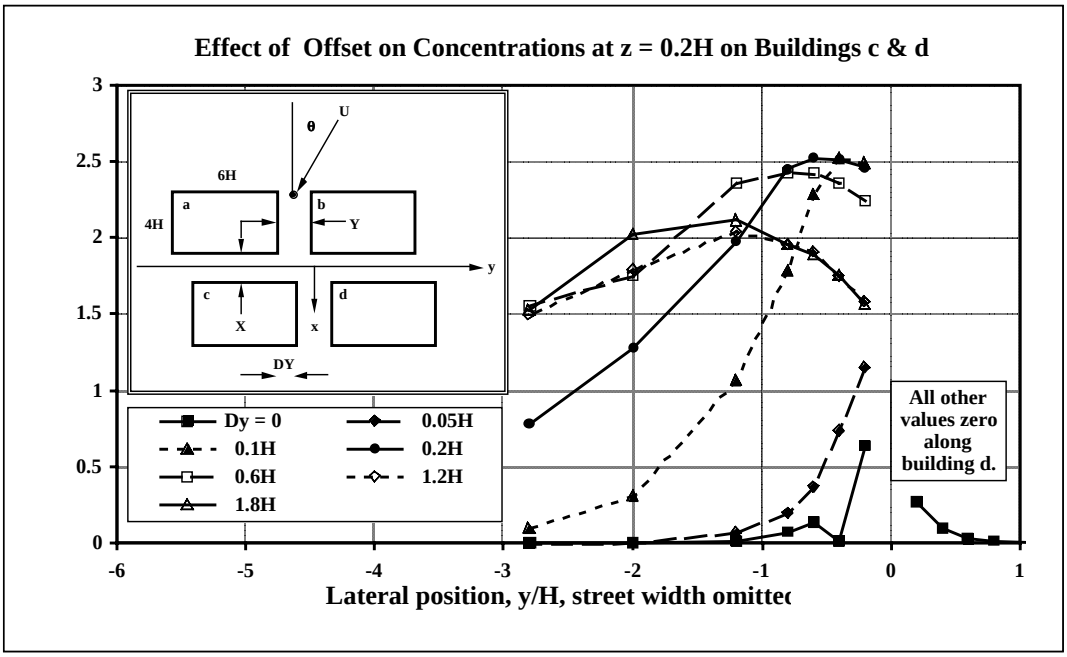

FIGURE 5.27 Effects of lateral offset in a group of four buildings on concentration levels along the cross-wind buildings (at a height $z = 0.2H$), from Scaperdas *et al* (1998a,b); street widths $X = Y = H$

by the Briggs urban curves (Table 3.2) except relatively close to the source where σ_z was dominated by local mechanical turbulence induced by the flow in and above the roughness elements. This is supported by the data shown in Figure 3.4, where the Briggs urban plume spreads are lower than the measured values in the wind tunnel measured at the shortest distances from the source.

5.4 Aerodynamics of arrays of obstacles

In comparison to dispersion studies, there are many wind tunnel data available on the topic of building aerodynamics and pressure forces, due to its wider range of interest to civil engineers. Relevant studies include Counihan (1971), Cook (1978, 1990a,b), Hussain and Lee (1980), Ho *et al* (1991, 1992), Theurer *et al* (1992), Bottema (1996), Petersen (1997) and Macdonald *et al* (1998b).

Hussain and Lee (1980) made measurements of velocity profiles in regular arrays of cubic obstacles and identified three regimes of flow, as follows.

(a) The isolated roughness flow regime which occurs when $\lambda_p < 8\%–10\%$ ($S/H > 2.2–2.6$). In this regime the obstacles are sufficiently far apart for their wake cavities to reattach before the next element is reached downwind (minimal aerodynamic interaction).

(b) The wake interference flow regime for $9\% < \lambda_p < 17\%$ ($1.2 < S/H < 2.4$). In this regime the separation region behind the obstacles does not have sufficient room to develop fully, and secondary flows occur between the cubes.

(c) The skimming flow regime exists for values of $\lambda_p > 15\%–21\%$ ($S/H < 1.2–1.6$). In this regime stable vortices are created behind the obstacles, and the flow which skims over the tops is decoupled from the secondary flow in the canyons between obstacles.

The specific density or element spacing for each of the above transitions is dependent of course upon the array geometry, obstacle shape and other variables. In most urban areas the flow

will be in the wake interference or skimming flow regimes (Turner, 1979; Spanton *et al*, 1996, 1998; Theurer, 1999).

There have been many attempts to relate the surface roughness z_o and displacement height d of the logarithmic boundary layer above a city to the urban geometry. Theurer (quoted in Plate, 1995) found that z_o and d could be approximated by functions of the two area densities λ_p and λ_f, with z_o related mainly to λ_f and d related mainly to λ_p. Petersen (1997) reviewed several existing models for predicting z_o in industrial complexes and compared the predictions with values measured in a wind tunnel simulation.

Macdonald (1997) and Hall *et al* (1996c) measured the mean wind speed profiles in regular arrays of cubic obstacles in a boundary layer wind tunnel using pulsed wire anemometry. They found that the mean wind speed in the obstacle canopy reduced dramatically with increasing area density. In very dense arrays ($\lambda_p > 40\%$), the flow below $z = H$ is effectively stagnant and the plume tends to meander randomly though the narrow gaps between obstacles. The influence of the obstacles tends to be limited to heights below $z = 2H$ or $3H$. At $z = 2H$ there were only small changes in the wind speed measured above the obstacle array over a wide range of packing density. Similar observations were also made by Rafailidis (1997), who found that the influence of the buildings on the mean wind was confined to within three building heights above ground. He also noted that in dense arrays the resulting skimming flow above flat-roofed buildings prevented the overhead flow from penetrating significantly into the street canyons.

The detailed functional dependence of the roughness length z_o and displacement height d on the area density of regular cube arrays has been derived by Macdonald *et al* (1998b), using wind tunnel data. Despite this development, more work needs to be done in the area of non-uniform arrays and additional work is required to look at the development of the internal boundary layers formed over changes in roughness.

Wind field measurements within the roughness canopy are relatively scarce, except for vegetation canopies and two-dimensional street canyons. Raupach *et al* (1981) review the topic, discussing both the mean flow and the turbulence structure. The mean velocity within the canopy is shown to be quite well represented by the empirical exponential wind profile:

$$U(z)/U(H) = \exp[-\alpha(1 - z/H)] \qquad (5.2)$$

where the coefficient α increases with array density. Clearly, the applicability of this profile must be limited as it does not admit flow reversal. Further, departures from equation 5.2 are also notable when the canopy resistance varies significantly with height (eg in forests). The shear stress and turbulent intensities, normalised by u^*, all fall with increasing depth below the canopy top, although the intensities relative to the local mean wind increase. Although there is some dependence on array density, turbulence velocity and length scale data from a wide range of cases collapse reasonably well when non-dimensionalised by u^* and H and plotted as functions of z/H.

Rotach (1995) presents and discusses measurements made in an urban environment (Zurich) using instrument masts mounted at street and roof level. Flow conditions fell within the skimming regime, but estimation of mean flow speeds within the street canyon was found to require knowledge of both the mean wind velocity and the stability of the urban boundary layer. Average wind profiles were strongly dependent on wind direction relative to the canyon, although the same was not observed of the turbulence characteristics. Turbulence levels were found to depend on stability, being greatest in unstable conditions. Stable stratification was rarely observed within the canyon.

6 Implications of recent experimental work

6.1 Extensions within the ADMS approach to treat building groups

Currently, ADMS reduces a building group to a single, effective building, the size of which is actually controlled by the model user through the decisions made in entering dimensions for the main and surrounding buildings. ADMS will create an effective building according to the algorithm outlined in Section 3.2.2, although the user may well choose to input its location and dimensions directly (eg having determined them from wind tunnel tests). Whichever approach is adopted, sensitivity to the definition of the effective building should be investigated as a part of subsequent dispersion calculations.

Some building groupings can be modelled explicitly, when suitable assumptions can be made about the mean flow. This is feasible when separations between buildings are large. What is meant by large in this context is that the flow field experienced by any building within an array can be expressed as a small perturbation (say, less than 30%) to the approach flow and that recirculation regions of adjacent buildings do not overlap. Typically, this implies along- and across-wind separations of around $2H$ to $3H$ or more, depending on building shape. The isolated building model can then be applied to each building in turn, using an appropriate approach flow determined by the buildings upwind.

The ADMS buildings effect model can also be applied in the wake downstream from an array of buildings. For this to be successful the wake strength and any streamline deflection over the array would have to be correctly specified. Recent work summarised in Section 5.1 has shown that the latter is the most important factor for elevated sources and that it can (at least in the range of circumstances examined) be specified through an effective building that is a function of the array geometry and orientation relative to the approach flow. Virtual source information would be required for a low level plume. Of course, the basic ADMS dispersion model can be applied to an extensive array, with specification of roughness length, zero-plane displacement and friction velocity to match the array conditions. This is valid once the plume size is large compared with the obstacle dimensions. Again, virtual source information would be required for emissions within the canopy. Reasonably reliable empirical parameterisations of the virtual source location and initial plume dimensions rests on the availability of sufficient empirical information (see, for example, Baechlin *et al*, 1992, for an example of this approach). Otherwise, site-specific wind tunnel studies could be carried out to determine this information.

Clearly, predictions already depend on user decisions in ADMS (and, presumably, similarly advanced models) and this dependency would increase if the buildings module were extended along the lines indicated above. At the very least, the user might wish to input virtual source data, effective building shapes and sizes, recirculation region scales, wake strengths and mean streamline deflections to replace the default algorithms expressed in the model. The user would be responsible for quality assurance in overwriting the defaults.

6.2 Considerations for modelling dispersion in large groups of obstacles

Many of the modelling criteria that have been identified as important for the dispersion around individual and small groups of obstacles are equally relevant for dispersion in large groups or arrays of obstacles. However, additional difficulties are introduced when dealing with large groups of obstacles. These include the characterisation or parameterisation of the modified boundary layer flow, identification of the relevant dispersion regime, and the interaction between the various time scales of the flow. The specification of the appropriate plume advection speed is essential in order to obtain correct estimates of the plume concentration in any kind of simple

Gaussian model, since concentration is inversely proportional to wind speed. The specification of the relevant mean wind speed for plume advection in obstacle arrays is therefore discussed first.

6.3 Characterisation of the bulk flow over urban roughness and the effect of limited fetch

Flow over urban surfaces can be simply approximated by a power law of the form:

$$U(z)/U_r = (z/z_r)^q \tag{6.1}$$

where U_r is the mean wind speed at a reference height z_r, and the exponent q ranges from 0.25 to 0.40. Alternatively a logarithmic profile with displacement height d can be used:

$$U(z)/u* = (1/\mathrm{k}) \ln[(z - d)/\mathrm{z_o}] \tag{6.2}$$

These profiles are only valid above the roughness sub-layer, well outside the urban canopy. The roughness sub-layer is defined by Raupach *et al* (1980) as the layer immediately above the roughness elements, extending to a height of about $z = H + 1.5S$, where S is the mean obstacle spacing. In the roughness sub-layer the obstacle wakes and other motions generated by the individual obstacles intrude into the mean flow field, and the wind profile deviates from the simple power law or log profile. Since the beginning phase of ground-level plume dispersion is within the urban canopy, some form of parameterisation of this lower level flow is required in a dispersion model.

The bulk properties of the urban canopy can be treated through spatial averaging, so that the flow in the canopy is subjected to a distributed drag force. This approach has been shown to be acceptable in plant and forest canopies (Kaimal and Finnigan, 1994), but has yet to be fully extended to urban conditions, where the individual canopy elements are much larger. Jerram *et al* (1995, 1997) have shown that a distributed drag model of the canopy can predict the observed mean flow conditions. Extension to the prediction of the turbulence field is needed, as well as the treatment of heat flux within the canopy and stability in the external flow.

Recent work at the University of Surrey with regular arrays of obstacles of uniform size has shown that the log law can be extended down to the top of the roughness canopy by applying it to the spatially averaged velocity, U_A, defined as

$$U_A(z) = (1/A_p) \int_0^{\mathrm{Plot}} \int_0^{\mathrm{Plot}} U(x,y,z)\, \mathrm{d}y\, \mathrm{d}x \tag{6.3}$$

where integration covers the plot area, A_p, occupied by an obstacle. Similarly the turbulence stress profiles reduce to conventional boundary layer profiles when processed in this manner. Matching theory based on spatially averaged flow in the canopy with that in the internal boundary layer offers a route to a full description of plume behaviour, except for the near-field where detail dominates. As yet, however, how to adapt equation 6.3 to random or highly irregular arrays is not entirely clear, although the general basis of spatial averaging has been analysed (Raupach and Shaw, 1982).

A further complicating factor in wind characterisation over urban terrain is that there are often distinct patches of roughness, so that the lower parts of the boundary layer are continually undergoing transition from one surface roughness to another. The derivation of the logarithmic velocity profile is based on the assumption of homogeneous terrain and equilibrium between shear production and dissipation of turbulent kinetic energy in the boundary layer. If x is a measure of the horizontal distance from a change in surface roughness, then the mean wind profile will only be in equilibrium with the new surface within an internal boundary layer of height $\delta_i(x)$. The wind structure at higher levels will be determined by the surface roughness upwind of the transition (Kaimal and Finnigan, 1994). As the wind encounters a new surface roughness, it either speeds up

over a smoother surface or slows down because of increased surface drag with associated vertical displacements. Acceleration is initially confined to the layer closest to the new surface, but is diffused vertically by turbulence until the effect of the change is felt throughout a growing boundary layer of height $\delta_i(x)$. The characteristic vertical velocity of this diffusion is the friction velocity u_*. Using similarity analysis, it is possible to derive a relationship between z_o, x and $\delta_i(x)$ (Panofsky and Dutton, 1984)

$$x/z_o = 2(\delta_i/z_o)[\ln(\delta_i/z_o) - 1] + 2 \tag{6.4}$$

For typical values of z_o, the internal boundary layer is about one-tenth of the fetch (Elliot, 1958), although only the lowest 10% of the internal boundary layer can be considered to be truly in equilibrium with the new surface (Wieringa, 1993). Special attention is required when treating transitions from open terrain to built-up areas. The distributed force model of Jerram *et al* (1995, 1997) is a promising approach to the simplified treatment of this type of problem and for modelling the bulk characteristics of the flow.

When an estimate of the surface roughness is required to characterise the flow above a built-up area, one can use standard tables of roughness estimates for various types of terrain, such as those found in Wieringa (1993). However, for general arrays of substantial obstacles, Lettau (1969) suggested that the roughness length could be related to the frontal area density of the obstacles via

$$z_0/H = 0.5\lambda_f \tag{6.5}$$

Lettau's equation predicts z_o to within a factor of two for simple cuboid obstacles when there is minimal aerodynamic interaction between them, ie when the area density λ_f is less than about 20%. Petersen (1997) showed that Lettau's equation provides good estimates of the roughness length associated with refineries, consisting of various geometrical shapes, in which the obstacle density is around 10%. However, this is much lower than the building packing density usually associated with built-up areas. For denser construction, the mutual interference between the obstacles reduces z_o/H below the value predicted by Lettau's equation. For arrays of cubic obstacles, Macdonald *et al* (1998a) derived a semi-empirical expression for roughness length that remains valid for much higher area densities where skimming flow occurs. It is

$$z_o/H = (1 - \lambda_p)\, a^{-\lambda p} \exp\{-[3.13\, \beta_s C_D (1 - \lambda_p)\, a^{-\lambda_p}\, \lambda_f]^{-0.5}\} \tag{6.6}$$

For typical cubic obstacles, the drag coefficient C_D = 1.2, the constant a = 4 and the sheltering coefficient β_s = 1 (nominally staggered array). Figure 6.1 shows the very good agreement between the expression in equation 6.5 and measured values of z_o in simple cube arrays tested in a wind tunnel.

Finally, in order to apply the logarithmic profile, one needs the value of u*. It is likely in most applications that the mean wind speed will be available from an airport site, corrected to 10 m height (U_{10}). If one assumes that the airport site is representative of open exposure with a roughness length of about 3 cm, then the mean wind speed at an arbitrary reference height z_r (say 100 m) will be

$$U_r = U_{10} \ln(z_r/0.03) / \ln(10/0.03) \tag{6.7}$$

The mean wind speed at a height z_r = 100 over the city will be almost the same as that at the airport. Therefore, the value of U_{100} calculated from the airport data can be substituted in the logarithmic profile to obtain u_* for the urban area. One then has a reasonable estimate of the urban velocity profile outside the urban roughness sub-layer. The next problem is to identify the plume advection velocity as a function of the plume growth.

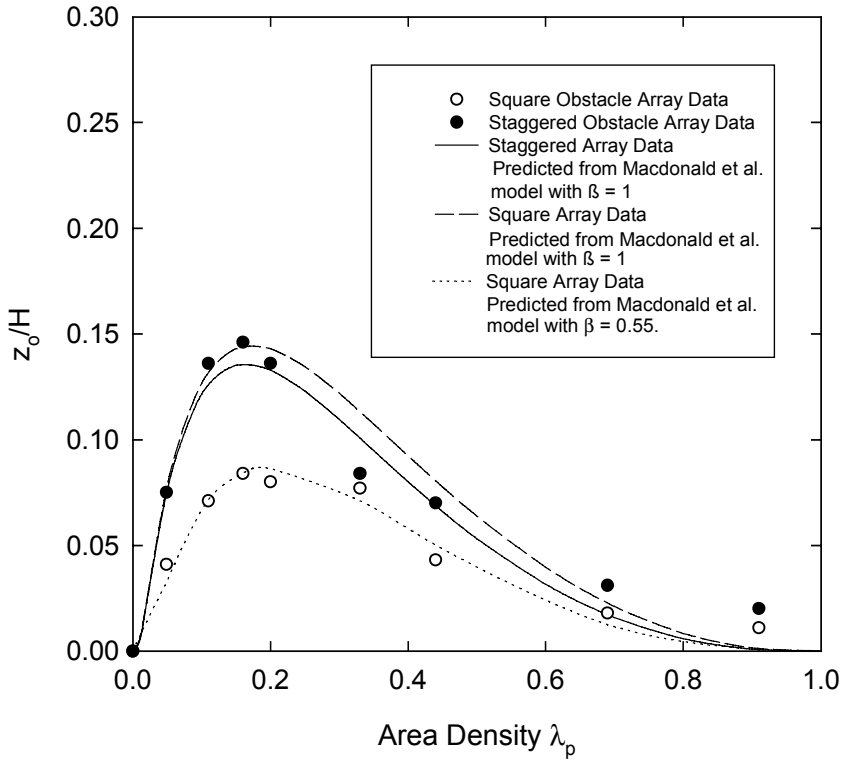

FIGURE 6.1 Comparison of measured and predicted roughness length as a function of area density from Macdonald *et al* (1998a)

6.4 Modelling the plume advection velocity in urban dispersion

If a plume is much larger than the surface obstacles ($\sigma_z >> z_o$), then the bulk surface roughness is usually a sufficient parameter to describe the effect of the obstacles. For a ground-based plume in a logarithmic shear layer, the effective plume velocity can be shown to be approximately

$$U_r = (u^*/k) \ln(0.45\sigma_z/z_o) \tag{6.8}$$

assuming a Gaussian concentration profile (Robins and Fackrell, 1998). Therefore the effective plume velocity is simply the mean wind velocity evaluated at a height $z = 0.45\sigma_z$. This gives the plume advection velocity in the third regime of urban dispersion.

In the near and intermediate ranges of urban dispersion, Hall *et al* (1996a,c) and Macdonald *et al* (1998b) have shown that for a ground-level release the plume distribution is generally well modelled by a reflected Gaussian profile

$$C(x, y, z) = (Q/2\pi\, \sigma_y \sigma_z\, U_c) \exp\,[\, -(y - y_p)^2/2\sigma_y^2] \times \{\exp[\, -(z - z_p)^2/2\sigma_z^2] + \exp[\, -(z + z_p)^2/2\sigma_z^2]\} \tag{6.9}$$

Here y_p is a measure of the lateral deflection of the plume and z_p is an effective source height or plume offset. The effective plume velocity can be evaluated from the integral

$$U_c = {}_0\int^{\infty}{}_{-\infty}\int^{\infty} C(x, y, z)\, U(z)\, dy\, dz \,/\, {}_0\int^{\infty}{}_{-\infty}\int^{\infty} C(x, y, z)\, dy\, dz \tag{6.10}$$

which is just a weighted average velocity (Csanady, 1973).

By integrating over the complicated structure of the velocity profile within the urban canopy and using the reflected Gaussian profile, one finds (see, for example, Macdonald, 1997)

$$U_c = f(a, u^*, d, z_o, \sigma_z, z_p) \tag{6.11}$$

The parameter a depends on the mean velocity profile. Below roof-top level Macdonald (1997) found that in low density ($\lambda_f < 30\%$) arrays the exponential profile, equation 5.2, provided a good fit to the observations. An example of this is shown in Figure 6.2. A similar parameterisation was also used by Nicholson (1975) to describe the below rooftop flow in street canyons. The final expression, equation 6.11, is quite complex, but can presumably be obtained from numerically solving the integral equation 6.10 with all the necessary parameters. Its asymptotic form is equation 6.8, which occurs when the fraction of plume within the urban canopy is small (say less than 10%).

The important conclusion to be drawn from the above analysis is that the plume advection velocity varies as a function of distance of travel. There is no simple and representative uniform advection speed that can be used in the near and intermediate regimes of dispersion where a substantial fraction of the plume falls within the urban canopy. A practical approach would be to generate a database of measured plume advection velocities from standard array geometry. In most cases the advection velocity can be represented fairly well by a two-parameter functional form (Macdonald *et al*, 1998c)

$$U_c/U_H = k_1 \ln(x/H) + k_2 \tag{6.12}$$

These complications do not occur in standard Gaussian plume models for high level releases in urban terrain. One of the consequences of the developing internal boundary layer over urban topology is that high level plumes may actually be released outside the internal boundary layer. In such a case the initial spread may not be influenced directly by the urban surface roughness. This is similar to the behaviour of plumes from stacks that extend above the separation streamline above an isolated building. The plume outside the boundary layer will be influenced mainly by the turbulence generated upstream, and will have an advection velocity close to that at the release height.

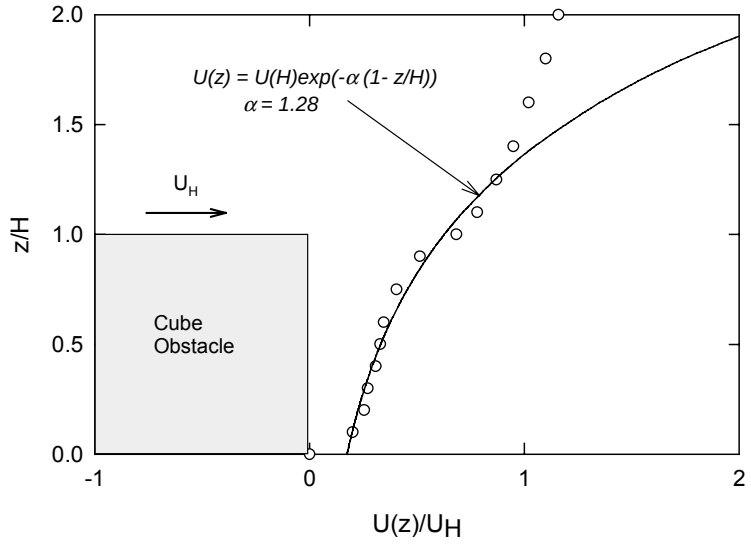

FIGURE 6.2 Velocity profile within the canopy of a low density obstacle array, from Macdonald (1997)

6.5 Plume partitioning and near-field dispersion in large obstacle arrays

For low level releases in a large array of obstacles, the initial growth of the plume will depend strongly on the details of the initial release point relative to the obstacles. Macdonald *et al* (1998b,d) note that the initial growth for a release inside an array is usually much greater than the growth of a plume released just upwind of an array. The latter problem is specific to plumes originating outside the built up area, which was the release condition in the experiments by Davidson *et al* (1995, 1996).

The initial growth of a plume released in an obstacle array can be modelled with a virtual source position, as is often done in the case of dispersion around individual buildings. In some cases the plume may be bifurcated by an initial obstacle interaction and further treatment may require two virtual sources. The proportion of material entrained into a wake of a downstream obstacle depends on the lateral offset of the source from the obstacle centreline. Mavroidis (1997) offers empirical functions for the entrainment fraction both for isolated obstacles and for a few cases within obstacle arrays. This partitioning can be handled in a relatively straightforward manner in a computer solution of the dispersion problem (see, for example, Robins *et al*, 1997). However, accurate prediction is very difficult, due to the inherent sensitivity of the near-field behaviour to small changes in geometry near the release. Theurer *et al* (1996) note that the semi-empirical SAMPU model has a weakness in this regime. In the near-field dispersion problem, it is not always possible to interpolate data for discrete wind directions (eg 0°, 30°, 45° and 90°), since profound effects may occur in the intervening angles. This would suggest that a separate model to deal with the first 100 m or so of the dispersion is required, which must somehow tie in to a simpler Gaussian plume model at an intermediate distance from the source.

Site-specific behaviour can also occur in the near-field when one building dominates the others, by being significantly taller or wider than the rest. Hall *et al* (1996c) give an example of a plume impacting on a building which is three times taller than the surrounding uniform array. Flow visualisation shows that the plume is entrained into the wake and drawn up to the height of the tall building. In dispersion results from arrays with staggered tall and short buildings having a height variability coefficient of $\sigma_H = 50\%$, Hall *et al* (1996a) note that the vertical dispersion coefficient σ_z tends to scale with the height of the taller buildings. This suggests that the mean height of the urban construction is an insufficient parameter to characterise its influence on the vertical development of the plume, and some account must be taken of the variability.

6.6 Averaging time effects in urban dispersion

In the full-scale atmosphere the obstacle-induced or topologically-induced lateral spreading that occurs in obstacle arrays in a wind tunnel is sometimes only apparent when the averaging time is relatively short. If the large-scale eddies in the atmosphere are sufficiently energetic, they may completely smear out the lateral spreading caused by the obstacles. In their scaled field experiments of obstacle-influenced dispersion, Davidson *et al* (1995, 1996) found that for 20-minute averages it was better to scale the data by upstream turbulence length scales (eg the integral length scale of the lateral wind fluctuations) then by obstacle scales. However, Macdonald *et al* (1997, 1998b) used smaller averaging times (3 minutes) in the field, corresponding to more uniform wind direction, and found that the obstacle scales were more effective for scaling and for comparison with wind tunnel data.

In general, wind tunnel data provide low estimates of σ_y and correspondingly (conservative) higher estimates of concentration than in the field. Field data, however, tend to be sensitive to averaging time. To account for this, the lateral spread of the plume can be decomposed

into small-scale turbulence and meandering components as is done in the NRPB-R91 model (Clarke, 1979). This idea is originally attributed to Gifford (1960) and has been used extensively by Moore (1976); lateral spread is represented as the statistical summation of two independent variance contributions:

$$\sigma_y^2 = \sigma_{yt}^2 + \sigma_{yw}^2 \tag{6.13}$$

Here σ_{yt} is the boundary layer turbulence spreading parameter, which in open terrain is effectively measured in the wind tunnel, and σ_{yw} is the wind direction meandering component, which is approximately related to the wind direction fluctuations via:

$$\sigma_{yw} = \sigma_\theta \, x \tag{6.14}$$

where x is the travel distance and σ_θ is the standard deviation of the wind direction fluctuations due to the large-scale eddies in the wind. An additional multiplier function $f(t/T_L) < 1$, where t is the plume travel time and T_L is a Lagrangian time scale, is also sometimes included (Draxler, 1976). The effect of the obstacle array appears as an enhancement of the turbulent diffusion parameter σ_{yt}, but this relative spread tends to become less influential with long averaging times that include the contributions of the large-scale atmospheric eddies.

In the vertical direction, the influence of the obstacles will always be important, since the size of the vertical atmospheric eddies tends to scale with height above the ground, even for long averaging times. Thus the plume is always larger than the maximum vertical eddy scale, which is unlike the situation in the lateral direction. Vertical dispersion effects such as the enhancement of σ_z and the effective lifting of the plume centre of mass in the array, z_c are therefore relevant both to instantaneous and longer time-averaged plumes.

A note should be made about the influence of the lateral shift of the plume that occurs at acute wind angles to the predominant street direction. If the plume deflection in an obstacle array is plotted as a function of mean wind direction, then the slope of the resulting curve is the derivative $\partial y_p/\partial\theta$. When the wind direction has variability σ_θ, this derivative modifies the lateral spread due to wind direction unsteadiness, so that

$$\sigma_{yw} = (\partial y_p/\partial\theta)\, \sigma_\theta \tag{6.15}$$

Macdonald (1997) notes that in the near and intermediate regimes of urban dispersion, this can be as large as the obstacle-induced lateral spread and the contribution defined in equation 6.14. Equation 6.15 thus represents an amplification of the spread caused by meandering of the wind.

6.7 Effect of wake residence times on dispersion

A final note should be made about the wake residence time of obstacles within large arrays. From flow visualisation studies of a meandering plume in an obstacle array in the field, Davidson *et al* (1995) noted that as the plume shifted laterally from one obstacle to another, the material entrained in a previous wake slowly diffused out after the main plume departed. The wake then acted as a secondary source of pollutant, and a number of neighbouring wakes could be observed releasing material at the same time. Surprisingly, this behaviour did not appear to have much affect on lateral spread, at least in a time-averaged sense. However, the wake residence time will certainly influence the longitudinal spread of a finite duration or time-varying release. When a short-duration release (a puff) of material passes into an array of obstacles, it diffuses into any wakes it encounters. It is then re-released on a time scale T_R, of the order of H/U_H, the wake residence time. If this time scale is larger than the duration of the initial puff, it will dramatically increase the longitudinal spread of the puff. For releases which are time varying, the effect will be

to smooth out any longitudinal discontinuities in the plume concentration. This is in addition to the longitudinal spread caused by the mean flow shear (Wilson, 1981; Robins and Fackrell, 1998) and is particularly relevant to problems associated with explosive or short duration accidental releases.

7 Limitations of current understanding

The most studied topic has been the dispersion of low level emission within extensive, regular arrays of obstacles and street canyons, although even here there are numerous outstanding questions which limit the development of acceptable dispersion models. Probably the least examined topic, at least in any systematic manner, is the dispersion of roof level and elevated emissions above small and moderately sized obstacles arrays, typical of large industrial sites. Current dispersion models have very limited capabilities to treat problems of this kind, although the inventive user may well achieve rather more than the basic model might appear to allow.

We must start by asking if general models for predicting dispersion affected by groups of buildings are even possible, or rather what types of problem might be amenable to modelling. In the preceding chapters we have pointed out the very real difficulties arising when the plume scale is small compared with the building scale; ie when small-scale flow and geometrical features are important. The uncertainties involved in any dispersion modelling for such circumstances must be considerably greater than those implicit in treating plumes which are large relative to the buildings. In other words, modelling will inevitably be more uncertain in the near-field than in the far-field. That being so, we need to understand and try to quantify the levels of uncertainty. So the answer to the initial question is 'yes', but the precision will be much less in some circumstances than in others, and the detail of the problem (mainly, the geometry) will generally be greatly simplified in its solution.

7.1 Array dispersion modelling

In the past there has been a tendency to perform rather narrowly focused urban dispersion experiments. This has been partially necessitated by the complexity of the problem, and the inability to vary more than a few input parameters in any one experiment. Unfortunately such an approach creates its own momentum and, if unchecked, can result in the exclusive attention on idealised problems that bear little resemblance to the physical reality. Areas that have been particularly neglected include flow and dispersion in irregular (but realistic) obstacle arrays, dispersion from sources above obstacle arrays, dispersion in the wakes of arrays, and dispersion affected by porous obstacles rather than arrays of solid elements. In the following section, some of the limitations are exposed and certain neglected aspects of the urban dispersion problem highlighted.

One of the shortcomings in the existing database arises from the tendency to model only regular arrays of obstacles with orthogonal winds (ie perpendicular to the obstacle faces) and the concentration on low level emissions. This tendency prevails in most physical modelling studies, both for small and large arrays of obstacles. It is often justified by the necessity to generate baseline data in which only a few selective parameters are varied, such as obstacle dimensions or obstacle spacing. In reality, there is generally a random nature to the shape and distribution of obstacles in an urban agglomeration or at an industrial site. This prompted Ho *et al* (1991, 1992) to design a 'random city' for the measurement of wind forces on a building located therein, although the specification of a random city is not simple as there is an infinite number of possible arrangements. Consequently, ensembles of configurations must be examined to obtain meaningful statistical information about the variability of measured parameters such as plume trajectory and spread. Certain practical questions are also raised, such as when does a particularly large building dominate the surrounding topology, so that some of the nearby buildings may be neglected? Finer detail, such

as architectural features, foliage, cuttings, bridges, and signs, may also influence matters. These are usually neglected in array simulations, but must have some influence on the micro-meteorology and dispersion behaviour. When can they be neglected? How does one parameterise a so-called random city or random site using a minimum number of parameters?

As already noted, the vast majority of research only considers orthogonal wind directions. In real problems the wind direction is variable, so that the orthogonal wind direction (within ±5°, say) is no more likely to occur than any other. Important physical phenomena, such as strong trailing vorticity, and the lateral deflection of the plume centreline along street canyons, do not occur for orthogonal winds.

Another feature which predominates the research effort is a focus on high mean wind speeds and neutral stability flows. Most street canyon models are only valid for roof-level wind speeds above about 2–3 m s^{-1}, yet the worst air pollution problems often occur when the mean wind speed is lower than this. In such conditions turbulence levels may be very low (stable case) or of the same order of magnitude as the mean wind (unstable case), and in both situations dispersion patterns may be quite unlike those in neutral stability. Secondary flows due to irregular surface heating and disturbance created by traffic or other human activities may significantly influence dispersion. Emission buoyancy and momentum also play an increasingly important role at low wind speeds.

7.2 Some modelling issues

The most difficult dispersion regime to model is the near-field, in the immediate vicinity of the source and adjacent buildings. This is just as true for an isolated building as for an array. Very high levels of spatial and temporal variability occur as the narrow, relatively undiluted plume is transported through the flow fields around individual obstacles. The mean concentration may be of little relevance in such situations, as short-term exposure to the plume implies peak concentrations that are orders of magnitude higher than the mean.

In the near-field, part of an emission may be diluted in a building wake, part may flow through the spaces between buildings, and part may simply rise up over the building canopy. Partitioning of the release between these different processes can become a necessary part of dispersion modelling. How this can be done is only partially understood at present. Algorithms to treat entrainment into the near-wake of an isolated building have been developed as part of the ADMS dispersion model. Perturbations to the mean flow field around a building in an array (due to surrounding obstacles) can be large. Modelling may not always be able to take full advantage of related data from studies of isolated obstacles, such as recirculating wake dimensions, wake residence times, and entrainment fractions. An approach similar to that incorporated in ADMS is plausible in treating near-wakes in arrays but the model parameters must become functions of the array geometry.

The characteristics of the wake of an isolated obstacle depend on approach flow conditions. For example, wake structure and decay in a highly sheared boundary layer with energetic, large-scale turbulence is not the same as that for an obstacle in a relatively smooth flow. The wind direction relative to the obstacle is also very important. A simple momentum wake occurs for winds normal to the front face, and there are analytical theories for this case. The roof vortices which arise for other wind directions may change the entire nature of the wake and there are no theories that treat these situations so empiricism must currently suffice. A common assumption in modelling arrays is that the incident flow characteristics are relatively unimportant within the array. This is not necessarily a valid assumption; it is certainly not true when wind speeds are low, particularly for lateral dispersion which is very sensitive to wind direction meander. Furthermore,

recent experiments on dispersion of emissions above small arrays have revealed wake behaviour similar to that behind a single block, with the same sensitivity to wind direction.

Modelling requirements and criteria for Reynolds number independence in wind tunnel studies have been discussed in Section 4.2. These have largely been developed for simple stack emissions affected by block-shaped obstacles and have not been evaluated for arrays. Snyder (1981) recommends a minimum Reynolds number of 11×10^3 for simulating flow around sharp-edged buildings. Is this excessive for array studies? The minimum allowable Reynolds number, where at issue, is something that currently needs to be verified in individual experiments. The same is true of simulation criteria for buoyant discharges.

7.3 Some validation issues

As already noted, the use of complex numerical and laboratory simulations of dispersion in arrays of obstacles has increased greatly in the past decade. However, several questions remain as to the validity of these methods and there is a need for strategic bench-marking. There is also a need to perform a structured inter-comparison in order to identify the relative merits of the available approaches (ie physical modelling, numerical modelling and full-scale measurements) and the importance of human factors (see, for example, Hall, 1997; Robins *et al*, 1998a). Situations where one method is more reliable, or provides more physical insight into a particular class of problem, need to be identified. Schatzmann *et al* (1997) discuss the problem of comparing the results of full-scale measurements of microscale atmospheric dispersion to physical model scale and numerical models of the dispersion. One of the difficulties encountered is that there are systematic differences in the types of data that result. For example, full-scale measurements are affected by background concentrations and are often dominated by variability and high intermittency, whereas wind tunnel models tend to give results which are more uniform, with less fluctuation. Large-scale wind direction variability is not a feature of wind tunnel simulations and statistically stationary data are readily attained, whereas field results are dependent on the averaging period and ensemble averaging is required. There is no precise definition of the full-scale averaging period equivalent to a wind tunnel mean concentration measurement, although values of around 15 to 30 minutes are often assumed. CFD predictions face the same difficulty, although frequently the issue of appropriate averaging time is not discussed.

At present, there are clear difficulties in bench-marking CFD methods (or for that matter wind tunnel methods) for predicting complex dispersion problems (whether or nor involving arrays), and in providing a sensible framework in which to assess their usefulness for regulatory purposes. These questions have been a major focus of attention in several recent workshops and conferences. For example, at the 5th International Conference on Harmonisation within Atmospheric Dispersion Modelling for Regulatory Purposes (Rhodes, Greece, 1998) the question of the statistical assessment of numerical models for dispersion forecasting was one of the major issues on the agenda. The issues remain to be resolved.

7.4 Simple models – are they possible?

To be pessimistic about the possibility of simple array dispersion models is easy, but there has been significant progress in recent years and some promising approaches have been developed. Common sense shows that increasing model complexity is not always beneficial, and it is undesirable to make models too complex by incorporating multiple corrections for minor details which may have a small effect on the overall output. The incorporation of superfluous detail in practical models is not desirable or justifiable, given the variability of real dispersion behaviour and data and the overall lack of precision in any field measurements. Where the limit lies is though a moot point.

Models should really cater to the level of detail required, and many simplifications are accordingly possible. As a specific example, the plume advection velocity in the near and intermediate regimes of array dispersion can be written as some complex function of the plume dimensions and logarithmic profile parameters (Macdonald, 1997):

$$U_c = f(u^*, d, z_o, \sigma_z, z_p, \text{etc}) \tag{7.1}$$

This is a complex parameterisation and, for practical purposes, such complexity may be unnecessary. An acceptable estimate of U_c in a screening model could be half the mean roof-top velocity, as this usually gives an answer to within ±50% of the true plume advection velocity for a low level release in the array canopy. This level of accuracy would be completely acceptable for some requirements. A similar philosophy can be used to simplify many other aspects of potential array dispersion model.

We have discussed the value of viewing array plume dispersion in progressive regimes, in order to isolate the main physical parameters of interest at each stage. In the very-near-field, there is the dominance of small-scale, local effects and these must be included systematically in order to develop modelling rules. However, the modelling will not account for fine detail and the uncertainty which this inevitably brings about must be understood and quantified. In the intermediate regime, more general parameterisation of the effects of buildings (by simple mean dimensions and measures of variability) becomes practicable. Finally, in the far-field, parameterisation of the array surface by just a few basic measures is feasible (ie the roughness length, the boundary layer height and the Monin-Obukhov length). The maximum influence of buildings occurs at relatively short distances (0 to 1000 m), when the turbulent eddies they produce are of a similar size to the plume dimensions.

This suggests a tiered model in which the various phases are treated independently of one another, with some means of smooth overlapping at the boundaries. This approach is much more feasible than a complex model which uses the same level of detail for treating the problem at each stage of the dispersion. Both the ADMS model (Robins *et al*, 1997) and the model recently developed for the UK Ministry of Defence by Hall *et al* (1997a) take advantage of this form of philosophy. Of course, the uncertainties in predictions vary from one tier or regime to the other, but this is really a small price to pay in achieving an overall modelling capability.

8 Modelling – prospects and limitations

In the previous section we outlined some of the shortcomings that limit efforts at modelling dispersion in the environment of urban or industrial sites and pointed out some of the limitations in the existing dispersion database. Current capabilities and fruitful areas of research and development are summarised below. The discussion largely concentrates on dispersion, although the flow is of course equally important. Indeed, adequate dispersion prediction is impossible without sufficient knowledge of the flow field. Research effort needs to address that link, so that where we talk of a dispersion experiment it is implicit that related flow studies are involved, and vice versa. The overall aim is to understand much more thoroughly the flow and dispersion processes and their relation to boundary and array conditions and then to express that understanding through a set of models and modelling recommendations. This implies both generating new knowledge and developing the extent of current knowledge and practice.

The full topic is divided into a number of sub-topics in order to simplify the discussion. To do this we use four dispersion regimes, two categories of source location, two of emission type and two of stability condition, as summarised in Table 8.1. This division largely reflects the balance of

research activity to date, which has concentrated on the behaviour of passive, low level emissions and neutrally stable atmospheric boundary layer conditions. Consequently, fine divisions are possible according to fetch and source position, but only broad ones for atmospheric stability and emission conditions.

The main techniques currently in use are: empirical rules, standard Gaussian plume models, modified Gaussian plume models, isolated building models, street canyon models, CFD and physical simulation. The status of these techniques is first summarised for each sub-topic, along with the uncertainty attached to their application. Uncertainty is described qualitatively as normal, moderate, high or very high. 'Normal' is taken to mean the level of uncertainty expected of a standard application of the modelling technique.

The prospects for developing better prediction capabilities are then summarised. In general, this will involve improving current methods, developing new methods and linking selected methods. For example, a model for exchanges between streets at an intersection might be developed and patched to a modified street canyon or isolated building model. Some potentially valuable research opportunities are listed, chosen with regard to their likely impact. The nature of these research topics reflects effort to date; in some areas activity can be concentrated on detail whilst in others it must address basic and at this stage wide-ranging issues. Some generic research topics are included following Table 8.1.

8.1 General topic areas

TABLE 8.1 General topic areas: obstacle arrays and dispersion

Dispersion regimes	**Behaviour**
Array, near-field	Very variable plume behaviour affected by fine topographical detail
Array, intermediate-field	Variable plume behaviour affected by general topographical detail
Array, far-field	Well-defined plume behaviour as a function of bulk surface properties only
Downwind of array	Generally well defined plume behaviour in decaying building wake
Source locations	**Consequence**
Within canopy	Plumes affected by local array details
Above canopy	Plumes affected by overall array characteristics
Emission properties	**Data**
Near-passive	Most wind tunnel and field research
Significant buoyancy (+ve or –ve), momentum	Little systematic research
Atmospheric stability	**Data**
Near-neutral atmosphere	Most wind tunnel and field research
Stable and unstable atmosphere	No systematic research

Research topics

To promote good modelling practice

(a) Systematic investigation of the effects of Reynolds number, geometrical scale and model detail on the quality of physical modelling studies.

(b) Systematic investigation of solution procedures, geometrical detail and turbulence modelling on the quality of CFD studies.

(c) Inter-comparisons of full-scale, model scale and numerical modelling of dispersion in arrays to illustrate and quantify uncertainty, understand capabilities and develop guidelines for application and applicability.

To extend the range of application of modelling procedures

(a) Longitudinal dispersion effects in arrays for short duration releases. How does this differ from the case of a simple rough surface and how can the differences be parameterised?

(b) Measurement of concentration fluctuations and the effect of averaging time on full-scale concentration measurements in urban dispersion. How does this differ from the case of a simple rough surface or an isolated building, and how can the differences be parameterised?

8.2 Passive emissions and near-neutral boundary layers

8.2.1 Near-field dispersion (1st and 2nd obstacles) for sources within the canopy

TABLE 8.2 Modelling possibilities and limitations; near-field region for sources within the canopy

Flow	*Very complex; local detail important; difficult to set up appropriate boundary conditions for modelling within an array, unless spacing is large or building of interest much larger than average*		
Dispersion	*Plume small compared with obstacles; great spatial variability; high level of fluctuations; local detail difficult to treat but may be dominant*		
Models of potential value	**Availability**	**Uncertainty**	**Specific comments**
Empirical rules	Some	Very high – moderate	Case by case applicability depends on available empirical data
Standard Gaussian plume	Not applicable	–	–
Modified Gaussian plume	Some	Very high	Case by case applicability depends on available empirical data
Isolated building	Yes	Very high	Acceptable if large building dominates, but local detail not treated
Street canyon	Yes	High	Modelling assumptions rarely satisfied in practice
CFD	Yes	Very high – moderate	Selection of grid, domain size and boundary conditions inevitably lead to high uncertainty
Physical simulation	Yes	High – moderate	Very detailed and extensive model usually required

Prospects for model developments

The main prospects are for improved empirical rules, the creation of models for specific applications (eg street intersections), the development of guidelines for best practice in CFD and physical simulation and the quantification (and possible reduction) of modelling uncertainties.

Research topics

To extend the measurement database (to further understanding and model development)

(a) Studies of near-field, obstacle-induced dispersion, including the role of the horseshoe and roof vortex systems for a building surrounded by others. How does this differ from the case of an isolated building?

(b) Studies of array street canyons with intersections (not the two-dimensional problem). How does this differ from simple street canyons? How is it to be modelled? How can exchanges between streets at an intersection be modelled and how can this be linked to canyon and building models? What is the rate of traffic induced flow and dispersion?

(c) Investigation of the importance of the relatively small-scale features of obstacle arrays. What can be ignored in a given configuration? The development of systematic rules for specifying geometry in an array.

(d) Empirical determination of upper bound non-dimensional concentrations in typical building and array configurations.

To develop models for specific applications

Detailed studies of 'special' urban dispersion topics, such as exchanges at street intersections, effects of tall buildings, closed courtyards, road tunnels and the influence of ambient conditions. Development of models for such special situations.

To understand the limitations of complex modelling techniques

(a) Systematic investigation of the effects of scale, model detail and source configuration on the quality of physical modelling studies.

(b) Systematic investigation of the effects of resolution, numerical error, solution schemes and turbulence models on the quality of CFD simulations.

(c) Inter-comparison of full-scale, model-scale and CFD data to quantify uncertainty and develop guidelines for applicability and application.

8.2.2 Intermediate-field dispersion (2nd to 4th or 5th obstacle) for sources within the canopy

TABLE 8.3 Modelling possibilities and limitations; intermediate-field region for sources within the canopy

Flow	*Complex; overall size and arrangement of buildings is important, but not detail*		
Dispersion	*Plume and obstacles of similar size; significant spatial variability, moderate level of fluctuations; modelling has to be 'patched' to near-field solution*		
Models of potential value	**Availability**	**Uncertainty**	**Specific comments**
Empirical rules	Some	High – moderate	Applicability depends on available empirical data
Standard Gaussian plume	Not applicable	–	–
Modified Gaussian plume	Some	High	Applicability depends on available empirical data
Isolated building	Not applicable	–	–
Street canyon	Not applicable	–	–
CFD	Yes	High – moderate	Large errors may be carried from near-field; issues as for near-field
Physical simulation	Yes	Moderate	Very detailed (near source) and extensive model usually required

Prospects for model developments

The reliability of empirical rules and modified Gaussian plume models rests on the extent of empirical data and significant improvements in performance and applicability should result from continuing experimental research. The creation of models for specific special situations is another area where progress can be anticipated.

Research topics

To extend modelling capabilities

(a) General studies of intermediate range dispersion in simple arrays. How can turbulence and topographically induced dispersion be jointly modelled? Can models for dispersion in the wakes of isolated buildings be adapted for use in arrays?

(b) Plume partitioning and fractional entrainment into obstacle wakes in array dispersion; residence time measurements in building wakes embedded in arrays. Can practical rules be established? Can the methods developed for single building be adapted for use in arrays? How are the parameters involved related to array geometry?

(c) Parametric studies of 'random' obstacle arrays and any asymmetrical concentration distributions which may result. How does dispersion in such cases differ from that in regular arrays?

To develop models for specific applications

Detailed studies of 'special' urban dispersion topics, such as exchanges at street intersections, effects of tall buildings, closed courtyards, road tunnels and the effects of ambient conditions. Development of models for such special situations.

To understand the limitations of complex modelling techniques

(a) Systematic investigation of the effects of scale, model detail and source configuration on the quality of physical modelling studies.

(b) Systematic investigation of the effects of resolution, numerical error, solution schemes and turbulence models on the quality of CFD simulations.

(c) Inter-comparison of full-scale, model-scale and CFD data to quantify uncertainty and develop guidelines for applicability and application.

8.2.3 Far-field dispersion (beyond 5th or 6th obstacle) for sources within the canopy

TABLE 8.4 Modelling possibilities and limitations; far-field region for sources within the canopy

Flow	*Perturbed boundary layer; only 'bulk' properties of array important*		
Dispersion	*Near-Gaussian behaviour, with canopy and roughness change included; modelling has to be 'patched' to near and intermediate-field solution*		
Models of potential value	**Availability**	**Uncertainty**	**Specific comments**
Empirical rules	Not needed		
Standard Gaussian plume	Yes	Moderate	Requires empirical virtual source (or similar) data
Modified Gaussian plume	Some	Normal	Requires empirical virtual source (or similar) data and rules to determine surface properties (z_o, d etc.)
Isolated building	Not applicable		
Street canyon	Not applicable		
CFD	Generally not needed		Modified Gaussian models generally suffice; 'size' of problem likely to be excessive
Physical simulation	Yes	Normal	Modified Gaussian models generally suffice; extensive model required (if near source detail important)

Prospects for model developments

Existing methods can generally be successfully adapted but further insight and data are needed for establishing rules for determining virtual origins (ie introducing the near and intermediate-range effects).

Research topics

To develop virtual origin and related rules

Systematic analysis of current near-field dispersion information, coupled with additional parametric studies. Can simple rules be based on array geometrical properties? What level of uncertainty follows? At what stage can near-field effects be safely ignored? Can area averaged or depth averaged models be used to provide a model of the flow field?

8.2.4 Downstream dispersion (beyond all obstacles) for sources within the canopy

TABLE 8.5 Modelling possibilities and limitations; downstream region for sources within the canopy

Flow	*Array wake; internal boundary layer; boundary layer*		
Dispersion	*Near-Gaussian form, rate of spread and plume height changes determined by wake decay; initial conditions uncertain if plume leaves array at the intermediate-field stage (errors largest in these circumstances)*		
Models of potential value	**Availability**	**Uncertainty**	**Specific comments**
Empirical rules	Not needed		
Standard Gaussian plume	Yes	Moderate – high	From far-field; no treatment of wake
		High	From intermediate-field; no treatment of wake
Modified Gaussian plume	Some	Normal – moderate	From far-field; using semi-empirical rules for wake decay
		Normal	From intermediate-field; using semi-empirical rules for wake decay
Isolated building	Not applicable	–	–
Street canyon	Not applicable	–	–
CFD	Generally not needed	High	Feasible with small arrays, otherwise 'size' of problem excessive
Physical simulation	Yes	Moderate	Extensive and moderately detailed model required

Prospects for model developments

This area has been subject to little systematic research and model development should respond well to research effort.

Research topics

To understand wake and dispersion behaviour

Studies of wake structure and decay and the influence of wind direction. What regimes of flow behaviour are possible and which are common? How is the wake affected by the openness of an array? How do wakes from arrays differ from those from isolated buildings? Can dispersion models for single buildings be adapted for arrays?

8.2.5 Elevated plumes above large and medium sized arrays

Prospects for model developments

Modelling capabilities are generally satisfactory, with only some details remaining to be resolved.

Research topics

To characterise flow conditions

Investigation of flow above the array roughness elements. How does the internal boundary layer develop? What is the lowest level at which the standard boundary layer profiles apply? Can area averaging be used to extend the log-law velocity profile towards the surface? What are the general relations between the array geometry and the roughness length and displacement height? What is the zone of influence of an isolated, larger than average roughness element?

TABLE 8.6 Modelling possibilities and limitations; fully elevated plume above large and medium sized arrays

Flow	*Internal boundary layer, main boundary layer*		
Dispersion	*Plume remains clear of surface; Gaussian form, rate of spread and plume height determined by local boundary layer conditions*		
Models of potential value	**Availability**	**Uncertainty**	**Specific comments**
Empirical rules	Not needed	–	–
Standard Gaussian plume	Yes	Normal – moderate	Plume clear of surface; uniform flow conditions
Modified Gaussian plume	Some	Normal	Plume clear of surface; dispersion matched to local flow conditions
Isolated building	Not applicable	–	–
Street canyon	Not applicable	–	–
CFD	Not needed	–	Can provide basic information about internal boundary layer growth
Physical simulation	Not needed	–	Can provide basic information about internal boundary layer growth

8.2.6 Plumes reaching surface at long-range; size much larger than obstacles

TABLE 8.7 Modelling possibilities and limitations; elevated plume reaching surface of large and medium size arrays at long range

Flow	*External boundary layer, roughness sub-layer, canopy layer, building wakes; flow conditions increasingly dominated by array roughness conditions*		
Dispersion	*Modified Gaussian plume dispersion responding to local flow conditions; no significant vertical concentration gradients within the canopy*		
Models of potential value	**Availability**	**Uncertainty**	**Specific comments**
Empirical rules	Not needed		
Standard Gaussian plume	Yes	Moderate	Ignore sub-layer, use array surface conditions
Modified Gaussian plume	Some	Normal – moderate	Incorporate models for sub-layer and internal boundary layer
Isolated building	Not needed		
Street canyon	Not needed		
CFD	Not needed		
Physical simulation	Not needed		Research tool for sub-layer processes

Prospects for model developments

Modelling capabilities are generally satisfactory, with only some details remaining to be resolved.

Research topics

To characterise flow conditions

Investigation of flow above the array roughness elements. How does the internal boundary layer develop? What is the lowest level at which the standard boundary layer profiles apply? Can area averaging be used to extend the log-law velocity profile towards the surface? What are the general relations between the array geometry and the roughness length and displacement height? What is the zone of influence of an isolated, larger than average roughness element?

To characterise exchange rates

Investigation of the exchange mechanisms between the canopy and the external boundary layer? How are external fluid and pollutant mixed into the canopy (and vice versa)? What are the

characteristic mixing and residence times associated with these processes? How do the roles of the dominant mechanisms reflect the array geometry?

8.2.7 Plume reaching surface at short-range; size similar to obstacles

TABLE 8.8 Modelling possibilities and limitations; elevated plume reaching surface of large and medium size arrays at short range

Flow	*External boundary layer, roughness sub-layer, canopy layer, building wakes*		
Dispersion	*Possibly complex; many forms of interaction possible depending on size and arrangement of array obstacles (eg direct impact on to building, entrainment into recirculation regions, wake downwash)*		
Models of potential value	**Availability**	**Uncertainty**	**Specific comments**
Empirical rules	Some	High – very high	Case by case applicability depends on available empirical data
Standard Gaussian plume	Yes	High	Many forms of interaction to be covered
Modified Gaussian plume	Some	Moderate	Adapted for specific situations
Isolated building	Some	High	Useful when a single large building dominates
Street canyon	Possible	High – very high	Need to model entrainment from external source
CFD	Yes	High – moderate	'Size' of problem may be excessive
Physical simulation	Yes	Moderate	Extensive (and moderately detailed) model may be required

Prospects for model developments

The reliability of empirical rules and modified Gaussian plume models rests on the extent of empirical data and significant improvements in performance and applicability should result from continuing experimental research. The creation of models for specific special situations is another area where progress can be anticipated.

Research topics

To extend modelling capabilities

(a) Investigation of mixing into simple arrays. Identification of the dominant pathways for mixing of external fluid and pollutant into the canopy. What are the characteristic mixing and residence times associated with these processes? How do the roles of the dominant mechanisms reflect the array geometry? Can models for dispersion near isolated buildings be adapted for use in arrays?

(b) General studies of dispersion with regular arrays. How does lateral spread differ above and within the canopy? In what circumstances do significant vertical concentration gradients exist within the canopy? Can (isolated) building wake models be adapted to these circumstances?

(c) Parametric studies of 'random' obstacle arrays and asymmetrical concentration distributions which may result. How does dispersion in such cases differ from that in and over regular arrays?

To develop models for specific applications

Detailed studies of 'special' topics, such as plume impact on to individual large buildings within an array, plume downwash, and entrainment into recirculation regions. Development of models for such special situations and their subsequent incorporation into general models.

8.2.8 Dispersion within porous arrays

TABLE 8.9 Modelling possibilities and limitations; dispersion within porous arrays

Flow	*Rapid flow development through array sensitive to structural details and wind direction; recirculation regions may exist*		
Dispersion	*Spreading rates and centre line path determined by complex flow field; rapid dilution and mixing associated with recirculation regions*		
Models of potential value	**Availability**	**Uncertainty**	**Specific comments**
Empirical rules	None		Useful for upper bound concentration estimation
Standard Gaussian plume	Not applicable		
Modified Gaussian plume	None		Models need to incorporate details of flow field
Isolated building	Some	High – very high	Useful only when a single large building dominates
Street canyon	Not applicable		
CFD	Yes	Moderate – high	Numerous modelling difficulties – explicit representation of structures not feasible
Physical simulation	Yes	Moderate – high	Numerous modelling questions – considerable detail may be required

Prospects for model developments

This topic has been subject to little systematic research, largely because it can be extremely complex. It is, however, very important to the analysis of the on-site behaviour of hazardous emissions and merits considerable attention. Overall, only slow progress can be anticipated, with more rapid developments in some specific areas.

Research topics

To develop flow models

(a) Systematic investigation of flow fields within arrays of porous obstacles. How does the mean flow develop as it passes through the array? How do the flow characteristics respond to the nature and porosity of array elements? In what situations does recirculation develop – either on average or intermittently? What changes arise from solid obstacles within an otherwise porous array?

(b) Studies of external flow fields to determine the relative importance of displaced and bleed flow and the exchanges between the external and internal flows.

Dispersion modelling

(a) Systematic investigation of dispersion within arrays of porous obstacles. Classification of regimes of plume behaviour. Development of models to cover individual regimes. Can simple rules be developed to estimate upper-bound concentrations?

(b) Mass balance studies to determine loss rates through the top and sides of arrays associated with flow deceleration (and possibly acceleration) through the array. Is this significant? How can it be incorporated within models?

To develop models for specific applications

Comparisons of flow and dispersion at ‘real sites’ with behaviour within idealised porous arrays. How can ‘real sites’ be approximated by simple porous arrays? What are the likely errors implicit in doing this?

8.2.9 Dispersion downstream from porous arrays

TABLE 8.10 Modelling possibilities and limitations; dispersion downwind from porous arrays

Flow	*Array wake, sensitive to porosity and wind direction; downwind recirculation may occur*		
Dispersion	*Near-Gaussian form, spread and height determined by wake decay; rapid mixing in recirculation regions (where they exist)*		
Models of potential value	**Availability**	**Uncertainty**	**Specific comments**
Empirical rules	None	–	–
Standard Gaussian plume	Yes	High	Only applicable far downwind
Modified Gaussian plume	Some	Moderate	Applicable downwind of recirculation (if any present); semi-empirical rules to determine wake regime, strength, effect of wind direction, etc
Isolated building	Some	High – very high	Useful when a single large building dominates
Street canyon	Possible	–	–
CFD	Yes	Moderate – high	Numerous modelling difficulties – particularly establishing appropriate flow conditions downwind of obstacle
Physical simulation	Yes	Moderate	Modelling difficulties include establishing appropriate flow conditions downwind of obstacle

Prospects for model developments

Research to date suggests that the development of linked modified Gaussian plume and recirculation region models is a realistic goal. To aid complex modelling we need to understand how the complex structure of a real site can be satisfactorily simulated.

Research topics

To understand and model the flow field

(a) The role of bleed flow in the development of array wakes. Is there common ground between building arrays and porous obstacles? How is the effective porosity of an array to be ascertained? Can a characteristic bleed flow be measured?

(b) Studies of wake structure and the influence of wind direction. What regimes of flow behaviour are possible and which are common? How is the wake affected by the openness of an array? How do wakes of porous obstacles differ from those of building arrays?

To develop simple dispersion models

Systematic studies of dispersion downwind from porous arrays. Development of models for the flow regimes encountered; patching such models together. How does dispersion reflect the physical form of the array?

To understand the limitations of complex modelling techniques

(a) Systematic investigation of the effects of Reynolds number, geometrical scale and model detail on the quality of physical modelling studies.

(b) Systematic investigation and development of 'porosity models' and assessment of their influence on the quality of CFD studies.

(c) Inter-comparisons of full-scale, model-scale and numerical modelling of dispersion in porous arrays to quantify uncertainty and develop guidelines for application and applicability.

To develop models for specific applications

Comparisons of flow and dispersion downstream from 'real sites' with behaviour downstream from idealised porous arrays. How can 'real sites' be approximated by simple porous arrays? What are the likely errors implicit in doing this?

8.2.10 Elevated plumes downstream from small regular and irregular arrays

TABLE 8.11 Modelling possibilities and limitations; dispersion downwind from small regular and irregular arrays

Flow	*Array wake, sensitive to wind direction; streamline deflection associated with wake decay*		
Dispersion	*Near-Gaussian form, rate of spread and plume path determined by wake decay*		
Models of potential value	**Availability**	**Uncertainty**	**Specific comments**
Empirical rules	None	–	–
Standard Gaussian plume	Yes	Moderate – high	Regular arrays: most applicable far downwind
		High – very high	Irregular arrays: most applicable far downwind
Modified Gaussian plume	Some	Normal – moderate	Regular arrays: semi-empirical rules to determine wake regime, strength, effect of wind direction, plume height, etc
		Moderate – high	Irregular arrays: model as equivalent regular array
Isolated building	Some	High	Useful if a single large building dominates
Street canyon	Not applicable	–	–
CFD	Yes	Moderate	Regular arrays: 'size' of problem limits precision
		Moderate – high	Irregular arrays: 'size' and 'detail' of problem limits precision
Physical simulation	Yes	Normal	Regular arrays
		Normal – moderate	Irregular arrays: detailed model required

Prospects for model developments

Research to date suggests that the development of modified Gaussian plume models is a realistic goal. To aid complex modelling we need to understand how the complex structure of a real site can be satisfactorily simulated.

Research topics

To develop simple dispersion models

(a) Systematic study of the effect of source height, location and array form. At what height do perturbations due to an array become negligible? Can arrays be represented as single obstacles in Gaussian plume and similar models? Can the rules developed for small arrays be extended to larger ones?

(b) The effect of wind direction on mean streamline deflections – is the modelling used for isolated buildings readily adapted to small arrays? How does the form and arrangements of an array affect matters?

(c) The variation of lateral spread with height, for low and high level releases. Does lateral spread need to be made a function of height?

To understand the limitations of complex modelling techniques

(a) CFD simulations to determine the practical limits imposed by 'problem size'. What does this imply about the application of CFD techniques? What are the relative effects of numerical error and turbulence model errors?

(b) Physical modelling studies to establish the degree of modelling detail required for the treatment of 'real sites'.

(c) Inter-comparisons of full-scale, model-scale and numerical modelling of dispersion to quantify uncertainty and develop guidelines for application and applicability.

8.3 Dispersion and obstacle arrays; atmospheric stability effects

TABLE 8.12 Modelling possibilities and limitations; stability effects

Flow	*Unknown effects of stability of approach flow and heat transfer within the obstacle array; stable or unstable conditions*		
Dispersion	*Unknown consequences of flow stability on dispersion behaviour*		
Models of potential value	**Availability**	**Uncertainty**	**Specific comments**
Empirical rules	As for near-neutral	High – very high	Little or no data from which to establish rules
Standard Gaussian plume	As for near-neutral	High – very high	Little or no data available for testing performance
Modified Gaussian plume	As for near-neutral	High	Little or no data available for developing methods and testing performance
Isolated building	As for near-neutral	High	Some data available for isolated buildings, none for large buildings within arrays
Street canyon	As for near-neutral	High	Little or no data available for developing methods and testing performance
CFD	Yes	High	Little or no data available for testing performance
Physical simulation	Very limited	High	Little or no data available for testing performance; few suitable facilities

Prospects for model developments

Development is severely hampered by lack of any systematic research. Remedy of this situation should result in rapid development of modelling capabilities, along with clarification of the potential and applicability of particular techniques.

Research topics

To understand the effects of ambient stability

Systematic study of the effect of ambient stability and approach flow conditions on dispersion behaviour within and above arrays. How important is stability? What is the effect on emissions from stacks of height comparable with the depth of the stable boundary layer?

To understand the effects of small-scale temperature variations

Systematic study of the changes in dispersion behaviour resulting from heat emission from buildings and other human/industrial activities when wind speeds are light. What is the significance of solar heating of building surfaces? How important are heat transfer effects and how are they to be modelled? What conditions lead to the highest concentrations for a given emission?

To evaluate model performance

Inter-comparisons of full-scale, model-scale and numerical modelling of dispersion to quantify uncertainty and develop guidelines for application and applicability.

8.4 Dispersion and obstacle arrays; emission effects

TABLE 8.13 Modelling possibilities and limitations; emission effects

Flow	*Heat and momentum content of emissions leads to self-induced dilution and (in some cases) escape from the canopy; local wind fields are created by traffic and other human activities*		
Dispersion	*Largely unknown effects of momentum and buoyancy on dispersion; some limited knowledge of the effects of vehicle wakes*		
Models of potential value	**Availability**	**Uncertainty**	**Specific comments**
Empirical rules	None	–	Guidelines needed to estimate when emission effects become important
Standard Gaussian plume	None	–	–
Modified Gaussian plume	Some	High – very high	Little or no data available for developing methods and testing performance
Isolated building	Some	High	Some models in place; reasonable body of data for isolated buildings
Street canyon	Some	High	Some simple modelling in place; further progress limited by lack of suitable flow and dispersion data
CFD	Yes	High	Little or no data available for testing performance
Physical simulation	Yes	High	Little or no data available for testing performance

Prospects for model developments

Development is severely hampered by lack of any systematic research, other than for mixing in vehicle wakes. Remedy of this situation should result in rapid development of modelling capabilities, along with clarification of the potential and applicability of particular techniques.

Research topics

To develop models for self-induced mixing and plume lift-off

Systematic studies of the behaviour of plumes emitted with momentum and buoyancy, addressing self-induced dilution and plume escape from the canopy layer. Can simple 'lift-off' rules be developed similar to those for an isolated building? How can self-induced mixing be included in models for near and intermediate-range dispersion in arrays?

To develop models for dense gas dispersion

Systematic studies of the behaviour of heavier-than-air emission within arrays. How is lateral spread enhanced and vertical spread diminished by gravitational effects? Can methods employed in open terrain be adapted for application to arrays? To what degree need standard entrainment velocity models be modified within arrays, especially for shallow clouds and plumes?

To develop models treating mixing in vehicle wakes

(a) Review existing and ongoing research. Can general rules be derived? How can vehicle wake dispersion be correctly incorporated into general dispersion modelling procedures?

(b) Systematic studies of modelling options for use with CFD and physical simulations. Can static simulators create appropriate local flow conditions?

9 References

Apsley D D (1988). A model for dispersion in the wake of large buildings. Swindon, National Power, CEGB Report RD/L/3359/R88.

Arya S P S (1975). Geostrophic drag and heat transfer relations for the atmospheric boundary layer. *Quart J R Meteorol Soc,* **101,** 147–61.

Baechlin W, Theurer W and Plate E J (1991). Wind field and dispersion in a built-up area – a comparison between field experiments and wind tunnel data. *Atmos Environ*, **25A,** 1135–42.

Baechlin W, Theurer W and Plate E J (1992). Dispersion of gases released near the ground in built up areas: experimental results compared to simple numerical modelling. *J Wind Eng Indust Aerodyn*, **41–44,** 2721–32.

Barrett C F (1970). An experimental study by means of a fluorescent tracer of diffusion in two urban areas. London, HMSO, Warren Spring Laboratory Report No. LR117(AP).

Benarie M M (1980). *Urban Air Pollution Modelling*. London, MacMillan Press.

Berkowicz R (1997). Modelling street canyon pollution: model requirements and expectations. *Int J Environ Pollut*, **8**(3–6), 609–19.

Berkowicz R, Hertel O, Sorensen N N and Michelsen J A (1997a). Modelling air pollution from traffic in urban areas. IN *Proceedings IMA Conference on Flow and Dispersion through Groups of Obstacles*, Cambridge, March 1994. Oxford, Clarendon Press, pp 121–42.

Berkowicz R, Hertel O, Larsen S E, Sorensen N N and Nielsen M (1997b). Modelling traffic pollution in streets. Roskilde, Denmark, National Environmental Research Institute.

Bottema M (1996). Roughness parameters over regular rough surfaces: experimental requirements and model validation. *J Wind Eng Ind Aerodyn*, **64,** 249–65.

Bottema M (1997). Urban roughness modelling in relation to pollutant dispersion. *Atmos Environ*, **31,** 3059–75.

Briggs G A (1973). Diffusion estimation for small emissions. ATDL Contribution File No. 79. Oak Ridge, Tennessee, Air Resources Atmospheric Turbulence and Diffusion Laboratory, NOAA.

Briggs G, Britter R E, Hanna S B, Havens J, King S B, Robins A G, Snyder W H and Steinberg K W (1997). Advances in dense gas dispersion modelling of accidental releases over rough surfaces during stable conditions. IN *Proceedings NATO/CCMS 22nd International Conference on Air Pollution Modelling and its Applications,* Clermont Ferrand, France, June 1997.

Buckland A T (1998). Validation of a street canyon model in two cities. *Environ Monit Pollut*, **52,** 255–67.

Carruthers D J, Holroyd R J, Hunt J C R, Weng W S, Robins A G, Apsley D D, Thomson D J and Smith F B (1994). UK-ADMS: a new approach to modelling dispersion in the earth's atmospheric boundary layer. *J Wind Eng Indust Aerodyn*, **52,** 139–53.

Castro I P and Dianat M (1983). Surface flow patterns on rectangular bodies in thick boundary layers. *J Wind Eng Indust Aerodyn*, **11,** 107–19.

Castro I P, Cowan I R and Robins A G (1999). Simulations of flow and dispersion around buildings. *J Aerosp Eng,* **12,** 145–60.

Clarke R H (1979). The first report of a Working Group on Atmospheric Dispersion: a model for short and medium range dispersion of radionuclides released to the atmosphere. Harwell, NRPB-R91.

Cook N J (1978). Wind tunnel simulation of the adiabatic boundary layer by roughness, barrier and mixing-device methods. *J Indust Aerodyn*, **3,** 157–76.

Cook N J (1990a). *The Designer's Guide to Wind Loading of Building and Structures. Part 1: Background, Damage Survey, Wind Data and Structural Classification.* Building Research Establishment. London, Butterworth.

Cook N J (1990b). *The Designer's Guide to Wind Loading of Building Structures. Part 2: Static Structures.* Building Research Establishment. London, Butterworth.

Coulson B J (1998). An experimental study of dispersion in an array of model cubes. MSc Thesis. Waterloo, Ontario, Canada, Department of Mechanical Engineering, University of Waterloo.

Counihan J (1969). An improved method of simulating an atmospheric boundary layer in a wind tunnel. *Atmos Environ,* **3,** 197–214.

Counihan J (1971). Wind tunnel determination of the roughness length as a function of the fetch and the roughness density of three-dimensional roughness elements. *Atmos Environ*, **5,** 637–42.

Counihan J, Hunt J C R and Jackson P S (1974). Wakes behind two dimensional surface obstacles in turbulent boundary layers. *J Fluid Mech*, **64,** 529–63.

Cowan I R, Castro I P and Robins A G (1997). Numerical considerations for simulations of flow and dispersion around buildings. *J Wind Eng Indust Aerodyn*, **67/68,** 535–45.

Csanady G T (1973). *Turbulent Diffusion in the Environment*. Dordrecht, Holland, D Reidel Publishing Co.

Davidson M J and Hunt J C R (1991). Atmospheric dispersion around groups of obstacles: wind tunnel and field investigations. Final report under MoD Research Grant RG 10874. Department of Applied Mathematics and Theoretical Physics, Cambridge University.

Davidson M J, Mylne K R, Jones C D, Phillips L J, Perkins R J, Fung J C H and Hunt J C R (1995). Plume dispersion through large groups of obstacles – a field investigation. *Atmos Environ*, **29,** 3245–56.

Davidson M J, Snyder W H, Lawson R E and Hunt J C R (1996). Wind tunnel simulations of plume dispersion through groups of obstacles. *Atmos Environ,* **30,** 3715–31.

Delaunay D (1996). Numerical simulation of atmospheric dispersion in an urban site: comparison with field data. *J Wind Eng Indust Aerodyn*, **64,** 221–31.

Dianat M and Castro I P (1984). Fluctuating surface shear stresses on bluff bodies. *J Wind Eng Indust Aerodyn*, **17,** 133–46.

DoE (1997). *The United Kingdom National Air Quality Strategy.* London, Department of the Environment.

Draxler R R (1976). Determination of atmospheric diffusion parameters. *Atmos Environ*, **10,** 99–105.

Elliot W P (1958). The growth of the atmospheric internal boundary layer. *Trans Amer Geophys Union*, **39,** 1048.

Fackrell J E (1984a). Parameters characterising dispersion in the near wake of buildings. *J Wind Eng Indust Aerodyn*, **16,** 97–118.

Fackrell J E (1984b). An examination of simple models for building influenced dispersion. *Atmos Environ,* **18,** 89–98.

Fackrell J E and Robins A G (1982). Dispersion of releases at an AGR site. CEGB Report RD/M/1172R81.

Fang C and Sill B L (1992). Aerodynamic roughness length: correlation with roughness elements. *J Wind Eng Indust Aerodyn*, **41–44,** 449–60.

Fedorovich E and Kaiser R (1998). Wind tunnel study of turbulence regime in the atmospheric convective boundary layer. IN *Buoyant Convection in Geophysical Flows* (E J Plate, Ed). Amsterdam, Kluwer Academic Publishers.

Foster P M and Robins A G (1985). The effects of buildings on low-level atmospheric discharges. CEGB Report No. TPRD/L/2888/R85.

Gandemer J (1981). The aerodynamic characteristics of windbreaks, resulting in empirical design rules. *J Wind Eng Indust Aerodyn,* **7,** 15–36.

Gifford F A (1960). Peak to average concentration ratios according to a fluctuating plume dispersion model. *Int J Air Water Pollut,* **3,** 253–60.

Gifford F A (1972). Atmospheric transport and dispersion over cities. *Nucl Safety*, **13,** 391–401.

Gifford F A and Hanna S R (1970). Urban air pollution modelling. IN *Proceedings of the 1970 International Air Pollution Conference of International Union of Air Pollution Control Associations,* Washington DC.

Gifford F A and Hanna S R (1973). Technical note: modelling urban air pollution. *Atmos Environ*, **7,** 131–6.

Griffiths R F (1994). Errors in the use of the Briggs parameterisation for atmospheric dispersion coefficients. *Atmos Environ*, **28,** 2861–5.

Griffiths R F, Mavroidis I and Jones C D (1998). Development of a fast-response portable photo-ionisation detector: model of the instrument response and validation tests in air. *Meas Sci Technol*, **9,** 1369–79.

Grimmond C S B and Oke T R (1998). Aerodynamic properties of urban areas derived from analysis of surface form. *J Appl Meteorol*, **38,** 1262–92.

Guenther A, Lamb B and Stock D (1990). Three-dimensional numerical simulation of plume downwash with a k–ε turbulence model. *J Appl Meteorol,* **29,** 633–43.

Hall R C (1996). Evaluation of modelling uncertainty; CFD modelling of near-field atmospheric dispersion. Final report to the European Commission. Epsom, WS Atkins, Report WSA/AM5017/R7.

Hall R C (1997). Application of computational fluid dynamics to near-field atmospheric dispersion. Atmospheric Dispersion Modelling Liaison Committee Annual Report 1995/96. Chilton, NRPB-R292.

Hall R C (1998). Uncertainties in CFD modelling of gas dispersion. *MEG Bulletin Issue*, **3,** February 1998.

Hall D J and Walker S (1995). Scaling rules for reduced-scale field releases of hydrogen fluoride. BRE Report No. CR 121/95. Garston, Building Research Establishment.

Hall D J, Spanton A M, Macdonald R and Walker S (1996a). A review of requirements for simple urban dispersion models. BRE Client Report CR 77/96. Garston, Building Research Establishment.

Hall D J, Spanton A M, Kukadia V and Walker S (1996b). Exposure of buildings to pollutants in urban areas – a review of the contributions from different sources. BRE Client Report CR 209/96. Garston, Building Research Establishment.

Hall D J, Macdonald R, Walker S and Spanton A M (1996c). Measurements of dispersion within simulated urban arrays – a small scale wind tunnel study. BRE Client Report CR 178/96. Garston, Building Research Establishment.

Hall D J, Spanton A M, Macdonald R and Walker S (1997a). A simple model for estimating dispersion in urban areas. BRE Client Report CR 169/97. Garston, Building Research Establishment.

Hall D J, Macdonald R, Walker S, Mavroidis I, Higson H and Griffiths R F (1997b). Visualisation studies of flows in simulated urban arrays. BRE Client Report CR39/97. Garston, Building Research Establishment.

Hall D J, Macdonald R, Walker S and Spanton A M (1998a). Measurements of dispersion within simulated urban arrays – a small scale wind tunnel study. BRE Client Report CR 244/98, Building Research Establishment Ltd., Garston, Watford, England.

Hall D J, Walker S C, Spanton A M and Kukadia V (1999). Pressure and concentration patterns on building forms in urban arrays. BRE Client Report CR 125/99. Garston, Building Research Establishment.

Hanjalic K, Obi S and Hadzic I (1998). Wall-jets and flows over wall-mounted cubical obstacles. 6th ERCOFTAC/IAHR/COST Workshop on Refined Flow Modelling. *ERCOFTAC Bulletin* No. 36, March 1998.

Hanna S R, Briggs G A and Hosker R P (1982). *Handbook on Atmospheric Dispersion*. Publication DOE/TIC-11223. Washington DC,US Department of Energy.

Hassan A A and Crowther J M (1998). A simple model of pollutant concentrations in a street canyon. *Environ Monit Assess*, **52,** 269–80.

Hayden P (1997). Dispersion from stacks over groups of buildings in neutral and stable flows. PhD Thesis. University of Surrey, School of Mechanical and Materials Engineering.

Hertel O and Berkowicz R (1991). The operation street canyon pollution model (OSPM). *Air Pollution Modelling and its Application* (H van Dop and D G Stryn, Eds). New York, Plenum Press, **15,** 741–9.

Ho T C, Surrey D and Davenport A G (1991). Variability of low building loads due to surroundings. *J Wind Eng Indust Aerodyn,* **38,** 297–310.

Ho T C, Surrey D and Davenport A G (1992). Low building load variability with application to codes. *J Wind Eng Indust Aerodyn,* **41–44,** 1787–98.

Hosker R P (1984). Flow and diffusion near obstacles. *Atmospheric Science and Power Production* (D Randerson, Ed). Publication DOE/TIC-27601. Washington DC, US Department of Energy, pp 241–326.

Hosker R P (1985). Flow around isolated structures and building clusters: a review. *ASHRAE Trans,* **91,** 1671–92.

Hosker R P and Pendergrass W R (1987). Flow and dispersion near clusters of buildings. NOAA Technical Memorandum ERL-ARL-153. Department of Commerce, USA.

Hoydysh W G and Dabberdt W F (1994). Concentration fields at urban intersections: fluid modelling studies. *Atmos Environ*, **28,** 1849–60.

Huber A H (1987). Performance of a Gaussian model for centreline concentrations in the wake of buildings. *Atmos Environ*, **22**(6), 1039–50.

Huber A H and Snyder W H (1976). Building wake effects on short stack effluents. *Pre-print Volume 3rd Symposium on Atmospheric Turbulence, Diffusion and Air Quality*, October 1976, Raleigh NC. Boston MA, American Meteorological Society, pp 235–42.

Hunt J C R, Abell C J, Peterka J A and Woo H (1978). Kinematical studies of the flows around free or surface-mounted obstacles: applying topology to flow visualisation. *J Fluid Mech,* **86,** 179–200.

Hussain M and Lee B E (1980). A wind tunnel study of the mean pressure forces acting on large groups of low-rise buildings. *J Wind Eng Indust Aerodyn,* **6,** 207–25.

Irwin H P A H (1981). The design of spires for wind simulation. *J Wind Eng Indust Aerodyn,* **7,** 361–6.

Jerram N, Perkins R J, Fung J C H, Davidson M J, Belcher S E and Hunt J C R (1995). Atmospheric flow through groups of buildings and dispersion from localised sources. IN *Wind Climate in Cities* (J E Cermak, Ed). Amsterdam, Kluwer Academic Publishers, pp 109–130.

Jerram N, Belcher S E and Hunt J C R (1997). Turbulent flow through a distributed force – a model for the wind within and above an urban canopy. IN *Flow and Dispersion through Groups of Obstacles* (R J Perkins and S E Belcher, Eds). Oxford, Clarendon Press.

Johnson G T and Hunter L J (1995). A numerical study of dispersion of passive scalars in city canyons. *Boundary-Layer Meteor,* **75,** 235–62.

Johnson G T and Hunter L J (1999). Some insights into typical urban canyon flows. *Atmos Environ*, **33,** 3991–4000.

Johnson W B, Ludwig F L, Dabberdt W F and Allen R J (1973). An urban diffusion simulation model for carbon monoxide. *J Air Pollut Control Assoc,* **23,** 490–98.

Johnson W B, Sklarew R C and Turner D B (1976). Urban air quality simulation modelling. IN *Air Pollution,* Volume 1, 3rd Edition (A C Stern, Ed). New York, Academic Press, pp 503–62.

Jones J A (1983). The fifth report of a Working Group on Atmospheric Dispersion: models to allow for the effects of coastal sites, plume rise and buildings on dispersion of radionuclides and guidance on the value of deposition velocity and washout coefficients. Chilton, NRPB-R157.

Kaimal J C and Finnigan J J (1994). *Atmospheric Boundary Layer Flows*. New York, Oxford University Press.

Kastner-Klein P and Plate E J (1999). Wind tunnel study of concentration fields in street canyons. *Atmos Environ,* **33,** 3973–80.

Kukadia V, Hall G J and Sharples H (1999). Ventilation of urban buildings in relation to external pollution: a review. BRE Client Report CR 524/99. Garston, Building Research Establishment.

Lee Y and Park H M (1994). Parameterisation of the pollutant transport and dispersion in urban street canyons. *Atmos Environ*, **28,** 2343–49.

Lee J T, Call D L, Lawson R E, Clements W E and Hoard D E (1991). A video image analysis system for concentration measurements and flow visualisation in building wakes. *Atmos Environ,* **25A,** 1211–25.

Lee R F, Perry S G, Cimorelli A J, Paine R J, Venkatram A, Weil J C and Wilson R B (1996). AERMOD – the developmental evaluation. IN *Proceedings, 21st NATO/CCMS International Technical Meeting on Air Pollution Modelling and Its Application*, November 1995, Baltimore MD. Boston, American Meteorological Society, pp 418–25.

Lettau H (1969). Note on aerodynamic roughness-parameter estimation on the basis of roughness-element description. *J Appl Meteorol,* **8,** 828–32.

Lucas D H (1972). Choosing chimney heights in the presence of buildings. IN *Proceedings International Clean Air Congress*, Melbourne, Australia, May 1972, pp 47–52.

Macdonald R W (1997). Physical modelling study of flow and dispersion around groups of buildings. PhD Thesis. Department of Chemical Engineering, UMIST, Manchester.

Macdonald R W, Griffiths R F and Cheah S C (1997). Field experiments of dispersion through regular arrays of cubic structures. *Atmos Environ*, **31,** 783–95.

Macdonald R W, Griffiths R F and Hall D J (1998a). An improved method for estimation of surface roughness of obstacle arrays. *Atmos Environ*, **32,** 1857–64.

Macdonald R W, Griffiths R F and Hall D J (1998b). A comparison of results from scaled field and wind tunnel modelling of dispersion in arrays of obstacles. *Atmos Environ*, **32,** 3845–62.

Macdonald R W, Hall D J and Walker S (1998c). Wind tunnel measurements of velocity within simulated urban arrays. BRE Client Report CR 243/98. Garston, Building Research Establishment.

Macdonald R W, Hall D J and Griffiths R F (1998d). Scale model study of building effects on dispersion in the urban canopy at intermediate distances. IN *Proceedings 5th International Conference on Harmonisation within Atmospheric Dispersion Modelling for Regulatory Purposes*, May 1998, Rhodes, Greece.

Manning A J, Nicholson K J, Middleton D R and Rafferty S (1998). Field study of wind and traffic to test a street canyon pollution model. *Environ Monit Assess,* **60,** 283–313.

Mavroidis I (1997). Atmospheric dispersion around buildings. PhD Thesis. UMIST Department of Chemical Engineering, Manchester, April 1997.

McElroy J L (1969). A comparative study of urban and rural dispersion. *J Appl Meteorol,* **8,** 19–31.

McHugh C A, Carruthers D J and Edmunds H A (1997). ADMS-Urban: an air quality management system for traffic, domestic and industrial pollution. *Int J Environ Pollut*, **8**(3–6), 666–74.

Meroney R N (1982). Turbulent diffusion near buildings. IN *Engineering Meteorology* (E J Plate, Ed). Amsterdam, Elsevier, pp 481–525.

Meroney R N, Pavageau M, Rafailidis S and Schatzmann M (1996). Study of line source characteristics for 2-d physical modelling of pollutant dispersion in street canyons. *J Wind Eng Indust Aerodyn*, **62,** 37–56.

Meroney R N, Rafailidis S and Pavageau M (1997). Dispersion in idealised canyon streets. IN *Air Pollution Modelling and Its Applications XI* (S E Gryning and F Schiermeier, Ed). Proceedings of the 21st NATO CCMS International Technical Meeting on Air Pollution Modelling and its Applications, November 1995, Baltimore, pp 317–24.

Mestayer P G and Sini J-F (1998). A comprehensive numerical simulation of traffic pollution in a street during a diurnal cycle. IN *Proceedings 5th International Conference on Harmonisation within Atmospheric Dispersion Modelling for Regulatory Purposes*, May 1998, Rhodes, Greece.

Moore D J (1976). Calculation of ground level concentration for different sampling periods and source locations. IN *Atmospheric Pollution*. Amsterdam, Elsevier, pp 51–60.

Morris H M (1955). Flow in rough conduits. *Trans ASCE,* **120,** 373–98.

Munn R E (1981). *The Design of Air Quality Monitoring Networks*. Air Pollution Series. London, Macmillan Publishers.

Murakami S and Mochida A (1988). 3-D numerical simulation of airflow around a cubic model by means of the k-ε model. *J Wind Eng Indust Aerodyn,* **31,** 283–303.

Nicholson S E (1975). A pollution model for street level air. *Atmos Environ*, **9,** 19–31.

Obasaju E D and Robins A G (1998). Simulation of pollution dispersion using small scale physical models – assessment of scaling options. *Environ Monit Assess*, **52,** 239–54.

Okabayashi K, Ide Y, Takahashi H, Kane N, Okamoto S and Kobayashi K (1991). A new wind tunnel technique for investigating gas diffusion behind a structure. *Atmos Environ*, **25A,** 1227–36.

Oke T R (1987). *Boundary Layer Climates,* 2nd Edition. London, Routledge.

Ohya Y, Neff D E and Meroney R N (1997). Turbulence structure in a stratified boundary layer under stable conditions. *Boundary-Layer Meteorol*, **83,** 139–161.

Panofsky H A and Dutton J A (1984). *Atmospheric Turbulence: Models and Methods for Engineering Applications.* New York, Wiley.

Pavageau M, Rafailidis S and Schatzmann M (1997). A comprehensive experimental databank for the verification of urban car emission dispersion models. *Int J Environ Pollut*, **3-6,** 738–46.

Perera M D A E S (1981). Shelter behind two dimensional solid and porous fences. *J Wind Eng Indust Aerodyn,* **8,** 93–104.

Petersen R L (1997). A wind tunnel evaluation of methods for estimating surface roughness length at industrial facilities. *Atmos Environ*, **31,** 45–57.

Petersen R L and Hosoya N (1991). Development of hybrid model for assessing concentrations of toxic effluent at air force installations. Prepared for HQ AFESC/RDVS, Tyndall Air Force Base, Florida.

Petersen R L and Ratcliff M A (1989). *Effect of Homogeneous and Heterogeneous Surface Roughness on Heavier-than-air Gas dispersion,* Volumes I and II. API Publication Nos 4491 and 492. Washington DC, American Petroleum Institute.

Petersen R L, Hosoya N and Moss M (1991). Development of hybrid model for assessing concentrations of toxic effluent at air force installations. Paper 91-83.21. IN *Proceedings of the 84th Annual Meeting of the Air and Waste Management Association*, Vancouver BC, June 1991.

Plate E J (1971). The aerodynamics of shelter belts. *Agri Meteorol*, **8,** 203–22.

Plate E J (1995). Urban climates and urban climate modelling: an introduction. *Wind Climate in Cities* (J E Cermak, Ed). Amsterdam, Kluwer Academic Publishers, pp 23–9.

Plate E J (1999). Methods of investigating urban wind fields – physical models. *Atmos Environ,* **33,** 3981–90.

Plate E J and Baechlin W (1988). Wind tunnel tests as part of a warning system for accidental gaseous spills. *J Wind Eng Indust Aerodyn,* **29,** 165–74.

Poreh M (1997). Bulk properties of dispersion from ground level sources over a non-isotropic canopy. IN *Flow and Dispersion through Groups of Obstacles* (R J Perkins and S E Belcher, Ed). Oxford, Clarendon Press.

Poreh M and Kacherginsky A (1981). Simulation of plume rise using small wind-tunnel models. *J Wind Eng Indust Aerodyn*, **7,** 1–14.

Puttock J S and Hunt J C R (1979). Turbulent diffusion from a source near obstacles with separated wakes. Part I, an eddy-diffusivity model. *Atmos Environ*, **13,** 1–13.

Rafailidis R (1997). Influence of building area density and roof shape on the wind characteristics above a town. *Boundary-Layer Meteorol,* **85,** 255–71.

Rafailidis R and Schatzmann M (1996). Velocity measurements above the urban roughness and inside street canyons with aspect ratios *B/H* = 1/2 and *B/H* = 1. Meteorologisches Institut, Universität Hamburg.

Rafailidis R and Schatzmann M (1997). Physical modelling of car exhaust dispersion in urban street canyons – the effect of slanted roofs. IN *Proceedings of the 21st NATO/CCMS International Technical Meeting on Air Pollution Modelling and its Applications*. Baltimore, November 1995.

Raine J K and Stevenson D C (1997). Wind protection by model fences in a simulated atmospheric boundary layer. *J Wind Eng Indust Aerodyn,* **2,** 159–80.

Raul R and Bernard P S (1991). A numerical investigation of the turbulent flow field generated by a stationary cube. *Trans ASME./J Fluids Eng,* **113,** 216–22.

Raupach M R and Shaw R H (1982). Averaging procedures for flow within vegetation canopies. *Boundary-Layer Meteorol*, **22,** 79–90.

Raupach M R, Thom A S and Edwards I (1980). A wind tunnel study of turbulent flow close to regularly arrayed rough surfaces. *Boundary-Layer Meteorol,* **18,** 373–97.

Raupach M R, Antonia R A and Rajagopalan S (1991). Rough-wall turbulent boundary layers. *Appl Mech Rev,* **44,** 1–25.

Roberts P T, Fryer-Taylor R E J and Hall D J (1994). Wind tunnel studies of roughness effects in gas dispersion. *Atmos Environ*, **28,** 1861–70.

Robins A G and Castro I P (1977). A wind tunnel investigation of plume dispersion in the vicinity of a surface mounted cube. *Atmos Environ*, **11,** 291–311.

Robins A G and Fackrell J E (1980). Laboratory studies of dispersion near buildings. IN *Proceedings CEC Symposium on Radioactive Releases and their Dispersion in the Atmosphere,* RISO, Denmark, April 1980.

Robins A G and Fackrell J E (1998). An experimental study of the dispersion of short duration emissions in a turbulent boundary layer. *Air Pollution VI* (C A Brebbia, C F Ratto, C F and H Power, Eds). Southampton,WIT Press, pp 697–707.

Robins A G, Carruthers D J and McHugh C A (1997). The ADMS building effects module. *Int J Environ Pollut*, **8**(3–6), 708–17.

Robins A G, Hayden P and Teasdale I (1998a). Dispersion from elevated sources above obstacle arrays – modelling requirements. IN *Proceedings 5th International Conference on Harmonisation within Atmospheric Dispersion Modelling for Regulatory Purposes*, May 1998, Rhodes, Greece.

Robins A G, Hall R, Cowan I, Bartzis J and Algergel A (1998b). Wind tunnel and CFD modelling of building affected near field dispersion. IN *Proceedings 5th International Conference on Harmonisation within Atmospheric Dispersion Modelling for Regulatory Purposes*, May 1998, Rhodes, Greece.

Robins A G, Speirs L J and Roberts P T (1999). The structure of wakes from three-dimensional porous obstacles in a deep, turbulent boundary layer. IN *Wind Engineering into the 21st Century* (A Larsen, L Larose and F M Livesey, Eds). Rotterdam, A A Balkema, Volume 3, pp 1717–24.

Robins A G, Castro I P, Hayden P, Steggel N, Contini D and Heist D K (2000). A wind tunnel study of dense gas dispersion in a stable boundary layer over a rough surface. *Atmos Environ* (in press).

Rodi W, Ferziger J H, Breuer M and Pourquié M (1997). Status of large eddy simulation: results of a workshop. *Trans ASME./J Fluid Eng,* **119,** 248–62.

Rotach M W (1995). Profiles of turbulence statistics in and above an urban street canyon. *Atmos Environ,* **29,** 1473–86.

Sayre W W and Albertson M L (1963). Roughness spacing in rigid open channels. *Trans ASCE,* **128,** 343–71.

Scaperdas A, Colevile R and Robins A G (1998a). Understanding flow patterns at street canyon intersections using wind tunnel and CFD simulations. IN *Proceedings EUROTRAC Symposium 98*, Garmisch-Partenkirchen, Germany, March 1998.

Scaperdas A, Colevile R and Robins A G (1998b). Dispersion modelling at urban street canyon intersections: a comparison of CFD with wind tunnel modelling. IN *Proceedings 5th International Conference on Harmonisation within Atmospheric Dispersion Modelling for Regulatory Purposes*, Rhodes, Greece, May 1998.

Shatzmann M, Rafailidis S and Pavageau M (1997). Some remarks on the validation of small-scale dispersion models with field and laboratory data. *J Wind Eng Indust Aerodyn,* **67–68,** 885–93.

Schulman L L, Strimaitis D G and Scire J S (2000). Development and evaluation of the PRIME plume rise and building downwash model. *J Air Waste Manage Assoc* (in press).

Schulze R H (1999). Procedures used to develop and adopt newer dispersion models in the USA. Presented at *6th International Conference on Harmonisation within Atmospheric Dispersion Modelling for Regulatory Purposes*, Rouen, France, October 1999.

Sini J-F, Anquetin S, Mestayer P G (1996). Pollutant dispersion and thermal effects in urban street canyons. *Atmos Environ,* **30**(15), 2659–77.

Snyder W H (1981). Guidelines for fluid modelling of atmospheric dispersion. Washington DC, USEPA Report No. EPA-600/8-81-009.

Snyder W H and Lawson R E (1994). Wind tunnel measurements of flow fields in the vicinity of buildings. IN *Proceedings 8th Joint Conference on Applications of Air Pollution Meteorology with AWMA*. Boston, American Meteorological Society, pp 244–50.

Snyder W H and Castro I P (1997). Surface Reynolds number effects in rough-wall boundary layers. Presented at 3rd European Fluid Mechanics Conference, Gottingen, September 1997.

Spanton A M, Hall D J and Walker S (1996). A survey of aerodynamic characteristics of some UK urban areas. BRE Client Report CR 177/97. Garston, Building Research Establishment.

Spanton A M, Hall D J and Walker S (1998). A Survey of the aerodynamic characteristics of some UK areas. BRE Report CR 177/98. Garston, Building Research Establishment.

Speirs L J (1998). Wake dispersion on process plant: enhancing VOC emissions control. EngD Portfolio, University of Surrey, October 1998.

Theurer W (1995). Point sources in urban areas: modelling of neutral gas clouds with semi-empirical models. IN *Wind Climate in Cities* (J E Cermak, Ed). Amsterdam, Kluwer Academic Publishers, pp 485–502.

Theurer W (1999). Typical building arrangements for urban air pollution modelling. *Atmos Environ,* **33,** 4057–66.

Theurer W, Baechlin W and Plate E J (1992). Model study of the development of boundary layers above urban areas. *J Wind Eng Indust Aerodyn,* **41–44,** 437–8.

Theurer W, Plate E J and Hoeschele K (1996). Semi-empirical models as a combination of wind tunnel and numerical dispersion modelling. *Atmos Environ*, **30,** 3583–97.

Turner D B (1979). Atmospheric dispersion modeling: a critical review. *J Air Pollut Control Assoc,* **29,** 502–19.

Turner D B (1994). *Workbook of Atmospheric Dispersion Estimates: An Introduction to Dispersion Modeling,* 2nd Edition. London, CRC Press.

Turner D B, Bender L W, Pierce T E and Petersen W B (1989). Air quality simulation models from EPA. *Environ Software,* **4,** 52.

US-EPA (1992). Users guide for the industrial source complex dispersion model, Volume II. Description of model algorithms. Washington DC, USEPA Report EPA-450/4-92-008b, March 1992.

US-EPA (1998). The National Air Quality Standards. Washington DC, USEPA, http://www.epa.gov/.

VDI (1987). VDI-RICTLINIE 3783/1 1987. Ausbreitung von stoerfallbedingten Freisetzungen-Sicherheitsanalyse. VDI-Handbuch Reinhaltung der Luft, Bd. 1. Dusseldorf, VDI-Verlag (available in English).

Wedding J B, Lombardi D J and Cermak J E (1977). A wind tunnel study of gaseous pollutants in city street canyons. *J Air Pollut Control Assoc,* **27,** 557–66.

Weil J C (1996). A new dispersion model for stack sources in building wakes. IN *Proceedings 9th Joint Conference on Applications of Air Pollution Meteorology with AWMA*. Boston, American Meteorological Society, pp 333–7.

Wieringa J (1993). Representative roughness parameters for homogeneous terrain. *Boundary-Layer Meteorol,* **63,** 323–63.

Wilson D J (1979). Flow patterns over flat roofed buildings and application to exhaust stack design. *ASHRAE Trans*, **85,** 284–95.

Wilson D J (1981). Along-wind diffusion of source transients. *Atmos Environ*, **15,** 489–95.

Wilson D J and Britter R E (1982). Estimates of building surface concentrations from nearby point sources. *Atmos Environ,* **16,** 2631–46.

Wilson D J and Chui E H (1987). Effect of turbulence from upwind buildings on dilution of exhaust gases. *ASHRAE Trans,* **93,** 2186–97.

Wooding R A, Bradley E F and Marshall J K (1973). Drag due to regular arrays of roughness elements of varying geometry. *Boundary-Layer Meteorol,* **5,** 285–308.

Yamartino R J and Wiegand G (1986). Development and evaluation of simple models for flow, turbulence and pollution concentration fields within an urban street canyon. *Atmos Environ,* **20,** 2137–56.

Yersel M, Goble R and Morrill J (1983). Short range dispersion experiments in an urban area. *Atmos Environ*, **17,** 275–82.

Zannetti P (1990). *Air Pollution Modeling.* New York, Van Nostrand Reinhold.

APPENDIX
Notation

A	frontal area
A_d	mean lot area of obstacles in an array
A_f	mean frontal area of obstacles in an array
A_p	mean plan area of obstacles in an array
A_S	street cross-sectional area
a	constant
a_1, a_2	constants
b	constant
b_S	constant
b_1, b_2	constants
C	mean concentration
C_b	box model average concentration
C_D	drag coefficient
C_d	direct component of concentration in a street
C_L	lea side concentration
C_{non}	non-dimensional concentration
C_o	background concentration
C_R	average concentration in recirculation region
C_S	concentration on recirculation region boundary
C_u	upwind concentration
C_W	windward side concentration
C_Y	lateral concentration profile
C_Z	vertical concentration profile
C_θ	concentration average over wind direction range
c_B	turning moment coefficient
D	boundary layer depth
Dy	lateral street offset
d	zero-plane displacement
F_B	buoyancy flux
F_M	momentum flux
$F(\theta)$	probability distribution of wind direction fluctuations
f	general function
f_y, f_z	plume spread functions
$g(\zeta)$	wake lateral profile function
H	building height
h	stack height
$h(\eta)$	wake vertical profile function
h_e	effective stack height
h_{max}	limit stack height for building effect
K	non-dimensional concentration
k	von Karman's constant
k_1, k_2	constants

L	building length
L_B	building length scale
L_R	recirculation region length
L_y	wake lateral length scale
L_z	wake vertical length scale
M(p,n)	porous fence model reference code
m	growth law exponent
N_h	stack height factor for building effects, h_{max}/h
N_v	traffic flow rate or vehicle density
n	number of plates
p	porosity of plate
Q	emission rate
Q_R	effective emission rate from recirculation region
q	velocity power law exponent
$q_{\alpha\beta}$	plume strength constant in wake region $\alpha\beta$
R_H	obstacle Reynolds number, $U_H H/\nu$
Re*	roughness Reynolds number, $u^* z_o/\nu$
S	spacing between buildings; spacing factor, Section 5.1
S_R	surface area of recirculation region
S_S	street element plan area
s	distance from source
T_L	Lagrangian time scale
T_R	recirculation region concentration decay time scale
t	time
U	mean wind speed
U_A	spatially averaged velocity
U_c	plume convection speed
Ue, $\underline{U}_{ref}$	reference speed at edge of boundary layer
U_H	roof level mean wind speed, $U(H)$
U_n	wind component normal to street
U_p	wind component parallel to street
U_r	reference wind speed at height z_r
U_S	street level wind speed
U_W	mean velocity in wake
U_{10}	10 m wind speed
U_{100}	100 m wind speed
u	longitudinal velocity perturbations in wake
u'	longitudinal turbulence velocity
u^*	friction velocity
$u_{\alpha\beta}$	wake strength constant in wake region $\alpha\beta$
$\langle u_n c \rangle$	concentration flux across the recirculation region boundary
V	mean lateral velocity
V_R	volume of recirculation region
V_S	volume of street element
V_v	average vehicle speed
v	mean lateral velocity perturbation
$\langle v^2 \rangle$	mean lateral turbulence stress

W	building width; mean vertical velocity, Section 4.3
W_S	street width
w	mean vertical velocity
w'	vertical turbulence velocity
$\langle w^2 \rangle$	mean vertical turbulence stress
X, Y	street widths
x	distance downwind
x'	distance from the leading edge of building
x_o	virtual origin position
x_R	location of end of recirculation region, $L_R + L/2$
x_{Rmax}	location of maximum recirculation region height
x_s	source position
y	distance across-wind
y_p	lateral position of plume centre
z	height above surface
z_B	building effect region height
zc	plume centre height
z_o	roughness length
z_{oref}	reference roughness length
z_{o1}	upwind roughness length
z_{o2}	downwind roughness length
z_p	plume height
z_R	recirculation region height
z_{Rmax}	maximum recirculation region height
z_r	reference height
z_{SL}	mean streamline height
α	velocity profile constant
$\alpha\beta$	wake region label
β	constant
β_s	sheltering constant
γ	geometrical scale ratio
Δh	change in effective stack height
Δu	wake centreline velocity perturbation
Δx	longitudinal face to face spacing of obstacles in an array
Δy	lateral face to face spacing of obstacles in an array
Δz	mean streamline deflection
Δv^2	perturbation lateral turbulence stress
Δw^2	perturbation vertical turbulence stress
$\Delta\rho$	density difference
$\Delta\tau$	perturbation shear stresses
δ_i	internal boundary layer depth
ε	source strength ratio, Q_R/Q
ζ	normalised lateral coordinate, y/L_y
η	normalised vertical coordinate, z/L_z
θ	wind direction
κ_x	diffusivity for longitudinal turbulent diffusion

κ_y diffusivity for lateral turbulent diffusion
κ_z diffusivity for vertical turbulent diffusion
λ_p plan area density, A_p/A_d
λ_f frontal area density, A_f/A_d
ν kinematic viscosity
ν_y lateral eddy viscosity
ν_z vertical eddy viscosity
ρ ambient density
ρ_s density of emission
σ plume spread
σ_B building-affected plume spread
σ_H standard deviation of building heights
σ_L standard deviation of building lengths
σ_o initial plume spread
σ_W standard deviation of building widths
σ_y lateral plume spread
σ_{yt} lateral plume spread due to boundary layer turbulence
σ_{yw} lateral plume spread due to wind direction meandering
$\sigma_{y\alpha\beta}$ lateral plume spread in wake region $\alpha\beta$
σ_z vertical plume spread
$\sigma_{z\alpha\beta}$ vertical plume spread in wake region $\alpha\beta$
σ_θ standard deviation of wind direction fluctuations
φ density distortion function
ψ plume spread function

Suffices

B equivalent building
H building height
i building number
M model
p plume
R recirculation region
u undisturbed flow
x longitudinal direction
y lateral direction
z vertical direction

Superiors

(*W*) wake
(*E*) undisturbed flow